AD-A063 964 HUGHES RESEARCH LABS MALIBU CALIF F/G 20/7
SATELLITE POSITIVE ION BEAM SYSTEM.(U)
OCT 78 T MASEK
UNCLASSIFIED F19628-76-C-0066
AFGL-TR-78-0141 NL

1 OF 3
ADA
063964

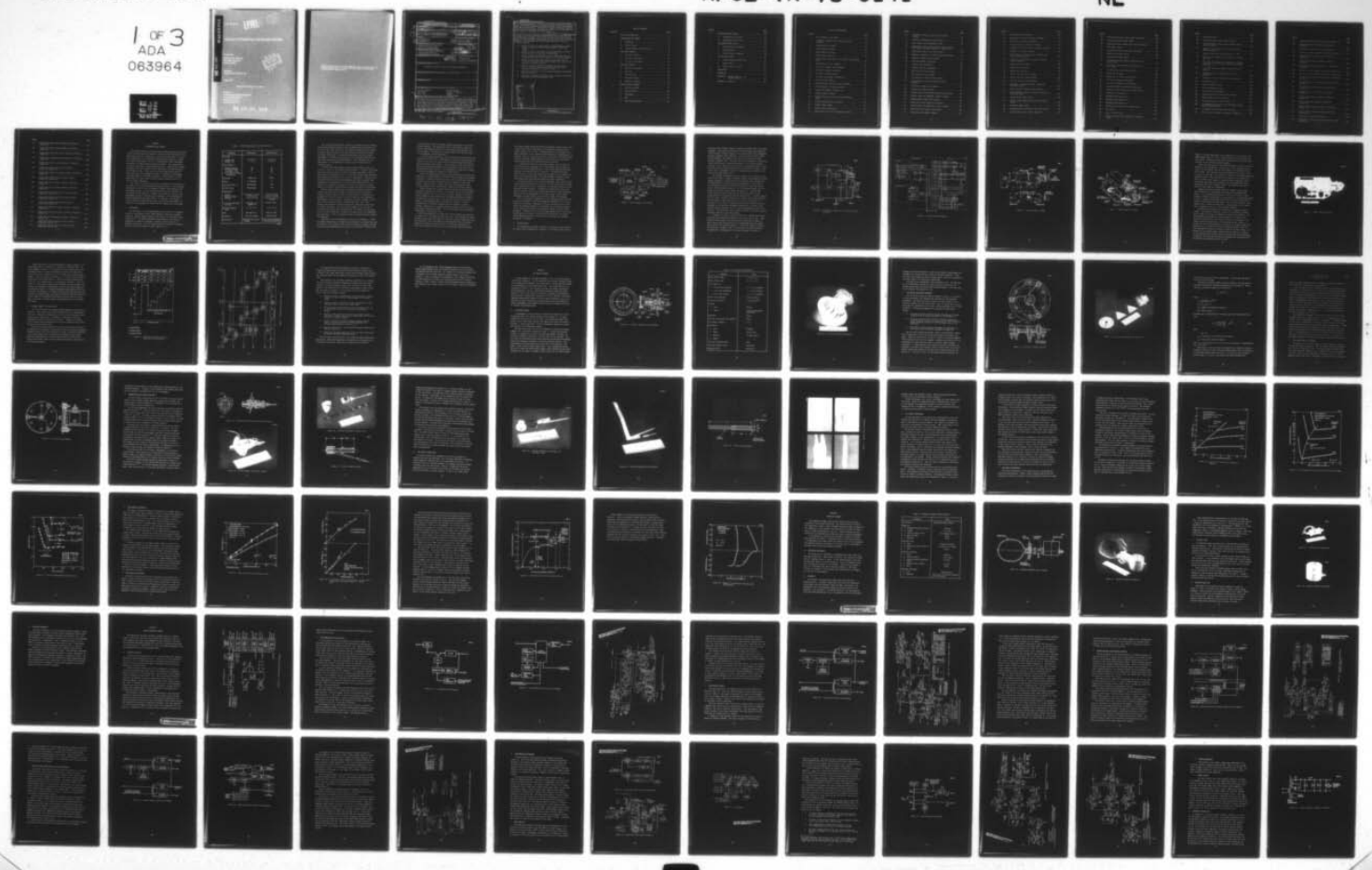

AFGL-TR-78-0141

LEVEL II

12

SATELLITE POSITIVE ION BEAM SYS

Tommy Masek

Hughes Research Laboratories
3011 Malibu Canyon Road
Malibu, CA 90265

Final Report
1 October 1975 to 30 October 1978

October 1978

UNCLASSIFIED

SECURITY CLASSIFICATION OF THIS PAGE (When Data Entered)

REPORT DOCUMENTATION PAGE	READ INSTRUCTIONS BEFORE COMPLETING FORM
1. REPORT NUMBER: AFGL-TR-78-0141	2. GOVT ACCESSION NO.
3. RECIPIENT'S CATALOG NUMBER	
4. TITLE (and Subtitle): SATELLITE POSITIVE ION BEAM SYSTEM. AD-A051 154	5. TYPE OF REPORT & PERIOD COVERED: Final Report, 1 Oct 75 - 30 Oct 78,
6. PERFORMING ORG. REPORT NUMBER	
7. AUTHOR(s): Tommy Masek	8. CONTRACT OR GRANT NUMBER(s): F19628-76-C-0066
9. PERFORMING ORGANIZATION NAME AND ADDRESS: Hughes Research Laboratories, 3011 Malibu Canyon Road, Malibu, California 90265	10. PROGRAM ELEMENT, PROJECT, TASK AREA & WORK UNIT NUMBERS: 62101F, 66900103
11. CONTROLLING OFFICE NAME AND ADDRESS: Air Force Geophysics Laboratory, Hanscom AFB, MA 01731, Monitor/Herbert Cohen/LKB	12. REPORT DATE: Oct 78
	13. NUMBER OF PAGES: 256
14. MONITORING AGENCY NAME & ADDRESS (if different from Controlling Office)	15. SECURITY CLASS. (of this report): UNCLASSIFIED
	15a. DECLASSIFICATION DOWNGRADING SCHEDULE

16. DISTRIBUTION STATEMENT (of this Report)

Approved for public release; distribution unlimited.

17. DISTRIBUTION STATEMENT (of the abstract entered in Block 20, if different from Report)

18. SUPPLEMENTARY NOTES

19. KEY WORDS (Continue on reverse side if necessary and identify by block number)

Ion beam systems	Hallow cathodes
Ion sources	Spacecraft charging
Xenon ions	SCATHA
	Graphite grids

20. ABSTRACT (Continue on reverse side if necessary and identify by block number)

The Satellite Positive Ion Beam Systems (SPIBS) program was initiated by the Air Force Geophysics Laboratory (AFGL) Aeronomy Division with the long-range objective of operating an ion-ejection instrument on the Air Force SCATHA (Spacecraft Charging at High Altitude) satellite. This report describes the development details for breadboard, engineering, and flight models of the SPIBS instrument. A fourth model, a rocket model SPIBS, was built ~~under contract F19628-6-76-0272~~ for use in a

over

DD FORM 1 JAN 73 1473 EDITION OF 1 NOV 65 IS OBSOLETE

UNCLASSIFIED

SECURITY CLASSIFICATION OF THIS PAGE (When Data Entered)

172 600

rocket charging experiment. This report provides a description of all phases of the SPIBS instrument development process and the key technical difficulties and successes. Corroborative results obtained by AFGL personnel using the delivered instruments are referred to as appropriate to support the most significant conclusions.

The flexibility of the SPIBS instrument should make it a valuable tool in the study of satellite charging on SCATHA and on other space vehicles. The SPIBS design provides a life of more than 300 hr and satisfies the SCATHA satellite instrument requirements on mass, power, EMI, and quality assurance. The instrument has been designed and built to have the following features:

- Ability to eject an unneutralized ion beam having a current range of 0.3 mA to 2.0 mA at beam energies of 1 keV and 2 keV.
- Ability to eject a partially or fully neutralized ion beam having the above current and voltage ranges.
- Ability during beam operation to use a neutralizer that can be biased from -1 kV to +1 kV relative to spacecraft ground.
- Ability to emit electrons, without an ion beam, from the neutralizer filament (which can be biased from -1 kV to +1 kV relative to satellite ground).
- Ability to detect neutralizer emission and net currents (ions or electrons) between the SPIBS instrument and satellite ground down to a level of 2 μA.
- Operation with xenon to avoid possible expellant interactions with the satellite.
- Provisions for ground operation of the ion source and system during the satellite integration phase.

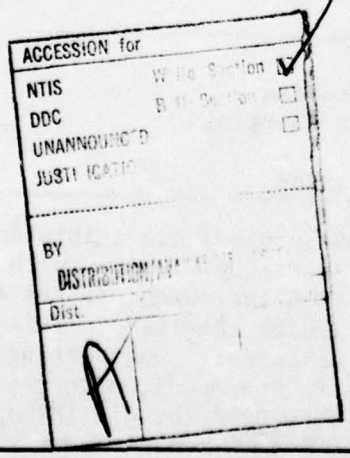

TABLE OF CONTENTS

LIST OF ILLUSTRATIONS

SECTION 1

INTRODUCTION AND SUMMARY

The Satellite Positive Ion Beam System (SPIBS) program was initiated by the Air Force Geophysics Laboratory (AFGL) Aeronomy Division with the long-range objective of operating an ion-ejection instrument on the Air Force SCATHA (Spacecraft Charging at High Altitude) satellite. Within the overall AFGL program, the task of developing the SPIBS instrument was awarded to Hughes Research Laboratories (HRL). The responsibility for other tasks (such as requirements definition, qualification testing, integration with the satellite, flight operations, and data reduction was retained by AFGL. This report, covering slightly more than two years, describes the development details for breadboard, engineering, and flight models of the SPIBS instrument. A fourth model, a rocket model SPIBS, was built under contract F19628-C-76-0272 for use in a rocket charging experiment.

This report is intended to provide a straightforward description of all phases of the SPIBS instrument development process. Since problems encountered are often vital in gaining a complete understanding of the development process, the key technical difficulties and successes are incorporated in the main text. However, the run-by-run account of the development process is presented as an appendix to avoid confusing the general program flow with many details. In addition, corroborative results obtained by AFGL personnel using the delivered instruments are referred to as appropriate to support the most significant conclusions.

A. BACKGROUND

The motivation for the SCATHA program and for SPIBS is the general interest in developing a better understanding of spacecraft charging processes. Several papers related to this subject are available in the literature.[1-6] The SPIBS requirements were derived by AFGL from consideration of spacecraft charging in general and the objectives of SCATHA in particular. The requirements defined for SPIBS are presented in Table 1 and are discussed in some length in Ref. 7.

Table 1. SPIBS Requirements and Characteristics

Parameter	Requirement	Characteristic
Ion beam		
Current, mA	0.3 to 2.0	0.3 to 2.0
Energy, keV	1 to 2	1 and 2
Input power, W		
Maximum startup	60	55
1 mA beam, 1 keV	25	30
2 mA beam, 2 keV	--	45
Full beam and biased neutralizer	--	55
Expellant	Noble gas	Xenon
Weight	7.8 maximum	7.4
Operating life, hr	300 minimum	>300
On/Off cycles	200 minimum	>200
Neutralizer		
Control	Ion beam on or off	On/off control
Emission range	2 μA to 2 mA	2.5 μA to 2.5 mA
Biasing	-1 kV to +1 kV	-1 kV to +1 kV in 10 steps
Ion source enclosure and cover	Preflight test capability	Blowoff cover
External magnetic field	<1 G at 10 cm	1 G at 12 cm
EMI	MIL STD 461 A	AFGL to test
Vibration	20 g rms random	AFGL to test
Decel grid	Shielding from space plasma	Decel grid operated at PPA ground potential

6327

The ion beam current levels, chosen to be greater than the maximum photoelectron emission expected from the SCATHA spacecraft ground, were set at 0.3 mA, 1 mA, and $\geq$ 2 mA. The upper value was chosen to provide a dynamic range for possible ion-beam currents consistent with power and weight limitations. To minimize interference with other SCATHA experiments, the SPIBS structure exposed to the ambient plasma must be kept close to spacecraft ground potential. This translates into the requirement for a grounded-surface (decel grid) following the ion accelerator grid.

The SPIBS instrument design evolved through several cycles, primarily as a result of ion source design evolution. Initially, the system input power goal was about 25 W with a lifetime requirement of 100 hr. Ion sources then available in the 1 to 2 mA beam current range used filament cathodes and met neither of the basic requirements. The key factor in meeting the power and life requirements was a lower cathode; lower temperatures are available only by using "oxide-coated" emitters. In addition, the initially available ion sources were operated on argon simply as a carryover from previous work and as a matter of convenience.

Several cathode designs were investigated in prototype argon ion sources including coated filaments, and various miniature "flower" cathodes using wire mesh to store the oxide mixture. Lifetimes were generally less than 50 hr and it was not obvious how any significant improvements could be achieved. Generally, the power required to maintain a given discharge current increased with time. This trend probably indicated that the work function was increasing as the result of several mechanisms. The free surface elements (e.g., barium or strontium) are maintained in equilibrium by the transport of new atoms from the oxide storage site to replace the atoms lost by ion bombardment and evaporation. Both the transport process and evaporation are temperature dependent.

Apparently, when ion bombardment losses are not dominant, a stable equilibrium temperature is achieved and reasonably long cathode lives can be obtained. For instance, flower cathode lifetimes of several thousand hours have beem demonstrated with mercury ion thrusters.[8] However, when

ion sputtering of the free elements becomes significant, the process becomes unstable. The temperature must be increased to supply the active oxide elements being lost by sputtering; the evporation rate then increases. Eventually, the cathode heater fails from hot spots or from weakness at high temperature.

To avoid cathode sputtering, the ion energy must be relatively low (probably less than 30 V). Unfortunately, the argon discharge tends to operate in the 40 to 50 V region with the plasma conditions needed to obtain reasonable beam currents. The discharge voltage can be driven down with increased discharge neutral atom density, but this results in unacceptable gas flowrates. The combination of argon with an oxide cathode was subsequently rejected as a SPIBS option.

With the recognition that both the gas and the cathode design were significant, a limited number of tests of oxide cathodes were performed with xenon. Although long duration tests were not conducted, operation on xenon with discharge voltages around 30 V appeared to have more promise. However, when it became clear that ion sputtering energy was the dominant factor, interest was focused on the hollow cathode.

Hollow cathodes were rejected initially because of the anticipated high power required for starting. For instance, the 8-cm ion thruster cathode required about 30 to 35 W for starting. However, the typical hollow cathode has the advantage that the emitting surface is exposed to relatively low energy ions. This probably results from the high-density, low-resistance plasma in and near the cathode. In most configurations, a "keeper" electrode near the cathode is used for starting. Generally, the cathode-to-keeper voltage is 10 to 20 V less than the main discharge voltage. Thus, the emitting surface experiences bombardment by lower energy ions.

Since the probability was high that a hollow cathode would provide the needed life, the primary concern was power. By isolating the cathode thermally and using a re-entrant thin wall tube design, conduction losses were minimized. With this approach, starting power (into the cathode heater) was reduced to about 20 to 25 W. Xenon was retained as the first choice expellant because of its more desirable plasma properties.

The hollow cathode design selected was eventually found to have a life of more than 1,000 hr operating at acceptable gas flowrates with a keeper voltage of 20 to 25 V. Because time was of the essence, only minor variations in the original cathode design were investigated. In addition, argon or other gases were not tested with the hollow cathode because the primary program objective was to develop a satisfactory system design within the available resources and time.

A significant benefit of the hollow cathode, one that probably would not have been available from a conventional oxide cathode, was a low steady-state operating power. After keeper and main discharge ignition, the cathode heater is turned off. The keeper discharge requires about 5 W, but this power also contributes to ion production and is not totally parasitic. The oxide cathodes originally tested undoubtedly would have required substantial power continuously.

As noted in Table 1, the system maximum input power was increased from the initial optimistic 25 W level. The 60 W peak level was found to be conservative for both startup and for full-power operation (2 mA beam with biased filament). Although the cathode heater draws less than 25 W during startup, power processing efficiency and housekeeping power contribute significantly to the power demand. Under normal conditions, an input power of about 55 W was found to be adequate.

This rather general explanation of the cathode approach selection process was intended to show the fundamental dependence of the system design on the cathode. Although the contract technical work took two years, the schedule dictated by the delivery of the flight instrument to the satellite allowed for no significant design iterations after go-ahead. Therefore, the ion source design approach had to be selected essentially at the outset. With only minor variations, the system design approach proposed at the start of the contract was followed throughout the program.

B. SYSTEM CONCEPT

The requirements and goals outlined in the previous section led to the system shown schematically in Figure 1. The basic system consists

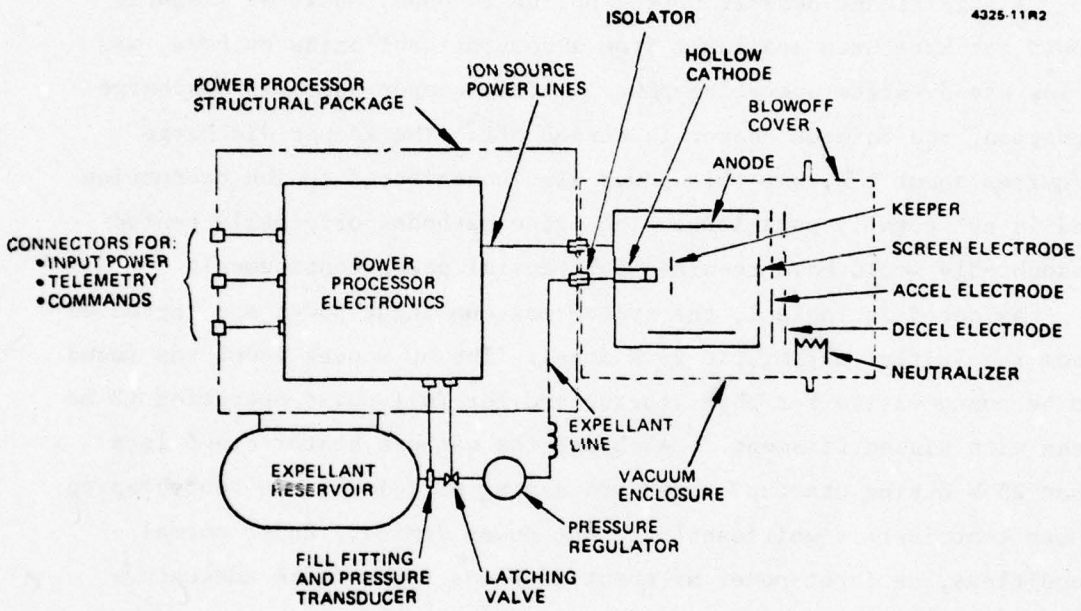

Figure 1. Block diagram of the SPIBS.

of an ion source assembly (ISA), an expellant assembly (EA), and a power processor. Xenon gas is delivered to the porous plug in the source at 7 psia through a pressure regulator and latching valve from a reservoir initially charged to about 800 psig. Power for the ion source valve, analog telemetry, and command functions are provided by the power processor assembly (PPA). The PPA circuitry is packaged on conventional circuit cards within a structural enclosure. An ion source vacuum enclosure, with a cover that is opened by electroexplosive devices, provides protection for the ion source prior to operation in space. This blowoff cover is designed to allow for complete ground checkout of ion source and system before launch.

Ion thruster technology was used to develop the ion source in the areas of ion optics, cathode, discharge chamber, and expellant line high voltage isolation. Positive xenon ions extracted from a Penning-type discharge plasma are accelerated electrostatically to high velocity. The discharge is operated at the beam potential to allow the ions to exit at near the ground potential. In the discharge plasma, ions are formed by collisions between atoms and electrons. A conventional hollow cathode is used to generate the electrons, which are then accelerated into the plasma by the discharge voltage. An axial magnetic field is used to restrict electron flow radially and increase electron-atom collisions. Downstream from the ion accelerating grids is a neutralizer in the form of redundant thermionically emitting filaments. Depending on the satellite experiment requirements, the neutralizer could be used to neutralize all or a fraction (including zero) of the ion beam. The neutralizer can be biased to $\pm$1000 V to control satellite potential relative to the space plasma.

A schematic of SPIBS is shown in Figure 2 to indicate the general electrical interconnections between the ion source and the PPA. Additional system functions and interfaces are illustrated in Figure 3. These figures show the locations of key measurements and the current paths and show the grounding approach. Layout and isometric drawings are presented in Figures 4 and 5 to illustrate the SPIBS instrument configuration; a photograph of the flight instrument is shown in

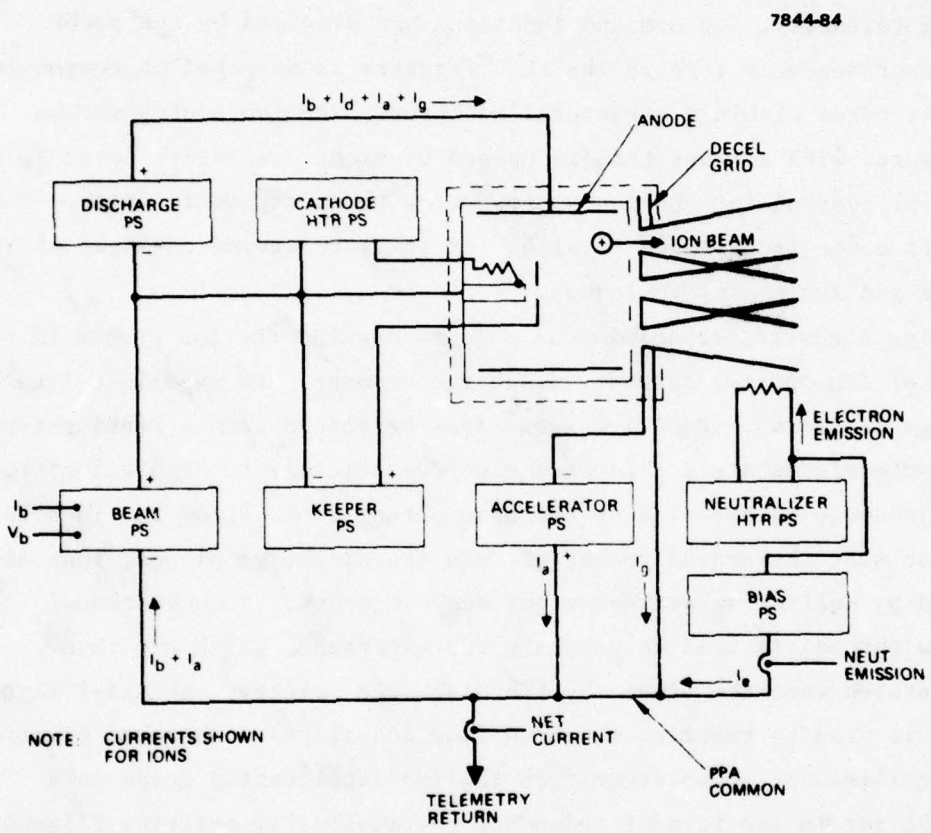

Figure 2. Schematic of SPIBS for ion source and power processor.

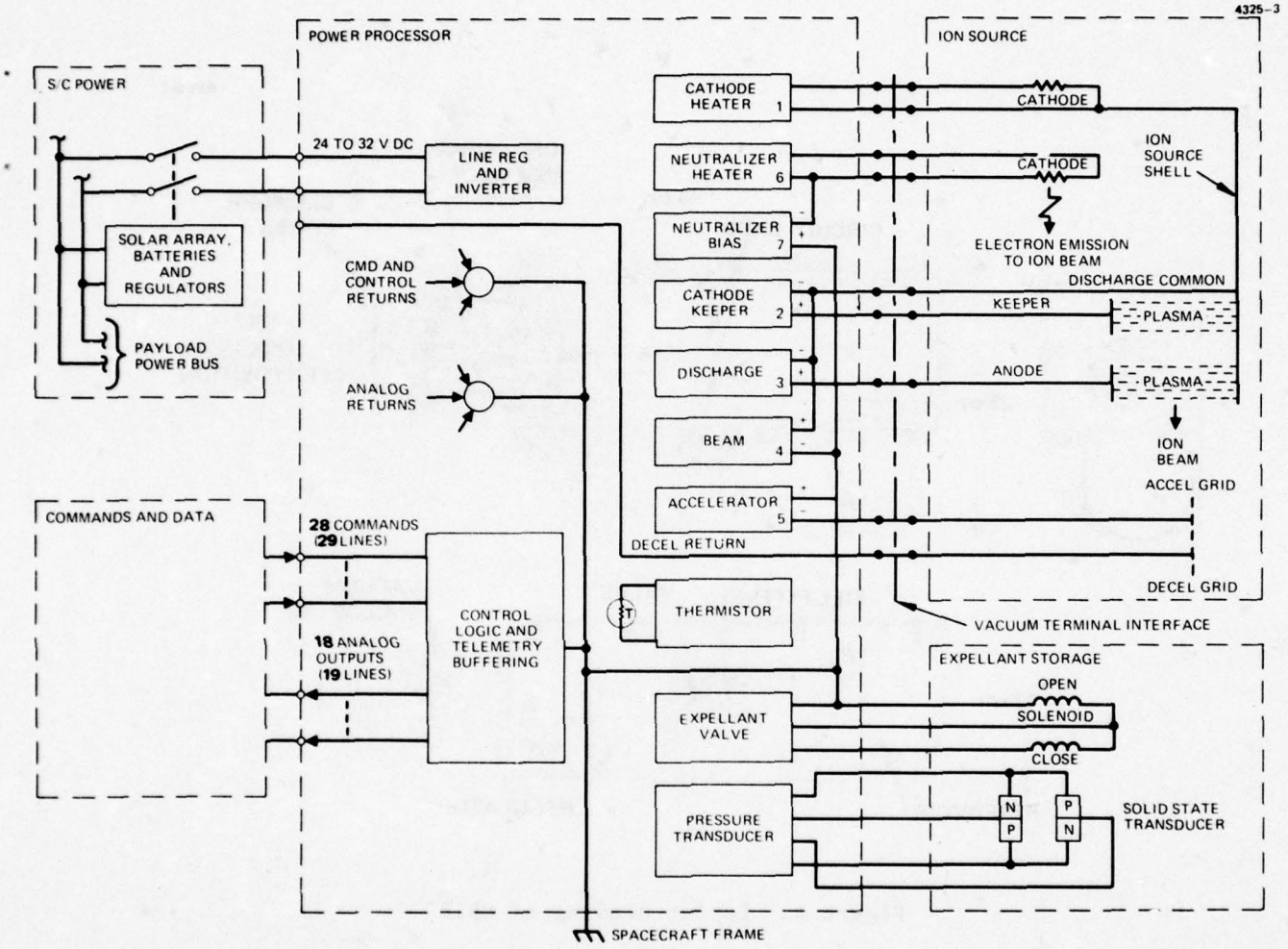

Figure 3. System interface diagram.

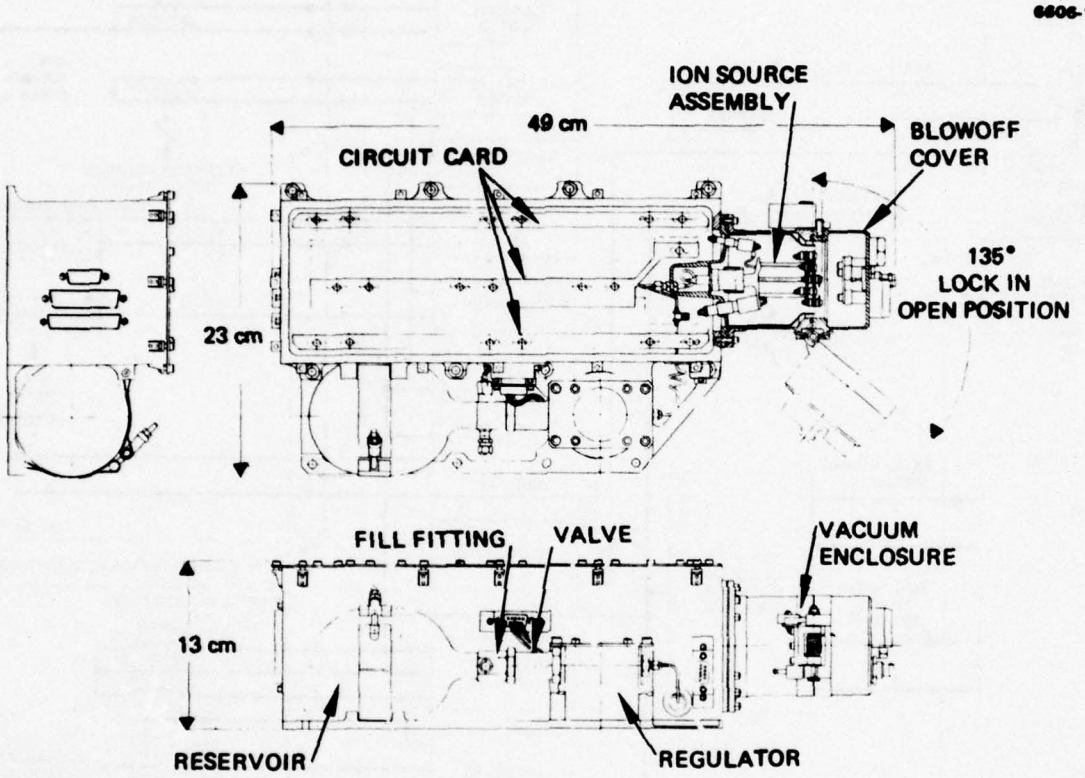

Figure 4. Layout drawing of SPIBS.

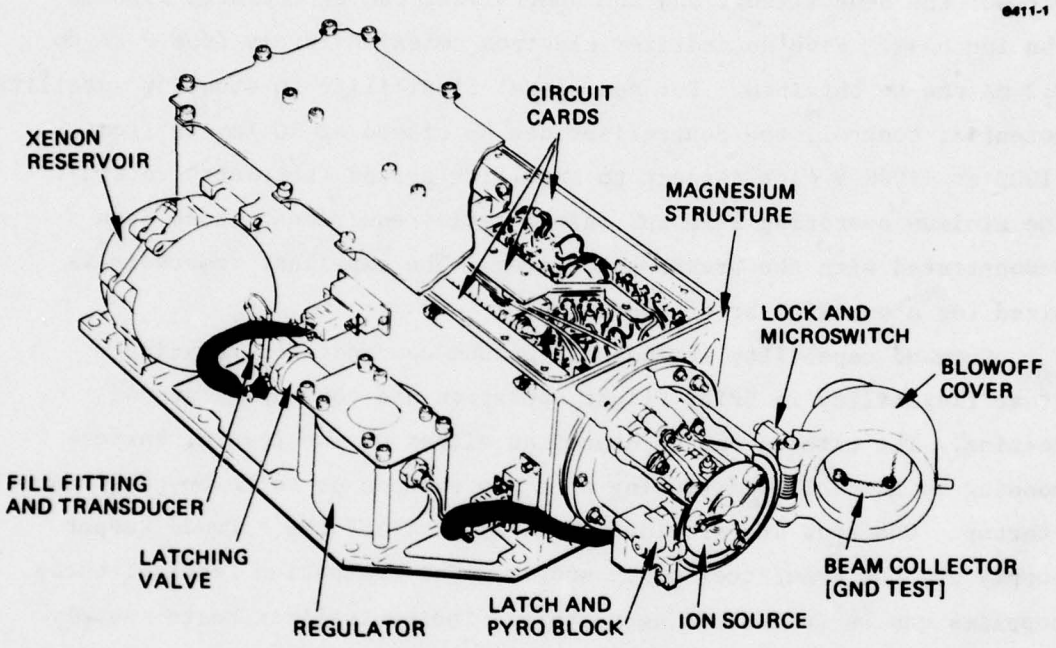

Figure 5. SPIBS isometric drawing.

Figure 6. Overall dimensions of the package are 49 x 23 x 13 cm; the flight model weight is 7.4 kg. Several features of the blowoff cover can be noted, including the open and closed positions and the ion beam collector to be used during ground checkout.

Major characteristics of the SPIBS instrument are listed in Table 1 along with the requirements. The ion source can be operated with or without the neutralizer, and the neutralizer can be operated without the ion beam. Five neutralizer electron emission levels from 2 μA to 2.2 mA can be obtained. For additional flexibility in studying satellite potential control, the neutralizer can be biased at 10 levels from -1000 to +1000 V with respect to satellite ground (telemetry return). The minimum operating life and on/off cycle requirements have been demonstrated with the breadboard system. The expellant reservoir is sized for about 2000 hr of operation.

Command capability includes 29 ground commands for relatively great flexibility in SPIBS flight operation and convenient ground testing. The cathode can be heated at either of two levels, corresponding to initial conditioning of a new cathode or to lower-power normal startup. Commands are provided to turn on or off the cathode keeper supply and the beam/accel power supply. For evaluation testing, these supplies can be turned off separately. The neutralizer heater supply can be connected to either of the redundant filaments.

Performance and operation are monitored by 18 analog telemetry outputs. Two extremely important currents, the neutralizer emission and the SPIBS net current are measured by bipolar electrometers. The electrometers are designed to operate between -2.5 mA and +2.5 mA (positive corresponds to a net electron flow off the filament). The bipolar feature is required only for detecting the net current to ground, but the two electrometers are identical to simplify design and fabrication. For currents (positive or negative) greater than 2 μA, the electrometer outputs are accurate to $\pm$10% of the true current. In addition to the primary outputs defining source operation, telemetry is also provided for expellant reservoir pressure and PPA housekeeping. In addition, two flags are provided for defining bias voltage polarity and blowoff cover position (open or closed).

MC12378

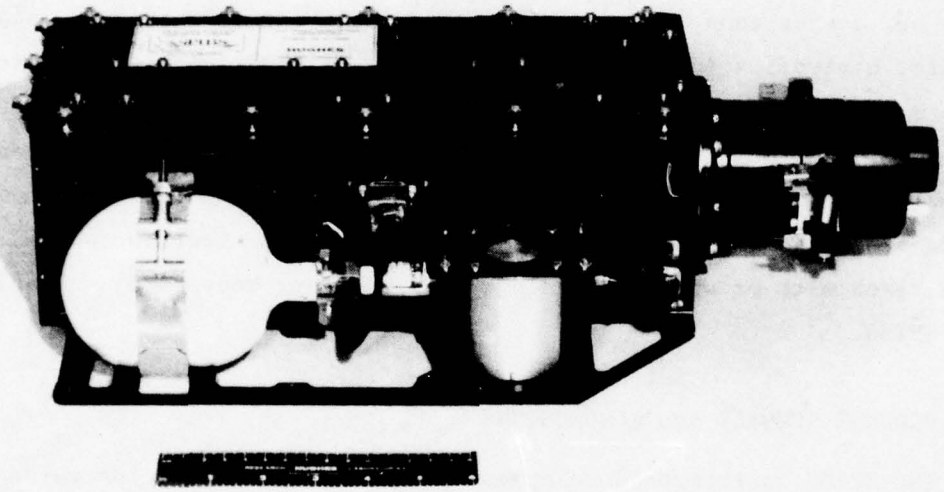

Figure 6. SPIBS flight instrument.

A good indication of system performance is shown in Figure 7, in which input power is presented as a function of operating mode. The first command, *instrument on*, activates the line regulator and ac distribution inverter to allow housekeeping functions to be monitored. The *cathode preheat* command turns on the cathode heater and discharge supply. After a few minutes (typically, 1 to 5 min), keeper voltage is applied and the discharge ignites. When the discharge voltage falls below 40 V, the cathode heater is automatically turned off. From this point on, a wide range of options are available for beam current, beam voltage, neutralization, and biasing. A few of the typical modes are illustrated in Figure 7. Although biasing is illustrated only for full beam power, the complete bias range of ± 1 kV can be used with any beam current or voltage setting. Since the system can be operated as an ion source alone, as a neutralized ion source, or as an electron source alone, each with or without biasing, 290 operating modes are available with SPIBS.

C. PROGRAM SUMMARY AND CONCLUSIONS

The SPIBS instrument development program phasing is illustrated in Figure 8. Three phases, with formal design reviews as dividing points, were used. During the breadboard phase, efforts were focussed on proving ion source feasibility. In addition, a breadboard system was assembled and tested for periods up to 600 hr. Approval to proceed with the xenon hollow-cathode-type ion source was given on 14 May 1976 during the first design review.

The first and second phases were used to prove system feasibility, including overall packaging, flight-type circuitry fabrication, expellant assembly testing, and system operation in vacuum. Successful demonstration of mass, input power, and functional capabilities was a major milestone highlighted at the second design review on 25 March 1977. Based on the design review results, approval was given to proceed with the flight instrument.

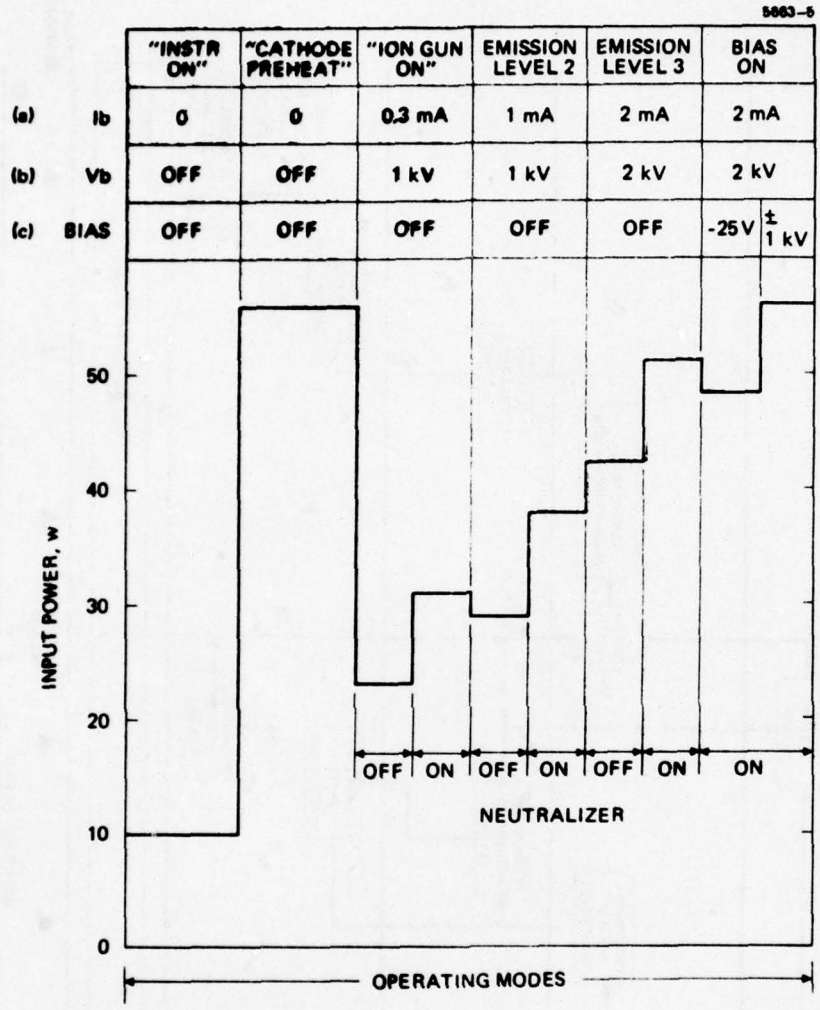

(a) BEAM CURRENT

(b) SCREEN VOLTAGE

(c) NEUTRALIZER BIAS

Figure 7. SPIBS typical input power as a function of operating mode.

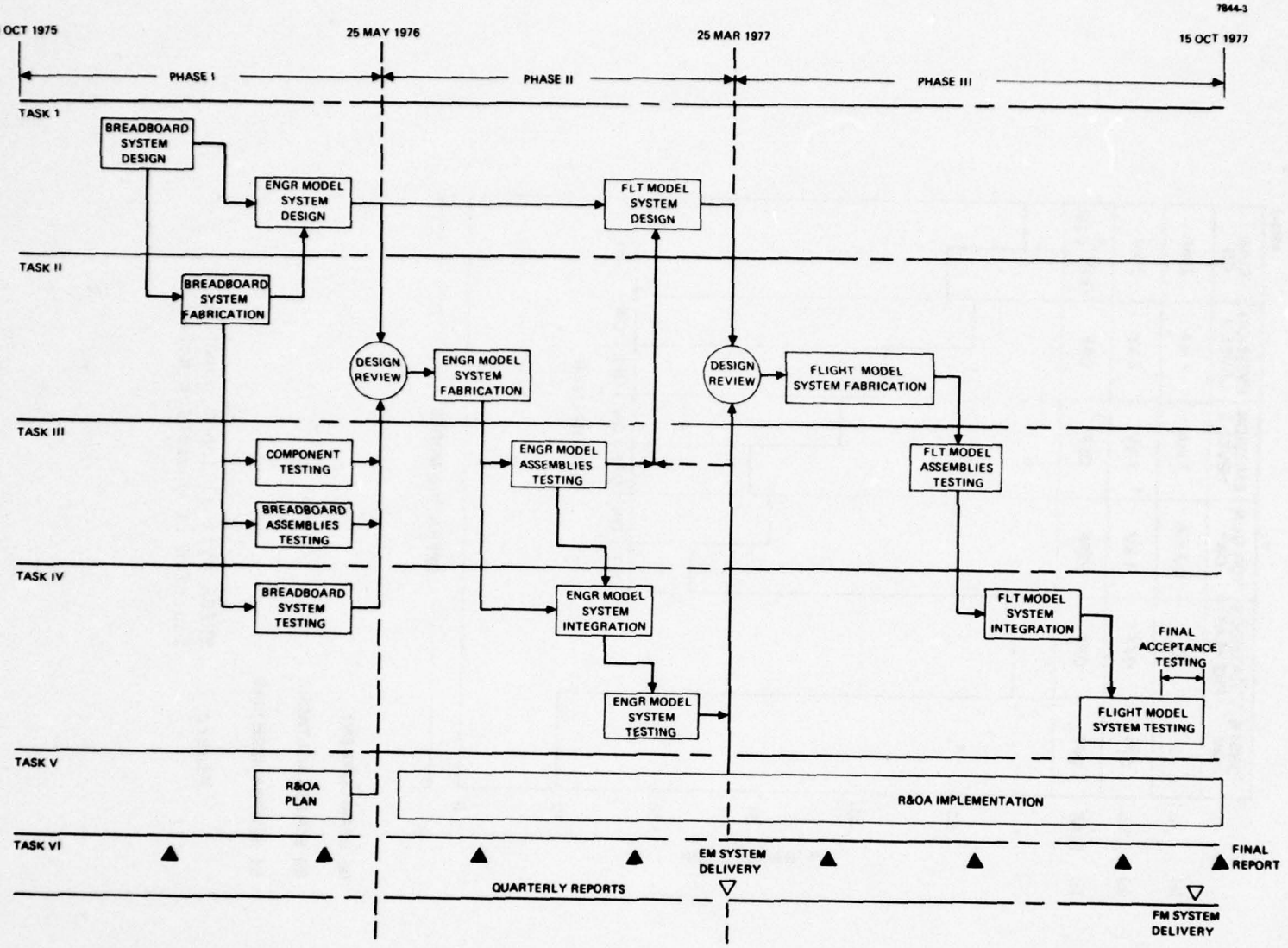

Figure 8. Program phasing logic diagram.

The flight model phase was primarily devoted to building the flight instrument using a relatively detailed quality assurance plan. A review of the flight model phase results and instrument characteristics was conducted before the instrument was delivered to AFGL on 15 October 1977.

The flexibility of the SPIBS instrument should make it a valuable tool in the study of satellite charging on SCATHA and on other space vehicles. The SPIBS design provides a life of more than 300 hr and satisfies the SCATHA satellite instrument requirements on mass, power, EMI, and quality assurance. The instrument has been designed and built to have the following features:

- Ability to eject an unneutralized ion beam having a current range of 0.3 mA to 2.0 mA at beam energies of 1 keV and 2 keV.
- Ability to eject a partially or fully neutralized ion beam having the above current and voltage ranges.
- Ability during beam operation to use a neutralizer that can be biased from -1 kV to +1 kV relative to spacecraft ground.
- Ability to emit electrons, without an ion beam, from the neutralizer filament (which can be biased from -1 kV to +1 kV relative to satellite ground).
- Ability to detect neutralizer emission and net currents (ions or electrons) between the SPIBS instrument and satellite ground down to a level of 2 μA.
- Operation with xenon to avoid possible expennant interactions with the satellite.
- Provisions for ground operation of the ion source and system during the satellite integration phase.

With the basic characteristics of the SPIBS instrument having been demonstrated, additional experimental and analytical investigations are now needed to assess the interaction of SPIBS with the satellite.

It is anticipated that charge exchange between the ionized and neutral xenon leaving SPIBS will partially reduce the flux of energetic ions emitted from the satellite. As a result of the charge exchange ions, a subsequent flux of SPIBS component surface material can also be expected. Tests to determine the composition, flux, energy distribution, and beam properties of charged and uncharged particles are currently underway at AFGL. However, Faraday probe measurements made by Hughes and AFGL indicate that a major portion of the ion beam is emitted as energetic ions.

SECTION 2

ION SOURCE ASSEMBLY

The key element of the SPIBS instrument is the ion source assembly (ISA) shown in Figure 9. The ISA produces the ion beam, provides a mount for the neutralizer filaments, and incorporates a vacuum enclosure flange for interfacing with the vacuum-tight cover. ISA characteristics are presented in Table 2. This section discusses the design, fabrication, and performance of the ISA. Additional information regarding design evolution, various test results, and specific problems is presented in later sections. Specifically, Sections 5, 6, and 7 provide a relatively complete chronological record of the ion source development from a system point of view. Since most ion source efforts were constrained by system requirements, most detailed results must be interpreted in terms of overall system implications.

A. ION SOURCE DESIGN

A photograph of the ion source is presented in Figure 10 to aid in visualizing some of the design details shown in Figure 9. The major elements of the source are the ion optics (including neutralizer filaments), source body (which supports the magnets and anode) and cathode – isolator – porous-plug (CIP). The CIP subassembly supports the keeper and connects to the expellant assembly.

The ion source consists of a 2.4-cm-diameter cylindrical discharge chamber with a concentric cylindrical anode. A hollow cathode-keeper assembly is located at the end of the discharge chamber cylinder; the ion optics assembly is attached to the exit end of this cylinder. The ion source is cantilevered from three insulated and shielded feedthroughs (cable end terminals) attached to the vacuum enclosure enplate. The feedthroughs are tilted toward the center line of the source at a 10° angle to form a rigid conical support base. This configuration allows the use of a small vacuum enclosure endplate while maintaining sufficient clearance for the isolator assembly, which lies within the conical space

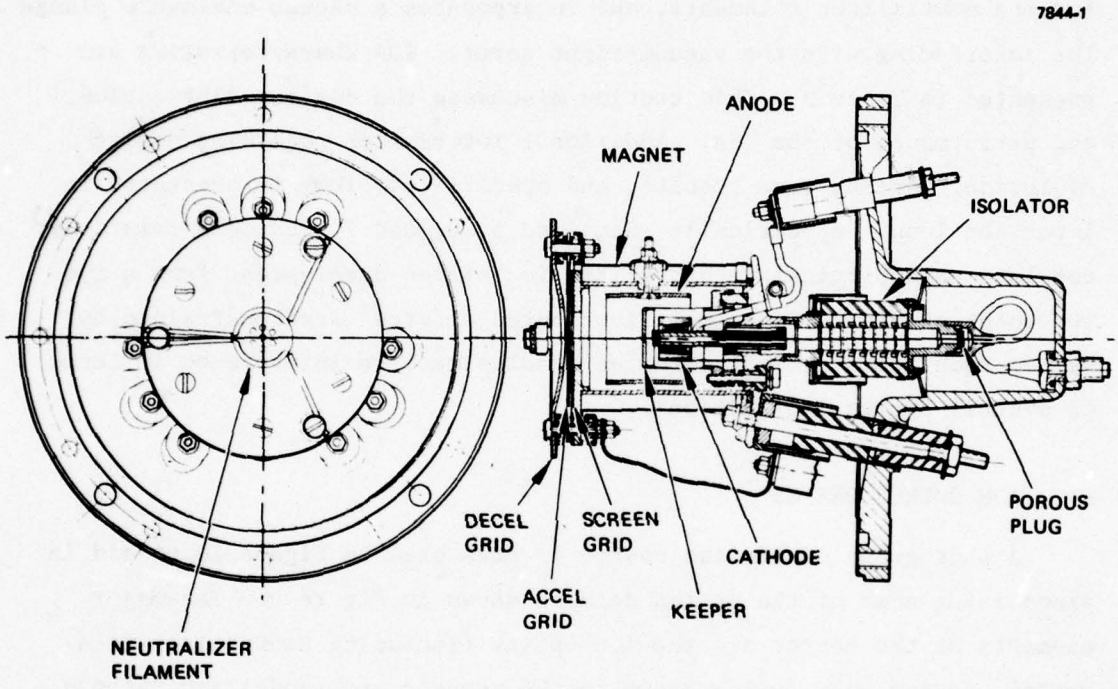

Figure 9. Ion source assembly layout drawing.

Table 2. Ion Source Characteristics

Parameter	Value
Beam current range	0.3 to 2.5 mA
Beam voltage range	0.5 to 2.5 kV
Grid apertures	
a. Screen grid (graphite)	7 — 0.15 cm diameter
b. Accel grid (graphite)	7 — 0.12 cm diameter
c. Decel grid (steel)	1 — 1.27 cm diameter
Grid-to-grid spacing	0.04 to 0.05 cm
Perveance (Xe ions)	4×10^{-9} A/V$^{3/2}$
Cathode	
a. Type	Hollow
b. Insert	Tungsten impregnated with oxide
Expellant	Xenon
Flowrate (equivalent ion current)	30 mA
Ion chamber diameter	2 cm
Neutralizer	
a. Type	Filament
b. Shape	Semicircular
c. Material	Ta doped with Yt
d. Number	2
Ion source assembly mass	490 g
Internal magnetic field	∿200 gauss
Estimated life	2000 hours

M11950

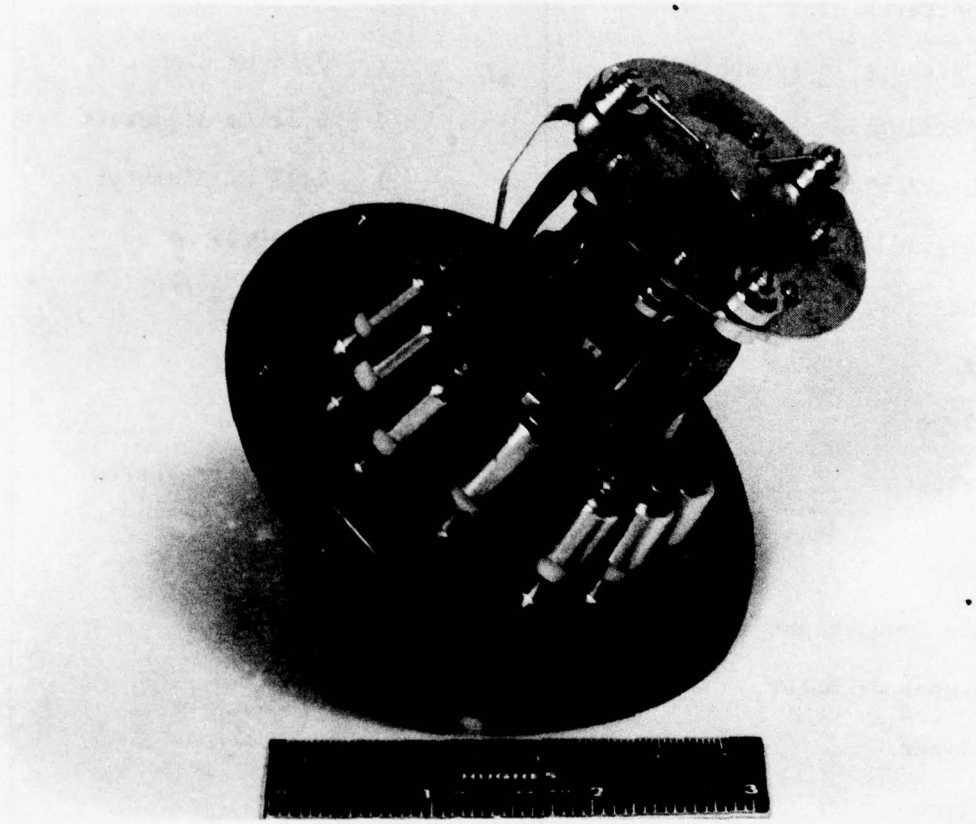

Figure 10. Ion source assembly photograph.

formed by the three insulators. Nine wiring insulator feedthroughs are arranged in a circular pattern around the enclosure endplate. These are also tilted toward the axis to allow sputter shields to be placed on the source end of the electrical feedthroughs.

The ISA can be evacuated by using the pumpout port. The open end of the feedthroughs outside the vacuum enclosure were potted with Uralane polyurathane to prevent high-voltage breakdown. This was found to be necessary for operation in air.

1. Ion Optics (Electrode Assembly)

The ion optics design is shown in Figures 11 and 12. It consists of three electrodes, two filament-type neutralizers, and shielded insulators. The decel electrode is used as the main support of the electrode assembly from the source body. Both the screen and the accel electrodes are supported from the decel through individual sets of three insulators. This mounting approach was selected for three major reasons:

- The decel could be centrally dished, allowing use of longer insulators and of sputter shields over the insulators.
- The decel electrode will operate at nominally spacecraft ground potential (between the negative accel and the positive screen potential and places a lower voltage stress on the insulators.
- With one electrode acting as the support for the other two electrodes, critical aperture alignment is simplified.

The ion optics design incorporates several novel features, including a single-aperture steel decel grid and graphite screen and accel grids. Steel was selected for the decel to reduce the external magnetic field created by the ion source magnets. Graphite was selected for the seven-aperture screen and accel grids to minimize charge-exchange sputtering. A single-aperture decel grid was selected to minimize the trapping of sputtered accel material, which in early tests was found to cause a significant buildup on the decel and subsequent shorting (see Section 5). The decel, accel, and screen grid aperture diameters are

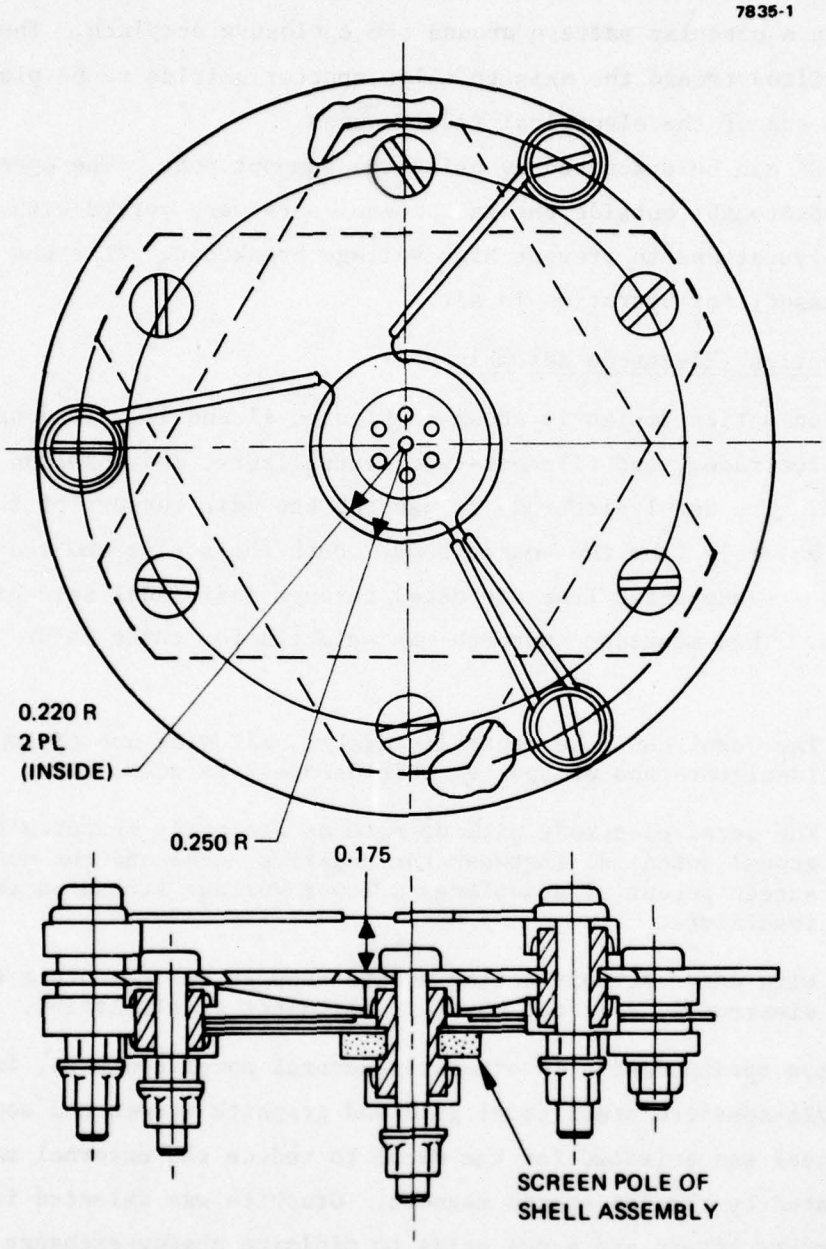

Figure 11. Ion optics assembly drawing.

M12001

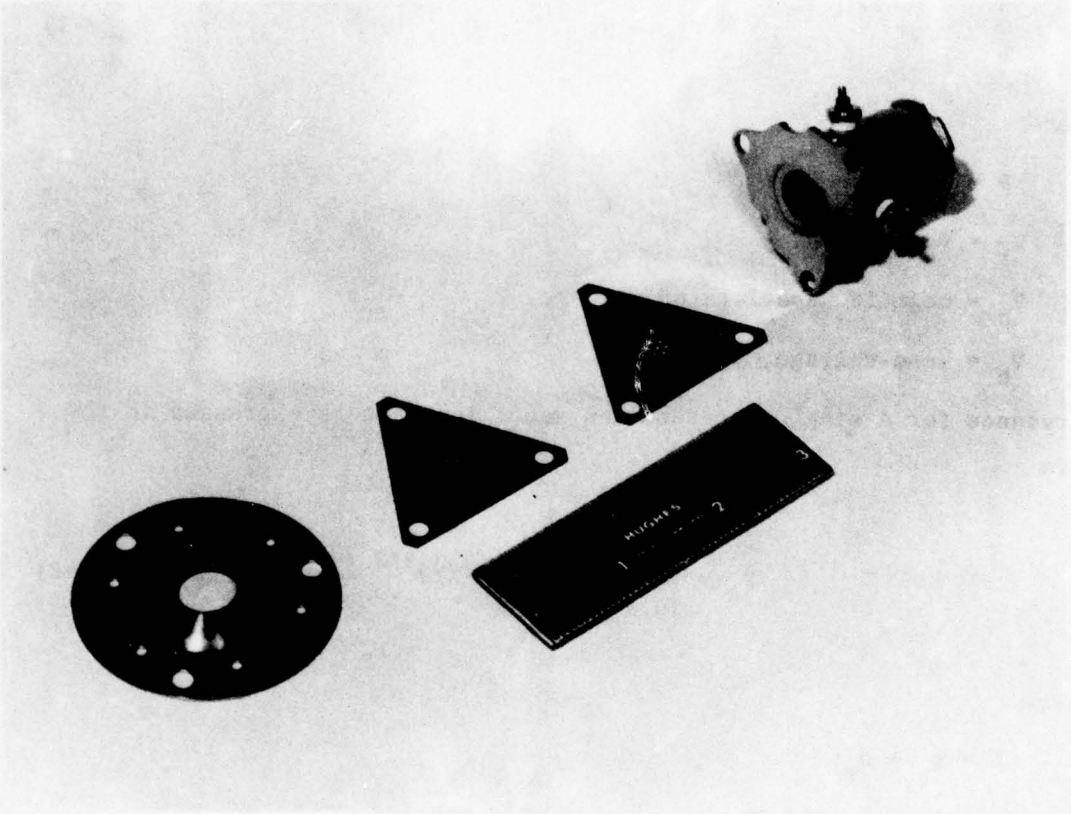

Figure 12. Ion optics photograph, exploded view.

1.27 cm, 0.12 cm, and 0.15 cm, respectively. Grid-to-grid spacings of 0.04 to 0.05 cm are used.

Selection of aperture number, aperture diameter, and grid spacing was based on empirical relations developed for ion thrusters.[9] Beam current I_b and beam voltage V_t are related by

$$I_b = PV_t^{3/2} \quad , A \quad , \tag{2-1}$$

where

P = perveance, $A/V^{3/2}$

$V_t = V_b + V_a$, V

V_a = negative accelerator voltage, V

V_b = beam voltage, V.

Perveance for a single aperture and xenon ions can be expressed in the form

$$P_a = \frac{6.8 \times 10^{-9}}{(0.336 + \frac{\ell}{d_s})} \quad , A/V^{3/2} \quad , \tag{2-2}$$

where

$\ell = \ell_g + d_s$

ℓ_g = screen grid to accelerator grid spacing

d_s = screen grid aperture diameter.

Using ℓ_g = 0.05 cm and d_s = 0.15 cm, the Xe ion perveance is approximately 4.1×10^{-9} $A/V^{3/2}$.

Empirically it has also been established that a minimum accelerator voltage is required to avoid "electron backstreaming" from the neutralizer or downstream plasma through the optics. The ratio of beam voltage to total voltage V_t is used to characterize the backstreaming limit:

$$R = \frac{V_b}{V_b + V_a} = \frac{V_b}{V_t} \leq 0.8. \qquad (2\text{-}3)$$

Thus, for beam voltages of 1000 V and 2000 V, accelerator voltages of 300 V and 600 V, respectively, were selected.

Total voltages of 1300 V and 2600 V result in beam currents (per aperture) of 0.19 mA and 5.4 mA. Since the ion chamber plasma density is nonuniform radially, these values must be reduced somewhat (about 25%) to obtain an average current capability for a given optics design. With an average beam current capability of about 0.14 A/aperture at 1300 V, seven apertures are needed to obtain a total beam current of 1 mA. At 2600 V, the optics design would support substantially more current than the required 2 mA. Experimental results presented in Section 5 show that these calculations, used in selecting an optics design, were slightly conservative (i.e., the measured perveance was found to be about 4.3×10^{-9} $A/V^{3/2}$.

The neutralizer filaments are mounted from the decel grid using shielded insulators as shown in Figure 11. The filament material is tantalum with yttrium added to reduce brittleness.[10] A filament length of 1.27 cm and a diameter of 0.18 mm was found to combine low heater power, adequate emission, and reasonable operating temperature. Filament location was determined experimentally through coupling tests (i.e., beam neutralization versus filament-to-beam voltage) and through life tests. A downstream position of 0.44 cm from the face of the decel grid and a radial position of 0.64 cm were selected. Details of the experiments related to filament positioning are presented in Section 5.

2. Ion Source Body (Ion Chamber)

A drawing of the ion source body is shown in Figure 13; exterior features are shown in Figure 12. The ion chamber shell has a diameter of 2.4 cm and a length of 3.6 cm. The anode, mounted from the shell with three insulator assemblies, has a diameter of 1.9 cm and a length of 1.8 cm. Both the shell and anode are stainless steel. A ferromagnetic (1018 steel) pole is attached to the optical end of the shell

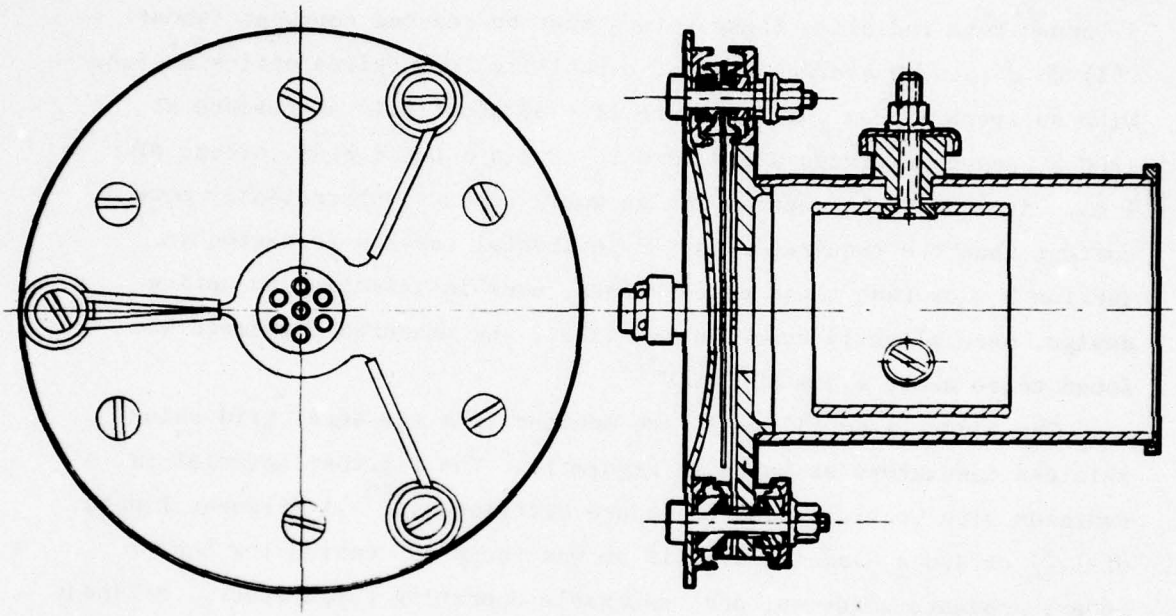

Figure 13. Ion source body drawing.

to provide internal magnetic field shaping and a mounting point for the electrode assembly. A flange is also attached to the cathode end of the shell to provide a mounting point for the CIP assembly.

3. Cathode-Isolator-Porous Plug (CIP)

The CIP includes several key parts of the SPIBS ion source, including the hollow cathode, keeper electrode, high-voltage isolator, and porous plug, as shown in Figure 14. A photograph of the CIP with the keeper removed is shown in Figure 15.

The CIP plug subassembly uses the technology developed for the 8-cm mercury thruster.[11,12] Xenon gas flowrate to the source is determined mainly by the porous plug, which reduces the pressure from the regulated 7 psia to a few Torr. The porous plug, fabricated from tungsten with a density of 80%, is 0.32 cm in diameter and about 0.14 cm thick. The plug is E-beam welded into a tantalum housing, with the sides E-beam sealed so that the gas flows through the full plug thickness.

To operate the source body at beam potential and the gas system at ground potential, an electrical isolator is required. The high-voltage isolator consists of an alumina (Al_2O_3) outer shell flanged on both ends, with alternating ceramic rings and stainless-steel mesh disks within the inner passage.[11,12] The disks function as barriers to electrons accelerated by the electric field. Within each gap, the applied field is below the minimum required for Paschen breakdown. The flanges provide a means for attaching the isolator to the porous plug (upstream) and the cathode (downstream). An exploded view of the isolator, source flange, and feedline is shown in Figure 16.

The structural part of the isolator subassembly is the alumina outer housing. Since alumina can withstand only limited bending or tension loads, the isolator housing is provided by the belleville washer between the upstream flange of the isolator and the enclosure endplate.

The hollow cathode assembly design is illustrated in Figure 17. This cathode is similar to the 5-cm and 8-cm ion-thruster cathodes with a modified mount,[11,12] The cathode assembly includes a reentrant-type mount, which has the effect of increasing the thermal conduction path

7835-2

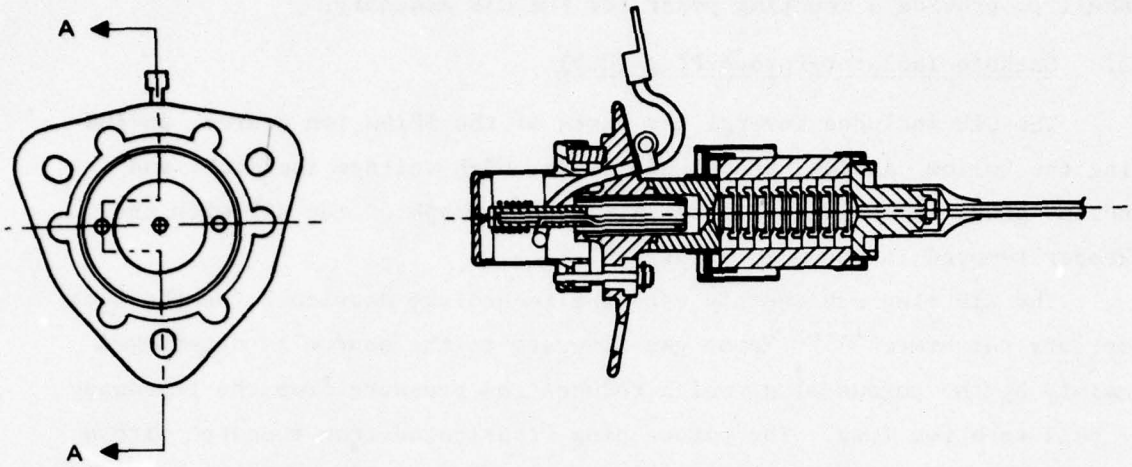

Figure 14. Cathode-isolator-porous plug (CIP) assembly.

M11999

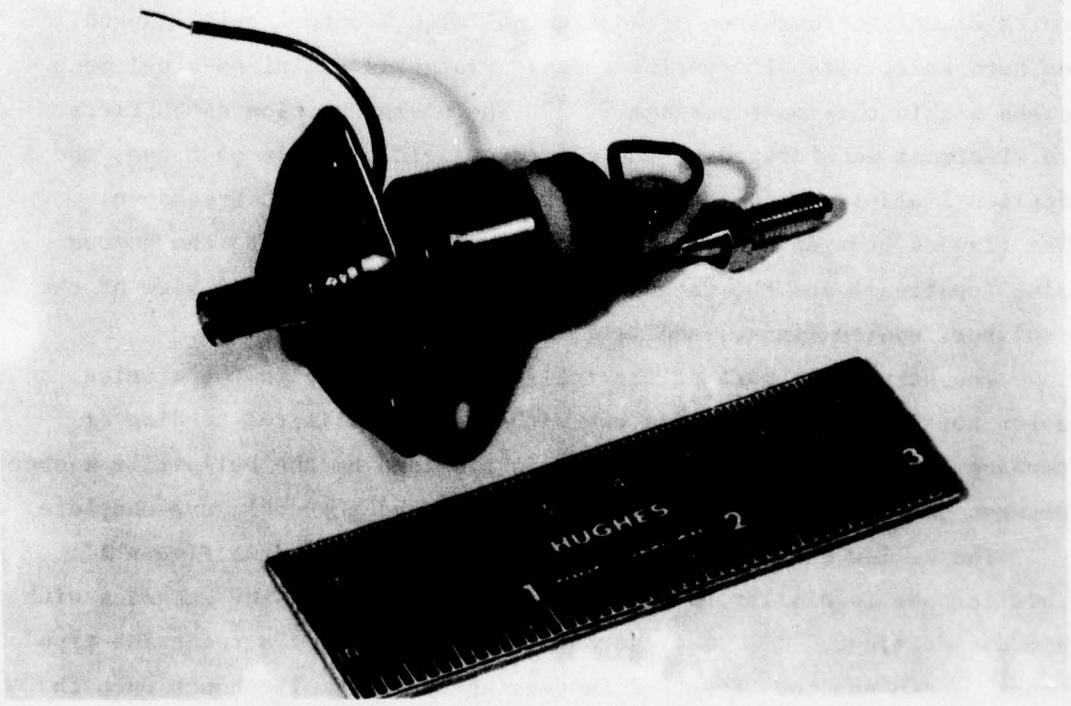

Figure 15. CIP photograph, with keeper removed.

M12003

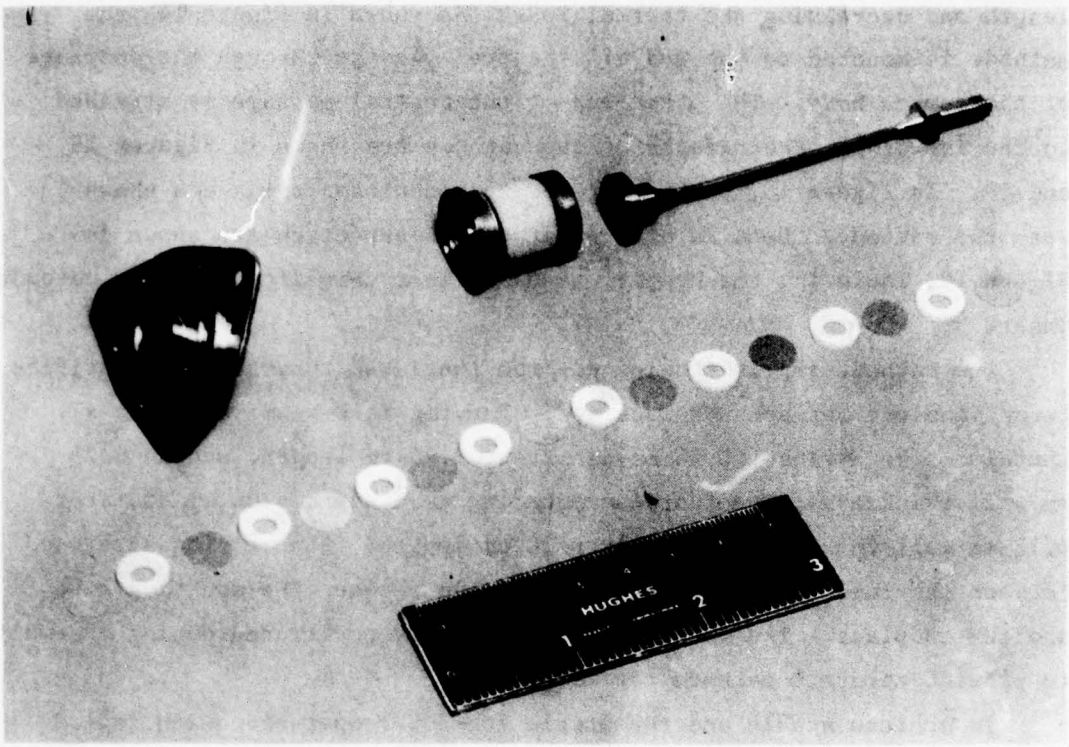

Figure 16. Isolator photograph, exploded view.

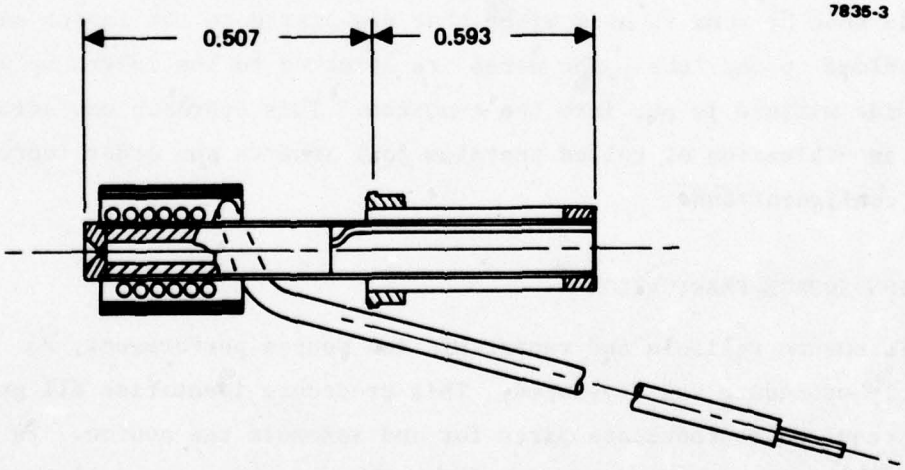

Figure 17. Cathode assembly drawing.

length and decreasing the thermal loss. As shown in Figure 14, the cathode is mounted to one end of a central passage through the endplate of the source body. The other end of the central passage is attached to the isolator. Photographs of the cathode are shown in Figures 18 and 19. In Figure 18, the keeper and its insulator rings are shown with the cathode. Details of the cathode construction are shown in Figure 19, including the heater, tantalum heat shielding, and the cathode insert.

The cathode tip is fabricated from thoriated tungsten. The orifice throat and chamber are EDM machined. The tip is E-beam welded to a tantalum tube having a 3.18 mm diameter, 2.79 cm length, and an 0.25 mm wall thickness. The tantalum mounting tube has a 4.00 mm diameter, 0.13 mm wall thickness, and about 1.0 cm length. Spacer rings are used between the feed tube and mounting tube and between the mounting tube and the endplate. The parts must be carefully positioned during assembly to provide accurate cathode tip alignment.

To achieve stable and repeatable low-power operation with hollow cathodes, a low-work-function insert is usually placed inside the cathode tube. The SPIBS cathode insert is made of oxide-impregnated porous tungsten and is shown in Figures 20 and 21. It is attached to the cathode tube by four rhenium wires that are brazed to the insert and spot welded to the tube. The wires are attached to the insert before the oxide mixture is put into the tungsten. This approach was selected after an evaluation of rolled tantalum foil inserts and other impregnated configurations.

B. ION SOURCE FABRICATION

To ensure reliable and repeatable ion source performance, an assembly procedure was developed. This procedure identifies all process steps required to fabricate parts for and assemble the source. In conjunction with the detailed drawings, the assembly procedure provides a written record for each source. However, a signed-off record was maintained only for the flight source since the procedure was evolved during the assembly of earlier sources. A copy of the flight model

M12002

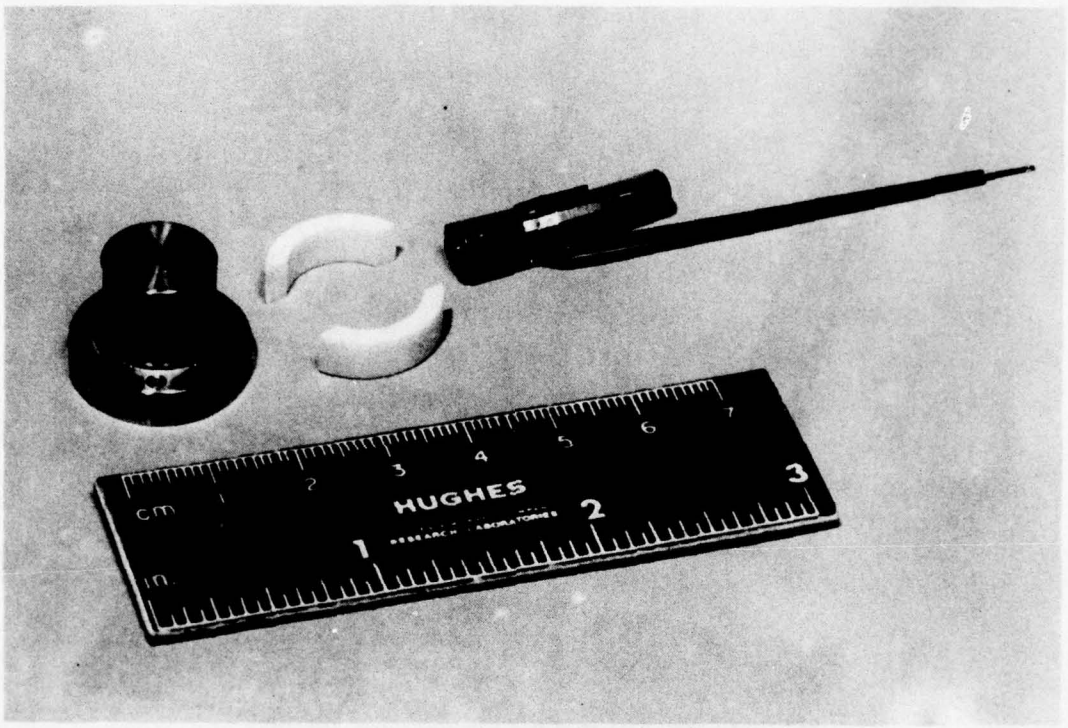

Figure 18. Cathode photograph, with keeper and insulator rings.

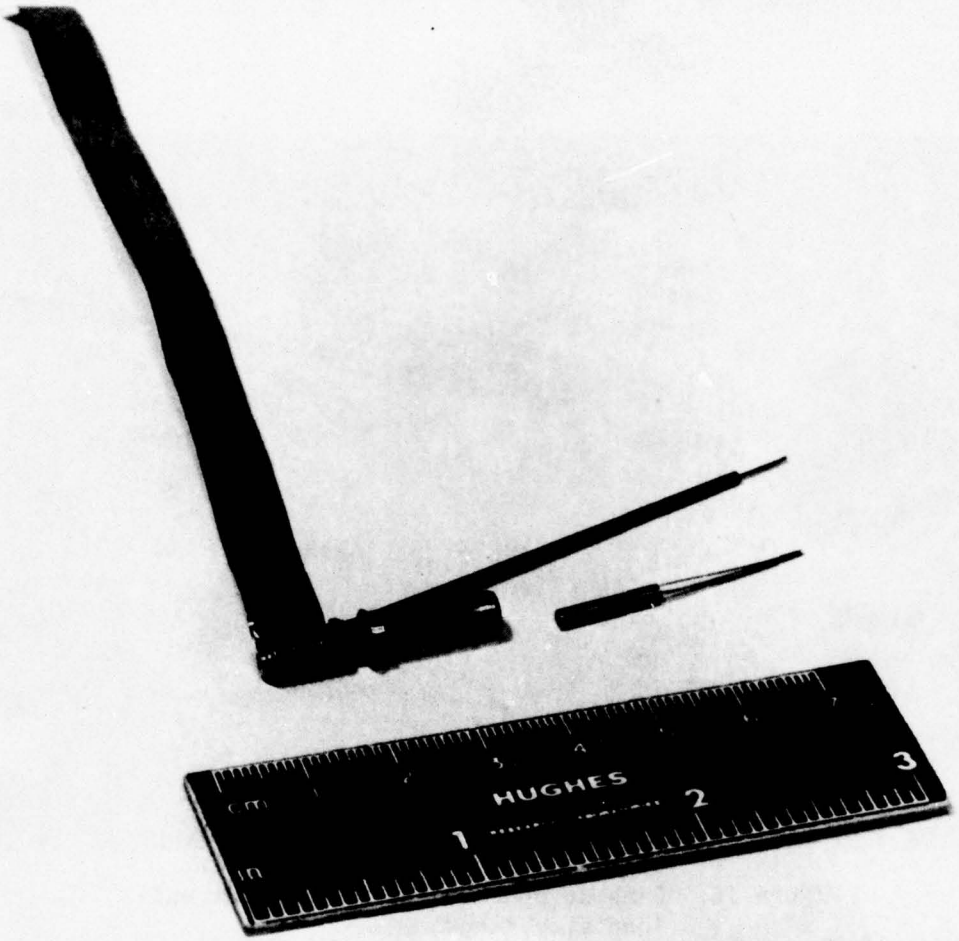

Figure 19. Cathode photograph during assembly.

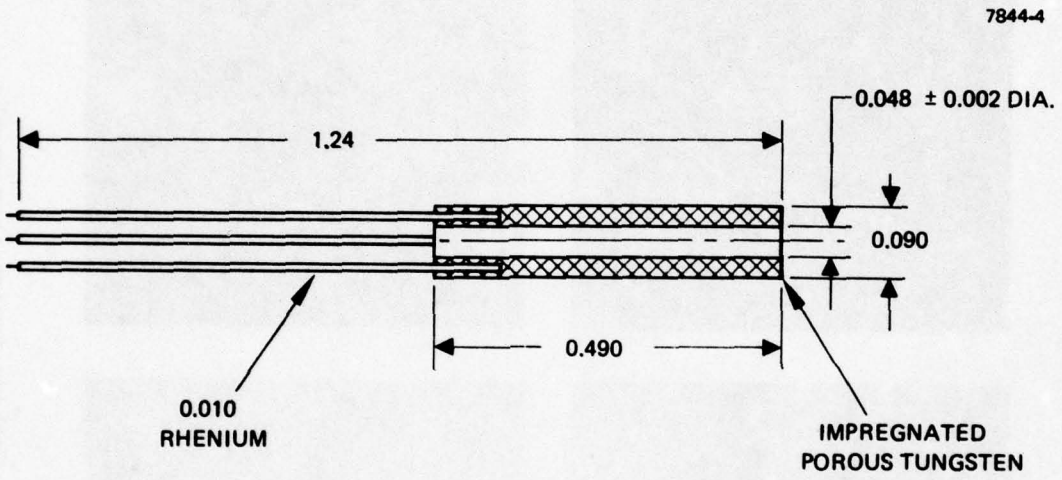

Figure 20. Cathode insert design.

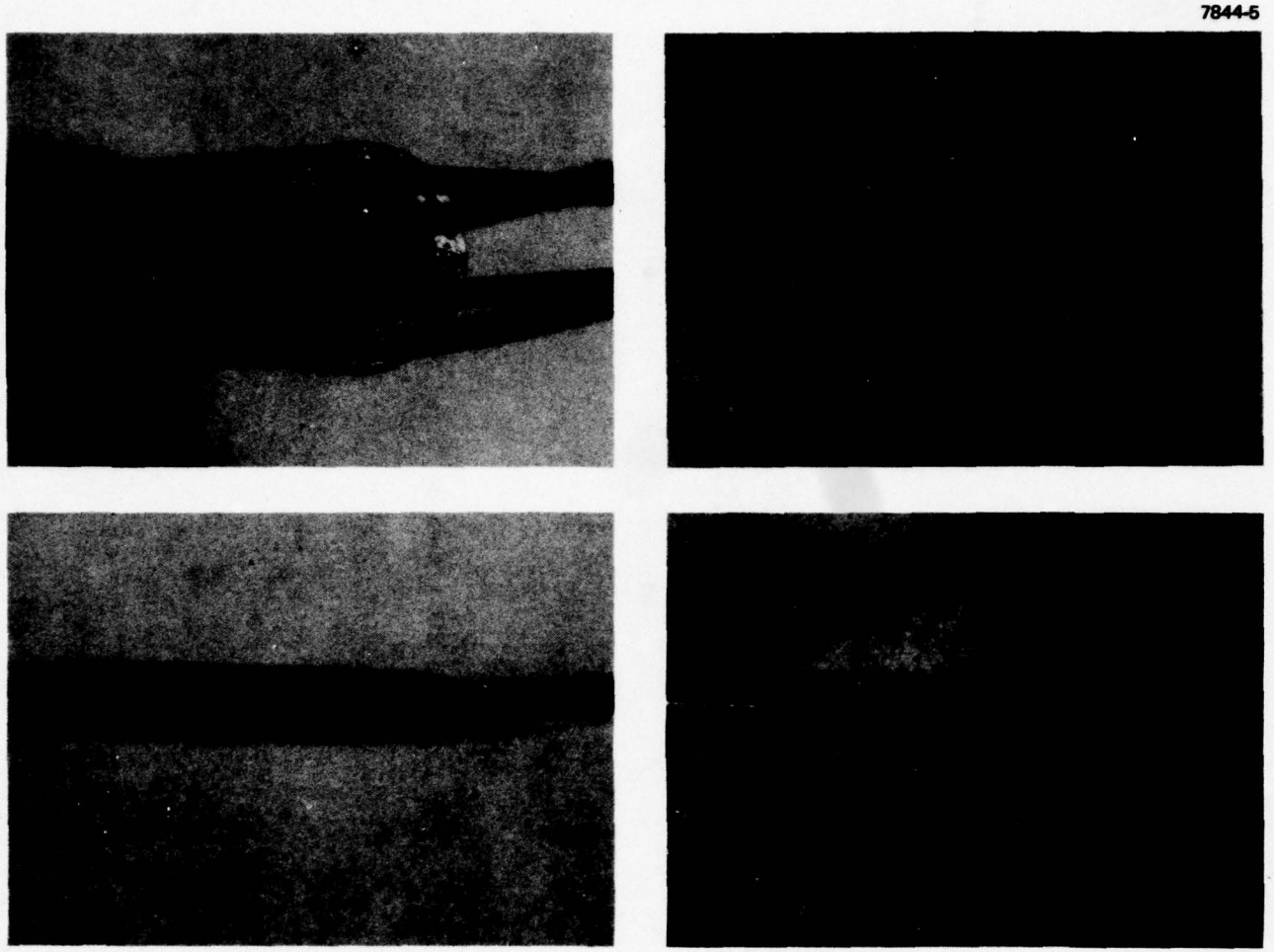

Figure 21. Cathode insert photographs.

assembly record was supplied to AFGL. Quality assurance procedures for each source are discussed in later sections.

During the program, four sources (including the rocket model) were fabricated. Except for design deficiencies identified and corrected in the breadboard and engineering models, no source failures were experienced due to workmanship. Minor problems resulting from handling or testing are discussed in later sections.

C. ION SOURCE PERFORMANCE

The data presented in this section are representative of the performance obtained with four similar sources (breadboard, engineering model, flight model, and rocket model). More specific information on each source is presented in later sections. (The rocket model is discussed in the final report on Contract AF19628-C-76-0272.)

For several reasons, interpreting and comparing the test results were a significant problem. First, source operation, including start-up, discharge stability and beam current/discharge current relationships, was found to depend on "gas system purity." It was generally easy to identify the "high purity" condition by the desirable source characteristics: (1) discharge ignition without keeper high voltage, (2) stable discharge at currents down to 10 to 20 mA, (3) stable operation without the keeper, and (4) relatively low discharge and keeper voltages. Poor, or bad, operation was also easily identified by the opposite of these characteristics. Unfortunately, when the source operated only moderately poorly, the reason was not always obvious, particularly at the beginning of the program. Several testing procedures were eventually established to allow the gas purity factor tc be separated from other performance characteristics. Once the "purity problem" was identified, many anomolous results were explained.

The second problem in data interpretation was gas flowrate uncertainty. Initially, a blowdown type gas system was used for supplying xenon. The breadboard source porous plug required a pressure of 18 to 22 psia to achieve a suitable flowrate. The engineering model, flight model, and rocket model sources were designed for about 7 to 8 psia to

simplify fabrication. With the blowdown system, flowrates could be estimated after a few hours of testings. Once regulators (for 7 psia) were obtained, flowrates were not measured, and the pressure was set to produce the desired discharge voltage and beam current.

A third factor in data comparison is source-to-source fabrication differences. Such differences might include screen grid aperture diameter or magnetic field strength. Although care was taken to make each source identical, fabrication tolerances, material variations, and magnet handling introduce some variations.

The fourth factor in data interpretation and comparison was instrumentation. With the current levels involved, voltmeter location in the circuits becomes critical since voltmeters draw current. In addition, tests were performed with both laboratory-type power supplies and metering as well as SPIBS power processing. Assuring that the hookups were correct was a constant concern. In addition, power supply wave forms (60-Hz sinesoidal or 20-kHz square wave) affect meter response and reading accuracy.

A fifth factor affecting data comparison is the ion source stabilization time. With the relatively low discharge and keeper current levels, cathode activation and ion source thermal time constants are apparently on the order of tens of minutes. Thus, run-to-run comparisons are somewhat dependent on the procedure used to obtain the data.

With these factors in mind, data scatter observed throughout the test program is not surprising. However, even with these uncertainties, all four sources performed quite similarly. With the technique of adjusting flowrate (i.e., pressure) to obtain the desired discharge voltage, variations due to fabricating tolerances tend to be reduced. Since only a small fraction of the gas is converted to ions (1 to 6%), minor flowrate variations between sources are not too significant.

1. Ion Optics Performance

Ion optics performance can be characterized by considering perveance and backstreaming. Typical results showing beam current and accelerator current as a function of total extraction voltage are shown

in Figures 22 and 23, respectively. The "perveance limit" line, determined from Figure 23, was taken to be the point at which accelerator current begins to increase as total voltage is decreased. This represents the point at which the beam starts to defocus. The measured perveance was about 4.3×10^{-9} $A/V^{3/2}$, in good agreement with the design value.

The curves in Figure 22 are typical of plasma ion sources. As total extraction voltage increases, the electric field at the screen grid penetrates further into the aperture. This penetration increases the area of the plasma sheath at the aperture and provides a larger source of ions for each beamlet. Beam currents below the perveance line are possible but at the sacrifice of higher accelerator current.

Backstreaming results are shown in Figure 24 for two sets of accelerator diameters. The format of beam current versus accelerator voltage is used because backstreaming is indicated by a rise in beam current. For the small aperture diameter (1.02 mm), accelerator voltages from 125 V (1 mA at 1 kV) to 185 V (2 mA at 2 kV) were needed to prevent backstreaming. With the larger aperture (1.52 mm), the minimum voltages increased to about 300 V and 400 V, respectively.

The SPIBS final accelerator aperture diameter was chosen based on tests discussed in Section 5. This diameter was determined by grid sputtering considerations. Lifetests demonstrated that smaller apertures were ion machined to about 1.2 mm. Thus, to avoid depositing the sputtered grid material on the optics, the initial diameter was made to be 1.2 mm.

Accelerator voltage was specified for the power processor design on the basis of Figure 24. To provide for accelerator aperture diameters up to 1.5 mm, the minimum voltage was set at 300 V for a beam voltage of 1 kV. Since the PPA was designed to provide an accelerator voltage directly proportional to beam voltage, an accelerator voltage of about 600 V is obtained with a beam voltage of 2 kV.

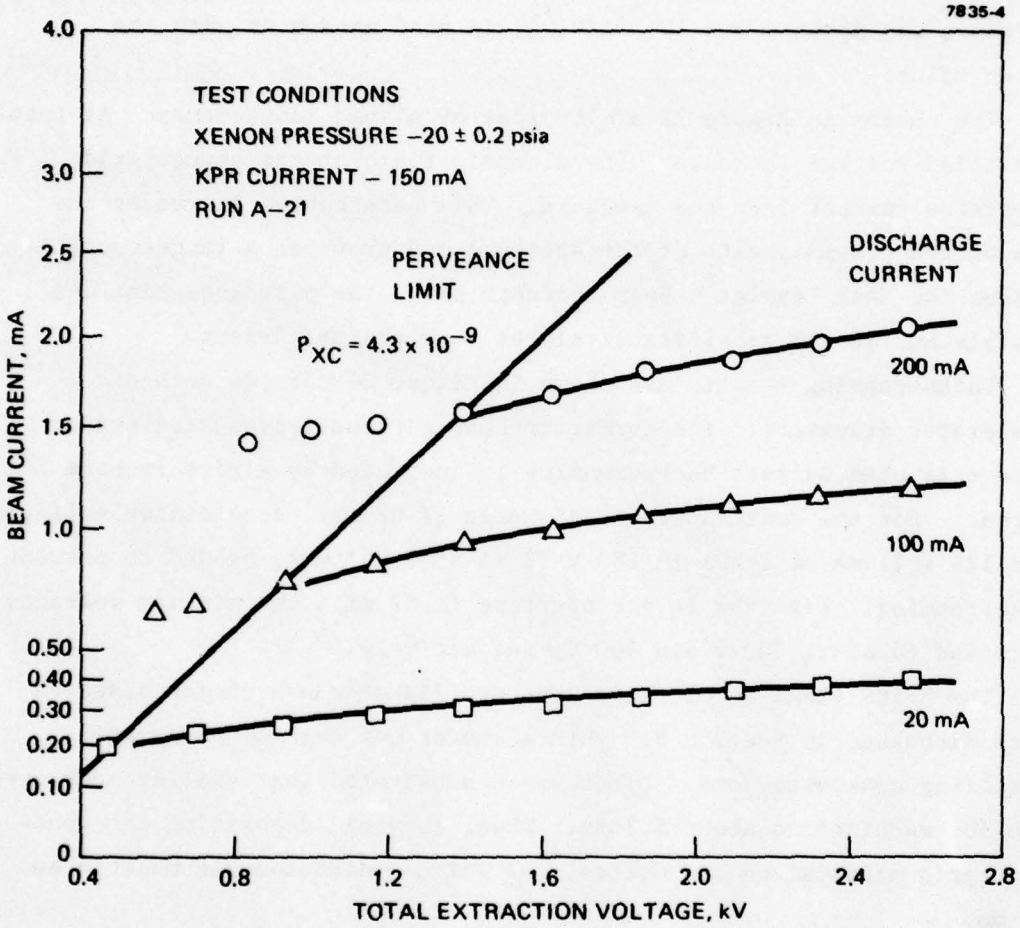

Figure 22. Beam current versus total extraction voltage.

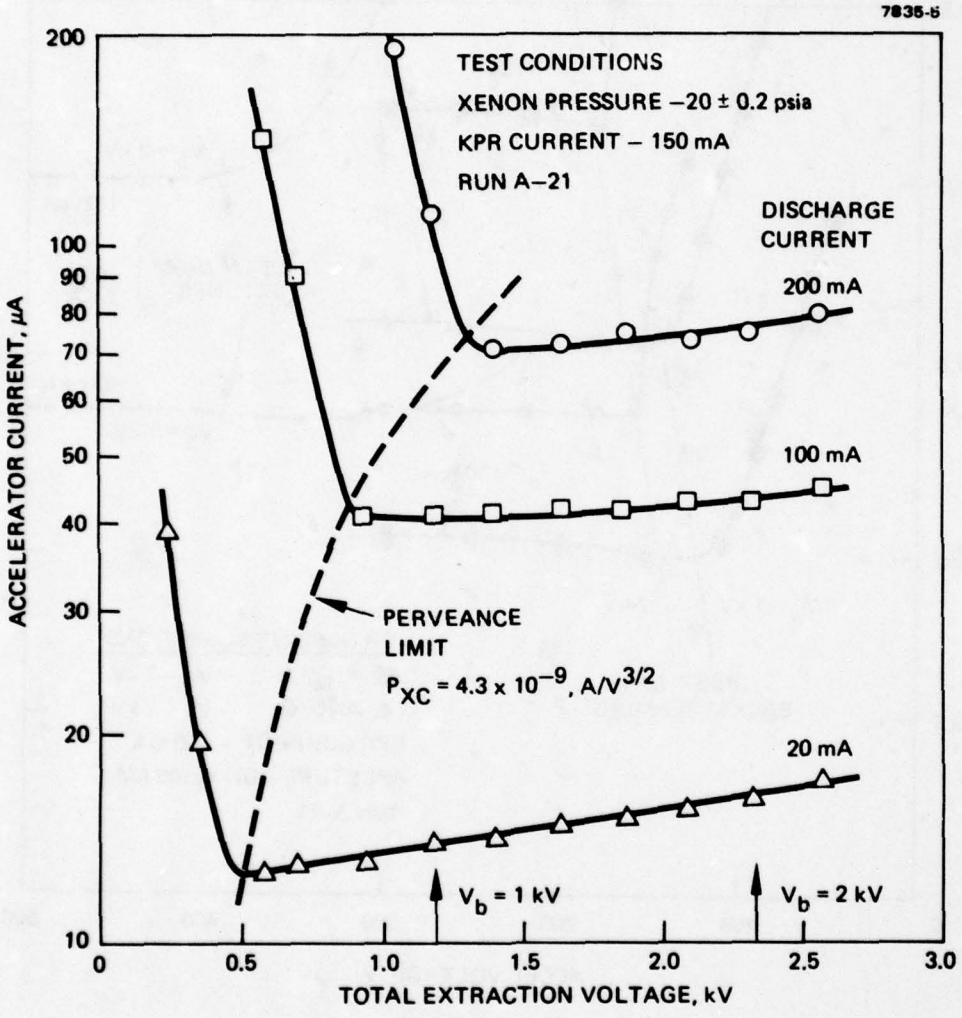

Figure 23. Accelerator current versus total extraction voltage.

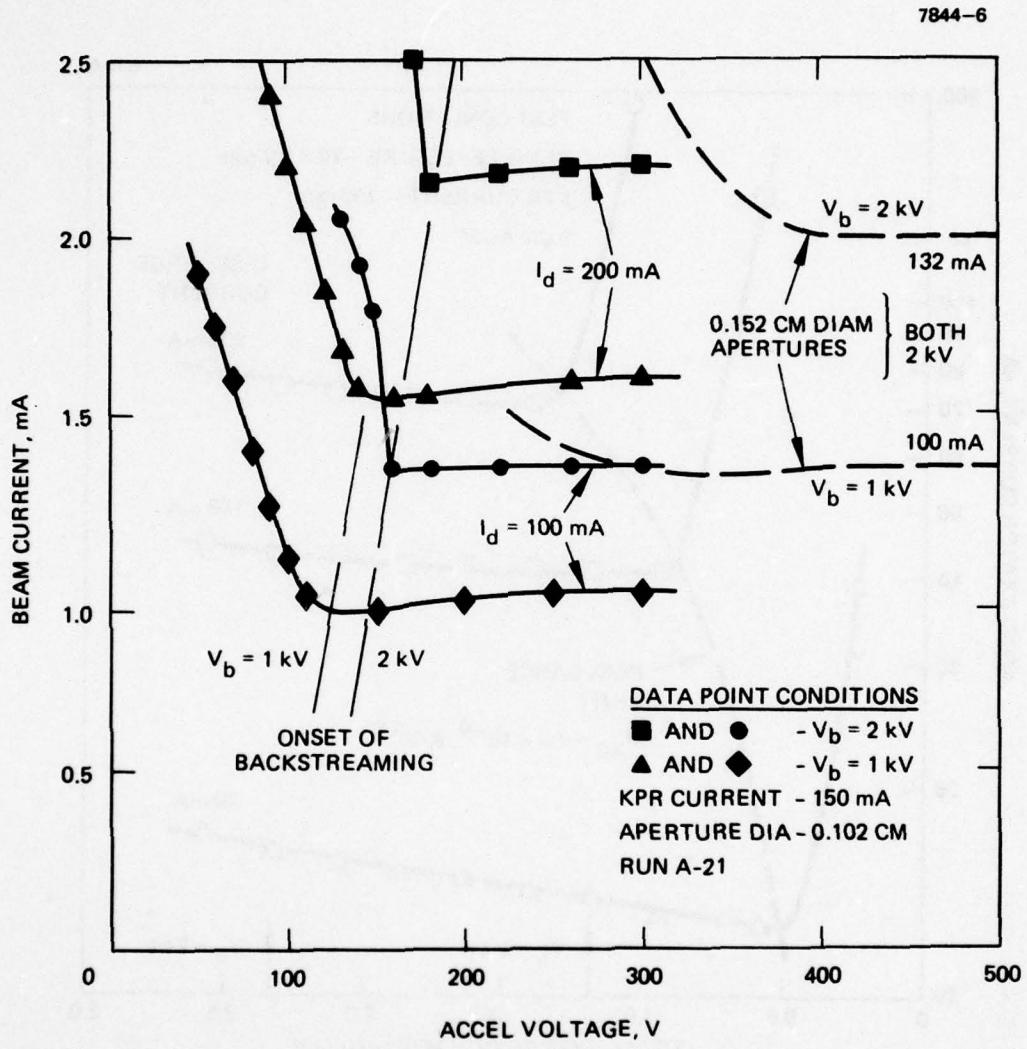

Figure 24. Electron backstreaming characteristics.

2. Ion Chamber Performance

The primary information needed to characterize ion chamber performance is beam current versus discharge current, as presented in Figure 25. These data are representative of the four sources tested. Typically, a beam current of 2.0 $\pm$ 0.2 mA is obtained with a discharge current of 200 mA and a beam voltage of 2 kV. The 0.3-mA variation is due to the factors discussed above. Although keeper current is important for start-up and to source stability at low discharge currents, keeper current has only a minor direct influence on geam current.

For SPIBS, beam current levels are set indirectly by setting discharge current levels. Each PPA was tested with its associated source to adjust the discharge current levels to the desired values. Typically, discharge currents of about 35 to 40 mA, 120 to 130 mA, and 190 to 200 mA were set.

As noted on Figure 25, the "beam current" shown is actually the current passing through the beam power supply. The beam supply current includes accelerator and decelerator currents as well as beam current (see Figure 10). To obtain the true beam current, the measured beam supply current would be reduced by the sum of accel and decel currents. Representative values of accel and decel current are shown in Figure 26. For SPIBS purposes, this fact is important for understanding system operation and correlating satellite results. However, the "net current" measurement will more accurately define the current leaving SPIBS (ions or electrons from the filament). Since neutralizer emission is also measured, net ion current emitted can be accurately obtained even with the neutralizer operating.

3. Neutralizer Performance

Neutralizer characteristics can be considered from several viewpoints. On the satellite, the primary goal is to provide the ability to eject a positive or neutral (in terms of space charge) beam. Since the beam is coupled to the neutralizer filament when it emits electrons, an additional objective is to bias the satellite relative to space plasma potential by biasing the filament. Without the ion beam, it may be possible to eject electrons using the bias supply alone.

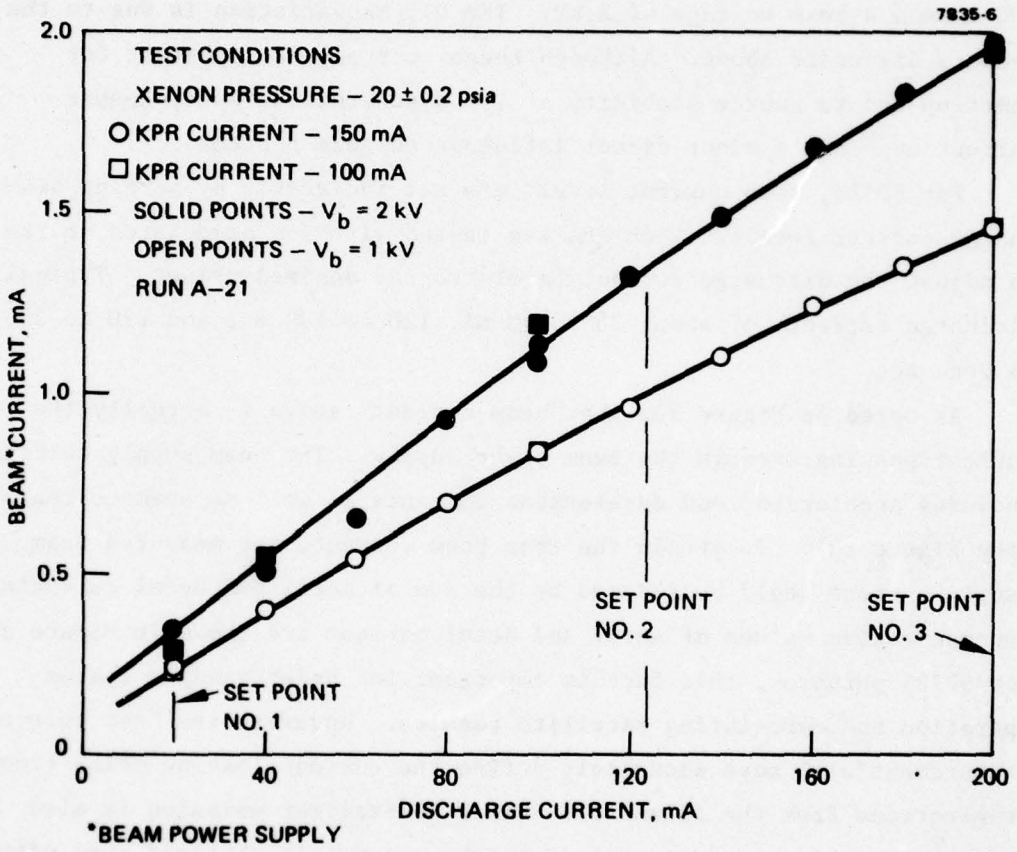

Figure 25. Beam current versus discharge current.

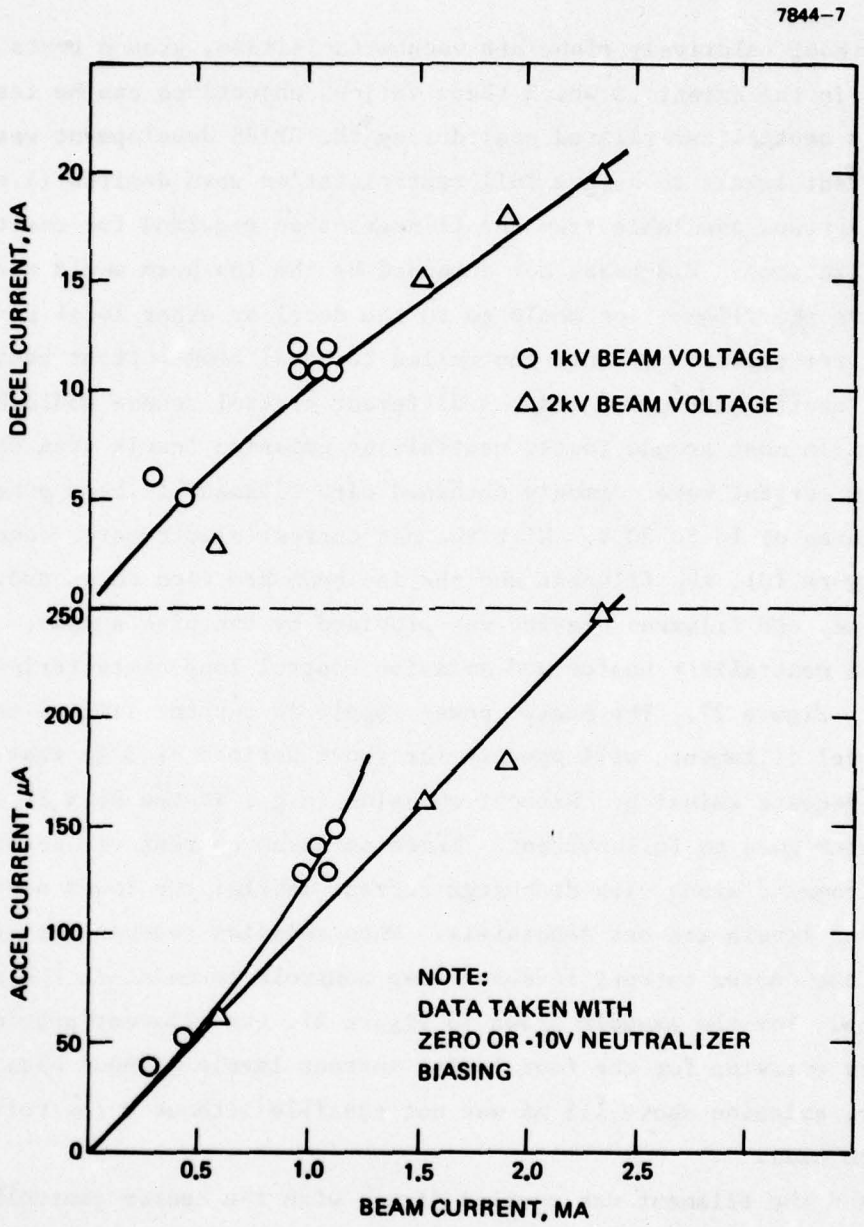

Figure 26. Accelerator current and decelerator current versus beam current for beam voltages of 1 kV and 2 kV.

Without relatively elaborate vacuum facilities, ground tests are limited in the extent to which these various objectives can be tested. The main neutralizer-related goal during the SPIBS development was to set current levels to assure full neutralization when desired (i.e., more electrons available from the filament than required for one-to-one neutralization). Electrons not demanded by the ion beam would either not leave the filament or would go to the decel or other local surfaces. Neutralizer emission was not controlled to equal beam current because, in the "neutralizer only" mode, a different control scheme would be needed. In most ground tests, neutralizer emission levels greater than the beam current were commonly obtained with filament to beam potential differences of 10 to 20 V. With the net current electrometer connected (see Figure 10), the filament and the ion beam are tied to ground. In this case, the filament biasing was provided by the bias supply.

The neutralizer heater and emission control loop characteristic is shown in Figure 27. The heater power supply is current limited at a safe level (filaments will operate for short periods at 3 A) that provides adequate emission. Without emission (e.g., if the beam if off), the heater goes to full current. Three emission current set points are set by command along with discharge current levels; two lower neutralizer emissions levels are set separately. When emission reaches the set value, the heater current feedback loop controls to maintain the set emission. For the example shown in Figure 27, the filament provided adequate emission for the four lowest current levels without biasing. However, emission above 1.5 mA was not possible without a few volts of negative bias.

Once the filament was coupled (i.e., with the heater controlling emission), biasing had a range of effects. For the three highest current levels, biasing caused only small reductions in heater power. However, at the low emission levels, negative biasing was apparently effective in attracting sufficient current to satisfy the emission loop, and the heater turned off. The ion current may have originated in the beam or in the vacuum chamber plasma near the source.

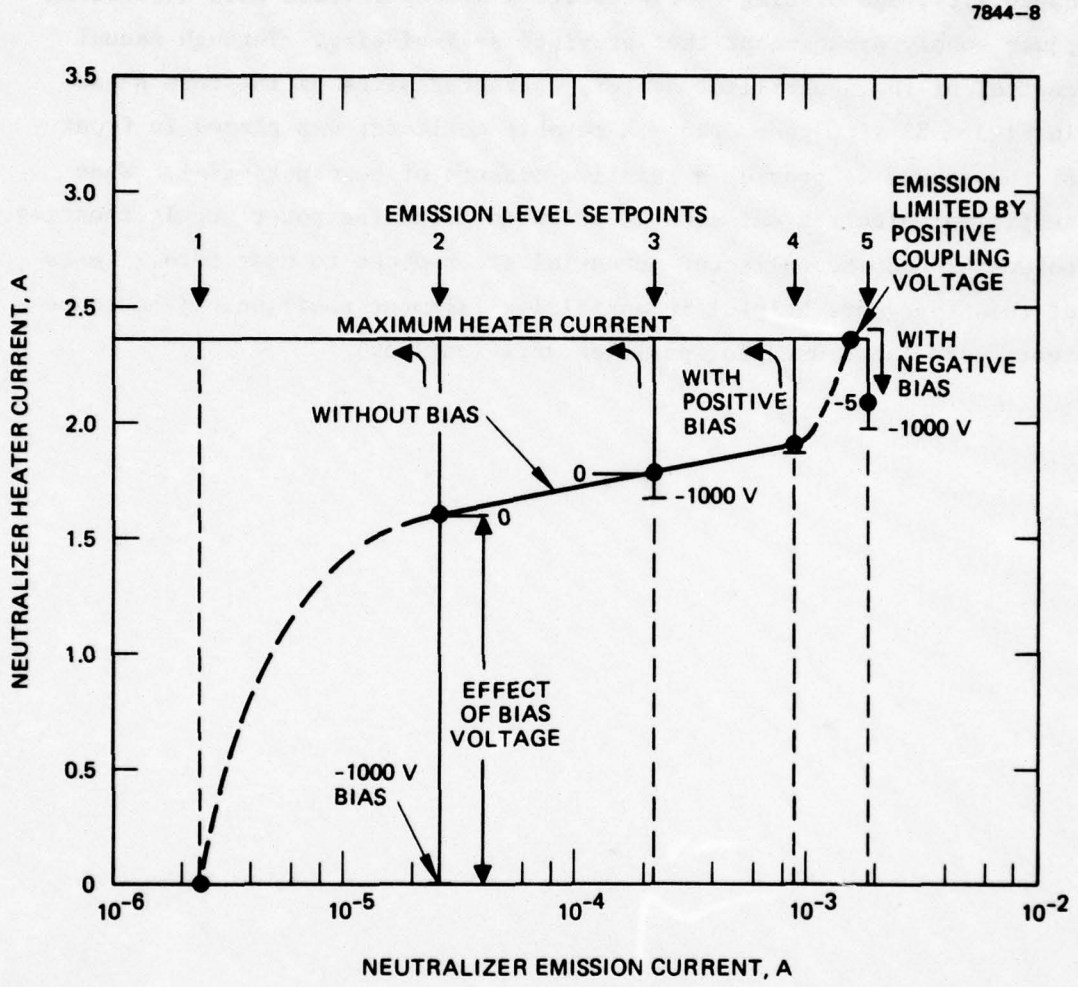

Figure 27. Neutralizer control loop characteristic.

Other examples of neutralizer operation are discussed in Section 5. Tests to establish filament position, neutralization capability, and biasing characteristics were performed with a floating power supply arrangement that provided self-biasing. Through manual control of the neutralizer heater, characteristics of the form shown in Figure 28 were generated. A movable collector was placed in front of the source to provide a relative measure of beam potential. When sufficient electron emission is provided, both the power supply floating potential and the collector potential are reduced to near zero. Tests of this type were helpful in optimizing filament position. (Endurance tests were later used for position verification.)

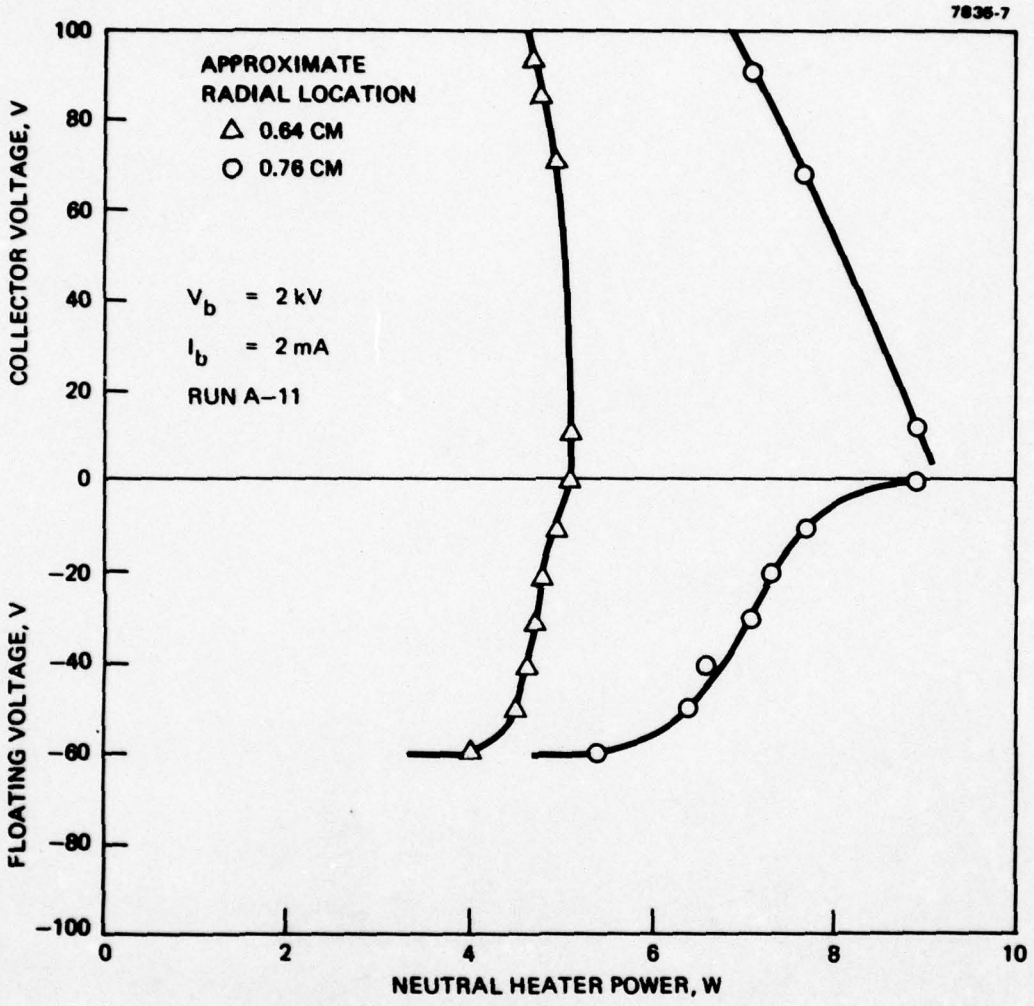

Figure 28. Example of neutralizer coupling using self biasing.

SECTION 3

EXPELLANT ASSEMBLY

The expellant assembly (EA) provides xenon storage, pressure regulation, and pressure monitoring. The characteristics of the EA are summarized in Table 3 and an assembly drawing is shown in Figure 29. The components in this assembly were selected on the basis of availability, flight qualifiability, and cost. Several options were considered but were generally more expensive and/or required development.

A photograph of a typical EA is presented in Figure 30; another view was shown in Figure 6. Mounting the EA to the system structure is accomplished with clamps around the reservoir and over the regulator. The regulator outlet is connected to the source with 1.5-mm-diameter stainless-steel tubing and Swagelock fittings.

A. RESERVOIR SUBASSEMBLY

The reservoir is a Department of Transportation (DOT) rated commercial aircraft part. When filled to 800 psi, this reservoir contains about 50 standard liters of xenon. At the design flowrate, this will provide about 1500 hr of source operation. As seen in Figures 29 and 30, a fitting is attached to the reservoir. This fitting contains a fill valve (Schrader type) and a pressure transducer. For xenon filling, the reservoir, fill fitting, and latching valve are shipped as a unit to the gas supplier.

B. RESERVOIR

The reservoir is manufactured using AISL 4130 steel and a spinning process. Although a significant fraction of the SPIBS mass is associated with the reservoir (about 9% empty, 12% filled), the availability of a rated pressure vessel was the main factor in its selection. Other vessels or a lightened version of the existing part could have been obtained but only at a significant cost for DOD rating.

Table 3. Expellant Assembly Characteristics

Parameter	Value
System type	Regulated, high pressure
Reservoir	
a. Maximum operating pressure	1000 psi
b. Volume	0.5 liter
c. Typical capacity (Xe)	50 standard liters
d. Mass (filled)	920 g
e. Material	Steel
Latching valve	
a. Type	Solenoid-latching
b. Operating current (100 ns)	1A-open; 0.1 A-close
c. Mass	180 g
Pressure regulator	
a. Type	Aneroid
b. Outlet pressure	7 ± 0.3 psia
c. Outlet pressure adjustable range	5-10 psia
d. Minimum inlet pressure	20 psia
e. Mass	460 g
Pressure transducer	
a. Type	Semiconductor
b. Mounting	Built into a screw and attached to fill fitting

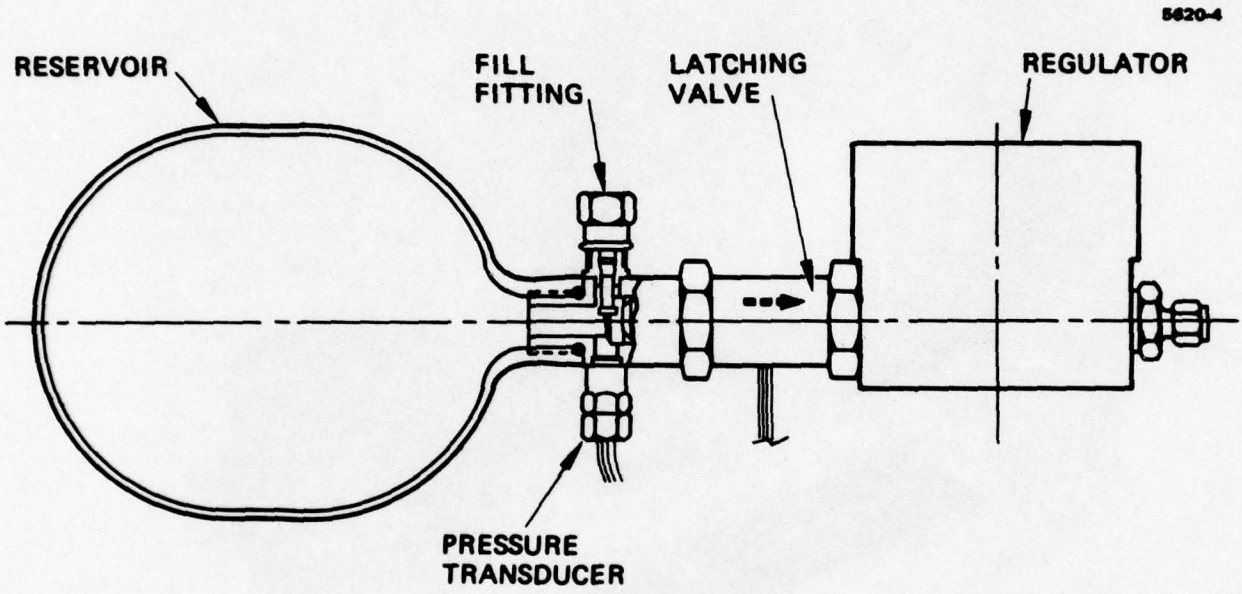

Figure 29. Expellant assembly layout drawing.

M11951

Figure 30. Expellant assembly photograph.

Xenon compressibility characteristics do not obey the ideal gas law. At the design pressure of 800 psi, a fraction of the xenon will be a liquid at temperatures below about 17°C. The implications of this possibility are being evaluated by AFGL personnel. However, if a liquid phase would cause a problem, a reservoir heater could be added for temperature control or the initial pressure could be reduced. Since the SPIBS expected operating time on SCATHA is only a few hundred hours, starting with less gas should not jeopardize the experiment.

C. LATCHING VALVE

A solenoid-operated latching valve is used between the reservoir and the regulator. This valve, shown in Figure 31, is manufactured by Carleton Controls Corp. Although the valve design was based on similar products developed by Carleton, this particular part was designed specifically for the SPIBS applications.

In tests with the first valves received, several leaks through the valve occurred. It was determined that ferromagnetic parts were rusting and producing small particles that fouled the valve seat. Nickel plating was used to protect these internal parts on later units and the initial valves were subsequently reworked.

Valve operation requires a 100-msec current pulse of about 1 A at 28 V to open and about 0.1 A to close. The higher opening power is required to overcome launch load restraints on the pintle. A single solenoid winding is used and the current directions are simply reversed between opening and closing.

D. PRESSURE REGULATOR

A photograph of the Carleton Controls regulator is shown in Figure 32. This is an aneroid-type regulator using a sealed bellows movement. Outlet pressure can be adjusted simply over a range of about 5 to 10 psia to match the flow impedance characteristics of the ion source porous plug. Accurate regulation is obtained over an inlet pressure range from 1000 psig to about 20 psia. This wide inlet pressure range allows essentially all the xenon to be used.

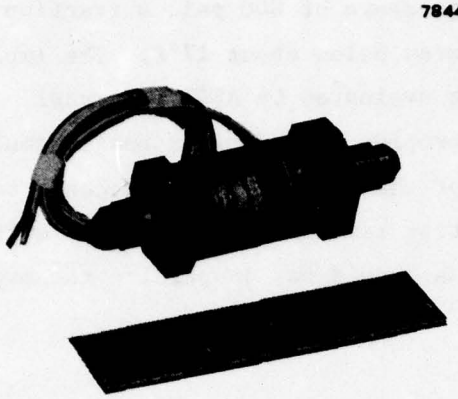

Figure 31. Latching valve photograph.

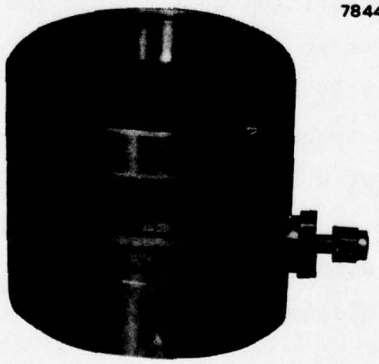

Figure 32. Pressure regulator photograph.

E. PRESSURE TRANSDUCER

A pressure transducer is used to monitor reservoir pressure. Since this measurement is mainly to provide status information, high accuracy is not required. The transducer selected, Entran Devices, Inc., P/N EPS-1032-1500, has the advantages of small size, low cost, and reasonably low sensitivity to temperature. Over a temperature range of -40 to +80°C, the output is within $\pm$10% of the correct value. A calibration curve is present along with telemetry calibration data in Section 7.

Difficulty was experienced with this transducer after all the SPIBS instruments had been delivered to AFGL. The particular transducer ordered referenced the semiconductor element to vacuum. Apparently, in vacuum the semiconductor degraded causing the transducers to fail. The same transducer is available in a hermetically sealed configuration and can be substituted for the original part. This problem was not encountered during tests at Hughes for which system operation in vacuum was limited to about a week per instrument.

SECTION 4

POWER PROCESSOR ASSEMBLY

The function of the power processor assembly (PPA) is to supply power to and control the ion source, operate the expellant valve, provide telemetry data, and accept commands from the satellite. This section describes the design implemented to meet the requirements discussed in previous sections. Simplicity, low cost, and minimum development risk were guiding factors in the PPA design effort.

A. ELECTRICAL DESIGN

A functional block diagram of the PPA, shown in Figure 33, indicates the general power-processing technique. Input power is first regulated at 21 Vdc. A 20 to 25 kHz square-wave free-running inverter then produces 42 Vac rms for each power supply. Saturable reactor type power supplies are generally used.

A major feature of this design is the achievement of electrical isolation between the input power lines, the command lines, telemetry, and the outputs of the various supplies. The isolation of the command lines is obtained by using relays. The relay coils provide electrical isolation, and magnetic latching provides nonvolatile storage of the received commands. The isolation between input, output, and the telemetry lines is achieved by using transformer isolation. Each individual supply has an output transformer and, where required, includes isolated voltage sense windings and a current transformer on the primary for voltage and current telemetry, respectively.

The discharge, neutralizer heater, cathode keeper, and accelerator supplies are fixed setpoint supplies and are saturable reactor current limited for short-circuit protection. The beam and cathode heater supplies use saturable reactors for both controllability and current limiting. The neutralizer bias supply is transistor regulated. The line regulator is a "buck" switching regulator which converts the unregulated 24 to 32 V input to a regulated 21 Vdc. An input filter is required to prevent the

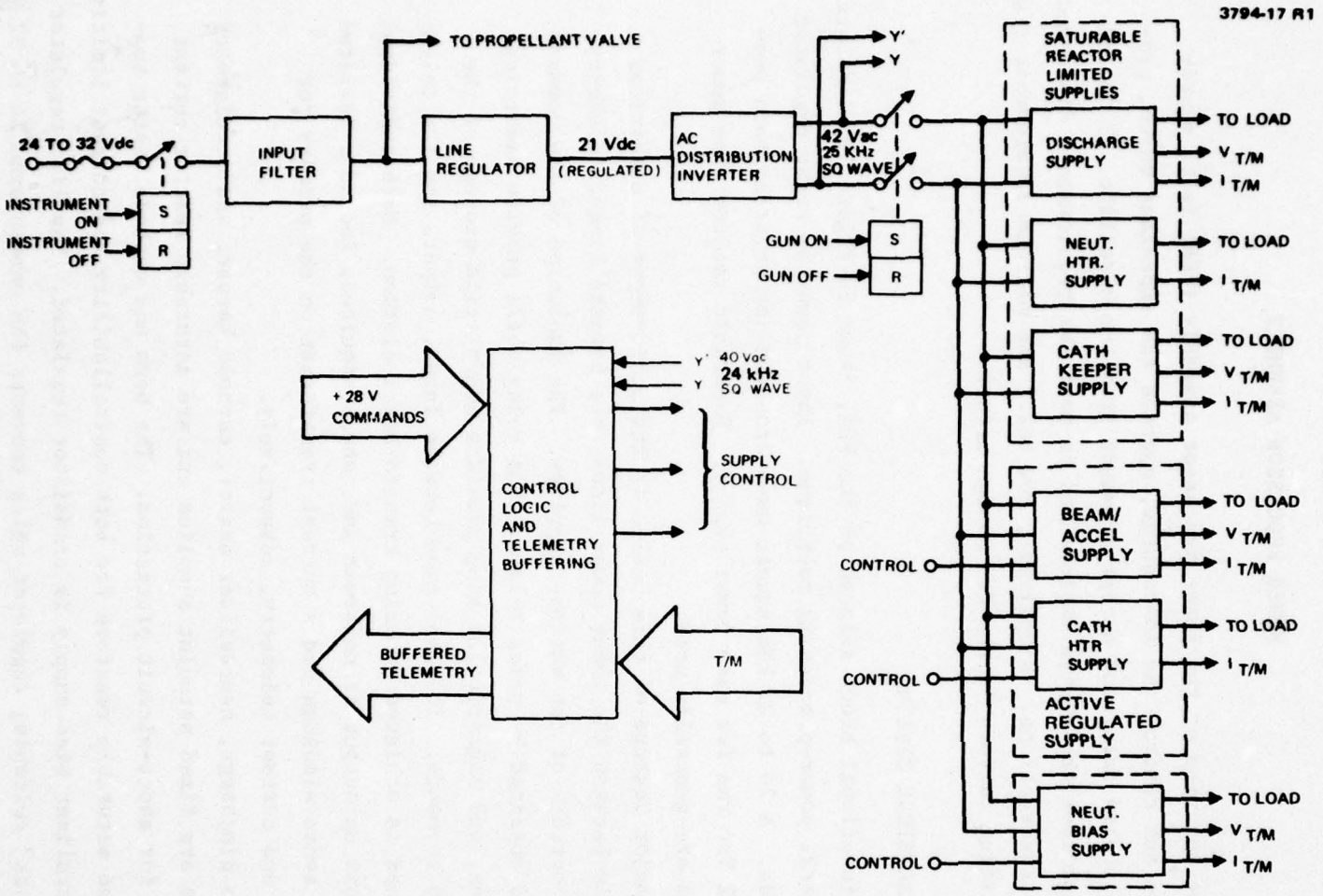

Figure 33. PPA functional block diagram.

ripple current generated by the line regulator from appearing on the input power bus lines.

1. Line Regulator and AC Inverter

A block diagram of the line regulator is shown in Figure 34. A switching regulator was chosen for this application to achieve the desired regulation with maximum efficiency. This regulator operates over an input range of 24 to 32 Vdc and provides a source of regulated 21-Vdc power for the ac distribution inverter. Preregulation of the bus power assures that the ac inverter output will be a constant amplitude square wave as required by the power supply saturable reactors.

The line filter will filter the ripple current produced by the switching regulator. The main requirements for the input filter are to be stable when a negative resistance device is connected to its output and to adequately reduce the ripple current returning to the power source.

An error amplifier compares the 21-V output with a reference and furnishes an error signal to the comparator. The comparator compares the output of the error amplifier with a ramp voltage supplied by the ramp generator. The comparator output is a pulsewidth-modulated wave that turns on and off the drive to the NPN power transistor switch. The input of the ramp generator is fed back from the output of the ac distribution inverter. Hence, the switching regulator and ac distribution inverter operate at the same frequency.

The ac distribution inverter receives regulated 21 Vdc from the line regulator and converts it to a square wave, 42 Vac rms for use by the power supplies. The block diagram for the ac distribution inverter is shown in Figure 35. The 21 Vdc is sent to the primary center tap of the output power auto transformer. A pair of push-pull power transistors are connected to the two legs of the primary of the output power transformer and are driven by a square-wave oscillator.

The schematic of the line regulator and ac inverter is shown in Figure 36 (drawing 1028500). The error amplifier AR2 compares the reference voltage created by zener diode VR1 to a voltage on a resistor R40, which is a function of the output voltage. The ramp generator is

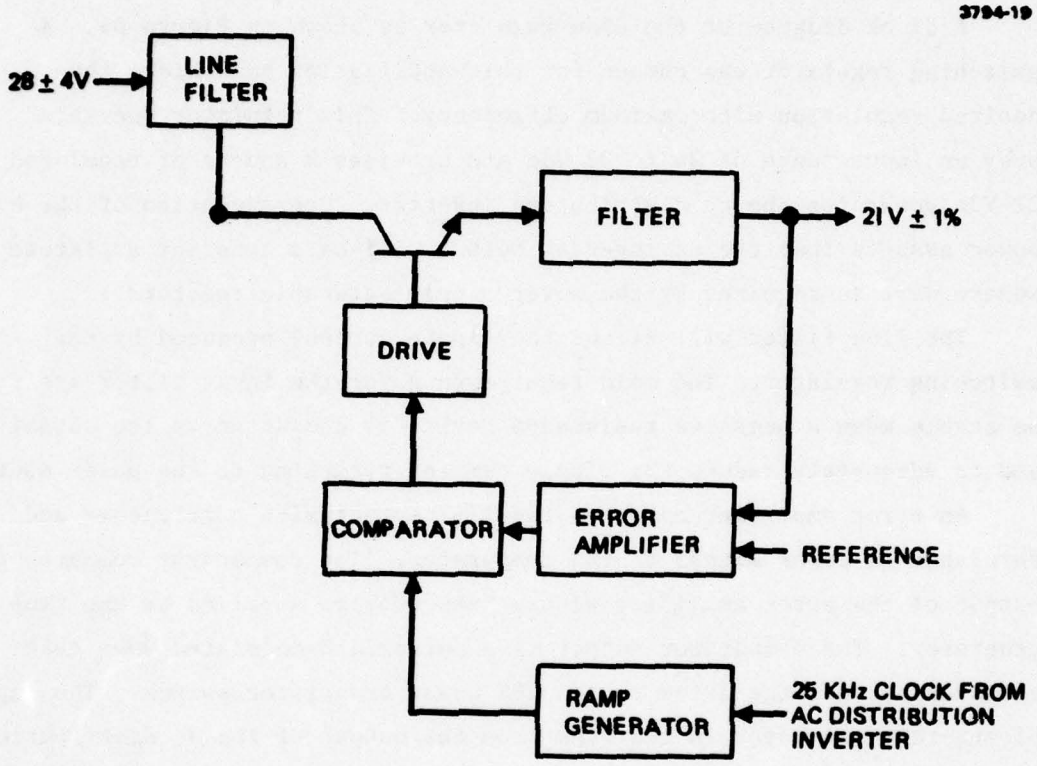

Figure 34. Line regulator block diagram.

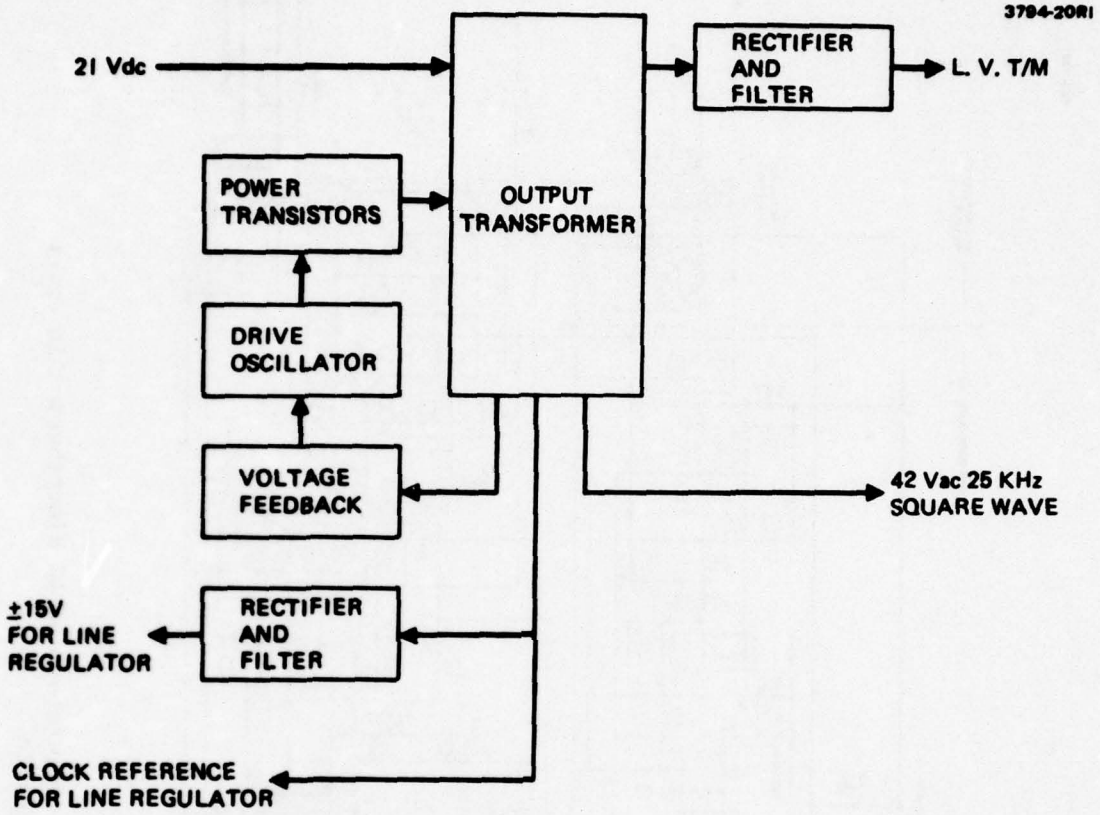

Figure 35. AC distribution inverter block diagram.

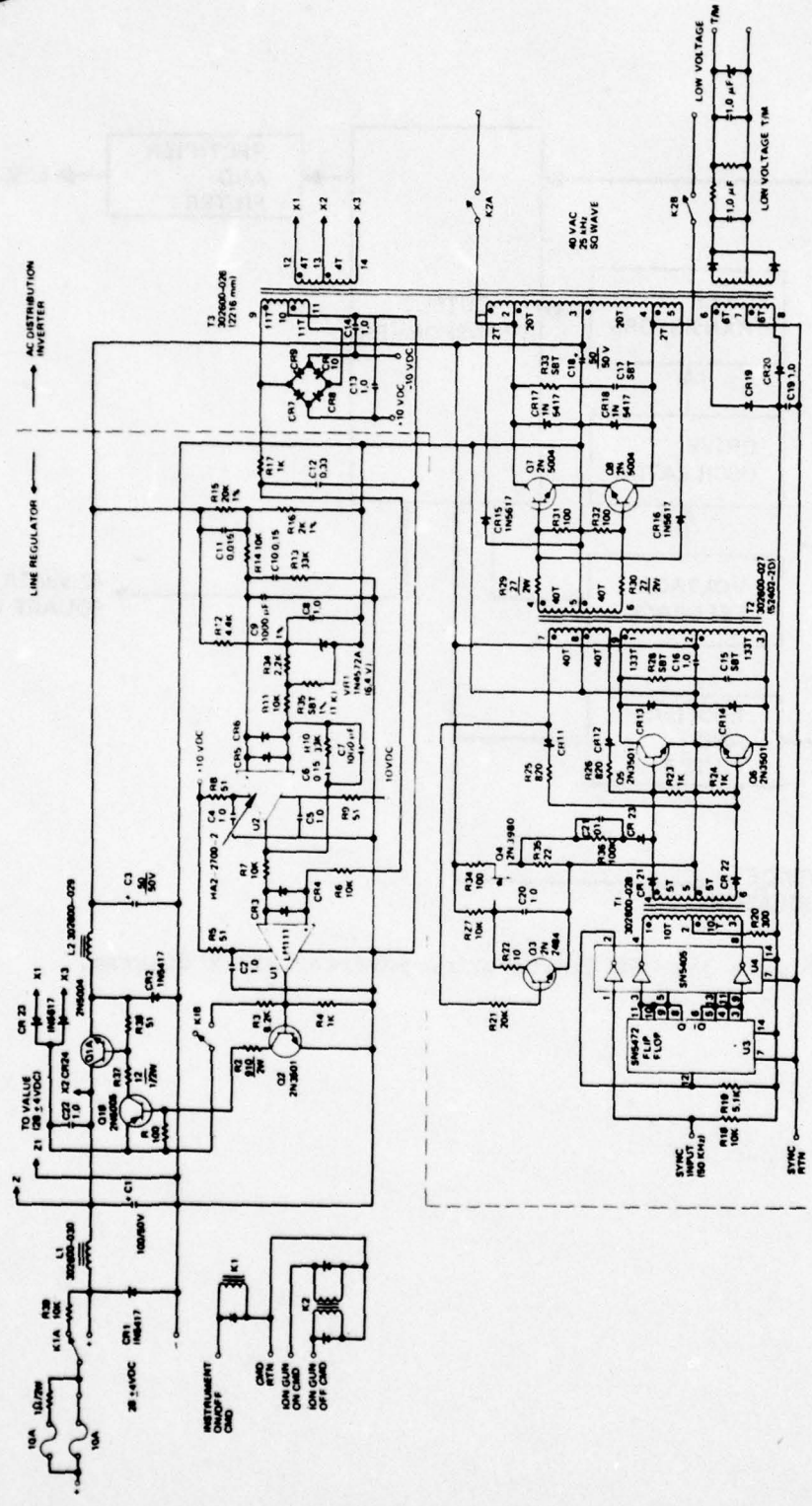

Figure 36. Line regulator and AC distribution inverter schematic.

comprised of resistor R41 and capacitor C16. This network produces a ramp voltage by integrating the clock reference square wave supplied from the ac distribution inverter. The comparator AR1 compares the output of the error amplifier AR2 to the voltage ramp on capacitor C16. The comparator turns transistor Q2 on and off, which, in turn, turns transistors Q9 and Q1 on and off in a pulsewidth-controlled fashion.

The connections of Q9 and Q1 shown in Figure 36 allow Q1 to saturate. Inductor L2 and capacitors C6 and C19 comprise the filter which averages the pulsewidth-controlled output of Q1 to obtain 21 Vdc. Diode CR10 is a commutating diode which furnishes a path for the current in inductor L2 when transistor Q1 turns off.

Resistor R5 is the oscillator starting resistor. It causes current to flow into the base of transistor Q5 or Q6. For example, the resistor could cause current to flow into the base of transistor Q5 causing it to turn on. Transistor Q5 will remain on because transformer T2 is phased so that positive feedback will occur. After several volt-seconds, as determined by the windings on T2, T2 will saturate, Q5 will turn off, and Q6 will turn on. This type of oscillator is basically a Royer circuit.

2. Screen/Accel Supply

The block diagram for the combined screen and accel supplies is shown in Figure 37. Since the output windings of screen and accel supplies are common to one output transformer, the output of T/M winding (also on the same transformer) is representative of either the screen or accel output voltages. Output current T/M for both supplies is isolated by individual output transformers.

The block labeled "control electronics" accepts level I or level II command pulses, which set the screen and accel output levels at +1000 or +2000 Vdc, and -300 or -600 Vdc, respectively. The relay shown in the primary winding of the output transformer turns both supplies off when receiving the "screen/accel off command."

A schematic of the combined screen and accel supplies is shown in Figure 38 (Drawing 1028190). The output voltages of the screen and

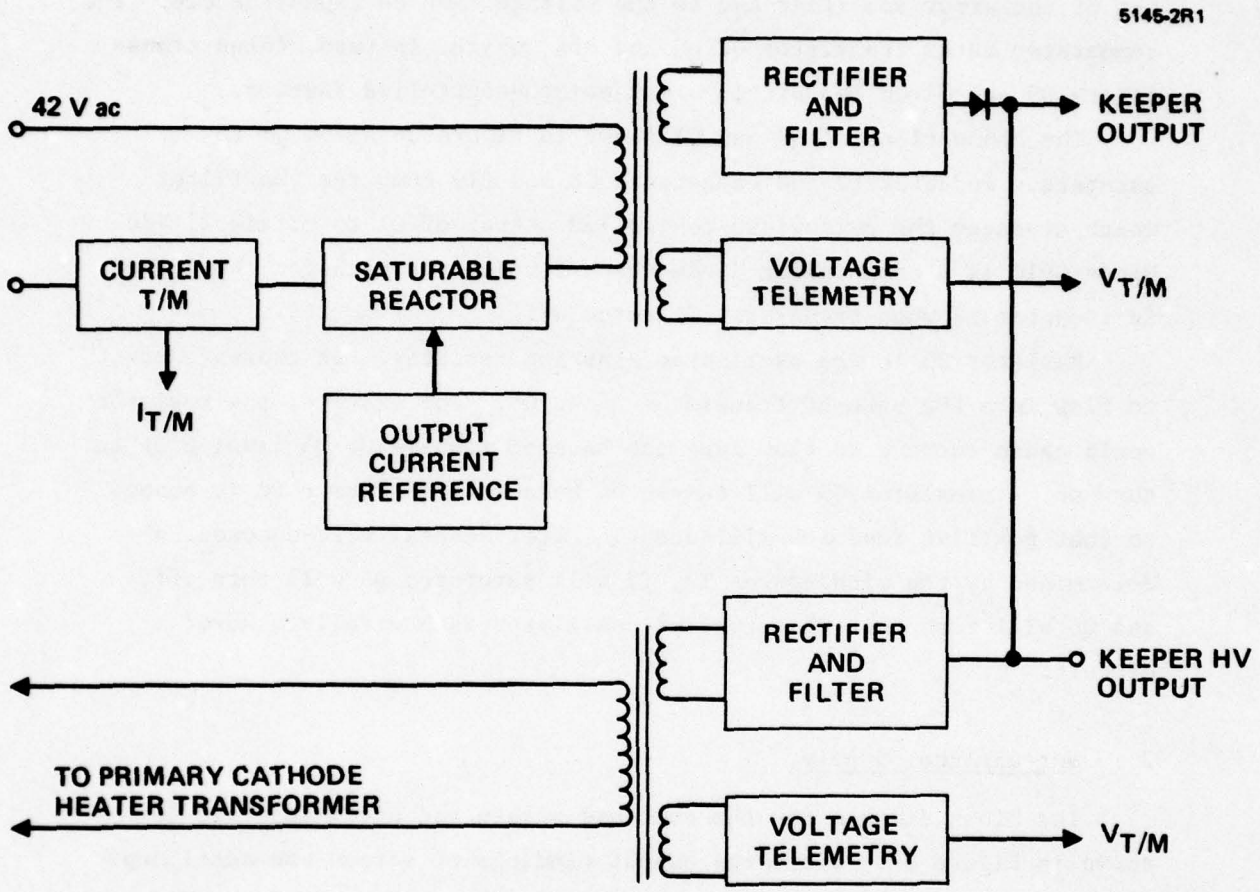

Figure 37. Screen/accel supply block diagram.

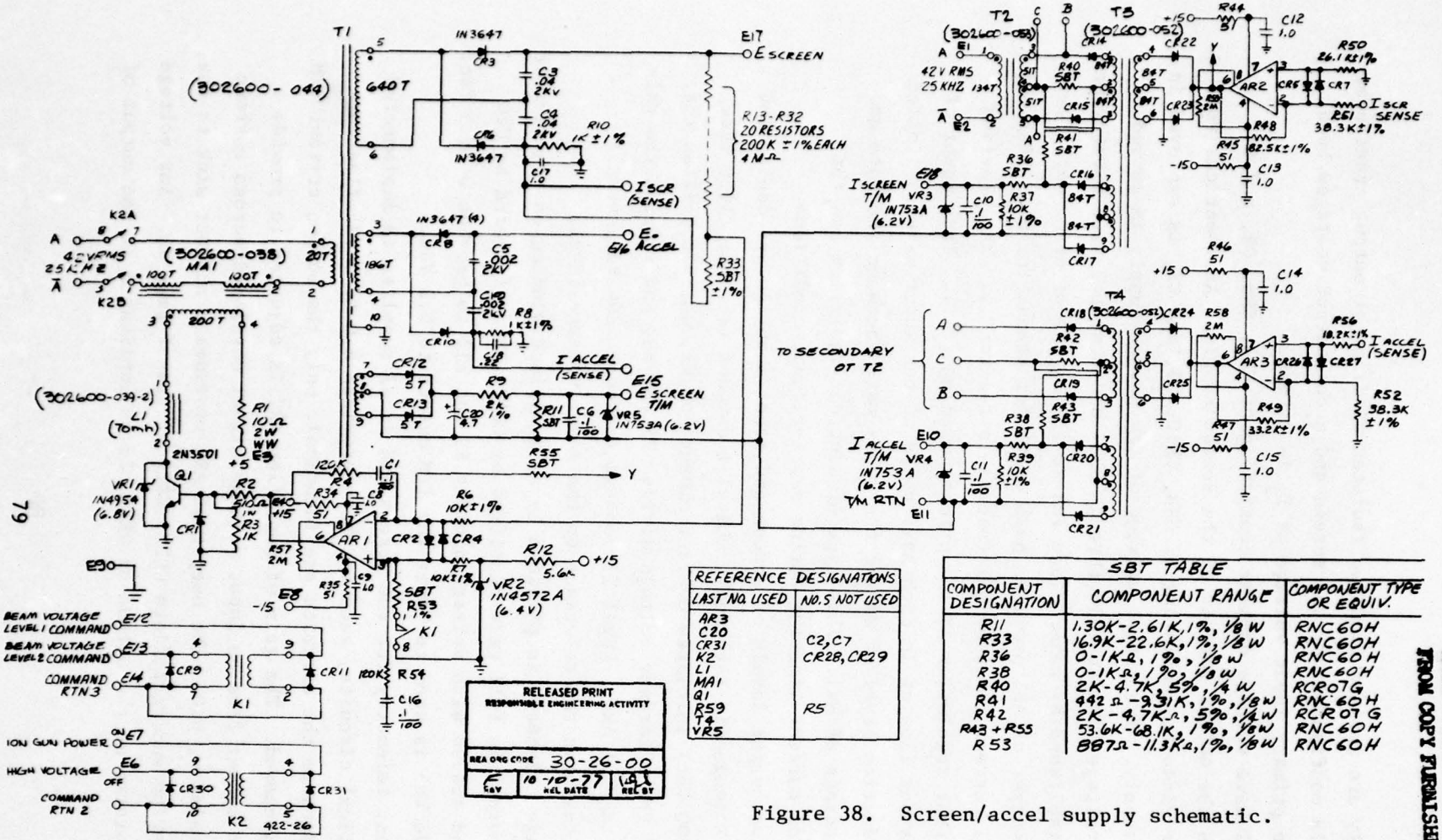

REFERENCE DESIGNATIONS	
LAST NO. USED	NO.S NOT USED
AR3	
C20	
CR31	C2, C7
K2	CR28, CR29
L1	
MA1	
Q1	
R59	R5
T4	
VR5	

SBT TABLE		
COMPONENT DESIGNATION	COMPONENT RANGE	COMPONENT TYPE OR EQUIV.
R11	1.30K-2.61K, 1%, 1/8 W	RNC60H
R33	16.9K-22.6K, 1%, 1/8 W	RNC60H
R36	0-1KΩ, 1%, 1/8 W	RNC60H
R38	0-1KΩ, 1%, 1/8 W	RNC60H
R40	2K-4.7K, 5%, 1/4 W	RCR07G
R41	442 Ω-9.31K, 1%, 1/8 W	RNC60H
R42	2K-4.7KΩ, 5%, 1/4 W	RCR07G
R43+R55	53.6K-68.1K, 1%, 1/8 W	RNC60H
R53	887Ω-11.3KΩ, 1%, 1/8 W	RNC60H

RELEASED PRINT
RESPONSIBLE ENGINEERING ACTIVITY
REA ORG CODE 30-26-00
E 5&V | 10-10-77 REL DATE | LA REL BY

5. RELAYS ARE TELEDYNE 421-26
4. OPERATIONAL AMPLIFIERS LM4250
3. DIODES ARE IN3600
2. CAPACITORS ARE IN μF, 50 VDC
1. RESISTORS ARE IN OHMS ±5% 1/4 W

NOTES-UNLESS OTHERWISE SPECIFIED

7. S.B.T. MEANS "SELECT BY TEST."
6. ±1% RESISTORS ARE 1/8 W

Figure 38. Screen/accel supply schematic.

accel supply are derived from two isolated windings of output transformer T_1. In this configuration, the screen and accel output voltages both vary as the primary input voltage of T_1 is varied.

A full wave voltage doubler consisting of CR3, CR6, CR, and C4 constitutes the output circuit of the screen supply. An identical voltage doubler circuit, consisting of CR8, CR10, C5, and C7, is employed in the accel supply. The output voltage of the screen supply is sensed through a voltage divider (R13 through R33) and compared with a reference voltage established by zener diode VR2 at the inputs of error amplifier AR1. The output of AR1 provides base drive for transistor Q_1, which sets the control current level of MA1 (saturable reactor 1). MA1 provides series current regulation to the primary winding of T1. The amount of primary current flowing in each half cycle of the input wave is limited by the conduction level of Q1 and the turns ratio between the gate and control windings of MA1. This type of control regulation has the advantage of current limiting during short-circuit conditions.

The two output levels of screen and accel supplies are controlled by relay K1 (magnetic latching). Level I command (screen: 1000 Vdc, accel: -300 Vdc) initiates contact closure of K1, which completes the circuit of the reference voltage divider R7 and R53 and reduces the reference voltage of AR1. Level II command (screen: 200 Vdc, accel: -600 Vdc) restores the reference to the zener voltage level.

Voltage telemetry is provided by an auxiliary winding on transformer T_1. The output is full wave rectified by CR12, CR13, filtered by C20 and C6, and scaled with voltage divider R9 and R11 to provide 0 to 5 Vdc. Zener diode VR5 is used to limit the T/M output to 6.2 Vdc.

Current telemetry for the screen and accel supplies is implemented with identical circuits, each of which provides a 0 to 5 Vdc floating output. Because the circuits are identical, only the screen current T/M will be discussed. The gain of amplifier AR2 is adjusted to provide a 0 to 5 Vdc output from an input voltage signal developed across current sensing resistor, R10. The output of AR2 provides a current sink to the output winding and rectifiers CR22, CR23 of transformer T3. Any voltage level generated at the output of CR22, 23 is duplicated at the output of

rectifiers CR16, CR17. R40 in the primary winding of T3, determines the current sink requirements of AR2 and establishes the available output power to the T/M output circuit. R41 provides a forward bias current for CR16, CR17 at low level T/M outputs.

3. Cathode Heater and Discharge Supplies

The block diagram for the cathode heater and discharge supplies is shown in Figure 39. A control loop is used between the "voltage sensing" block of the discharge supply and the "saturable reactor and control electrons" block of the cathode heater supply. Before discharge ignition takes place, the maximum cathode heater output current is established by current limiting resistors in the saturable reactor control winding. After discharge ignition, the feedback voltage from the discharge supply will suddenly decrease to a value less than the reference voltage in the heater control electronics. At this time, the cathode heater supply will be cutback to virtually zero output.

The output current levels of the discharge supply are 35, 125, and 250 mA and are set by level I, II, and III command signals to latching relays in the "discharge output current" block. Voltage and current T/M signals for both supplies are transformer isolated.

The cathode heater and discharge supplies circuit schematics are presented in Figure 40 (drawing 1028191). The discharge supply is a constant current supply in which output voltage is sensed to control the cathode heater current. As in the screen supply, a current limiting feature is designed into both output transformer control magnetics.

The output current level is selected by latching relays K1 and K2, which are operated by the discharge level commands. A voltage sense winding on the discharge supply output transformer, T3, furnishes a voltage proportional to the output voltage and is used to control the electronics in the heater supply. Operational amplifier AR1 compares this voltage with a reference voltage and varies the base drive to transistor Q1, which controls the cathode heater output current. Two levels of heater current can be selected by latching relays K3 and K4, which are operated by the input heater level commands.

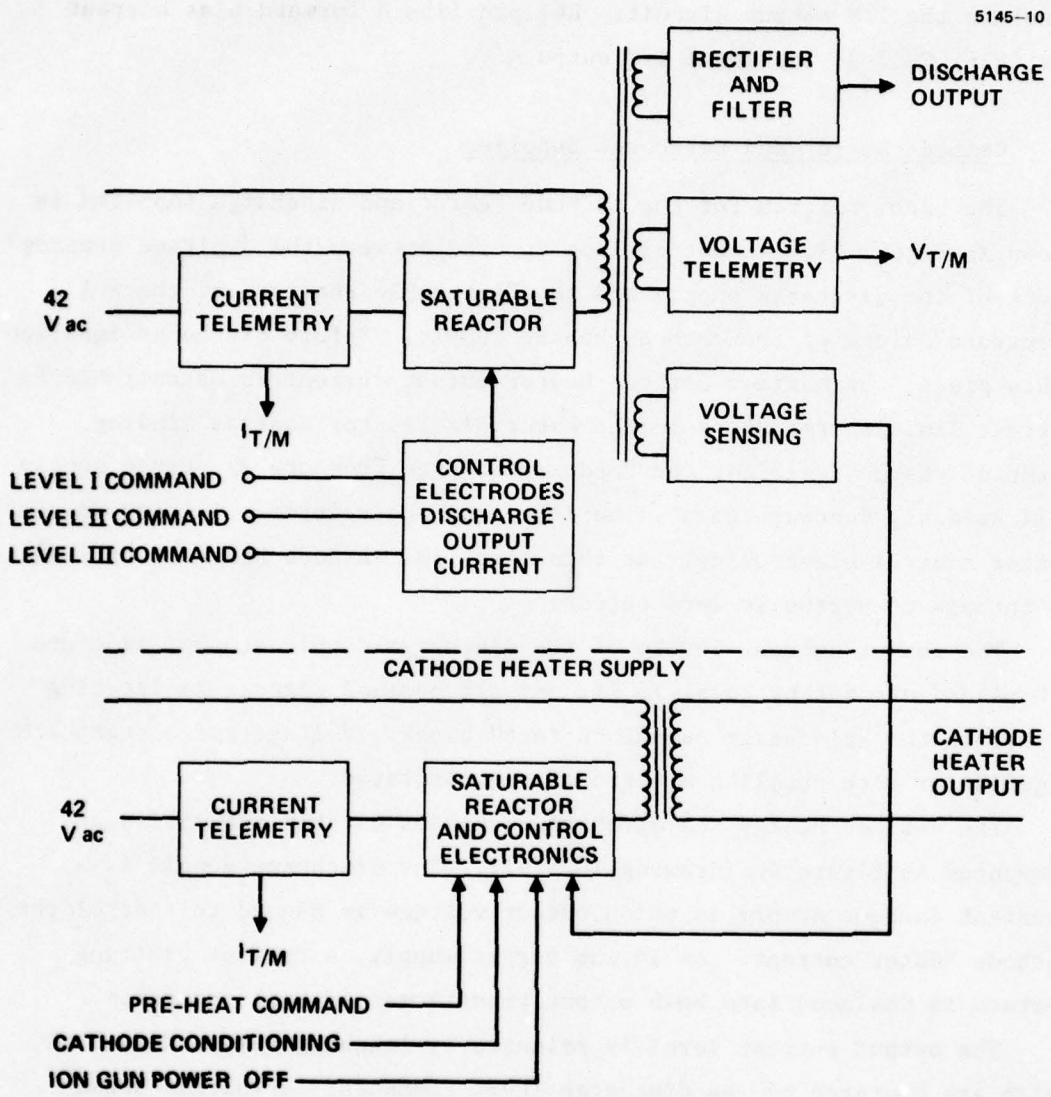

Figure 39. Cathode heater and discharge supplies block diagram.

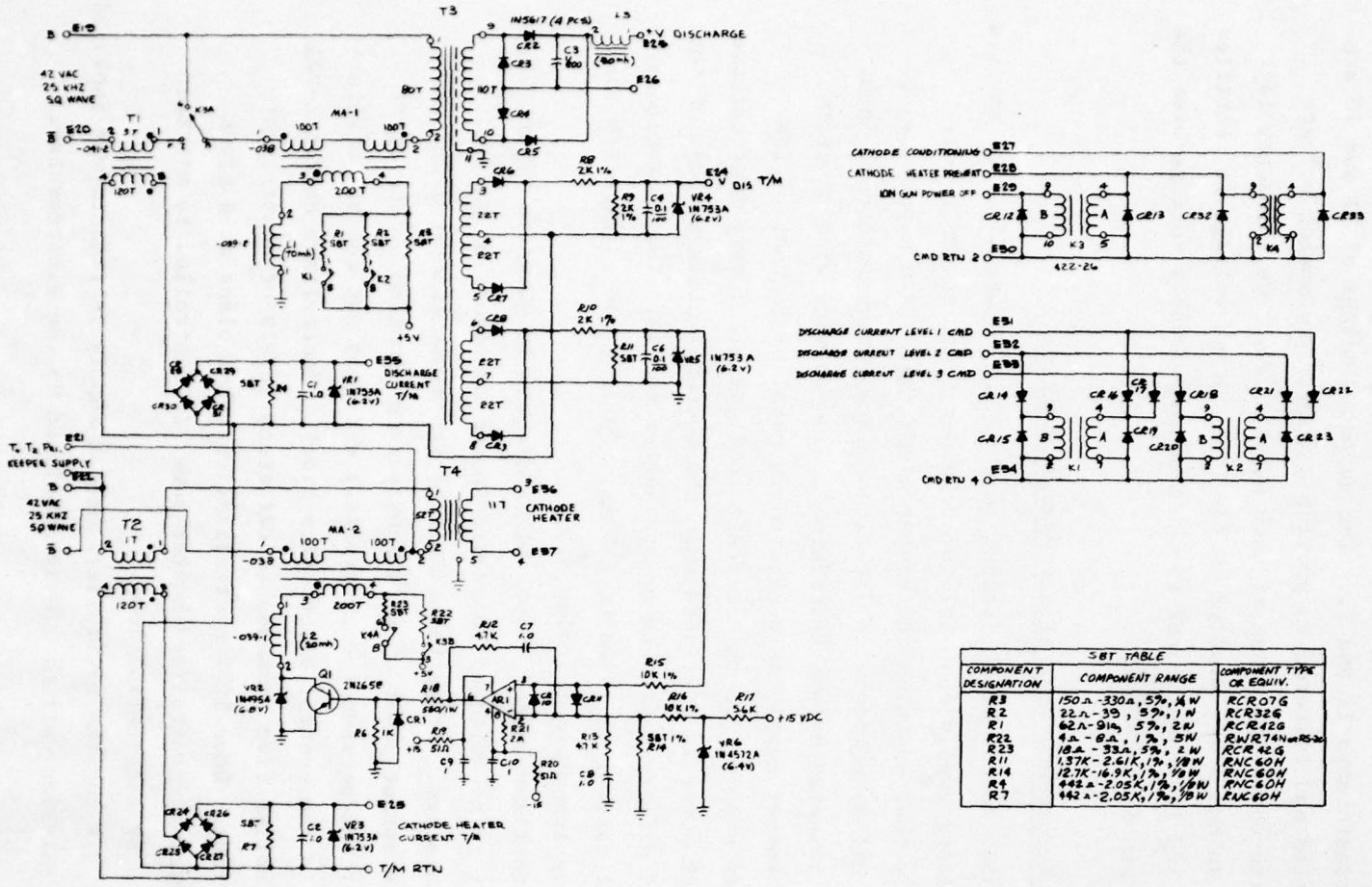

SBT TABLE		
COMPONENT DESIGNATION	COMPONENT RANGE	COMPONENT TYPE OR EQUIV.
R3	150Ω - 330Ω, 5%, ¼ W	RCR07G
R2	22Ω - 39Ω, 5%, 1 W	RCR32G
R1	62Ω - 91Ω, 5%, 2W	RCR42G
R22	4Ω - 8Ω, 1%, 5W	RNR74N or RS-2G
R23	18Ω - 33Ω, 5%, 2W	RCR42G
R11	1.37K - 2.61K, 1%, ⅛W	RNC60H
R14	12.7K - 16.9K, 1%, ⅛W	RNC60H
R4	442Ω - 2.05K, 1%, ⅛W	RNC60H
R7	442Ω - 2.05K, 1%, ⅛W	RNC60H

NOTES: UNLESS OTHERWISE SPECIFIED
1. OPERATIONAL AMPLIFIERS ARE LM4250
2. DIODES ARE IN3600
3. CAPACITORS ARE IN MFF, 50 VDC
4. RESISTORS ARE IN OHMS, 5%, ¼ W
5. RELAYS ARE TELEDYNE #21-28
6. ±1% RESISTORS ARE 1/8 W.
7. SBT MEANS "SELECT BY TEST"

Figure 40. Cathode heater and discharge supplies schematic.

Current telemetry for both discharge and heater supplies is provided by current transformers T1 and T2. The output windings of T1 and T2 are bridge rectified and filtered to provide a 0 to 5 Vdc analog voltage over the entire operating range of each supply. Voltage telemetry is derived from an auxiliary winding on T3. The output voltage is rectified and filtered and is proportional to the discharge output voltage over the operating range of the supply.

4. Cathode Keeper and Neutralizer Heater Supplies

The cathode keeper block diagram is shown in Figure 41. It consists of a high-voltage supply that initiates keeper ignition and a low-voltage supply that sustains the keeper discharge. Each supply can be turned on or off by commands to latching relays, which interrupt input power to the selected output transformer. The primary winding of the high-voltage keeper supply is connected in parallel to that of the cathode heater supply. In this circuit configuration, very fast cathode heater cutback power is initiated when the keeper ignites because of the low reflected primary impedance of the keeper supply. The low-voltage keeper output current is fixed at 235 mA. Current and voltage T/M for this supply is transformer isolated.

The neutralizer heater supply block diagram is shown in Figure 42. Its output is relay switched to provide power to either of the two neutralizer heaters. It is turned off by the *neutralizer heater off* command. The output power of this supply is controlled by the error signal difference between the neutralizer emission current and a reference signal in the control electronics block. Neutralizer heater level commands establish five commandable reference levels of neutralizer emission current. Once 100% neutralization takes place at a given reference setting, neutralizer heater power is controlled to maintain this emission by the control loop.

Current T/M for the neutralizer heater supply is transformer isolated. Neutralizer emission current T/M is furnished by the electrometer.

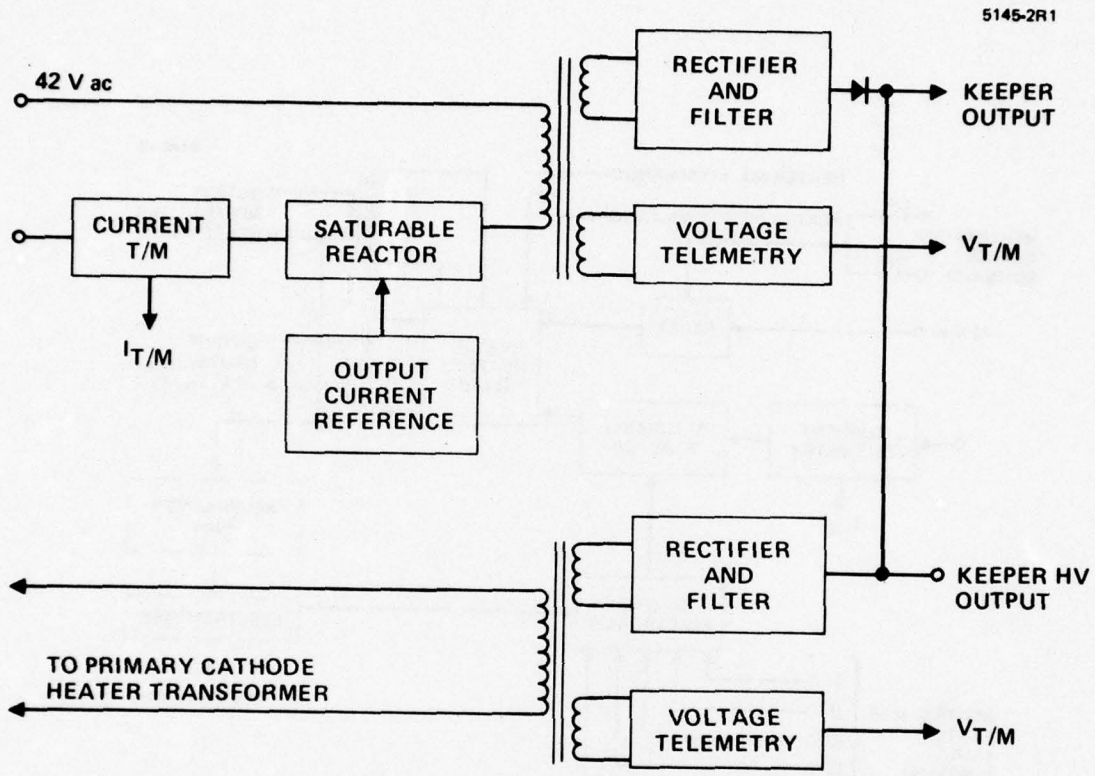

Figure 41. Cathode keeper supply block diagram.

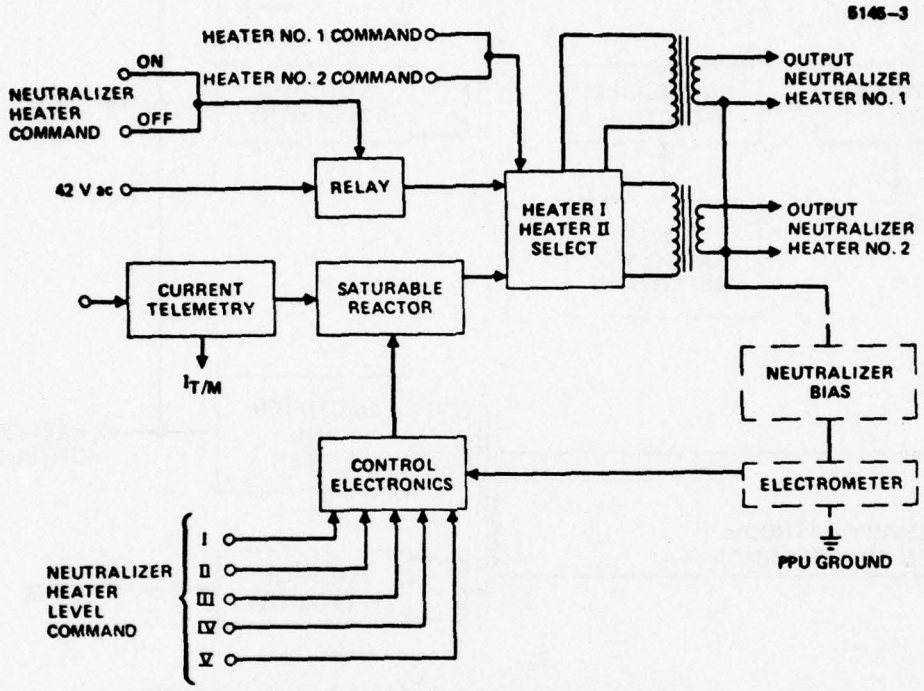

Figure 42. Neutralizer heater supply block diagram.

A schematic of the cathode keeper supply is shown in Figure 43 (drawing 1028192). The supply includes a high-voltage module for keeper ignition and a low-voltage module to sustain the keeper discharge in normal operation. The high-voltage winding on T2 provides 1000 Vdc after being rectified by CR12 through CR15. The output current is limited to 20 mA because T2 derives its power from the magnetic amplifier in the cathode heater supply. At the 1000-Vdc output level, a telemetry voltage winding on T2 provides a 5 Vdc signal at the output of CR10, CR11, and R-C filter circuit.

The low-voltage output is derived from T3 with its output full wave rectified by CR16 and CR17. CR18 is a high-voltage diode which protects the output circuit of T3 from high voltage stresses before ignition takes place. Current limiting is accomplished by the action of saturable reactor MA1. The output of the keeper supply is turned on and off by latching relay K7.

Current telemetry is implemented with transformer T1 and its associated rectifier-filter output circuit. This provides a 0 to 5 Vdc analog signal proportional to the keeper load current.

The circuit of the neutralizer heater supply is identical to that of the cathode heater supply with the exception that the neutralizer heater current is controlled by the neutralizer emission current. Five level commands, which operate latching relays K3, K4, K5, and K6, change the reference signal on amplifier AR1. An increase in the reference level at the input of AR1 corresponds to an increase in heater current, which results in an increase in neutralizer emission current. The current supplied to the heater becomes stabilized when the emission current signal reaches the level of the reference voltage at the inputs of AR1. The option of selecting either one of two neutralizer heaters is implemented by latching relay K2. Neutralizer heater current telemetry is derived from transformer T4. The output, which is rectified and filtered, provides a 0 to 5 Vdc signal, which corresponds to the applied heater current.

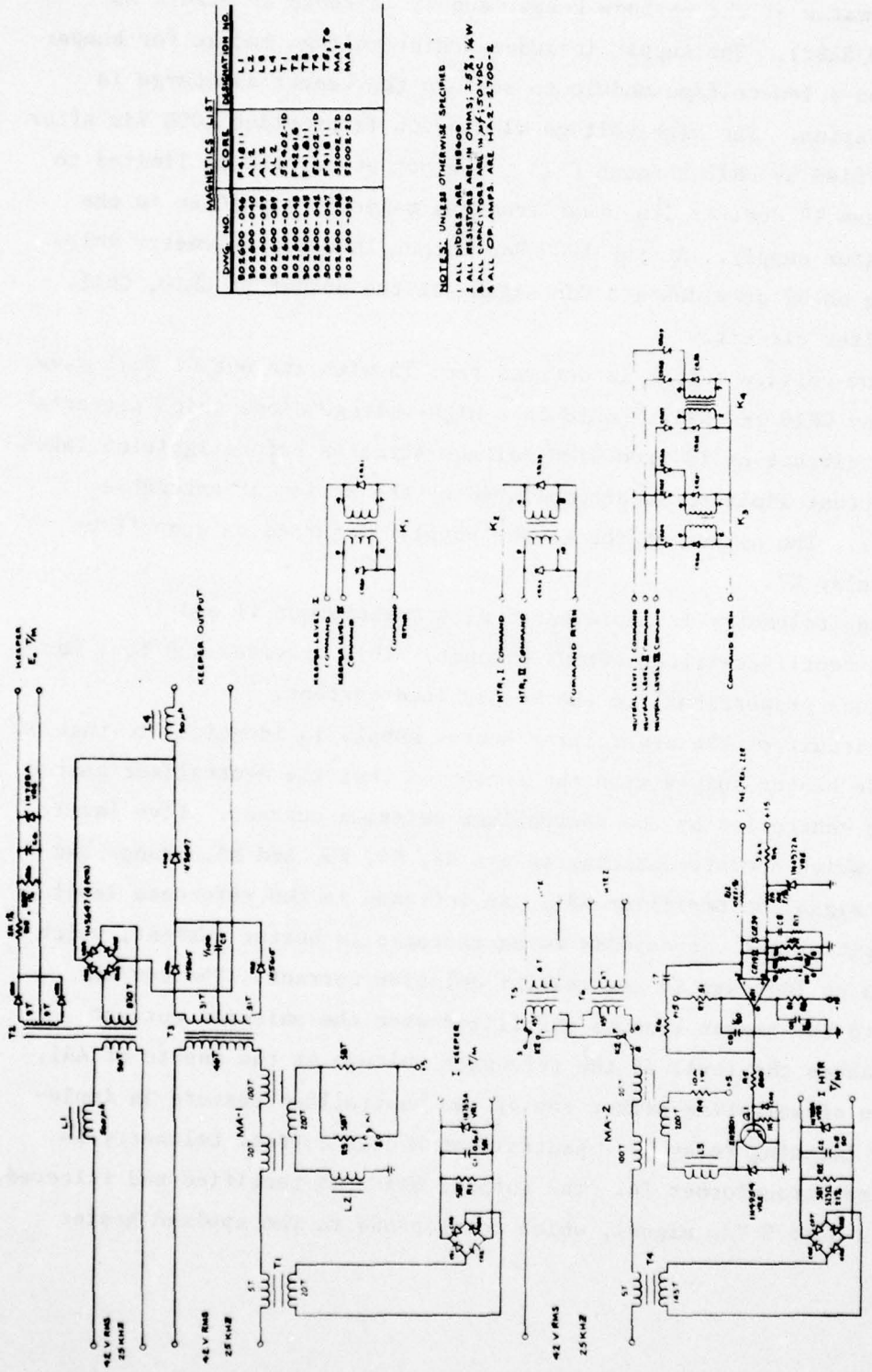

Figure 43. Cathode keeper and neutralizer heater schematic.

5. Neutralizer Bias Supply

A block diagram of the neutralizer bias supply is shown in Figure 44. The 42 Vac input passes through an isolation transformer and goes to two similar series regulated supplies. Each supply (one for positive bias and one for negative) consists of a series pass transistor that has current limiting, a step up transformer, a voltage doubler, and an error amplifier. The zener reference is common to both supplies. On receiving a polarity command, a relay selects the desired supply.

The neutralizer bias supply design is shown schematically in Figure 45 (Drawing 1028406). The basic design consists of positive and negative voltage-regulated supplies and a commandable relay (K6) that selects the desired supply. The negative supply consists of an output transformer T3 and a full-wave voltage doubler CR17, CR18, C19, and C20. The output voltage is sensed by operational amplifier AR1 through resistors R27 through R31 and compares this voltage to the reference provided by zener diode VR2. The operational amplifier linearly drives Q4, which varies the voltage on the primary of transformer T3 to close the regulation loop. Transistor Q3 and resistor R5 are included to provide current limiting. The positive supply is similar in design to the negative supply but has a series string of 3 mA constant current diodes CR21 through CR32 across the output. These diodes provide a path for the current that the supply must sink. The different output levels are obtained by commands which activate relays K2, K3, K4, and K5. Amplifier AR3 and a magnetic telemetry isolator will generate a telemetry signal that corresponds to the absolute output voltage. A polarity flag is used to indicate the polarity of the output.

6. Electrometers

The SPIBS system requires accurate telemetry measurements for the neutralizer emission current (I_{NE}) and SPIBS net current (I_{NET}) (i.e., current in the ground line) over a 3 decade range from 2 μA to mA with ±5 percent accuracy. Furthermore, measurement of the SPIBS net current is required to be bi-directional since the spacecraft net current may be

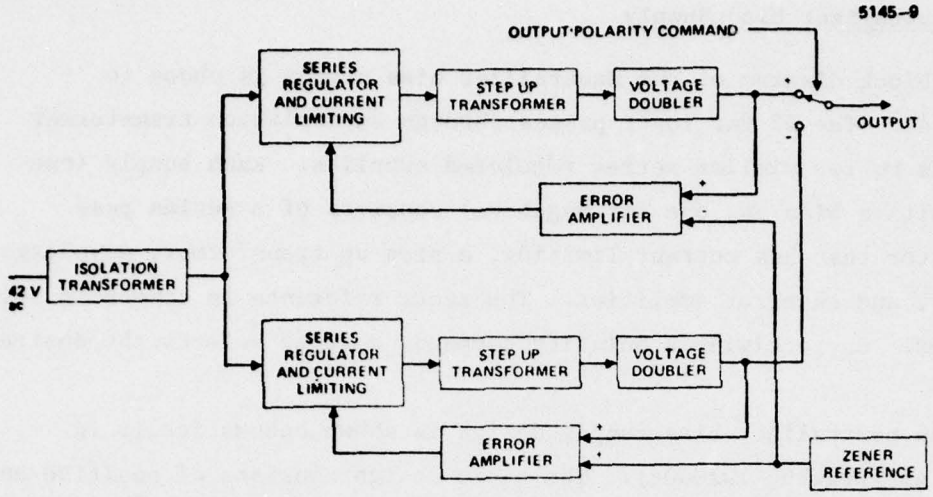

Figure 44. Neutralizer bias supply block diagram.

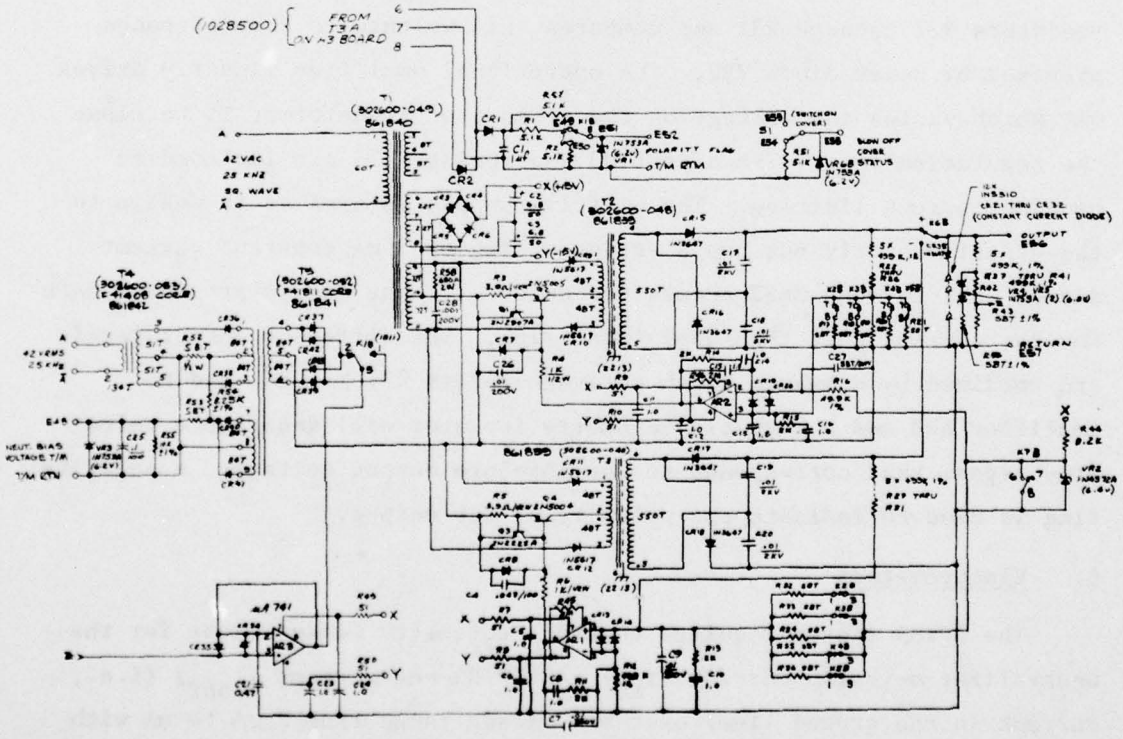

Figure 45. Neutralizer bias supply schematic.

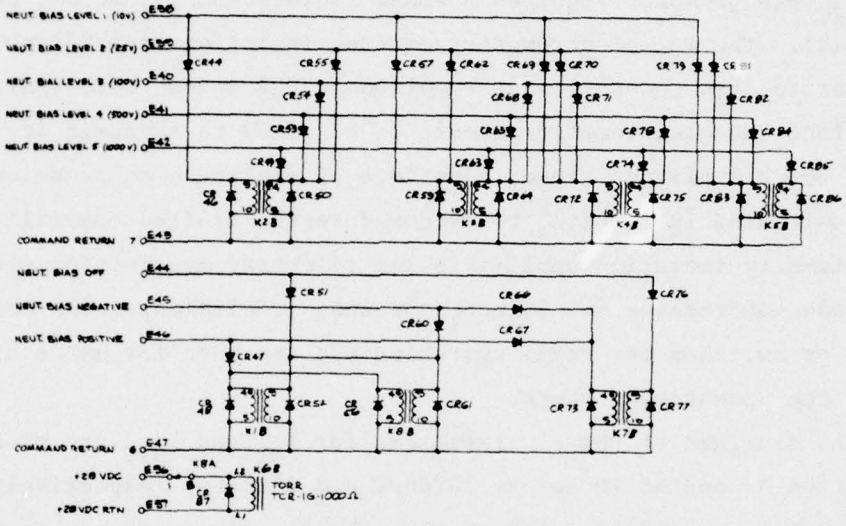

Figure 45. (Continued).

positive or negative. Finally, the unit is required to have a low source impedance such that the voltage across the input terminals does not exceed ±2 V at the highest input current (2 mA). A single design is used to meet both the emission and net current requirements.

A block diagram of the SPIBS electrometer configuration is shown in Figure 46. I_{NET} can be conveniently measured at S/C common and be supplied directly to the telemetry acquisition system without isolation. The I_{NET} electrometer requires a small isolated supply at S/C common potential. The I_{NE} electrometer requires isolation from S/C potential and operates from housekeeping supplies at PPA common potential.

Since the electrometer circuit is required to maintain accuracy over a 60-dB amplitude range, some form of amplitude compression or range switching is required to accommodate the limited capability of the telemetry isolation amplifiers and telemetry acquisition systems. Amplitude compression was selected because it eliminates the need for relays or switches for range switching and the need for extra bits to define the measurement range.

The diagrams of the electrometers for I_{NE} and I_{NET} are presented in Figures 47 and 48 (Drawings 1028602 and 1028706) respectively. The electrometers are similar except that the I_{NE} electrometer has additional telemetry magnetic isolation. The circuits are basically comprised of the following:

- A voltage regulator, comprised of AR1 and AR2, provides a precisely regulated 10-V bipolar supply for AR3, AR4, and AR5 and provides off-setting for AR6.
- An input circuit which provides for source impedance compression at the higher input current levels.
- Three amplifiers for linear decade ranges 0 ± 20 μA, 0 to ± 200 μA and 0 to ± 2 mA.* (2.5 mA full scale).
- An output summing amplifier for the 3 decades, with off-setting, to provide a 0- to +5-output for -2.5 mA to +2.5 mA input.

*The three amplifiers each operate over a ± 10-V output range and are designed to provide a precise supply rail and a 0 to ± 100-MV input range clamp when the input range for that amplifier is exceeded.

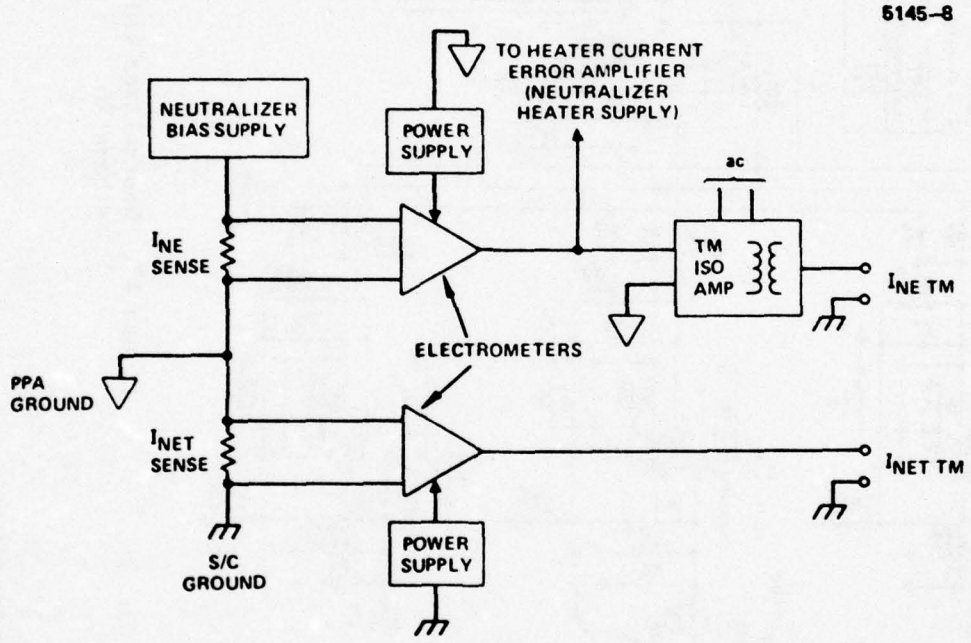

Figure 46. Electrometer block diagram.

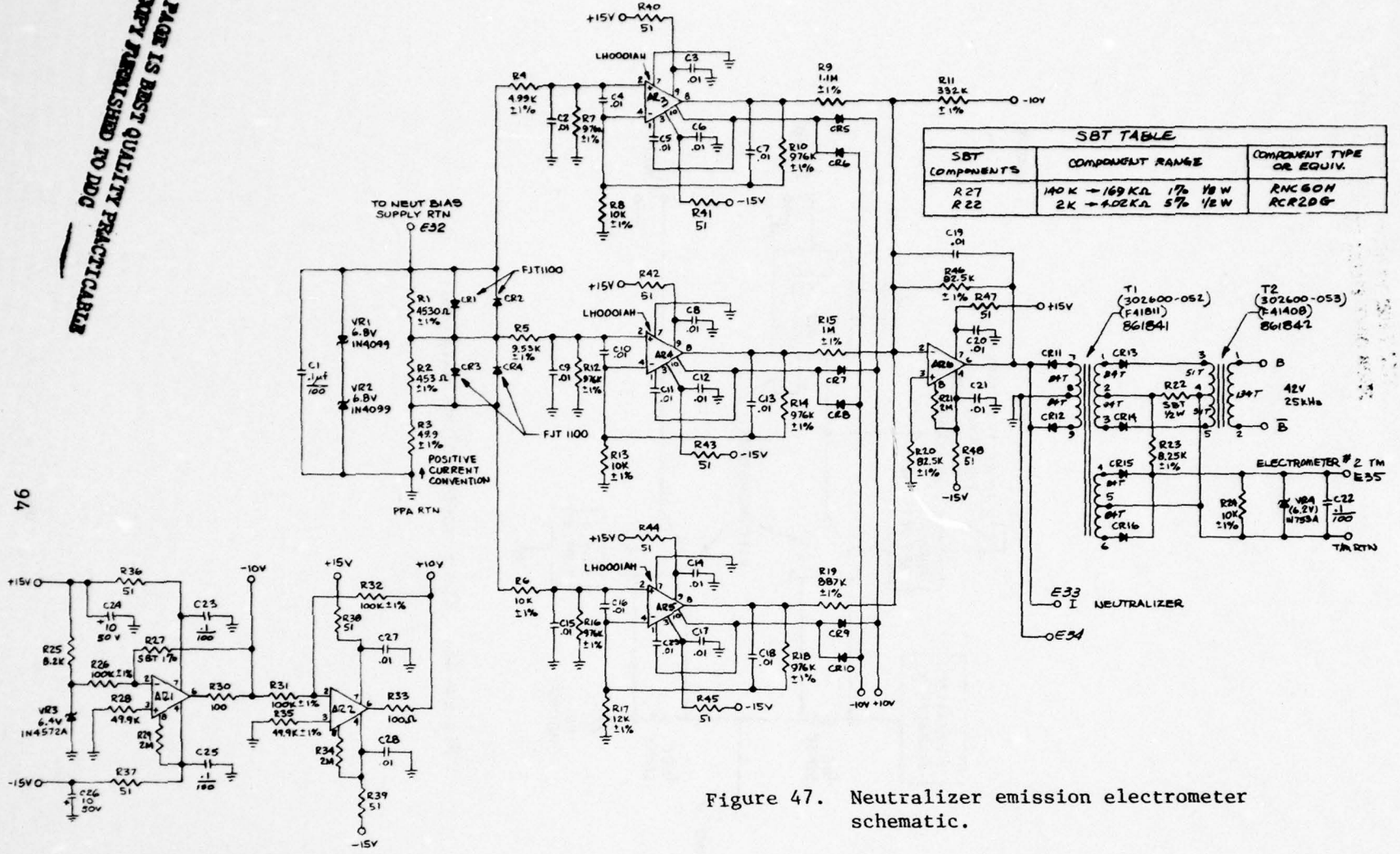

Figure 47. Neutralizer emission electrometer schematic.

4. OP. AMPS ARE LM4250
3. DIODES ARE IN3600
2. CAPACITORS ARE IN μf, 200 VDC
1. RESISTORS ARE IN OHMS ± 5% 1/4 W

NOTES: UNLESS OTHERWISE SPECIFIED

7. S.B.T. MEANS "SELECT BY TEST."
6. ±1% RESISTORS ARE 1/8 W.
5. ±15V BIAS FROM AC INVERTER

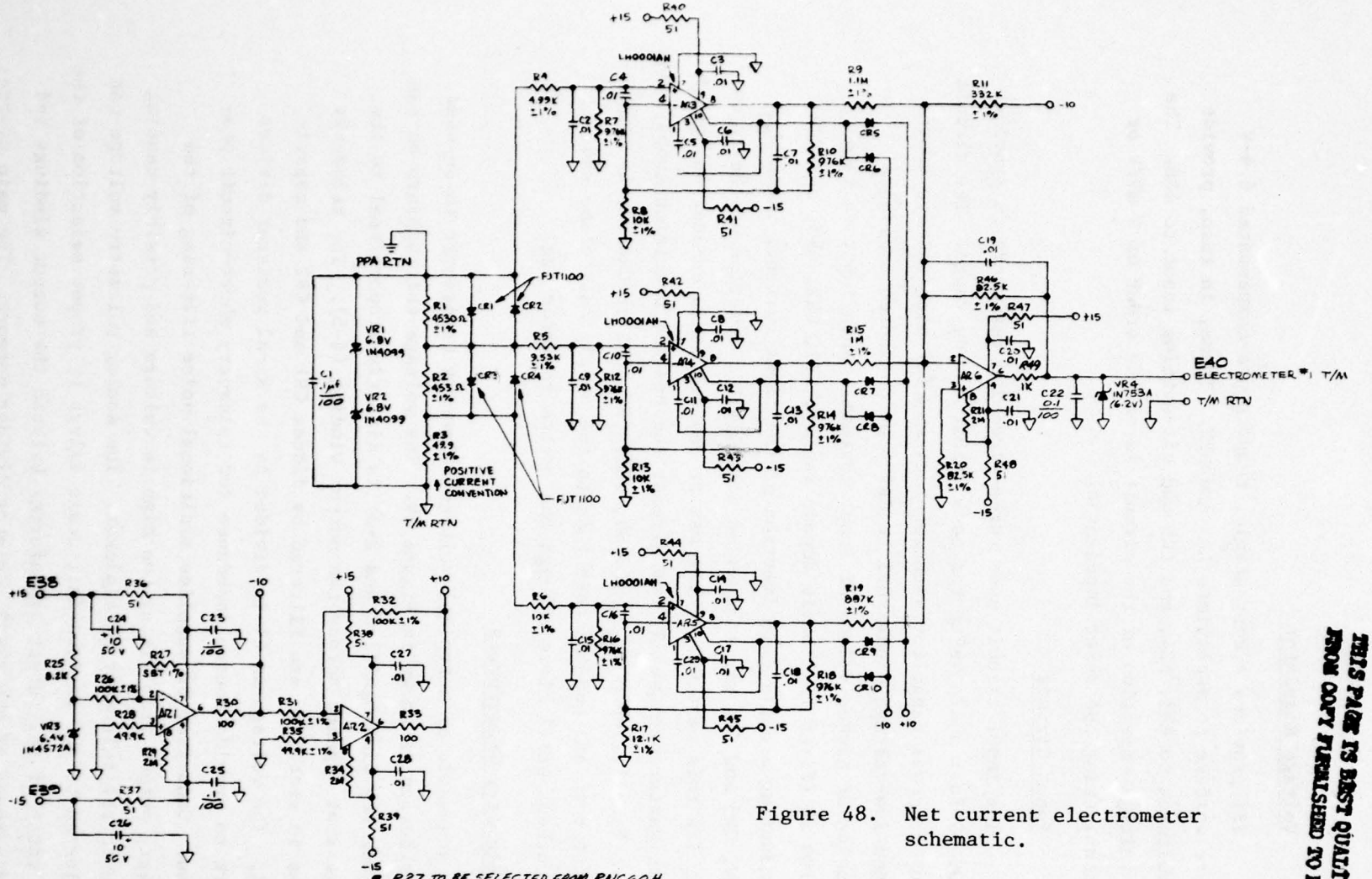

Figure 48. Net current electrometer schematic.

NOTES: UNLESS OTHERWISE SPECIFIED

1. RESISTORS ARE IN OHMS ± 5% ¼W
2. CAPACITORS ARE IN μf, 200 VDC
3. DIODES ARE IN3600
4. OP. AMPS ARE LM4250
5. ± 15 FROM PRESSURE TEMPERATURE AND DECEL TELEMETERING
6. ± 1% RESISTORS ARE ⅛ W.
7. S.B.T. MEANS "SELECT BY TEST."
8. R27 TO BE SELECTED FROM RNC60H 1%, ⅛ W. VALUE, 140K → 169K.

a. Voltage Regulator

VR3 provides a very stable, temperature-compensated 6.4-V reference voltage to amplifiers AR1 and AR2. These, in turn, provide ±10-V voltages to AR3, AR4, and AR5 and off-setting input to AR6. The supply voltage rejection of the circuit is on the order of 2 mV/V or less, considering the zener impedances.

b. Input Circuit

The input circuit uses three precision resistors to provide 0 to 100-mV full scale value for each linear decade range. The circuit contains a bypass capacitor with zener clamps for over-voltage protection, and low-voltage diodes CR1 to CR4 provide source impedance compression at higher values of input current. When input voltage $V_{R1} \leq 100$ mV (first full scale decade range), CR1, CR2, CR3, and CR4 are conducting a negligible fraction of the input current. When $V_{R2} \leq 100$ mV, CR3 and CR4 are conducting a negligible fraction of the input current (in this case CR1 or CR2 may or may not be in conduction, which does not matter because AR1 has already reached the precision supply rail clamp). Finally, when $V_{R3} \leq 100$ mV, CR1, CR2, CR3 or CR4 may be conducting, but both AR1 and AR2 have reached the supply rail clamp and all input current still flows through the bottom resistor leg.

7. Telemetry Transducers

A schematic of a typical voltage telemetry transducer to be used in this design is shown in Figure 49. The voltage that appears across the telemetry windings (1-2 and 2-3) is directly proportional to the voltage that appears across the output winding (4-5). The telemetry voltage is rectified and filtered by diodes CR1 and CR2 and capacitor C1. The voltage on C1 is divided by the R1-R2 resistor divider network to provide source impedance for telemetry short-circuit protection. Capacitor C2 supplies additional noise filtering of the telemetry output from rising too high in voltage and possibly causing damage to the telemetry multiplexer. The analog telemetry voltage can be adjusted to the various full scale values by proper selection of the turns ratio of the output transformer between the output windings and the adjustment of the R1-R2 resistor divider network. The main source

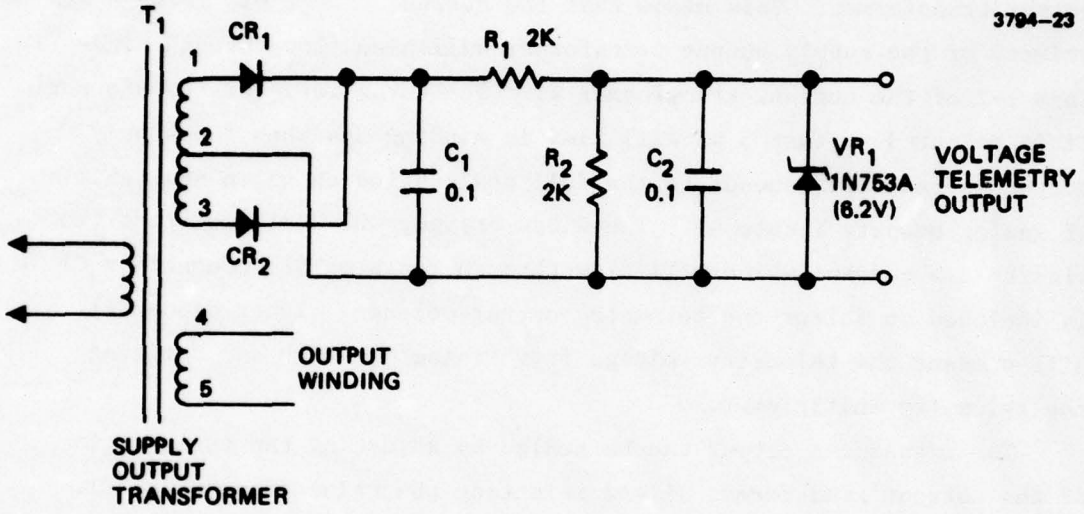

Figure 49. Voltage telemetry transducer schematic.

AD-A063 964 HUGHES RESEARCH LABS MALIBU CALIF F/G 20/7
SATELLITE POSITIVE ION BEAM SYSTEM.(U)
OCT 78 T MASEK F19628-76-C-0066
UNCLASSIFIED AFGL-TR-78-0141 NL

2 OF 3
ADA
063964

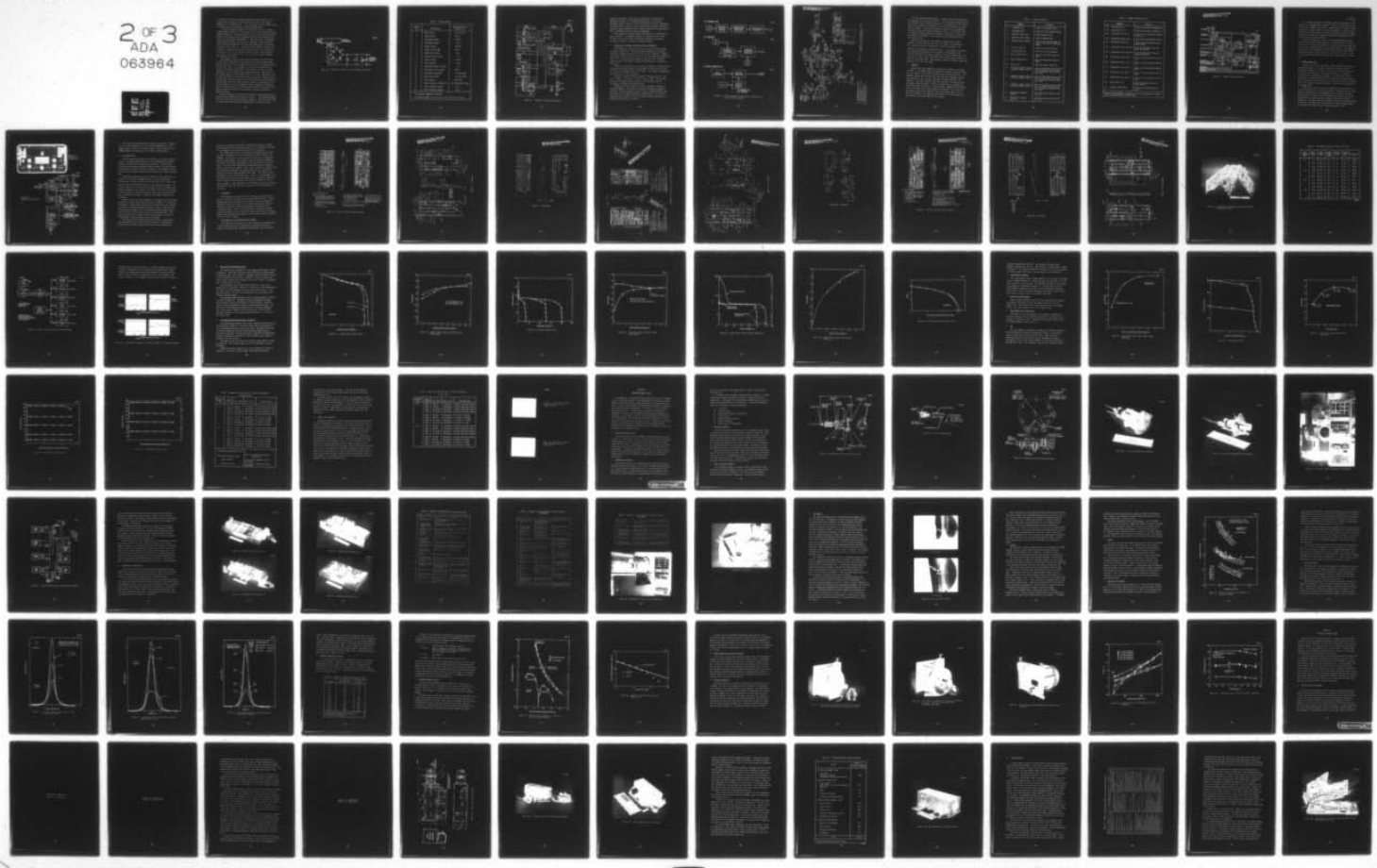

of error of this type of voltage transducer is the variation of the supply output voltage with varying load current due to the output impedance of the supply itself. This can be kept to an acceptable value by taking it into consideration during the design phase.

A current transducer typical of the design to be used is shown schematically in Figure 50. Transformer T1 is in series with the supply output transformer. This means that the current that flows through the primary of the supply output transformer will also flow through windings 1-2 of the current transformer T1. The turns ratio of transformer T1 is selected so that 5 mA will flow in winding 3-4 when the supply output current corresponds to the full scale value shown in the table of analog outputs (Table 4). The diode bridge, CR1-CR4, rectifies the winding 3-4 current which will flow through resistor R1. Capacitor C1 is included to filter the telemetry output voltage. Zener diode VR1 will prevent the telemetry voltage from rising too high and damaging the telemetry multiplexer.

The transducer output can be scaled by adjusting the turns ratio of the current transformer T1 and selecting the value of resistor R1. The main source of error encountered with this type of transducer arises from the fact that, in this design, it is placed in series with the primary of the output transformer. This is done so that the current transformer will not require high voltage insulation. Therefore, any additional loading on the secondary side of the output transformer, such as voltage telemetry, will be reflected on the current telemetry output. In most cases, this will appear as a "zero" offset and can be taken into consideration when the current telemetry channels are calibrated. One feature common to both the voltage and current transducers proposed is that the telemetry output is isolated electrically from the rest of the power processor electronics by utilizing the inherent isolation of magnetic devices.

Eighteen channels of telemetry are provided for monitoring the performance of the SPIBS system as shown in Table 4. The sensing locations for 14 of these quantities are shown in Figure 51. The other four telemetry channels are tank pressure (obtained from a transducer in the

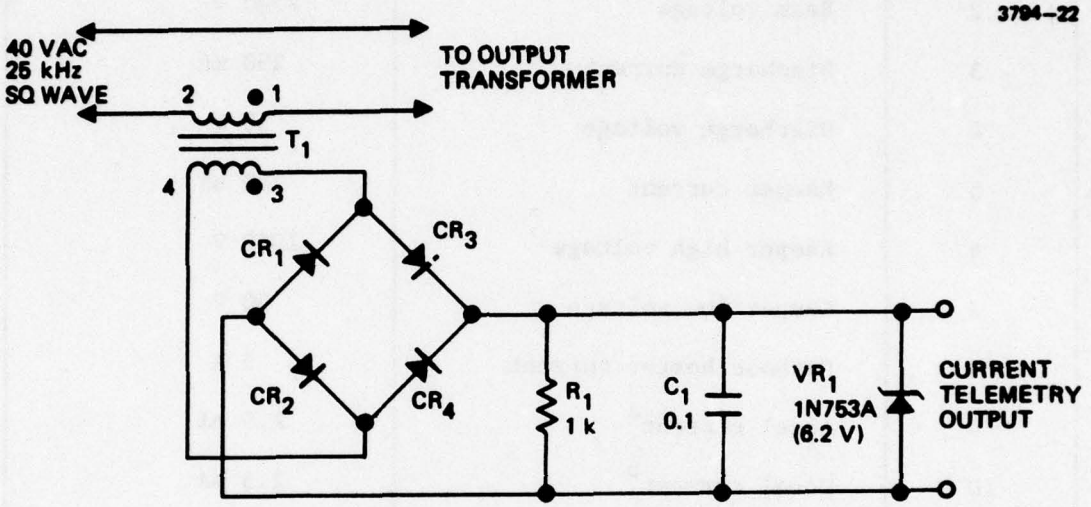

Figure 50. Schematic of typical current telemetry transducer.

Table 4. Analog Outputs

Channel No.	Description	Actual Value for 5 V Output, ±5%
1	Beam current	2.5 mA (±2%)
2	Beam voltage	2500 V
3	Discharge current	250 mA
4	Discharge voltage	50 V
5	Keeper current	250 mA
6	Keeper high voltage	1000 V
7	Keeper low voltage	50 V
8	Cathode heater current	5 A
9	Accel current[a]	2.5 mA
10	Decel current[a]	2.5 mA
11	Neutralizer heater current	5 A
12	Neutralizer bias voltage	1000 V
13	Neutralizer emission[b]	2.5 mA (±10%)
14	SPIBS net current[b]	2.5 mA (±10%)
15	Tank pressure	1500 psia
16	Power processor temperature	See calibration curve
17	PPA ac inverter current	1.5 A
18	PPA ac inverter voltage	50 V

[a] To indicate anomolous condition.

[b] In three ranges: 2.5 to 25 μA; 25 μA to 250 μA to 2.5 mA.

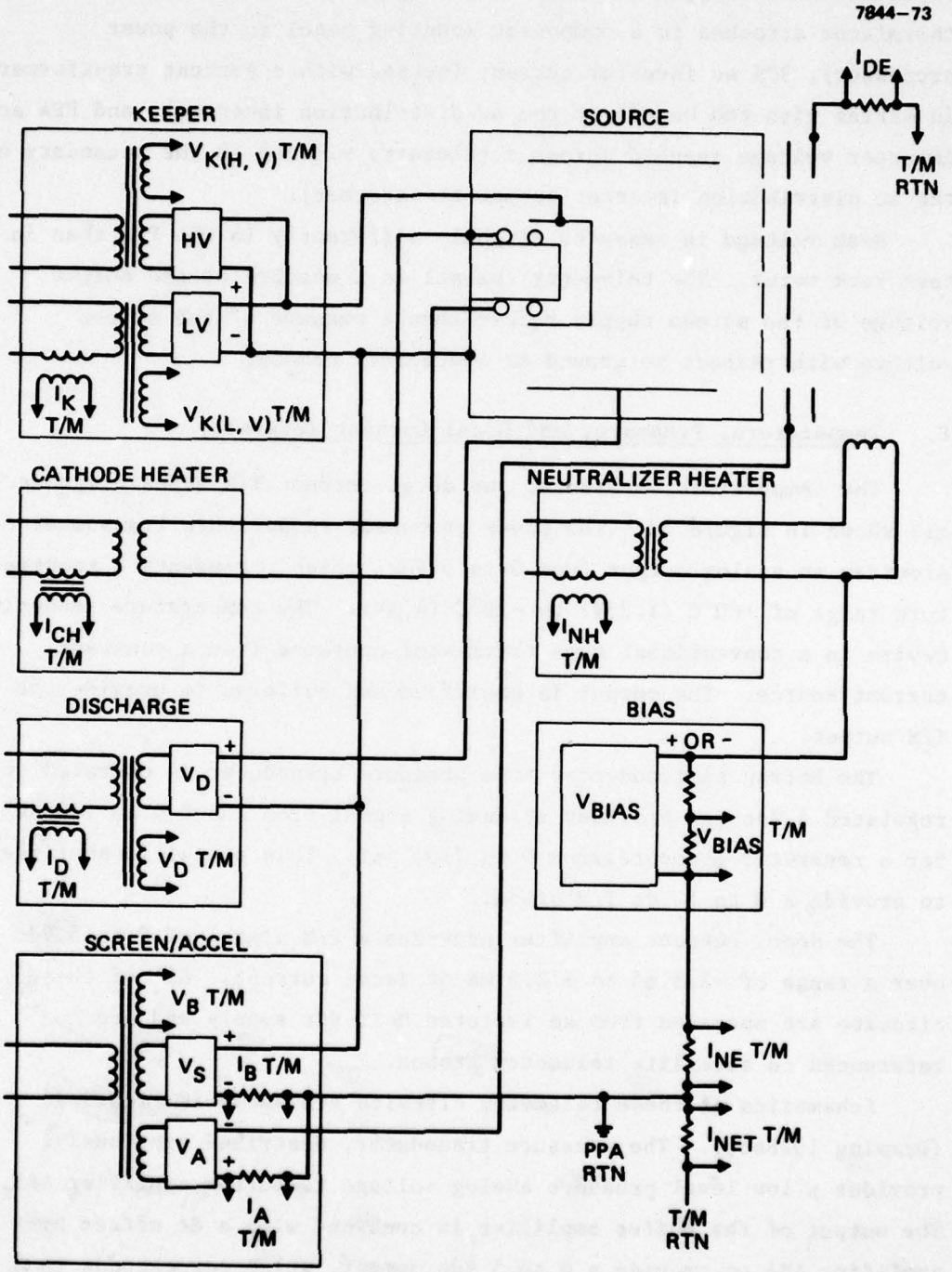

Figure 51. Schematic of sensing locations.

expellant assembly), power processor temperature (obtained from a thermistor attached to a component mounting panel in the power processor), PPA ac inverter current (sensed with a current transformer in series with the output of the ac distribution inverter), and PPA ac inverter voltage (sensed across a telemetry winding in the secondary of the ac distribution inverter output transformer).

Beam voltage is measured slightly differently in the PPA than in test rack meter. The telemetry channel is a measure of the output voltage of the screen supply rather than a measure of the screen voltage with respect to ground or spacecraft common.

8. Temperature, Pressure, and Decel Current Telemetry

The temperature, pressure, and decel current T/M block diagrams are shown in Figure 52. The power processor temperature transducer provides an analog output from 0 to 5 Vdc, which represents a temperature range of +60°C (1.25V) to -20°C (4.4V). The temperature measuring device is a conventional type thermistor operated from a constant current source. The output is amplified and buffered to provide the T/M output.

The Entran semiconductor type pressure transducer is operated from regulated 4 Vdc and provides an analog signal from about 0 to 120 mV for a reservoir pressure from 0 to 1500 psi. This signal is amplified to provide a 0 to 5 Vdc T/M signal.

The decel current amplifier provides a T/M signal of 0 to 5 Vdc over a range of -2.5 mA to + 2.5 mA of decel current. All of these circuits are operated from an isolated ±15 Vdc supply and are referenced to satellite telemetry ground.

Schematics of these telemetry circuits are shown in Figure 53 (Drawing 1028636). The pressure transducer, described previously, provides a low level pressure analog voltage to buffer amplifier AR3. The output of the buffer amplifier is combined with a dc offset by amplifier AR4 to provide a 0 to 5 Vdc output, which corresponds to a reservoir pressure of 0 to 1500 psi.

(a) TEMPERATURE

5145-4

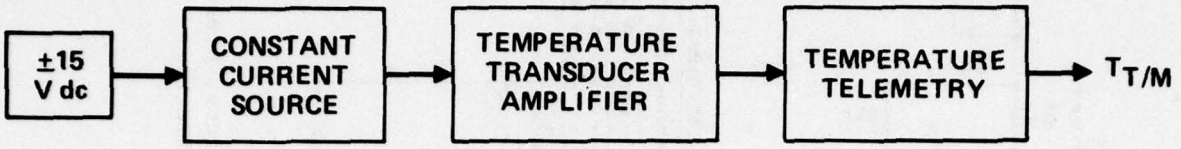

(b) PRESSURE

5145-5

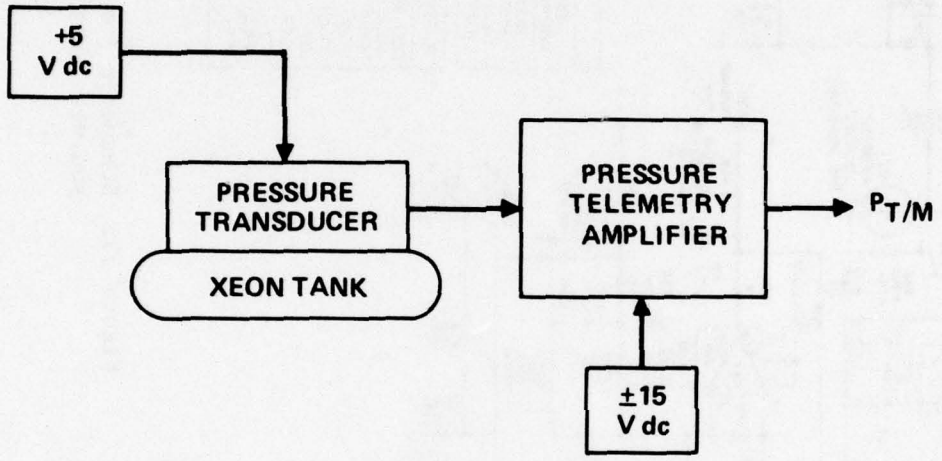

(c) DECEL CURRENT T/M

5145-6

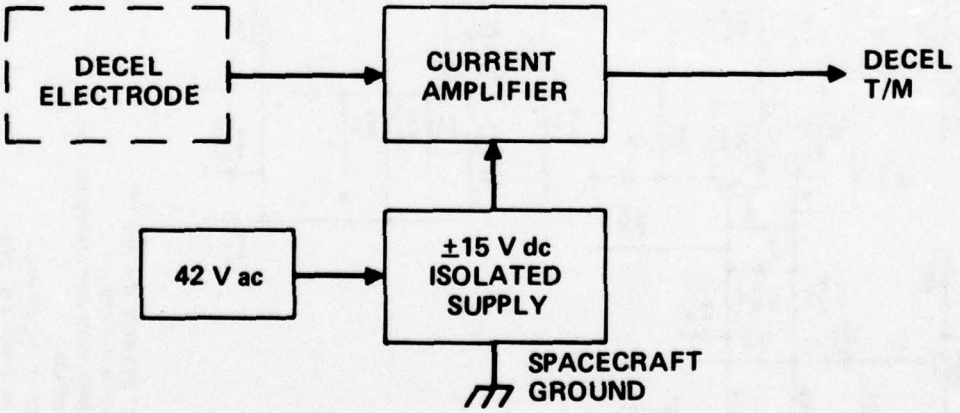

Figure 52. Block diagrams for temperature, pressure, and decel current telemetry.

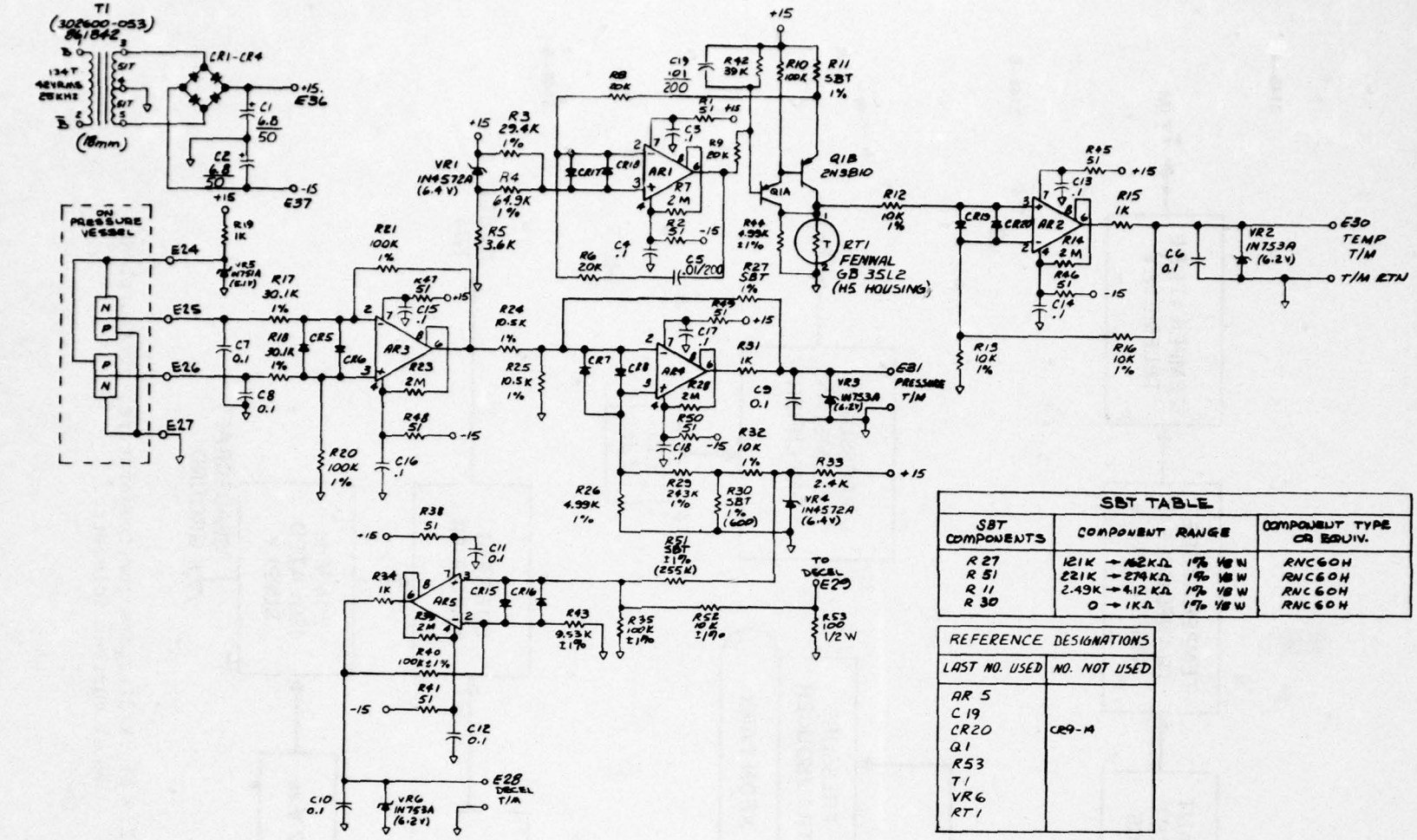

SBT TABLE		
SBT COMPONENTS	COMPONENT RANGE	COMPONENT TYPE OR EQUIV.
R 27	121K → 162KΩ 1% 1/8 W	RNC60H
R 51	221K → 274KΩ 1% 1/8 W	RNC60H
R 11	2.49K → 4.12 KΩ 1% 1/8 W	RNC60H
R 30	0 → 1KΩ 1% 1/8 W	RNC60H

REFERENCE DESIGNATIONS	
LAST NO. USED	NO. NOT USED
AR 5	
C 19	
CR20	CR9-14
Q 1	
R 53	
T 1	
VR 6	
RT 1	

6. S.B.T. MEANS "SELECT BY TEST."
5. ±1% RESISTORS ARE 1/8 W.
4. OPERATIONAL AMPLIFIERS ARE LM4250
3. DIODES ARE IN3600
2. CAPACITORS ARE IN μF 100 VDC
1. RESISTORS ARE IN OHMS, 5%, 1/4W

NOTES- UNLESS OTHERWISE SPECIFIED

Figure 53. Schematic for temperature, pressure and decel current telemetry.

For the temperature measurement, a constant current is supplied to the thermistor by the Q1-AR1 circuitry. The voltage that appears across the thermistor will be representative of the temperature of the surface to which the termistor is mounted (in this case, the baseplate of the power processor). Amplifier AR2 amplifies and buffers the thermistor voltage to obtain the required telemetry voltage. A calibration curve of telemetry voltage versus power processor temperature is used since the thermistor resistance versus temperature is characteristically a nonlinear function.

As shown in Figure 53, the pressure, temperature, and decel telemetry circuitry derives power from the output of transformer T1. This allows the pressure, temperature, and decel telemetry to be isolated from the power processing circuitry. The accuracy of pressure and temperature measurements will primarily be determined by the accuracy with which the initial calibration curves are generated. The decel current which flows through R53 (decel current sense resistor) is detected by amplifier AR5. When properly scaled, the output of AR5 will produce a 0 to 5 Vdc T/M signal.

9. Commands

Twenty-nine ground commands are available in SPIBS, as indicated in Table 5. The command function schematic presented in Figure 54 shows how the commands to the SPIBS accomplish their intended functions. All commands, except the expellant valve open and close commands, control the operation of one or more of the power processor supplies. The commands to the power processor with one exception can be grouped into two types, those that apply or remove AC input power to supplies and those that adjust the level of control signals. Examples of the former are ion gun power on and high-voltage off; examples of the latter are neutralizer bias levels 1 through 5 and beam voltage levels 1 and 2. The one exception to the functions described above is the reversing of the polarity of the bias supply output voltage.

Table 5. Command Capability

	Command	Function
1.	*Instrument on*[a]	Turns on instrument power
2.	*Instrument off*[a]	Turns off all instrument power
3.	*Expellant valve open*	Opens solenoid valve
4.	*Expellant valve closed*	Closes solenoid valve
5.	*Cathode heater preheat*	Turns on the cathode heater to Level 1 and turns on discharge supply
6.	*Ion gun power on*	Turns on the ion gun power
7.	*Ion gun power off*	Turns off the ion gun power
8.	*Beam voltage Level 1*	Sets the beam power supply to 1000 V
9.	*Beam voltage Level 2*	Sets the beam power supply to 2000 V
10.	*Keeper off*	Turns the keeper supply off
11.	*Discharge current and neutralizer emission Level 1*	Sets the discharge current reference to achieve 20 mA current; sets neutralizer emission level to 0.4 mA
12.	*Discharge current and neutralizer emission Level 2*	Sets the discharge current reference to achieve 125 mA current; sets neutralizer emission level to 1.2 mA
13.	*Discharge current and neutralizer emission Level 3*	Sets the discharge current reference to achieve 200 mA current; sets neutralizer emission level to 2.2 mA
14.	*Neutralizer emission Level 4*	Sets neutralizer emission level to 2 μA
15.	*Neutralizer emission Level 5*	Sets neutralizer emission level to 20 μA

Table 5. Command Capability (cont)

Command	Function
16. *Neutralizer No. 1*	Selects neutralizer filament No. 1
17. *Neutralizer No. 2*	Selects neutralizer filament No. 2
18. *Neutralizer heater on*	Turns on the neutralizer cathode heater on
19. *Neutralizer heater off*	Turns off the neutralizer heater
20. *Neutralizer bias off*	Turns off the neutralizer bias power supply
21. *Neutralizer bias positive*	Sets the neutralizer bias for positive polarity
22. *Neutralizer bias negative*	Sets the neutralizer bias for negative polarity
23. *Neutralizer bias Level 1*	Turns on the neutralizer bias to 10 V
24. *Neutralizer bias Level 2*	Turns on the neutralizer bias to 25 V
25. *Neutralizer bias Level 3*	Turns on the neutralizer bias to 100 V
26. *Neutralizer bias Level 4*	Turns on the neutralizer bias to 500 V
27. *Neutralizer bias Level 5*	Turns on the neutralizer bias to 1000 V
28. *High voltage off*	Turns off the beam and accel power supplies
29. *Cathode conditioning*	Turns on the cathode heater to Level 2

[a]In the SPIBS instrument, *instrument on/off* is implemented by connecting or disconnecting 28 V input power.

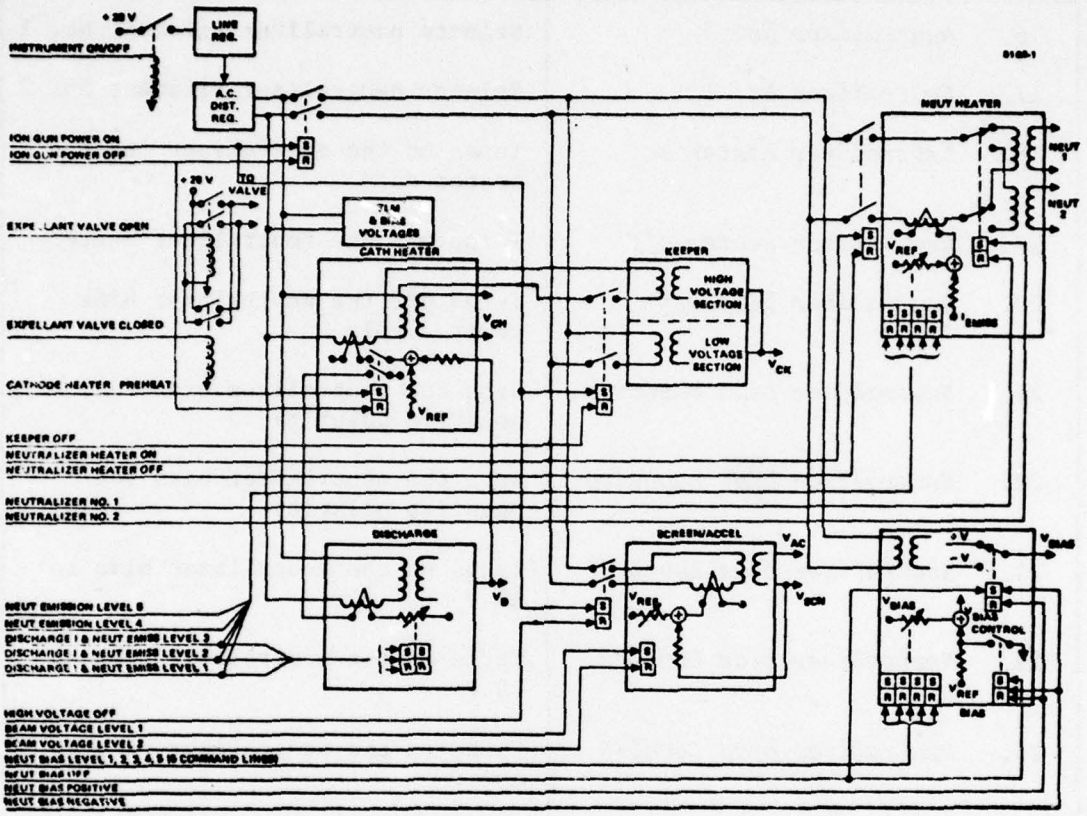

Figure 54. Command function schematic.

All commands received by the SPIBS, except the instrument on/off command, are momentary pulse commands. Therefore, SPIBS must possess the necessary "memory" to maintain a commanded mode of operation until commanded to change. Memory is provided by magnetic latching relays which remain in the set (S) or reset (R) condition until the opposite command is received. All command functions except instrument on/off are achieved with latching relays.

As shown in Figure 54, most level setting commands adjust the current through the control winding of a saturable reactor. The one exception is the bias supply where two series regulators are used, one in the positive supply and one in the negative supply. Also shown are the internal control functions that (1) turn off the cathode heater when the discharge voltage drops below a selected level and (2) turn off the keeper high voltage output when the cathode heater is turned off.

10. SPIBS Command Unit

Ground tests require a method for issuing commands to SPIBS and monitoring telemetry. The SPIBS command unit shown in Figure 55 contains the necessary circuitry to provide the following functions: (1) supply +28 V bus power to the power processor; (2) supply a continuous +28 V instrument on command; (3) generate any of the additional 26 commands described in the command list presented above; and (4) provide a front panel read out of the bus voltage, bus current, and the 18 telemetry inputs listed above. Figure 56 is a schematic of the command unit.

The power processor bus voltage is regulated by sensing the bus voltage at the input to the power processor to compensate for the line drop in the cable between the command unit and the power processor. The sensed bus voltage is used as the feedback signal in the voltage control loop of a commercial power supply capable of 0.05 percent regulation. The same sensed bus voltage is read when the VOLTS position is selected on the DVM input selector switch. When the AMPS position is selected, the output current of the bus supply is read.

Figure 55.
Command unit photograph.

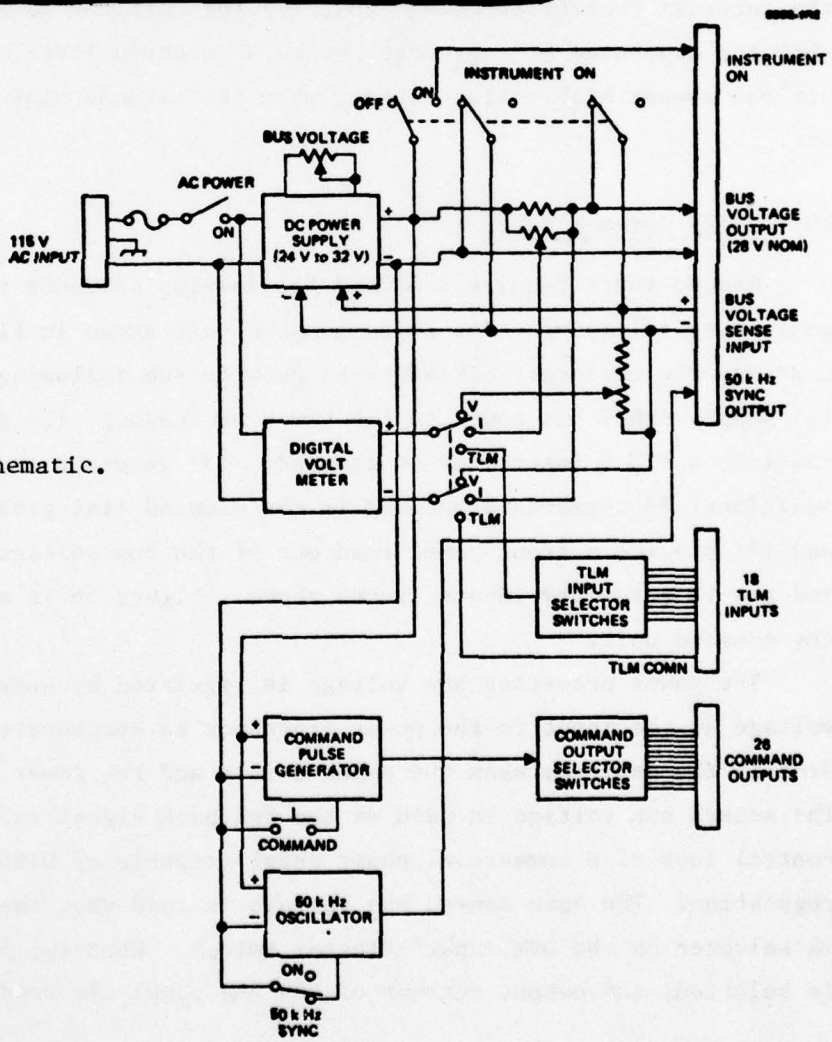

Figure 56.
Command unit schematic.

The output of the command pulse generator is one +28 V, 100 msec pulse for each depression of the front panel COMMAND button. The command pulse is routed to the proper output lead by setting the two COMMAND SELECT rotary switches to the desired command number.

B. PPA FABRICATION

The PPA fabrication process was tailored to the quality requirements of each SPIBS instrument model. The breadboard model PPA was assembled at HRL without detailed specifications. Various design difficulties and design adjustments needed to match ion source characteristics were worked out with the breadboard. The breadboard PPA did not include full command capability and provided only limited telemetry data.

The EM PPA fabrication process provided the first opportunity to evaluate the electronic packaging design. Several problems were encountered in fitting the parts and circuits onto three circuit cards and in fitting the harnessed cards into the structural enclosure. To fit the circuitry into the structural package defined for SCATHA, most magnetic components were bonded to the circuit cards rather than using a stud attachment. During the EM phase, shake tests were performed by AFGL on simulated PPA cards to prove that the bonding technique was acceptable.

EM PPU circuit cards were assembled at the Hughes Culver City plant by personnel familiar with flight electronics assembly in a clean room environment. Harness design and pin-to-pin wiring lists were prepared at Culver City from HRL schematics and parts layouts. Magnetics were fabricated by the Hughes Culver City Components and Materials Laboratory; other EM PPA parts were purchased or fabricated by HRL. The quality assurance level applied to the EM was primarily in terms of craftsmanship; complete inspection was not applied.

The flight model PPA fabrication process involved significantly more documentation and increased quality assurance. Drawings were released and controlled; complete wiring costs were developed and

checked; all electronics parts were screened and placed in a bonded store; magnetics were tested more rigorously; full inspection was given to the assembled circuit cards before and after harnessing.

The flight model circuit card designs and assembly process notes are shown in Figures 57, 58, and 59 (Drawings 1095560, 1095561, and 1095562). The structure of the circuit is machined out of magnesium stock for light weight. The terminal strips and magnetic components are bonded to the cards using Hughes process specification HP 16-103, Type 6. The electrical components are mounted between the terminal strips and hard-wired together. After initial electrical testing of the circuit cards is completed, the high-voltage areas are potted with uralane per HP 16-8 using aluminum oxide filler. The cards are then conformally coated with HP-16-66, type I, class I. A photograph of the flight PPA before potting and conformal coating is shown in Figure 60. The wire bundle in the foreground is eventually attached to the ion source terminals. When installed in the structural enclosure, the cards are secured on top and bottom with screws into nut plates mounted on the cards.

C. PERFORMANCE

The performance characteristics of the PPA can be described in terms of efficiency, regulation, and output characteristics. A block diagram showing efficiencies of the supplies is given in Figure 61. The quantities shown in Figure 61 are typical values; more specific details for each of the individual supplies is discussed in the following sections. Thus, for the conditions illustrated, the PPA overall efficiency is about 36 percent (15 W output with 41.9 W input). Without the neutralizer bias supply, the efficiency is about 48 percent (13 W out for 27 W input).

1. Line Regulator on AC Distribution Inverter

The efficiency and regulation of the combined line regulator and ac distribution inverter (including the line filter) is given in Table 6. These data were taken with the breadboard unit to show the

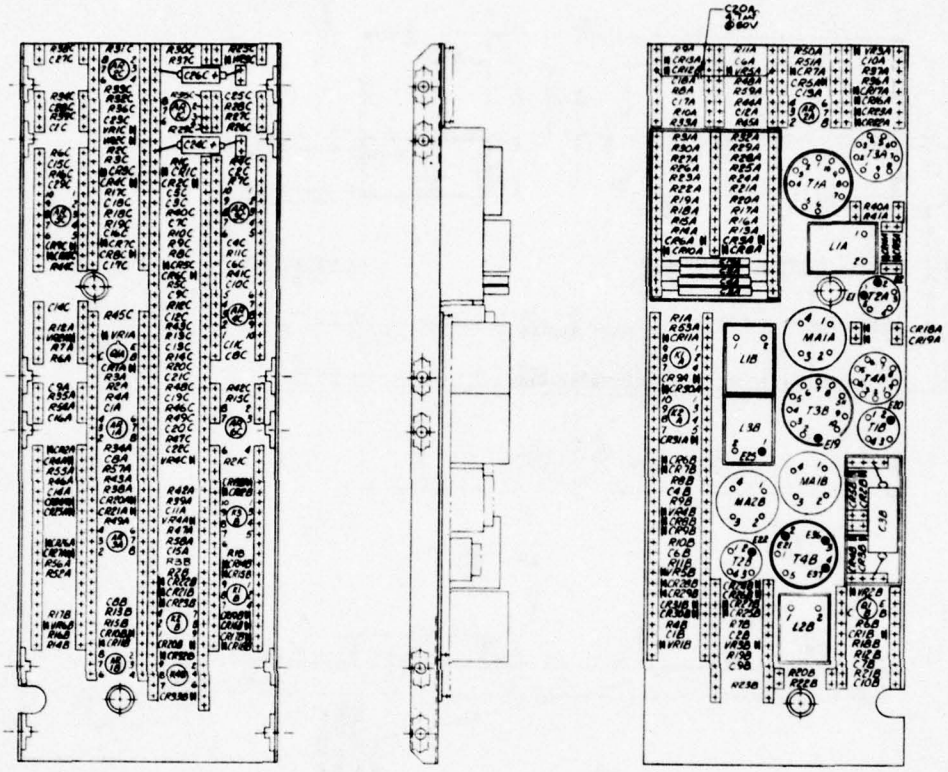

NOTES-UNLESS OTHERWISE SPECIFIED

1. INSTALL PER HP15-38.
2. BOND ALL FAYING SURFACES OF TERMINAL STRIPS MAGNETIC COMPONENTS AND SHEET PLASTIC LAMINATE PARTS, ITEMS 3,4,7 & 8, TO CKT BOARD AND EACH OTHER WHERE APPLICABLE PER HP16-103, TYPE G.
3. FOR SCHEMATIC DIAGRAMS SEE DWGS 1028190 (SCREEN ACCEL), 1028191 (CATHODE HTR AND DISCHARGE SUPPLY), 1028706 (ELECTROMETER #1).
4. ASSEMBLE PER HP11-53.
5. IDENTIFY PER MPB-5, TYPE II.
6. LETTER "A" OR "B" OR "C" ADDED TO COMPONENT REF DESIGNATOR FOR SCREEN ACCEL ("A" CKT), CATHODE HTR AND DISCHARGE SUPPLY ("B" CKT) AND ELECTROMETER #1 ("C" CKT).
7. "E" NO. DESIGNATIONS CODED "0".
8. POT H.V. AREAS WITH URALANE PER HP16-87 USING ALUMINUM OXIDE FILLER MMS 20-1795, TYPE I.
9. CONFORMAL COAT PER HP16-66, TYPE I, CLASS 2.
10. PERFORM PICKLING PROCESS PER HP4-65 PRIOR TO INSTALLATION OF NUT PLATES ON MAGNESIUM CIRCUIT BOARD (1095571).
11. APPLY MARKER DESIGNATORS PER MPB-5 TYPE I, CL B, GRADE A, FORM 2 USING LETRASET TRANSFER MARKING OVERCOAT MARKING DESIGNATORS PER MP6-66 TYPE I, CL 1 OR 2 USING HYSOL PC16 OR PC15 RESIN. MARK EVERY SIX TERMINAL.
12. AFTER TESTING, FILLET BOND C28, C38, C78, C88 C118 & R5A PER MP16-103 TYPE II, CLASS B.
13. BOND ITEMS 1,2,5 & 6, PER MP-25 TYPE 12.

Figure 57. Circuit card part layout drawing.

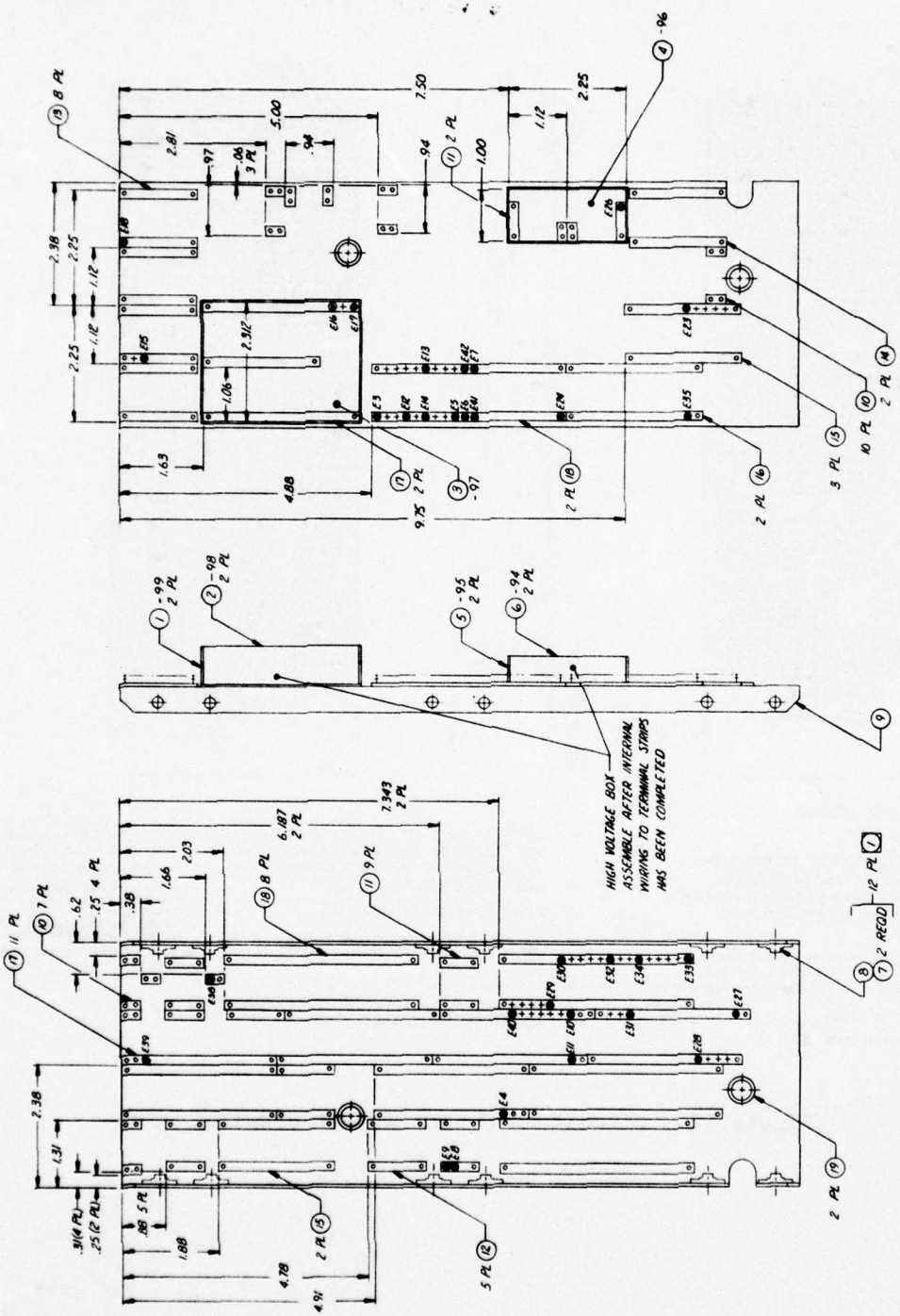

Figure 57. Continued.

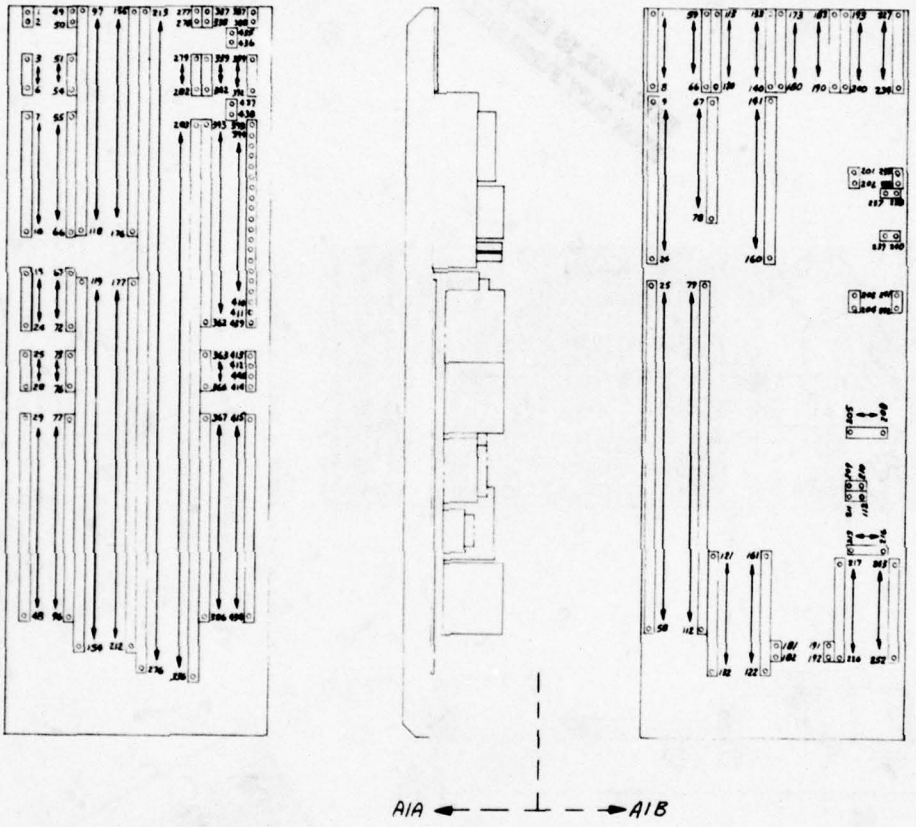

Figure 57. Continued.

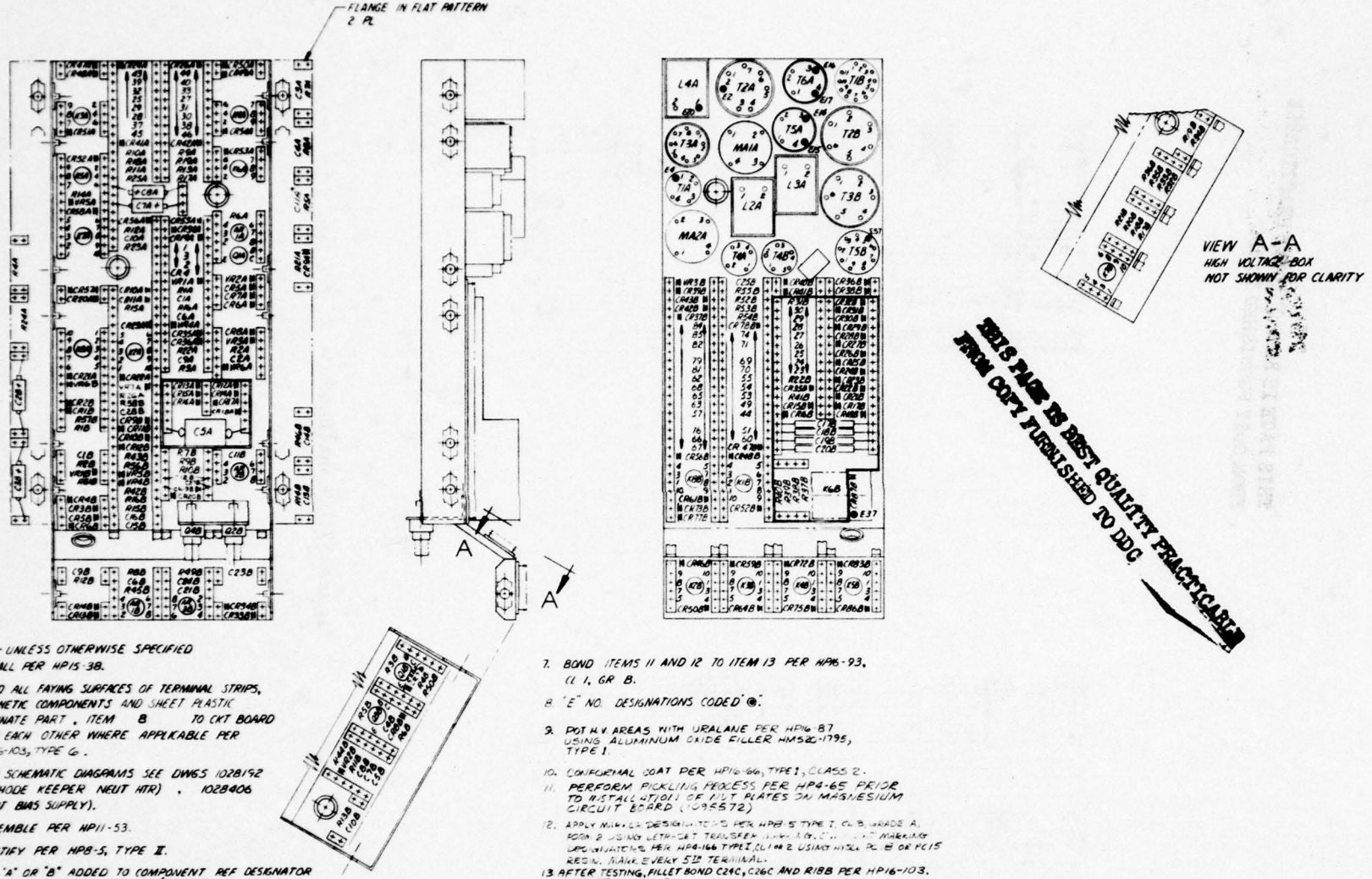

Figure 58. Circuit card part layout drawing.

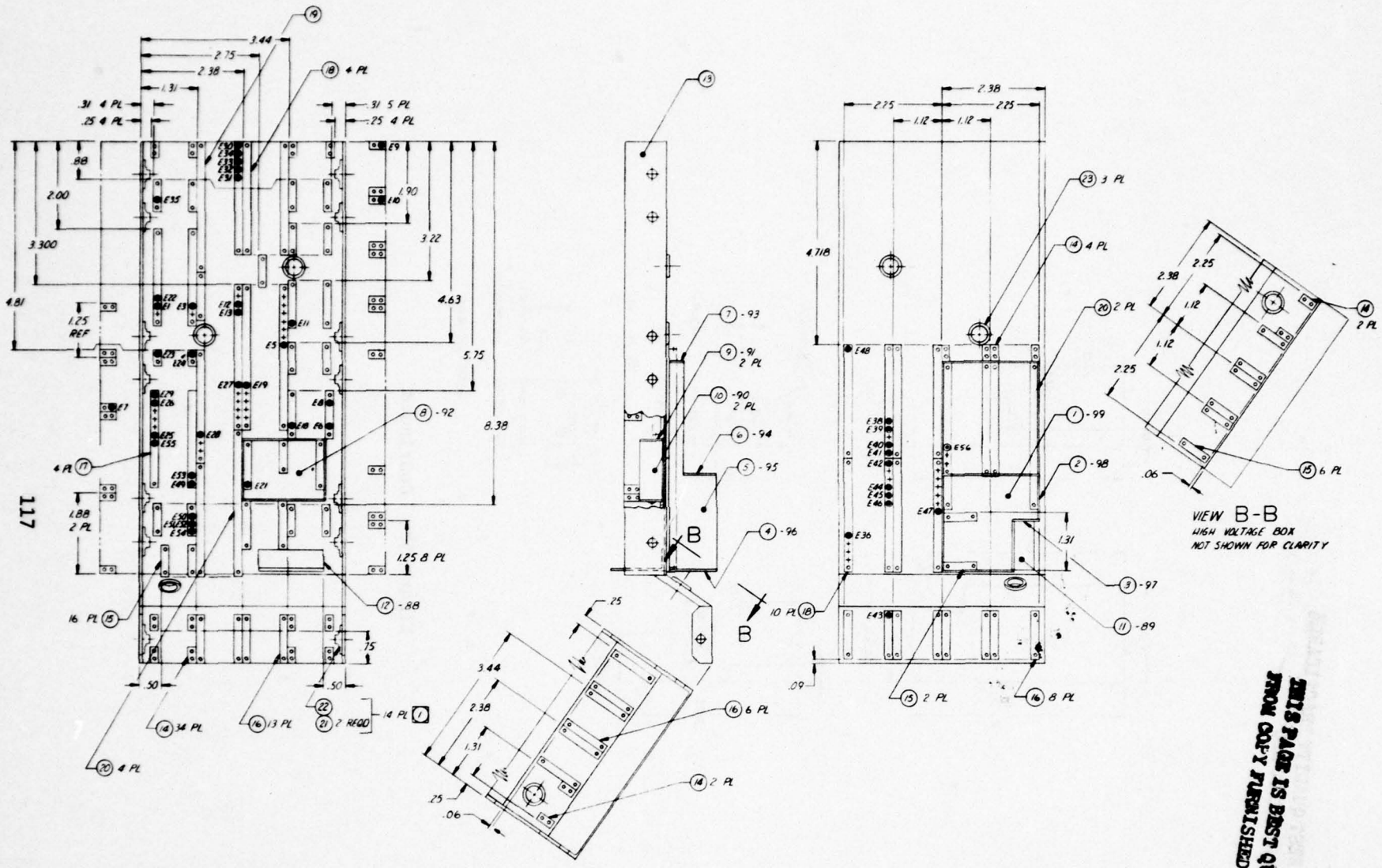

Figure 58. Continued.

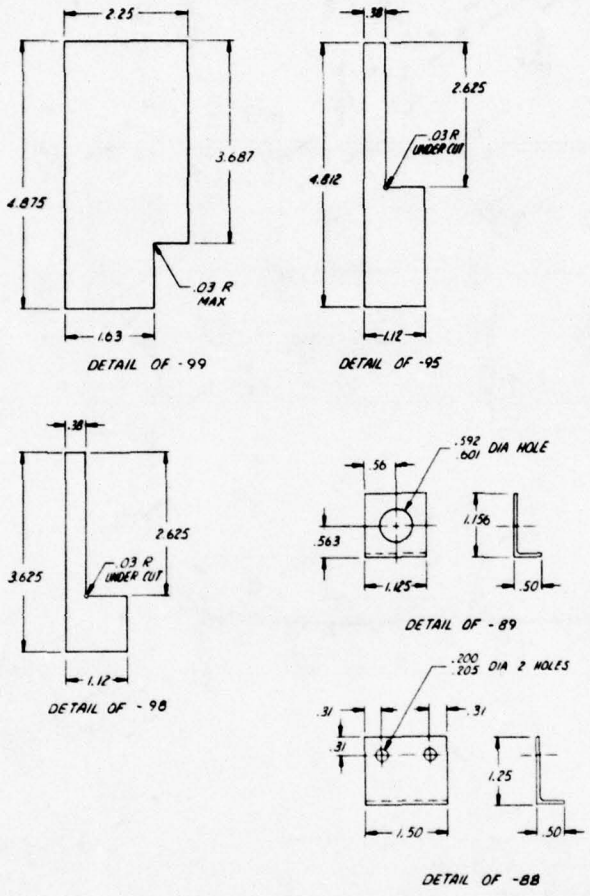

Figure 58. Continued.

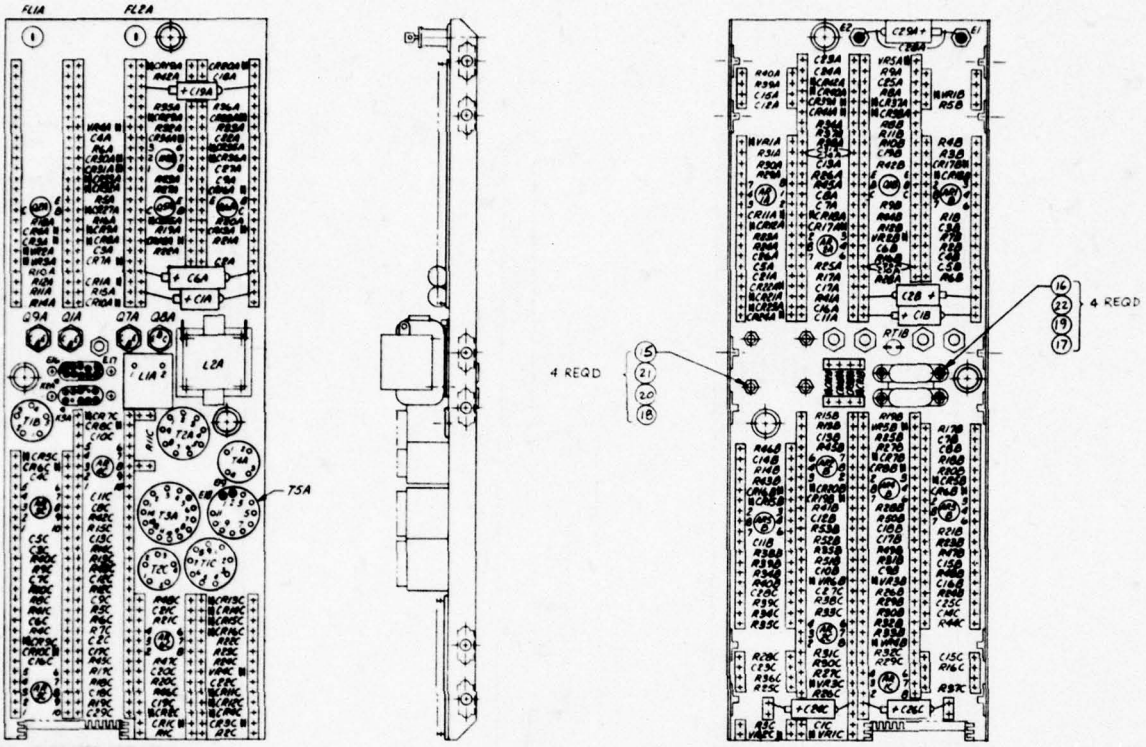

NOTES - UNLESS OTHERWISE SPECIFIED

1. INSTALL PER MP15-38.
2. BOND ALL FAYING SURFACES OF TERMINAL STRIPS, MAGNETIC COMPONENTS AND STRIP GROMMETS TO CKT BOARD PER MP16-103, TYPE G.
3. FOR SCHEMATIC DIAGRAMS SEE DWGS 1028500 (LINE REG AND AC DISTRIBUTION INVERTER), 1028636 (PRESS TEM TM), 1028602 (ELECTROMETER #2)
4. ASSEMBLE PER MP11-53.
5. IDENTIFY PER MP8-5, TYPE II.
6. LETTER "A" OR "B" OR "C" ADDED TO COMPONENT REF DESIGNATOR FOR LINE REG AND AC DISTRIBUTION INVERTER ("A" CKT), PRESS TEM TM ("B" CKT) AND ELECTROMETER #2 ("C" CKT).
7. "E" NO. DESIGNATIONS CODED "●".
8. CONFORMAL COAT PER MP1G-66, TYPE 1, CLASS 2.
9. PERFORM PICKLING PROCESS PER MP4-65 PRIOR TO INSTALLATION OF NUT PLATES ON MAGNESIUM CIRCUIT BOARD (1095573)
10. APPLY MARKER DESIGNATORS PER MP8-5 TYPE I, CL 3, GRADE A, FORM 2 USING LETRASET TRANSFER MARKING. OVERCOAT MARKING DESIGNATORS PER MP4-166 TYPE I, CL 1 OR 2 USING HYSOL PC15 OR PC18 RESIN. MARK EVERY 5TH TERMINAL.
11. AFTER TESTING, FILLET BOND C1A, C6A, C19A, C1B, C2B, C24C, C26C & C29A PER MP16-103, TYPE III, CLASS 3.
12. AFTER TESTING, BOND Q2A, Q5A AND Q6A PER MP16-99, TYPE 3.

Figure 59. Circuit card part layout drawing.

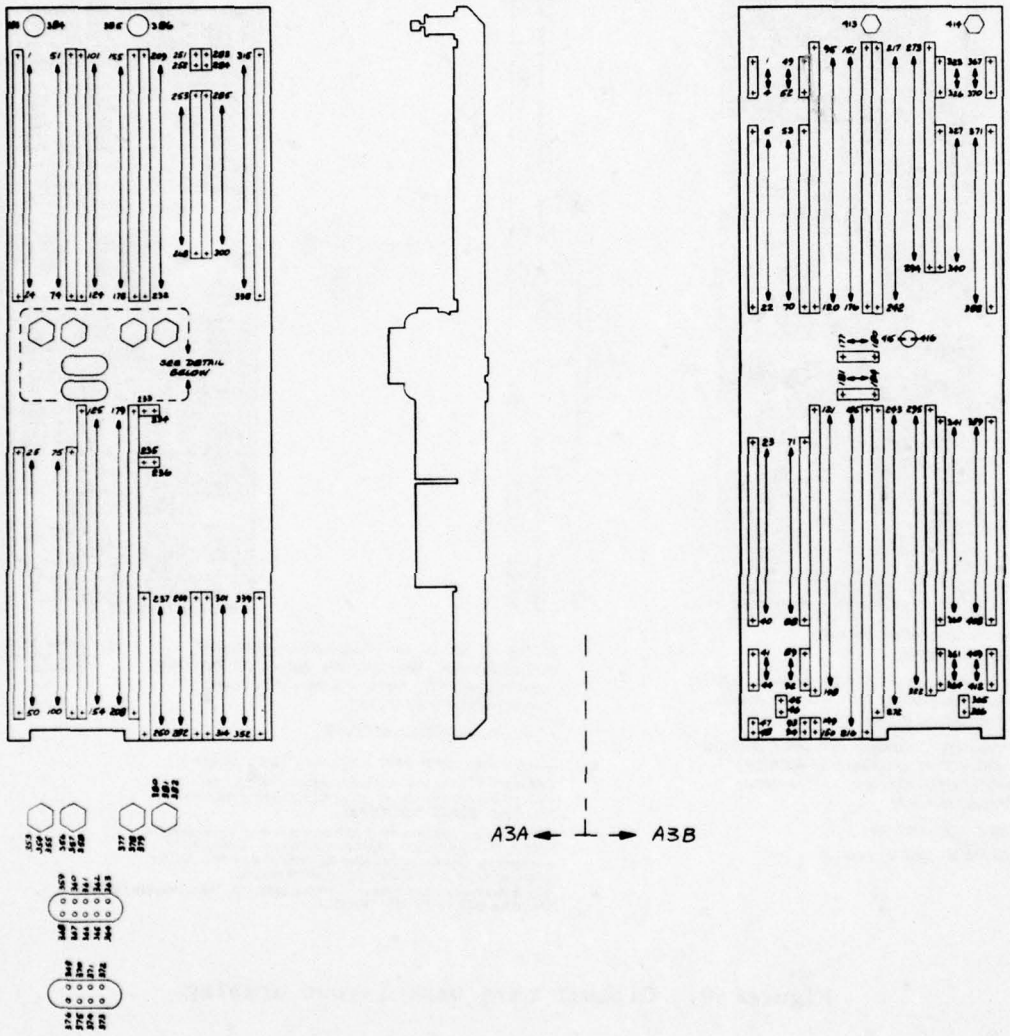

Figure 59. Continued.

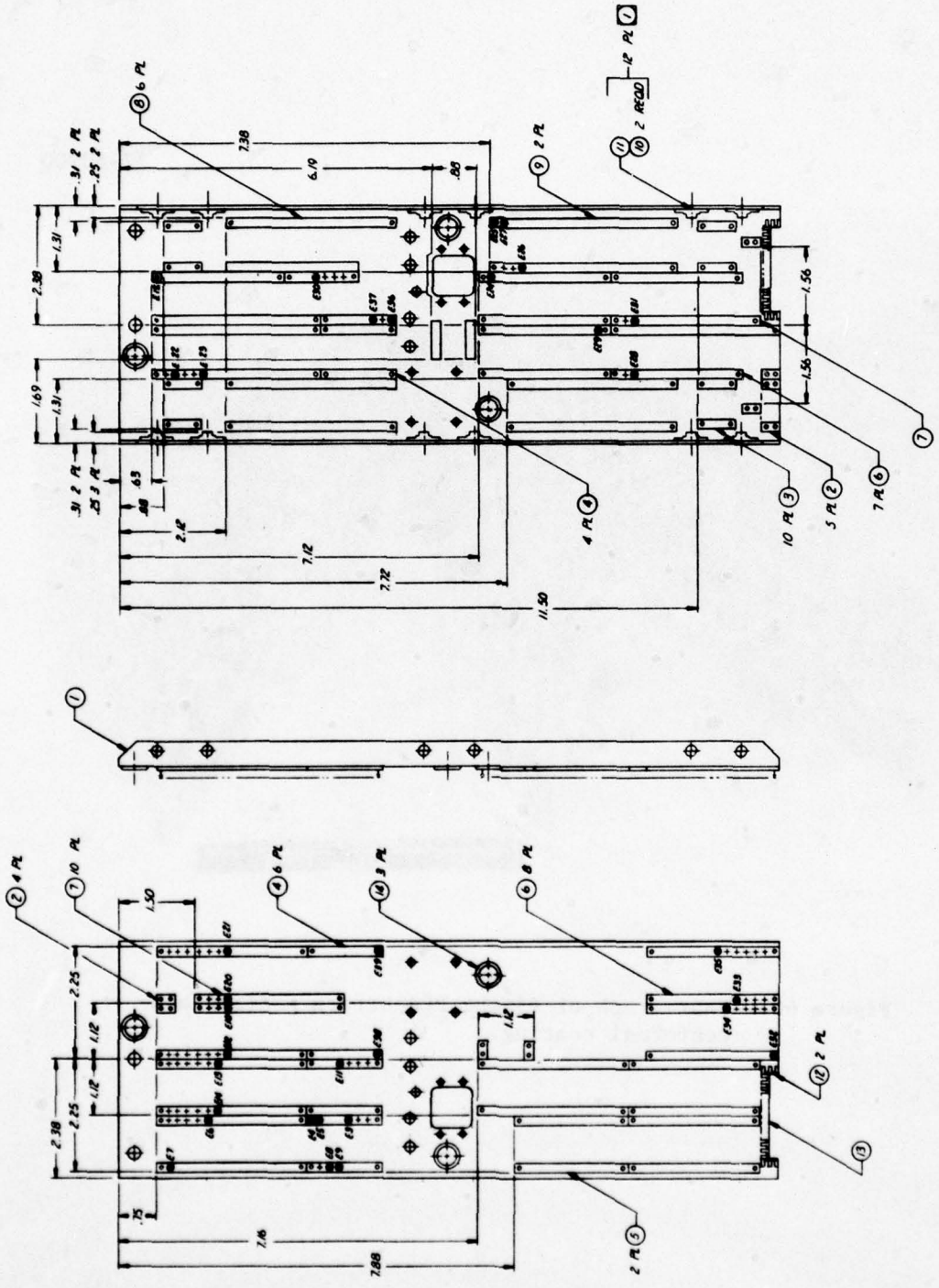

Figure 59. Continued.

77-60700

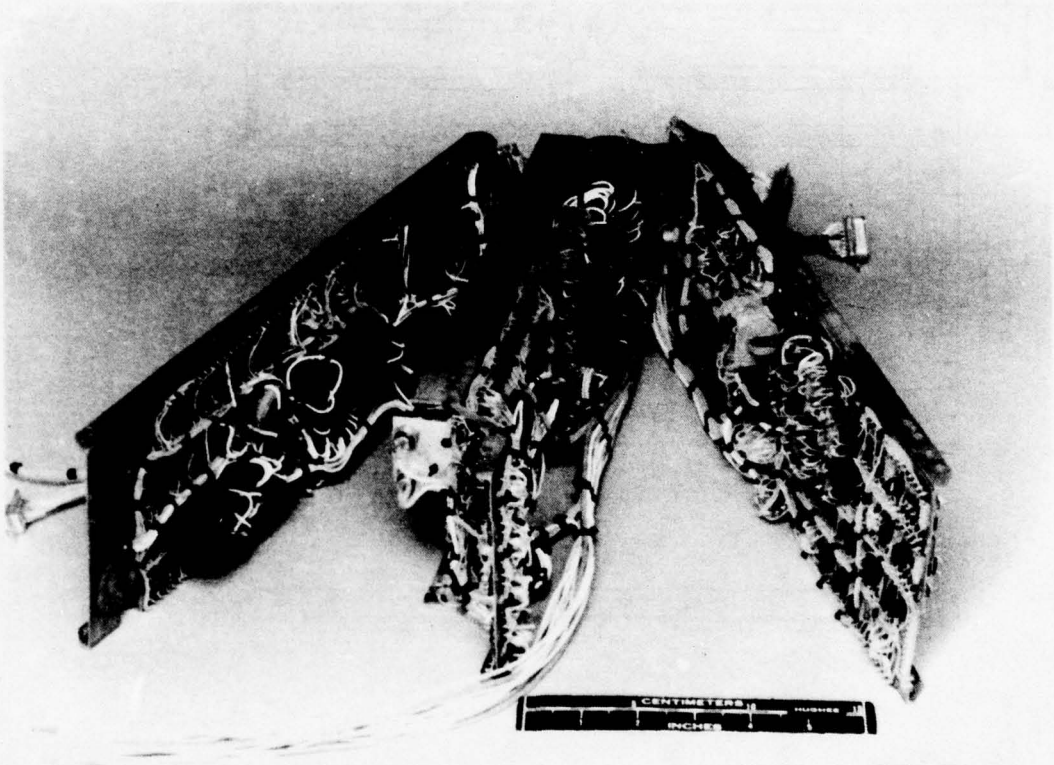

Figure 60. Photograph of flight PPA before potting and conformal coating.

Table 6. Line Regulator and AC Inverter Efficiency

Input Voltage, Vdc	Input Current, A	Input Power, W	Output Voltage, Vrms	Output Current, A	Output Power, W	Efficiency, %
21	1.3	27.3	41.5	0.5	20.75	76.01
	2.39	50.19	39.9	1.0	39.9	79.50
	3.15	66.15	37.0	1.5	55.5	83.90
25	1.28	32.0	42.3	0.5	21.5	66.09
	2.2	55.0	41.8	1.0	41.8	76.00
	3.25	81.25	40.5	1.6	64.8	79.75
30	1.0	30.0	42.3	0.5	21.15	70.5
	1.86	55.8	42.0	1.0	42.0	75.27
	2.76	82.8	40.5	1.6	64.8	78.26
35	0.87	30.45	42.3	0.5	21.15	69.46
	1.64	57.4	42.0	1.0	42.0	73.17
	2.3	80.5	40.5	1.5	60.75	75.46

T6327

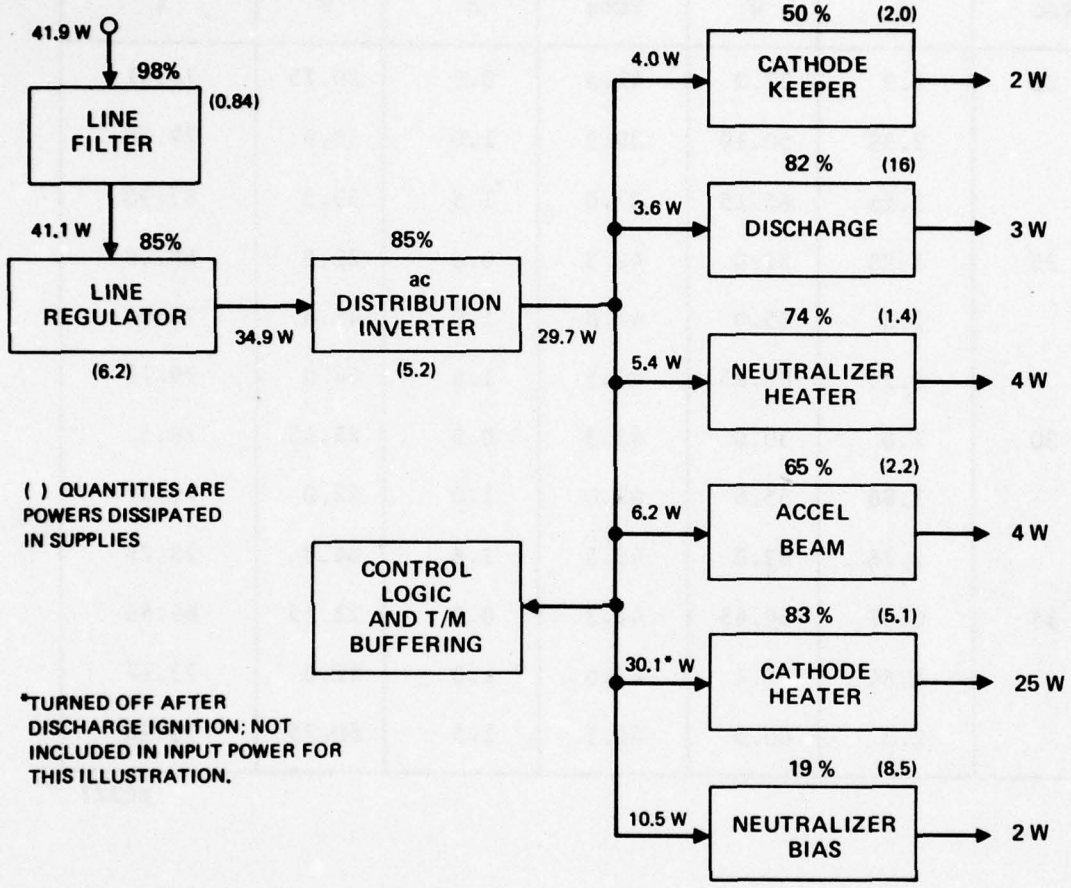

Figure 61. Power processor efficiency block diagram.

characteristics of the basic design. A resistive dummy load was used. Although slight differences exist between the breadboard and flight models (e.g., magnetics fabrication procedures), the characteristics shown in Table 6 should be representative of the final design. The inverter response to step changes in load current is shown in Figure 62.

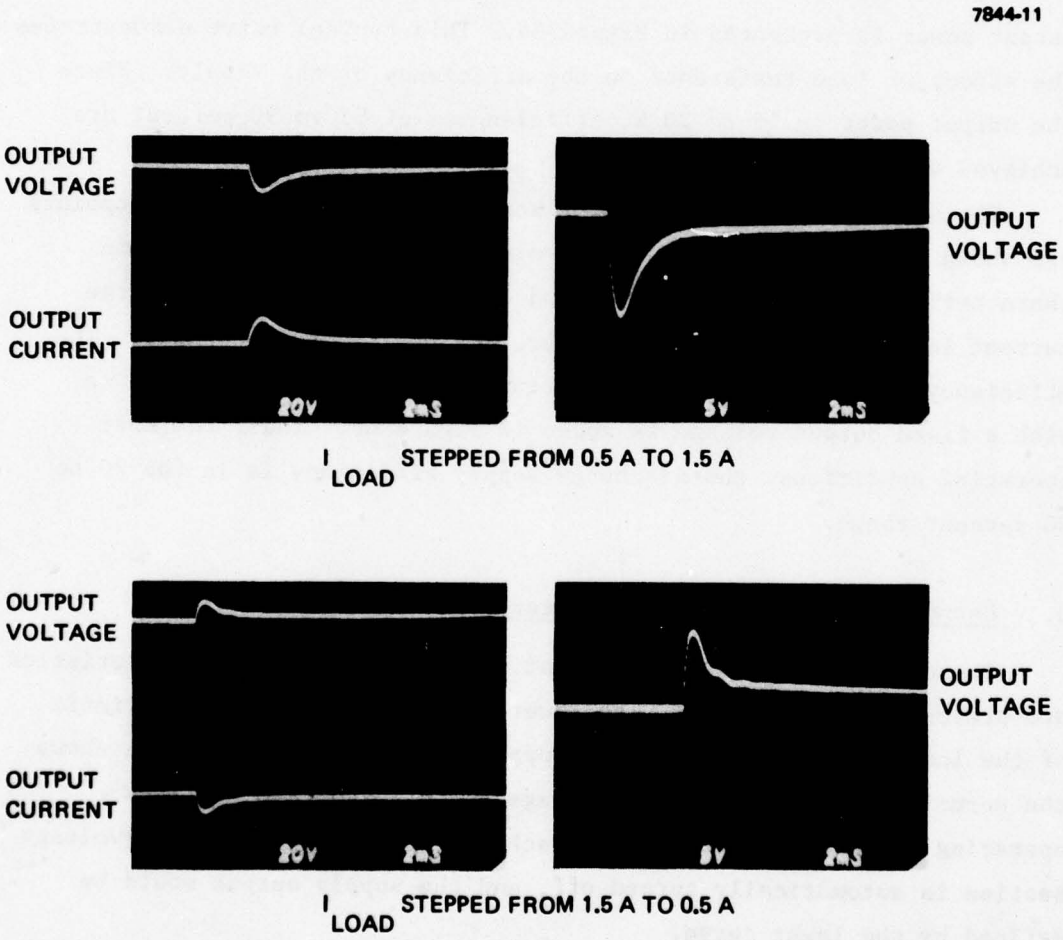

Figure 62. AC distribution inverter transient response to a step load change.

2. Cathode Heater/Discharge Supply

The output current regulation of the cathode heater supply is shown in Figure 63. This figure shows the typical regulation characteristic of the supply and is not intended to represent the final setpoint values. A current limiting characteristic is needed to prevent excessive current at turn-on when heater resistance is low (i.e., about 0.1 Ω compared with 1.2 Ω when heater is hot).

The efficiency of the cathode heater supply as a function of output power is presented in Figure 64. This typical curve demonstrates the effect of load resistance on the efficiency of the supply. Since the output power is 15 to 20 W, efficiencies of 85 to 90 percent are achieved with this supply.

The discharge supply characteristics for several current setpoints are shown in Figure 65. Discharge voltage is determined by plasma characteristics, which in turn depend on zenon flowrate. Discharge current levels are adjusted to produce the desired beam current. The efficiency of the supply when operating into a fixed load impedance with a fixed output voltage is shown in Figure 66. Thus, for most operating conditions, the discharge supply efficiency is in the 70 to 80 percent range.

3. Cathode/Keeper/Neutralizer Heater Supplies

The cathode keeper supply output current regulation characteristics are presented in Figure 67. The lower curve shows the characteristic of the low-voltage section of the supply alone. The upper curve shows the normal output with the low-voltage and high-voltage sections operating in parallel. Once the discharge is ignited, the high-voltage section is automatically turned off, and the supply output would be defined by the lower curve.

The keeper supply efficiency for a range of output power is shown in Figure 68. For a typical output of 6 W, the efficiency is about 80 percent.

Neutralizer heater supply output current regulation is shown in Figure 69. As with the cathode heater, the filament resistance

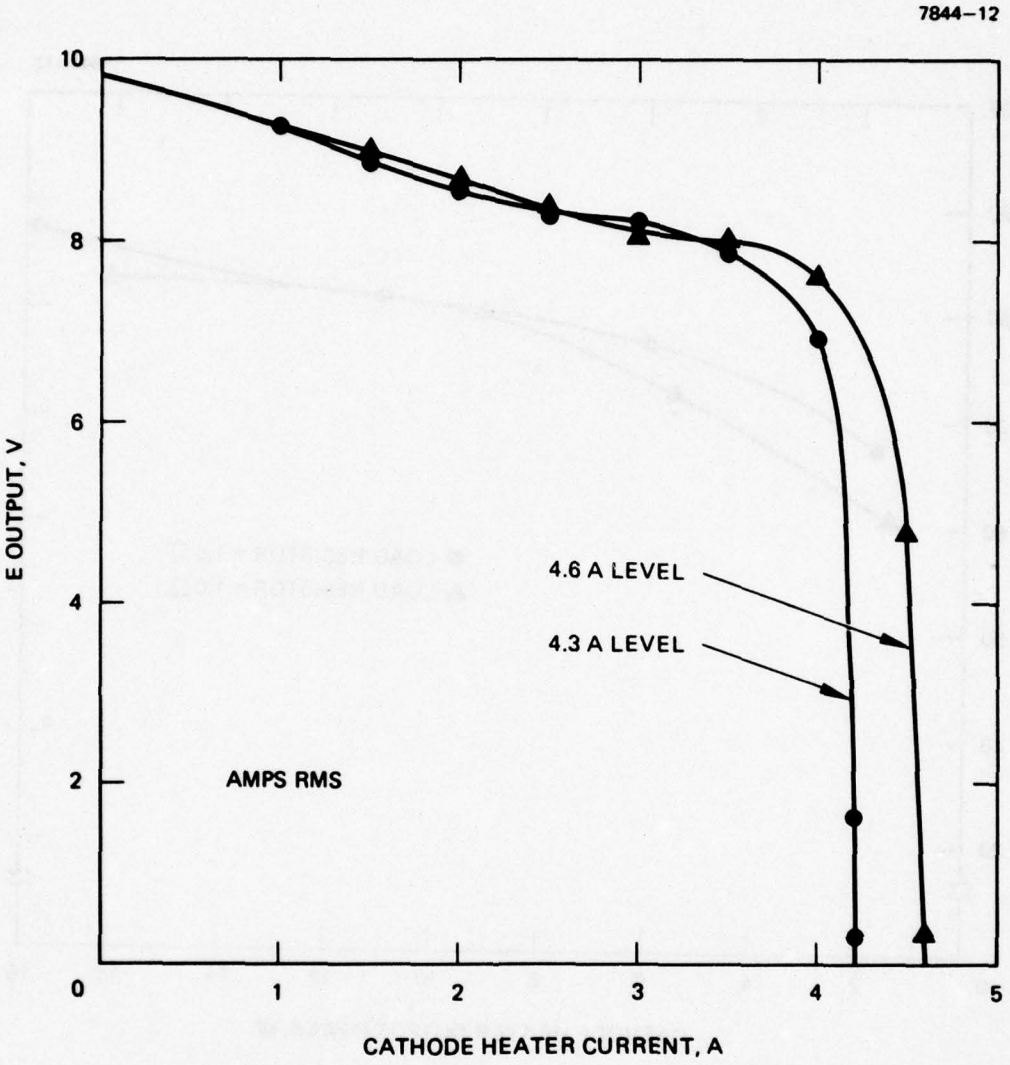

Figure 63. Cathode heater supply output.

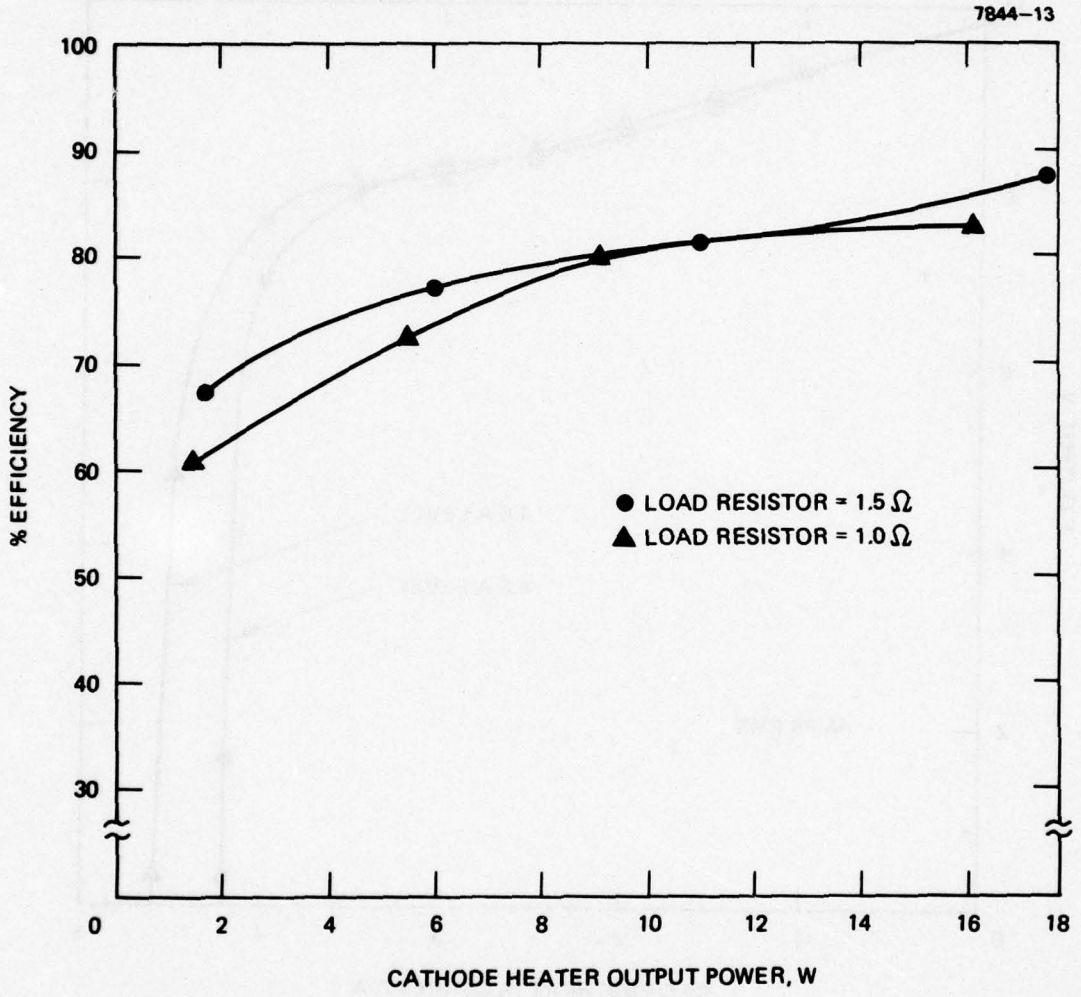

Figure 64. Cathode heater supply-efficiency versus power output.

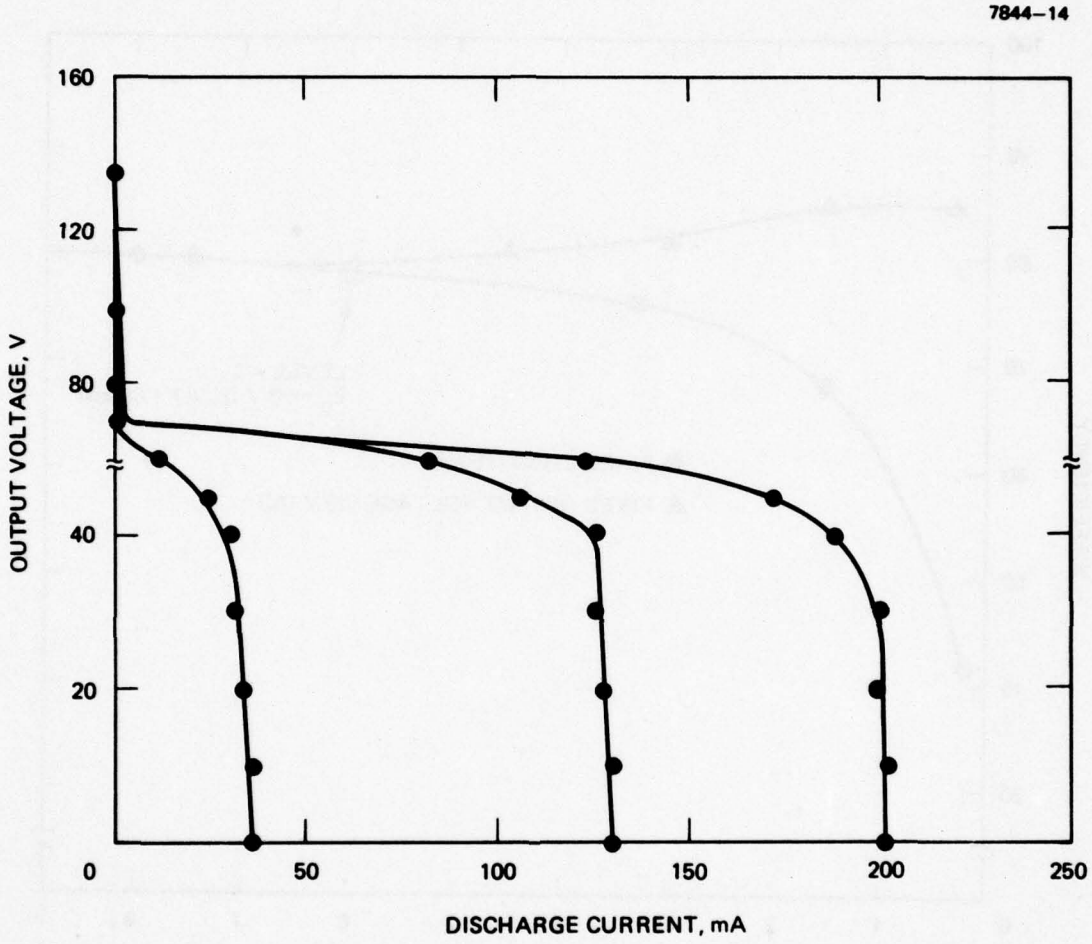

Figure 65. Discharge supply output.

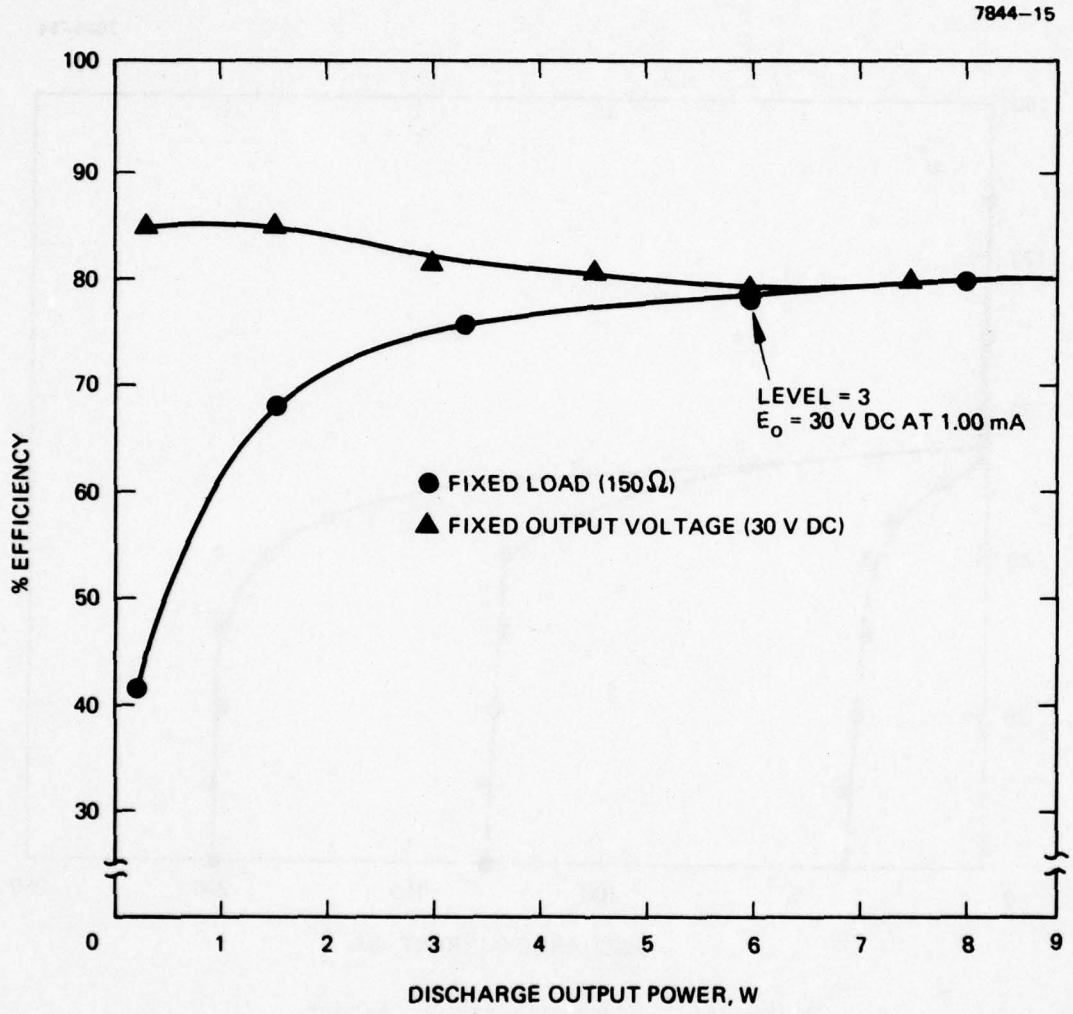

Figure 66. Discharge supply efficiency versus power output.

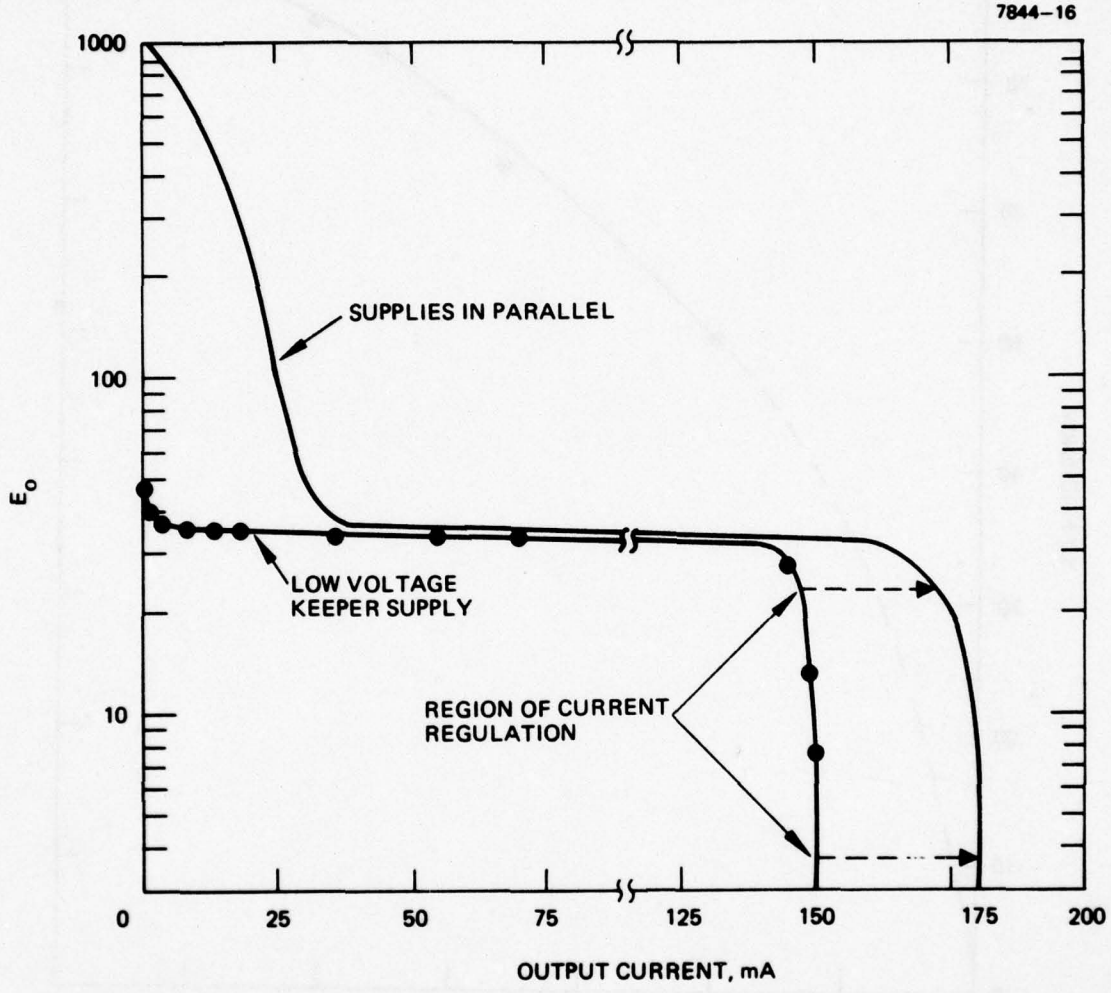

Figure 67. Keeper supply output current regulation.

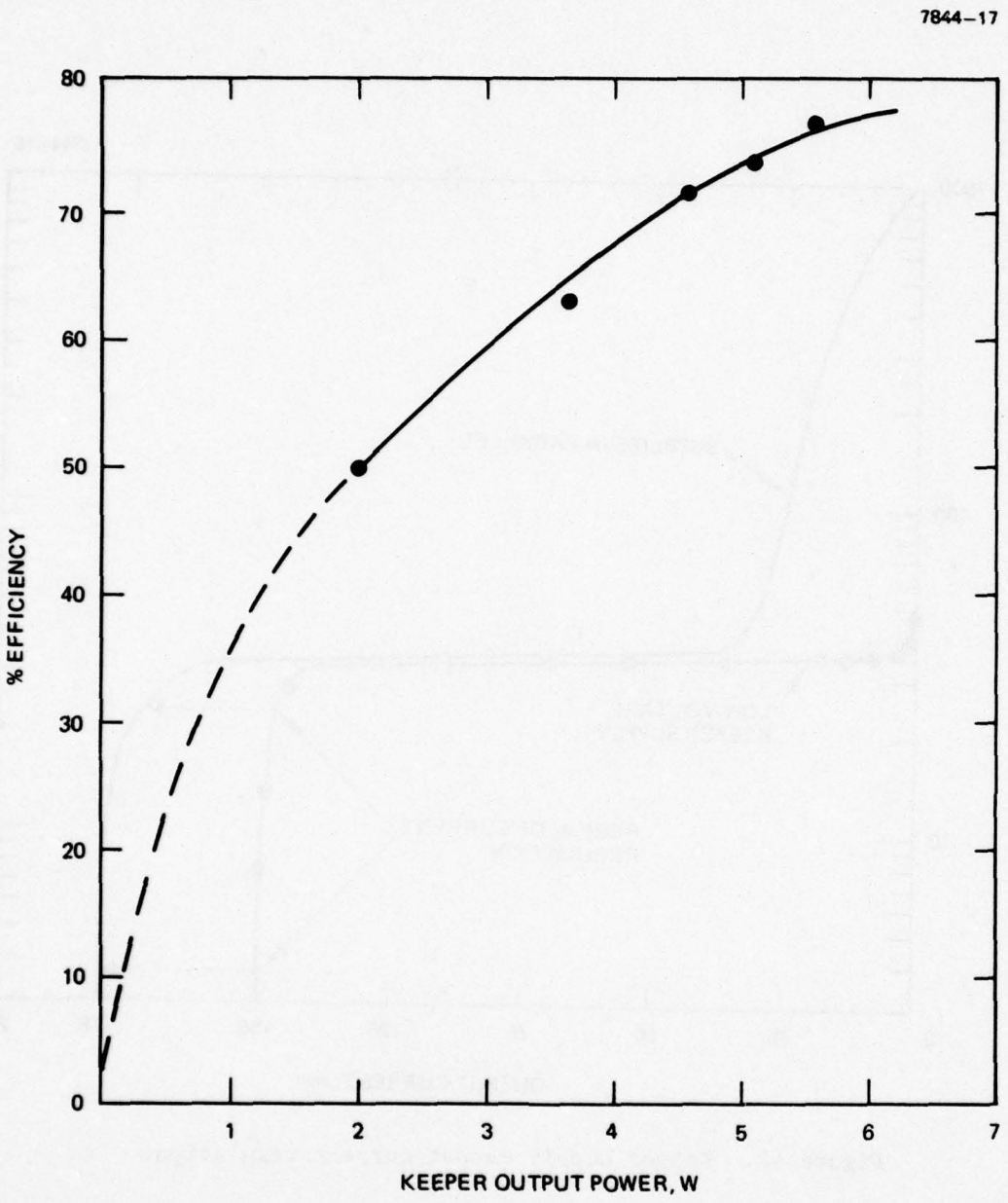

Figure 68. Cathode keeper-power output versus efficiency.

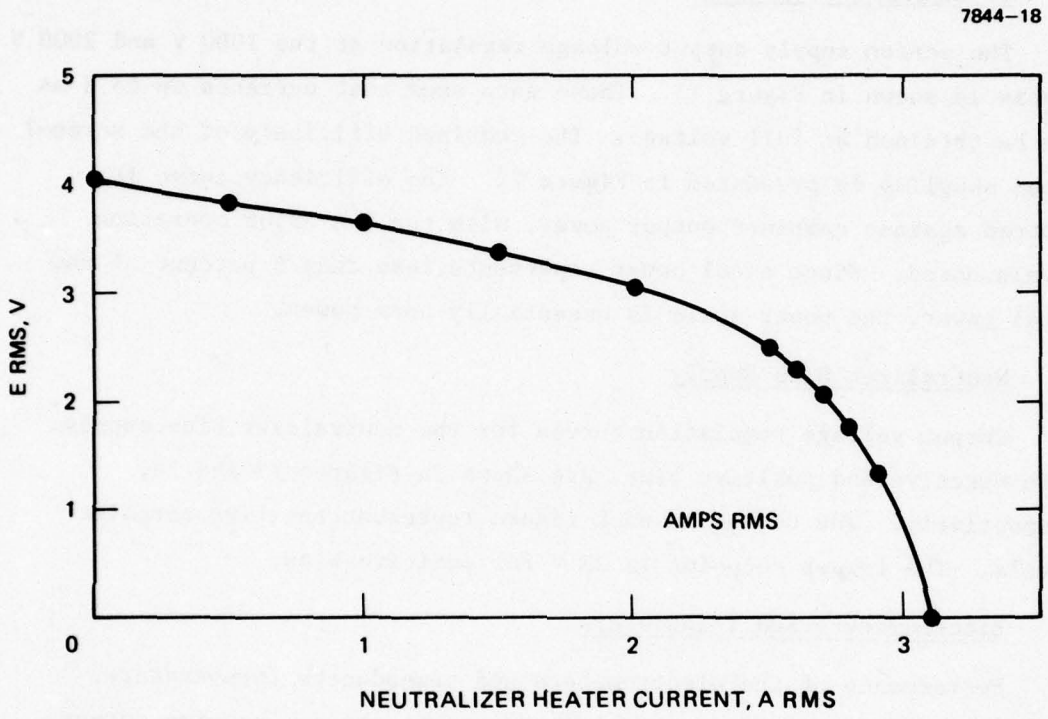

Figure 69. Neutralizer heater supply output.

increases significantly when hot. The current limiting feature prevents overheating at turn-on. The efficiency of this supply is shown in Figure 70. For typical operation at outputs of 2 to 6 W, the neutralizer heater supply efficiency is in the range of 75 to 85 percent.

4. Screen/Accel Supplies

The screen supply output voltage regulation at the 1000 V and 2000 V levels is shown in Figure 71. These data show that currents up to 3 mA can be obtained at full voltage. The combined efficiency of the screen/accel supplies is presented in Figure 72. The efficiency curve is plotted against combined output power, with the two major operating levels noted. Since accel power represents less than 5 percent of the total power, the power scale is essentially beam power.

5. Neutralizer Bias Supply

Output voltage regulation curves for the neutralizer bias supply, with negative and positive bias, are shown in Figures 73 and 74, respectively. The curves in each figure represent the five setpoint levels. The lowest setpoint is 25 V for positive bias.

6. Electrometers and Transducers

Performance of the electrometers and transducers (temperature, pressure, and decel) is best described through the calibration curves presented in Sections 6 and 7. Although these elements require power, the combined demand is less than 1 W.

D. EMI

The line regulator breadboard was checked for conducted emissions (CE01 and CE03) and conducted susceptibility (CS01) in the environmental testing area of the Culver City plant. These tests were conducted using the setup for this type of equipment described in MIL-STD-462, and the results were compared to the levels specified in MIL-STD-461A. Table 7 is a summary of the test data obtained during

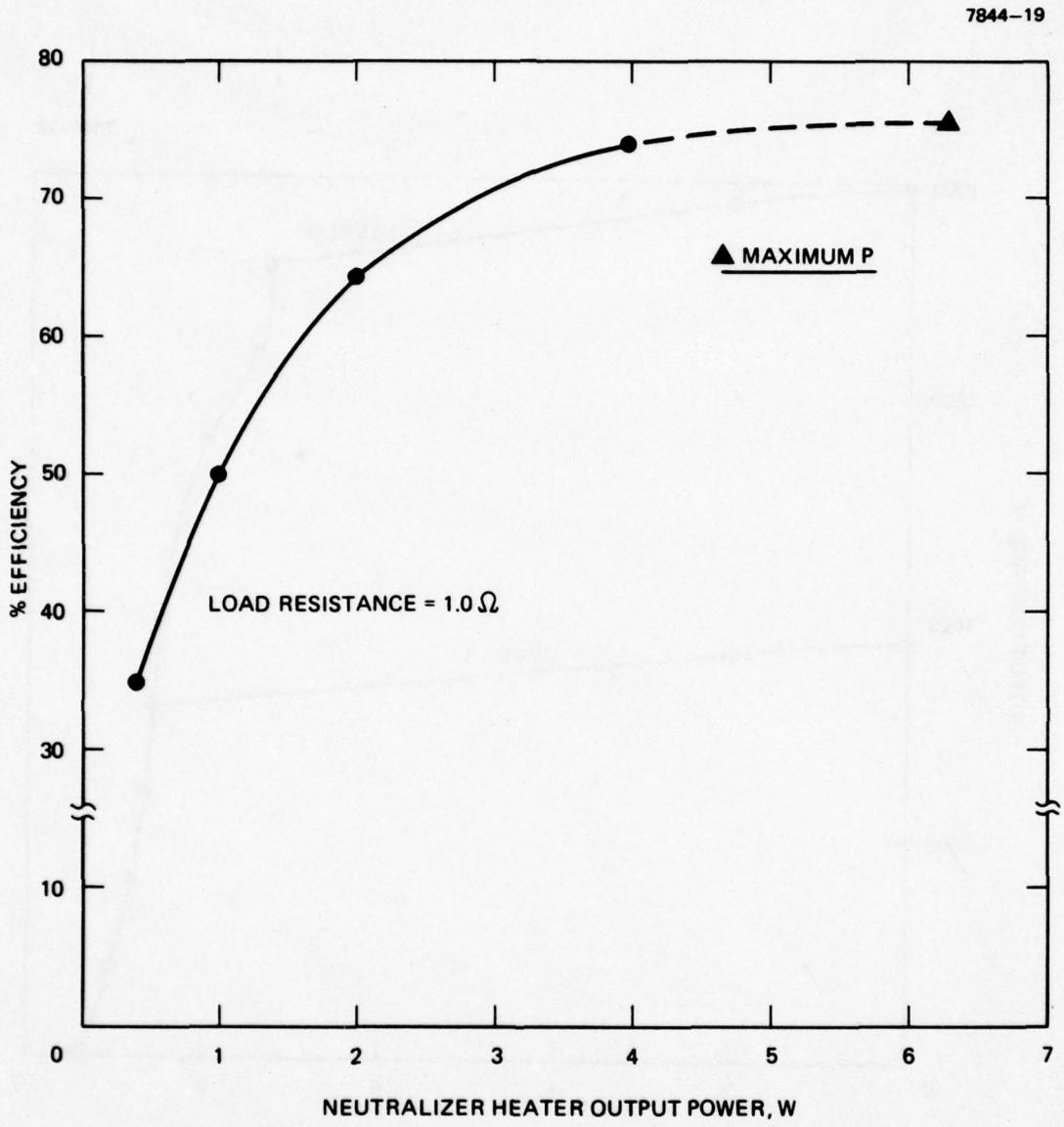

Figure 70. Neutralizer heater output power versus efficiency.

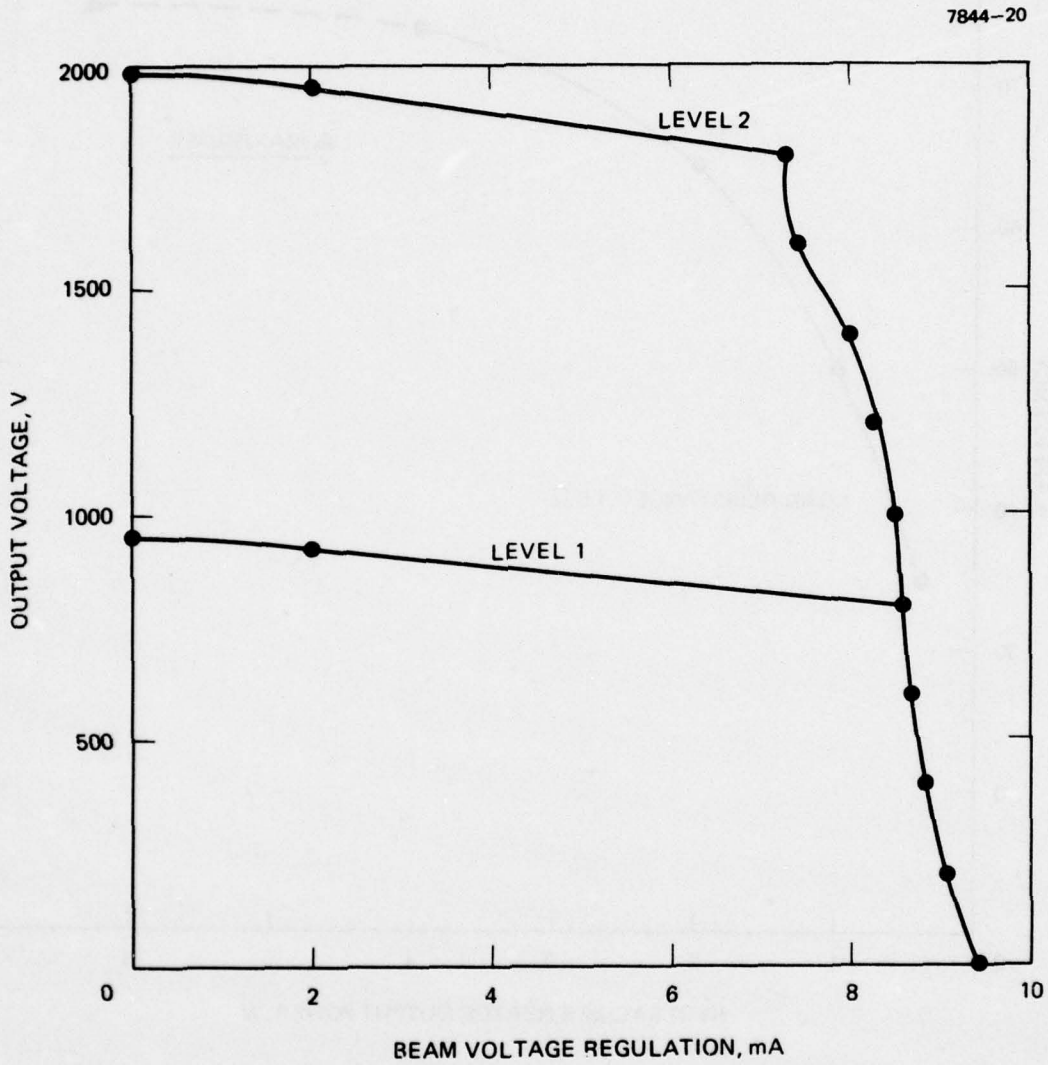

Figure 71. Beam supply output.

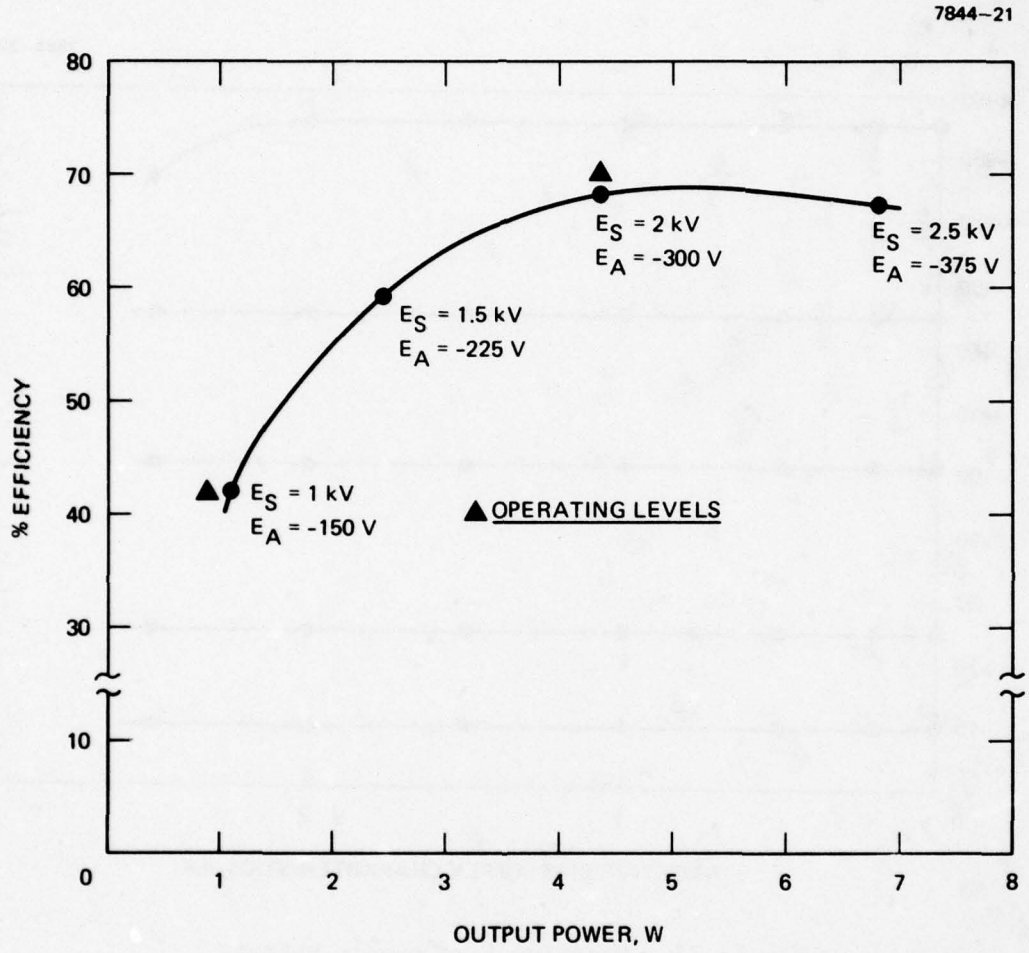

Figure 72. Screen/accel output power versus efficiency.

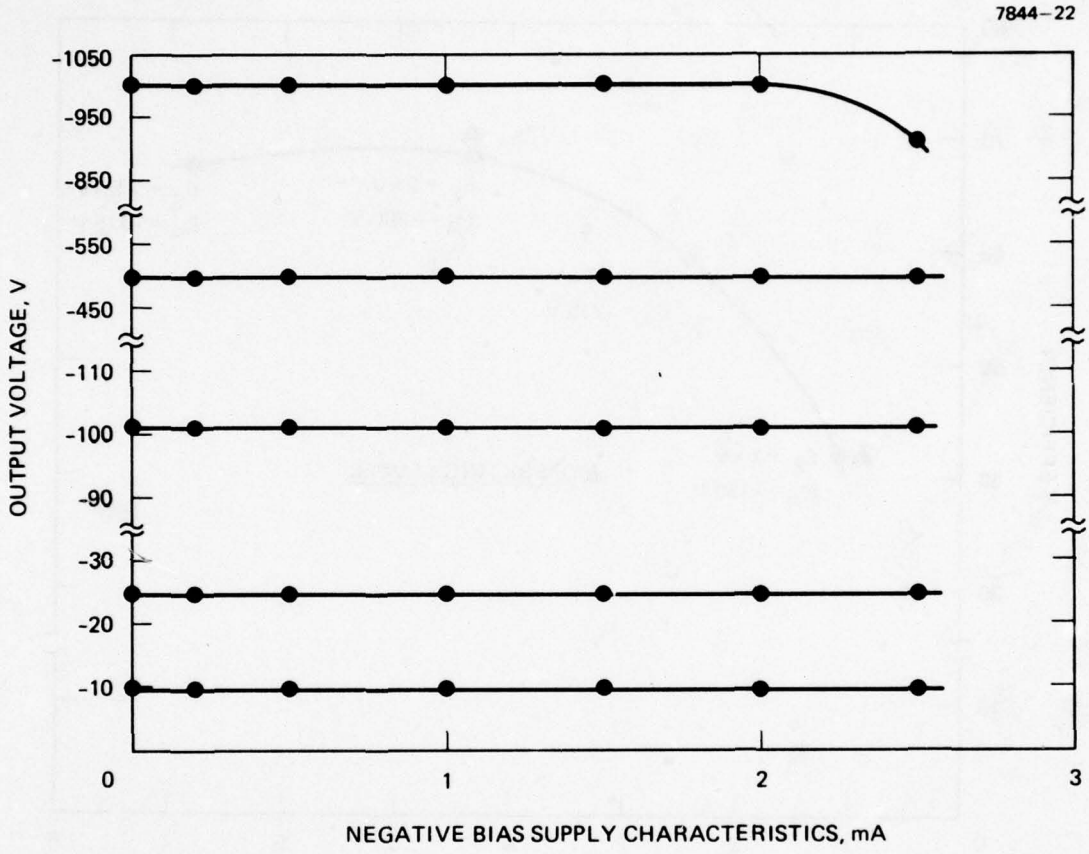

Figure 73. Negative bias supply output.

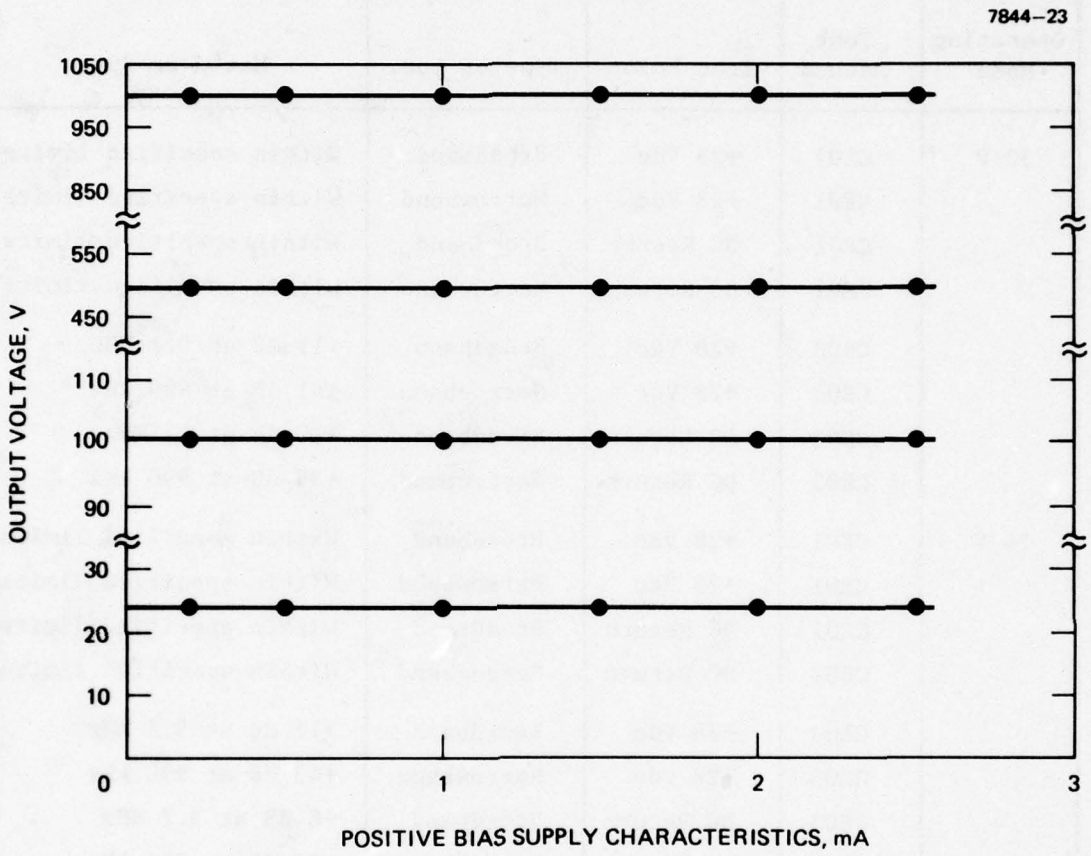

Figure 74. Positive bias supply output.

Table 7. Summary of EMI Test Data: SPIBS Line Regulator

(10 March 1976)

Operating Mode	Test Method	Test Point	Type of Int.	Max Over Spec.
32 V	CE01	+28 Vdc	Broadband	Within specified limits
	CE01	+28 Vdc	Narrowband	Within specified limits
	CE01	DC Return	Broadband	Within specified limits
	CE01	DC Return	Narrowband	Within specified limits
	CE03	+28 Vdc	Broadband	+11 dB at 3.1 MHz
	CE03	+28 Vdc	Narrowband	+41 dB at 990 kHz
	CE03	DC Return	Broadband	+10 dB at 15 MHz
	CE03	DC Return	Narrowband	+39 dB at 990 kHz
24 V	CE01	+28 Vdc	Broadband	Within specified limits
	CE01	+28 Vdc	Narrowband	Within specified limits
	CE01	DC Return	Broadband	Within specified limits
	CE01	DC Return	Narrowband	Within specified limits
	CE03	+28 Vdc	Broadband	+11 dB at 3.2 MHz
	CE03	+28 Vdc	Narrowband	+43 dB at 990 kHz
	CE03	DC Return	Broadband	+8 dB at 3.2 MHz
	CE03	DC Return	Narrowband	+35 dB at 950 kHz

Conducted Susceptibility Test:	
Test Method and Test Point	Worst Case Data Points (Lowest Threshold)
CS01, +28 Vdc	0.11 V rms at 1000 Hz (-28 dB threshold)
CS01, DC return	0.14 V rms at 1000 Hz (-26 dB threshold)

the first test. As noted in Table 7, the unit did not meet the specification for test method CE03 and did not pass the conducted susceptibility test.

The input filter to the line regulator was redesigned to reduce the amount of conducted emissions. The line regulator control loop was modified to reduce its susceptibility. The unit was then returned to the Culver City plant for retesting. The results of this test are summarized in Table 8. Improvements beyond these levels would require significant filter weight increases, and further changes were not introduced.

E. INPUT LINE TRANSIENTS

The major transient on the power bus occurs when power is applied to the PPA (Instrument On command). The current surge observed is the result of charging the line regulator input filter capacitor. Tests were performed on the breadboard system to determine the peak value of the turn on current surge. The first test performed used the input filter configuration present during the 10 March 1976 EMI test. A photograph of the surge current is shown in Figure 75. The peak current observed in this figure is 30 A. The line regulator was retested using the EMI filter additions before the 9 July 1976 EMI test. The results of the second transient test are shown in Figure 76. The initial 43 A peak observed in this figure, and not observed the previous test, is due to the addition of capacitance between the input filter choke and the input power bus. Since the additional current peak is of short duration and would not adversely affect the spacecraft fusing requirements, it was decided to finalize the filter design in the configuration used in the 9 July EMI test.

Table 8. Summary of EMI Test Data: SPIBS Line Regulator

(9 July 1976)

Operating Mode	Test Method	Test Point	Type of Int.	Max Over Spec.
32 V	CE01	+28 Vdc	Broadband	Within specified limits
	CE01	+28 Vdc	Narrowband	Within specified limits
	CE01	DC return	Broadband	Within specified limits
	CE01	DC return	Narrowband	Within specified limits
	CE03	+28 Vdc	Broadband	+2 dB at 2.29 MHz
	CE03	+28 Vdc	Narrowband	+11 dB at 1.85 MHz
	CE03	DC return	Broadband	+10 dB at 2.27 MHz
	CE03	DC return	Narrowband	+9 dB at 1.7 MHz
24 V	CE01	+28 Vdc	Broadband	Within specified limits
	CE01	+28 Vdc	Narrowband	Within specified limits
	CE01	DC return	Broadband	Within specified limits
	CE01	DC return	Narrowband	Within specified limits
	CE03	+28 Vdc	Broadband	Within specified limits
	CE03	+28 Vdc	Narrowband	+8 dB at 1.66 MHz
	CE03	DC return	Broadband	+2 dB at 2.28 MHz
	CE03	DC return	Narrowband	+10 dB at 1.73 MHz

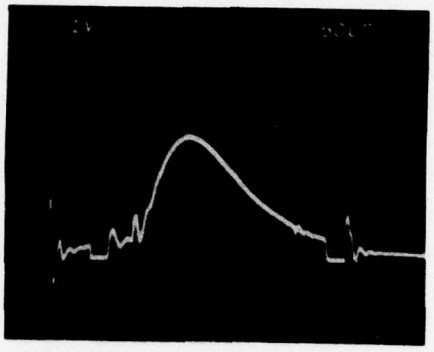

Figure 75. PPA turn-on current surge using EMI filter of 10 March 1976.

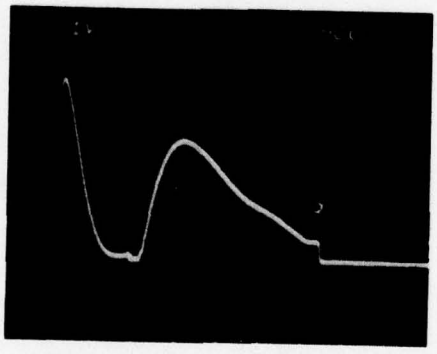

Figure 76. PPA turn-on current surge using EMI filter of 9 July 1976.

SECTION 5

BREADBOARD MODEL SYSTEM

The purpose of the breadboard model system was to prove the feasibility of the SPIBS concept. At the beginning of the program, several technical questions had been raised regarding ion source operation on xenon, use of a hollow cathode, ion-beam extraction without a neutralizer, and system power requirements. In addition, cost and schedule were major concerns. To answer these and many other questions, a breadboard ion source and a breadboard power processor assembly were developed. A great deal of the ion source testing was performed with the breadboard PPA. The breadboard EA consisted simply of a lecture bottle for xenon supply and a series of valves. Essentially, all basic feasibility questions were answered with this breadboard system. Demonstration of packaging and weight were the main characteristics not addressed in the breadboard phase.

A. BREADBOARD SYSTEM DESIGN

The detailed design of the breadboard system elements evolved as a result of a wide range of tests. Initial efforts focused on defining and refining the ion source electrical characteristics to the degree needed for PPA design. Subsequently, several minor design iterations occurred as the ion source was modified to meet performance and life requirements. Although the breadboard system was not constructed as a compact unit, the guiding objective in all tests was to develop functionally and electrically compatible elements that met the system requirements.

1. Breadboard Ion Source

The initial version of the breadboard source introduced several important features, including: (1) a compact low-power hollow cathode, (2) a three-electrode ion-optics design, (3) a porous plug for flow-rate control, and (4) a high-voltage isolator for the expellant line. Although the basic principals for these features were developed for

mercury ion thrusters, their application to a small, inert gas ion source was new.

The original source assembly design is shown in Figure 77. Hollow cathode and ion optics assemblies are shown in Figures 78 and 79, respectively. Photographs of the breadboard assembly and the CIP are presented in Figures 80 and 81, respectively. During the breadboard phase, the following areas were investigated:

- Ion optics
- Cathode insert
- Neutralizer filament configuration
- Keeper orifice
- Cathode heater tie-down
- Number of magnets
- Source-body to CIP mounting

2. Expellant Assembly

The gas system used throughout most of the breadboard phase (until a SPIBS pressure regulator was installed) is shown in Figure 82. This photograph shows the xenon lecture bottle, manual regulator, 1-liter reservoir, Heise pressure gauge, Granville-Philips controlled leak valve, and miscellaneous shutoff valves. The two valves mounted on the vacuum flange allowed the gas lines and the ion source feedline to be evaculated directly into the vacuum chamber. Maintaining a clean gas system was found to be necessary for successful source operation.

With the lecture bottle valve closed, the reservoir and gas lines back to this valve were evaculated. With proper valving, the reservoir was then filled to an appropriate pressure (5 to 10 psig) and sealed-off from the lecture bottle. During source testing, the decrease in reservoir pressure was used to measure flowrate.

3. Power Processor Assembly

In the breadboard phase, two types of power supplies were used: laboratory and SPIBS breadboard circuit. The laboratory supplies and metering can be seen in Figure 82. The basic circuit diagram and meter locations are shown in Figure 83. In the laboratory supply

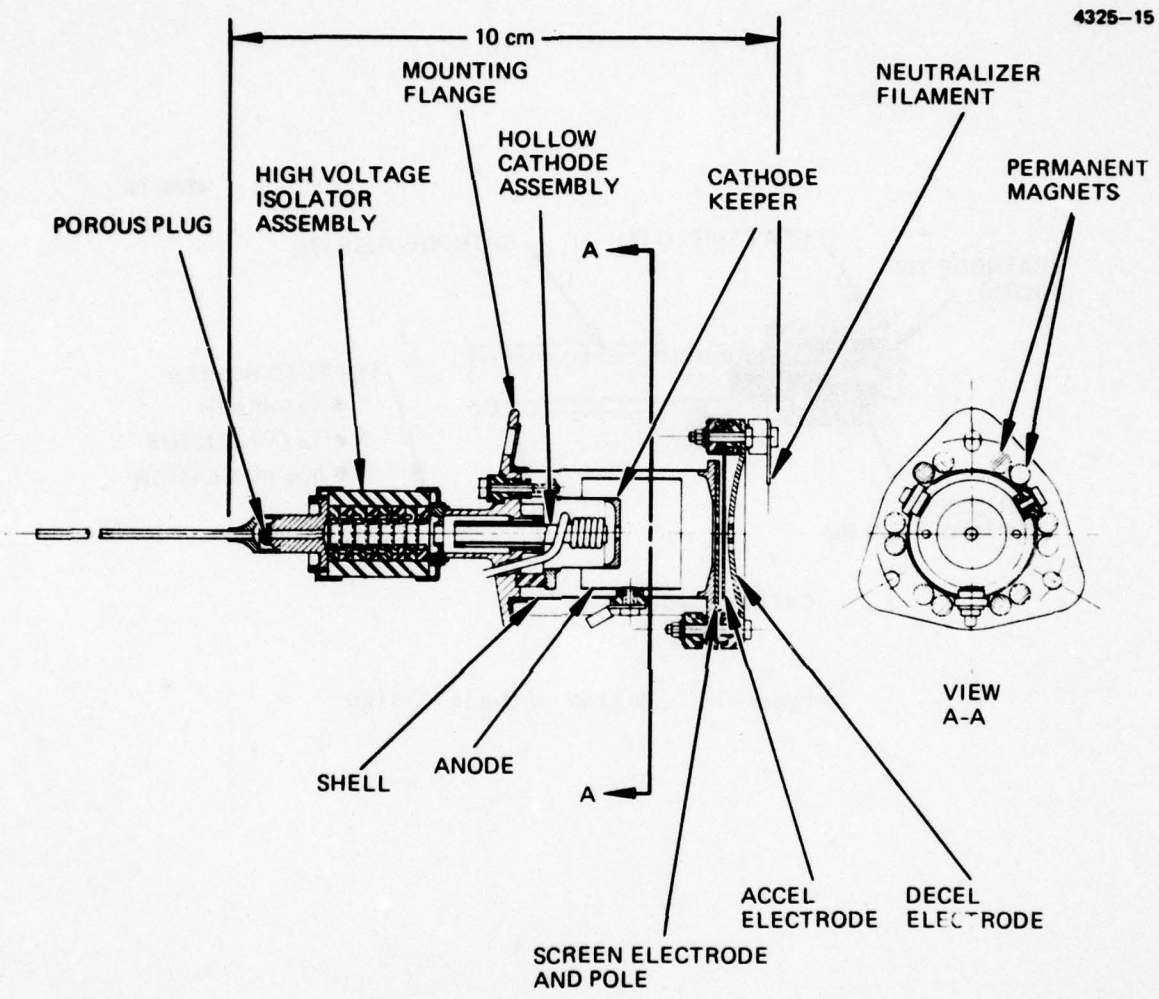

Figure 77. Breadboard ion source assembly layout.

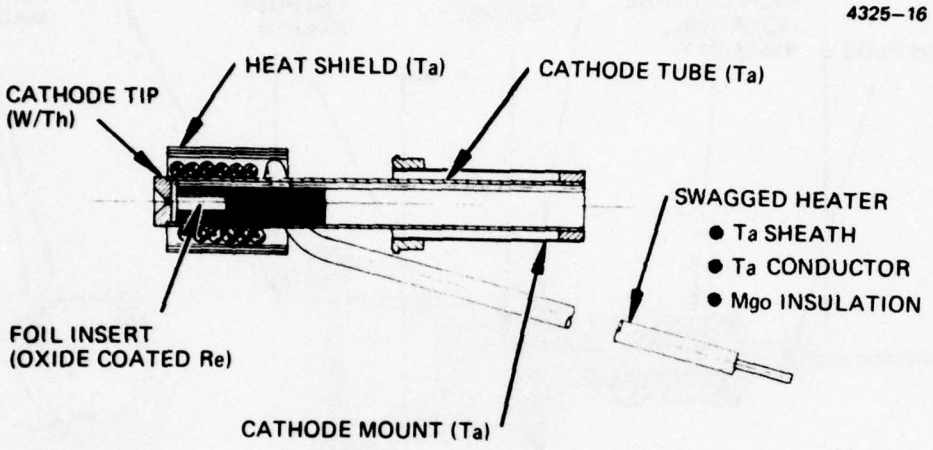

Figure 78. Hollow cathode design.

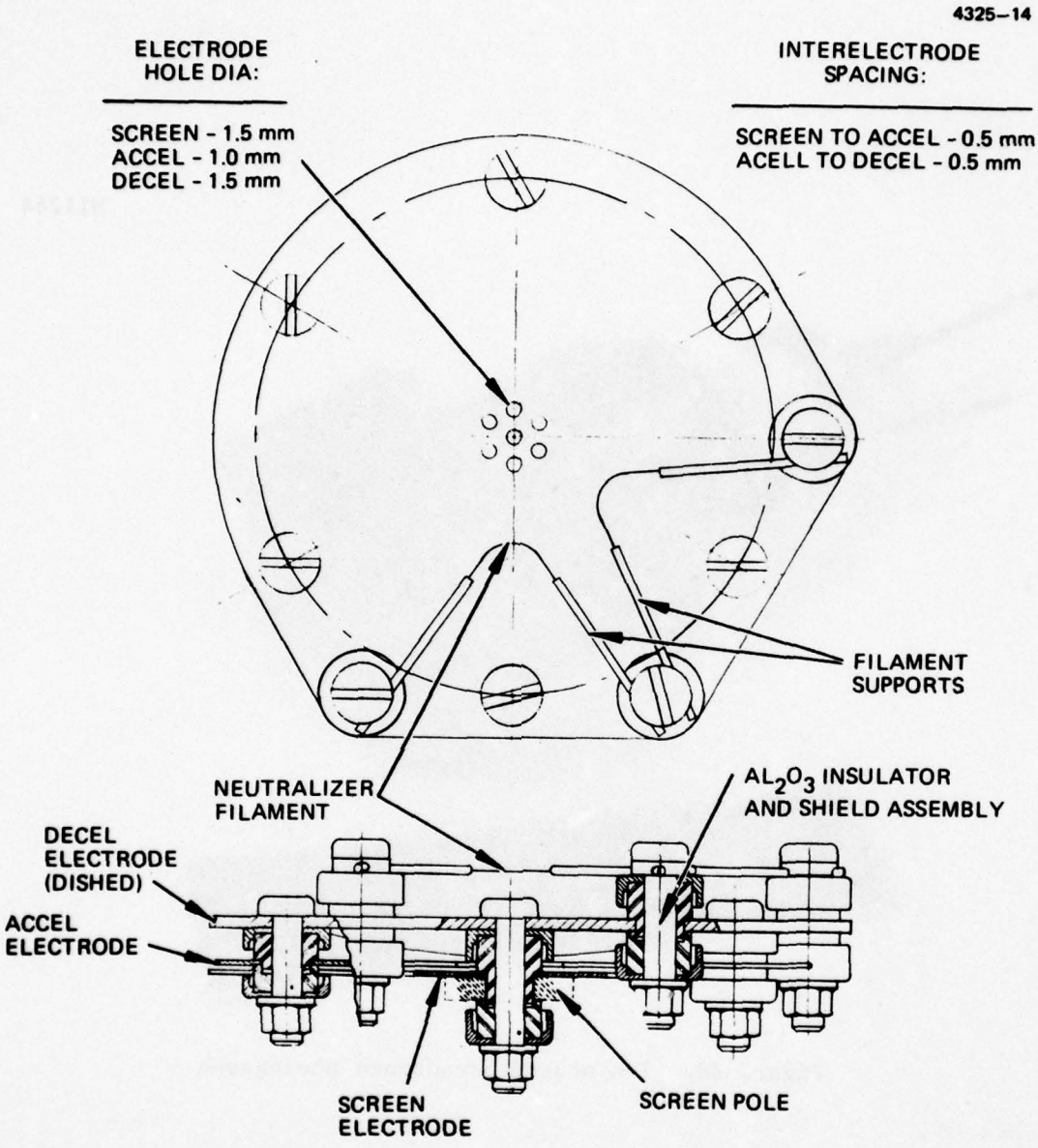

Figure 79. Breadboard ion optical system design.

M11264

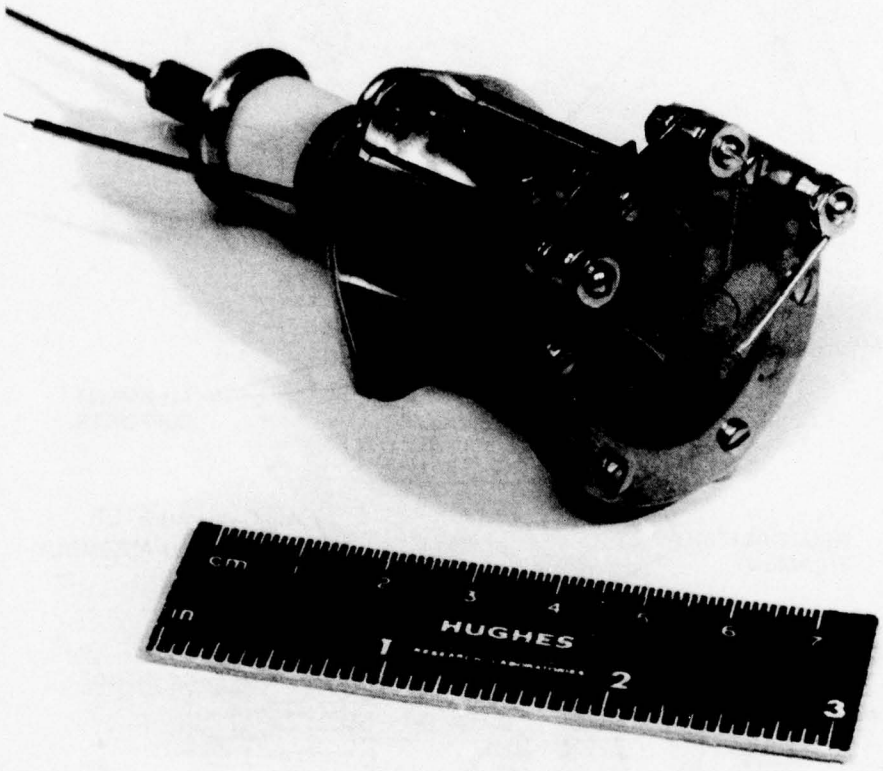

Figure 80. Ion source breadboard photograph.

M11265

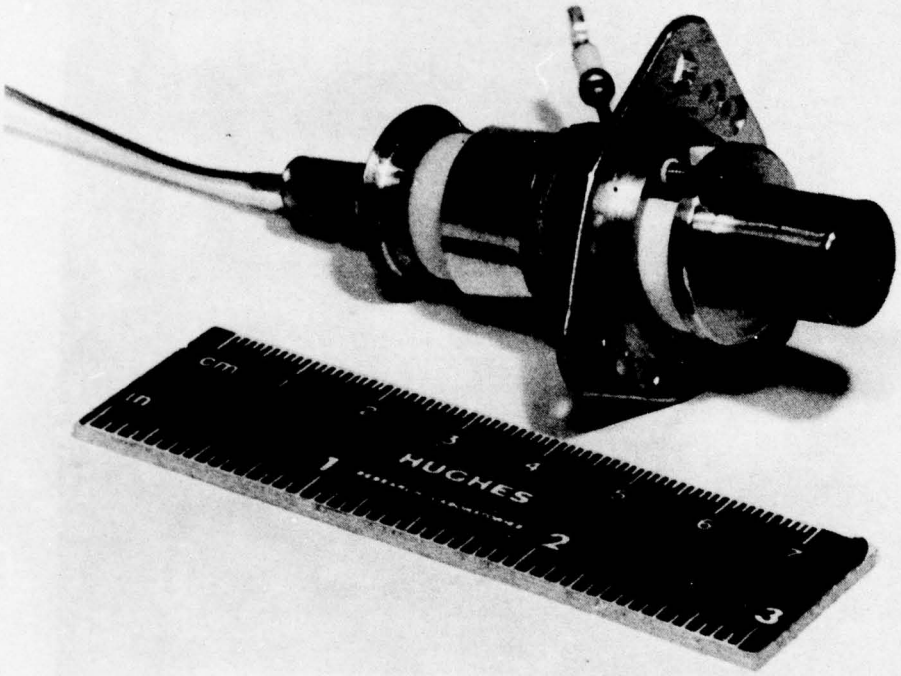

Figure 81. Ion source breadboard CIP photograph.

M11362

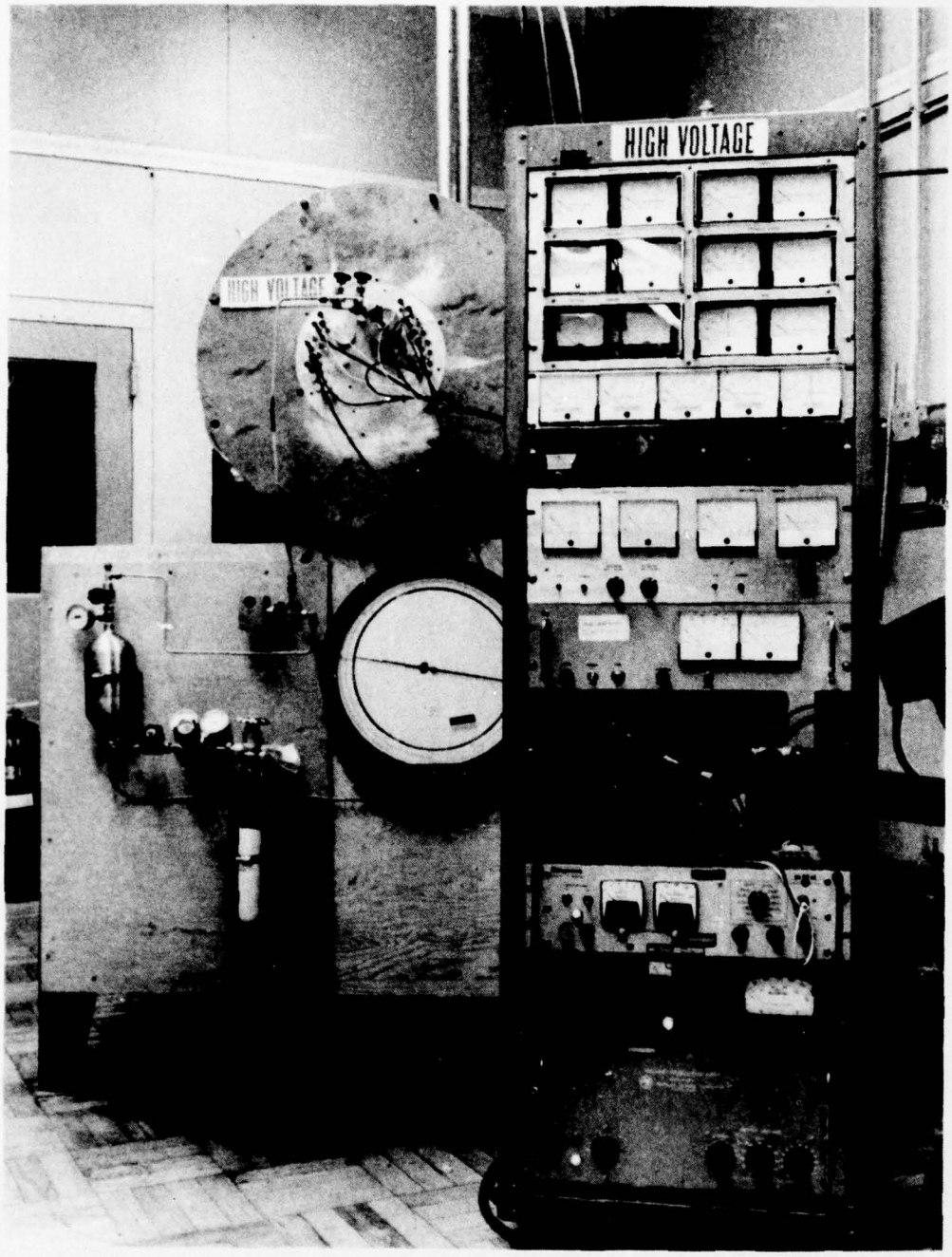

Figure 82. Expellant assembly breadboard configuration.

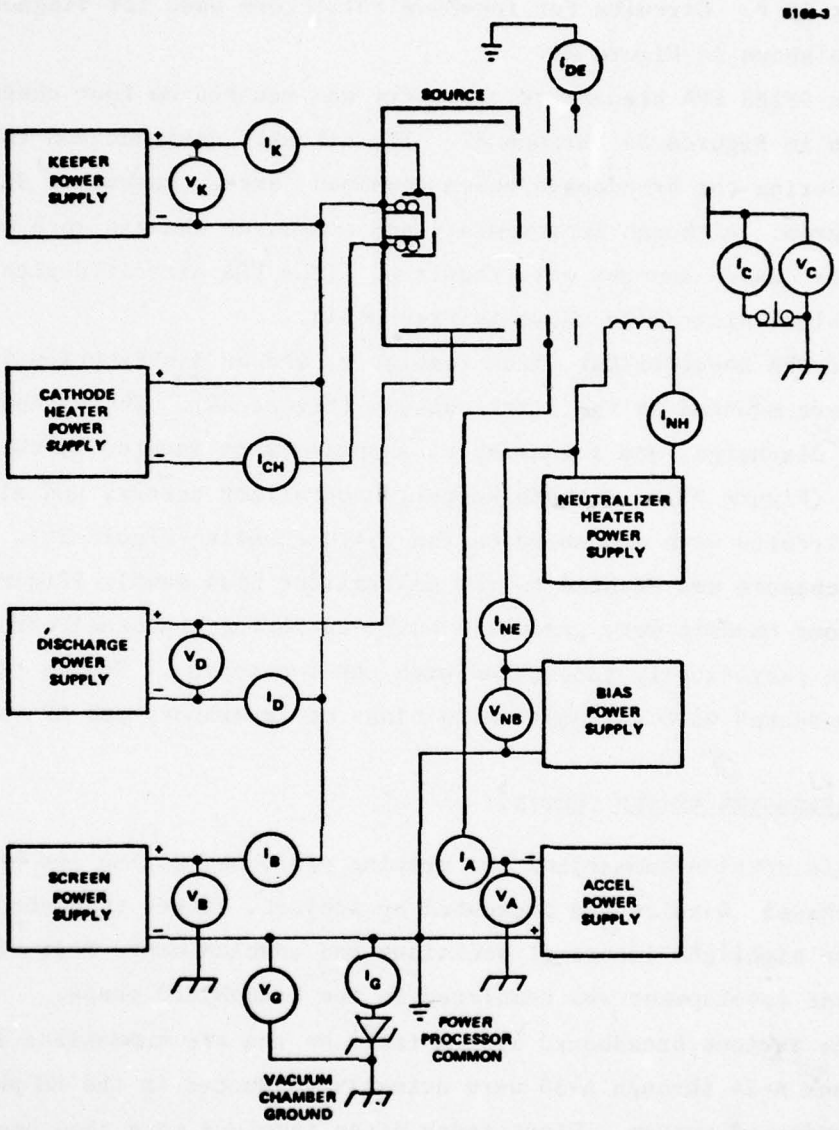

Figure 83. Laboratory power supply and metering schematic.

setup, a neutralizer bias supply was not used and self-biasing was achieved by allowing the power processor "common" to float negative relative to ground. This floating potential was limited by zener diodes to about 65 V. Circuits for ion-beam collectors used for diagnostics are also shown in Figure 83.

The SPIBS PPA breadboard circuitry was mounted on four chassis as shown in Figures 84 through 87. The circuits designed and implemented during the breadboard phase remained largely unchanged during the program. Although improvements and component changes were made, few major design changes were required. (The PPA circuit design functional block diagram is shown in Figure 61).

The PPA input filter, line regulator, and ac distribution inverter cards were mounted on the first chassis (Figure 84). The cathode heater, discharge, and screen/accel supplies were mounted to the second chassis (Figure 85). Cathode keeper, neutralizer heater, and electrometer circuits were assembled on the third chassis (Figure 86). The fourth chassis was devoted to the neutralizer bias supply (Figure 87). These four chassis were gradually built-up during the breadboard phase and were periodically integrated with the ion source. Source tests were conducted with various combinations of laboratory and PPA supplies.

B. BREADBOARD SYSTEM TESTING

This section summarizes the testing performed during the breadboard phase. Results are presented by subject, rather than chronologically to highlight important decisions and conclusions. Most of the component development was completed in the breadboard phase.

The various breadboard system tests by run are summarized in Table 9. Test runs A-34 through A-38 were actually conducted in the EM phase using the breadboard system. Since tests often involved more than one objective, several runs are referenced in more than one discussion. The initial breadboard ion source test configuration is shown in Figure 88. The ion source is shown in Figure 89. The ground screen and probes used for beam diagnostics can be seen in Figure 89.

M11364

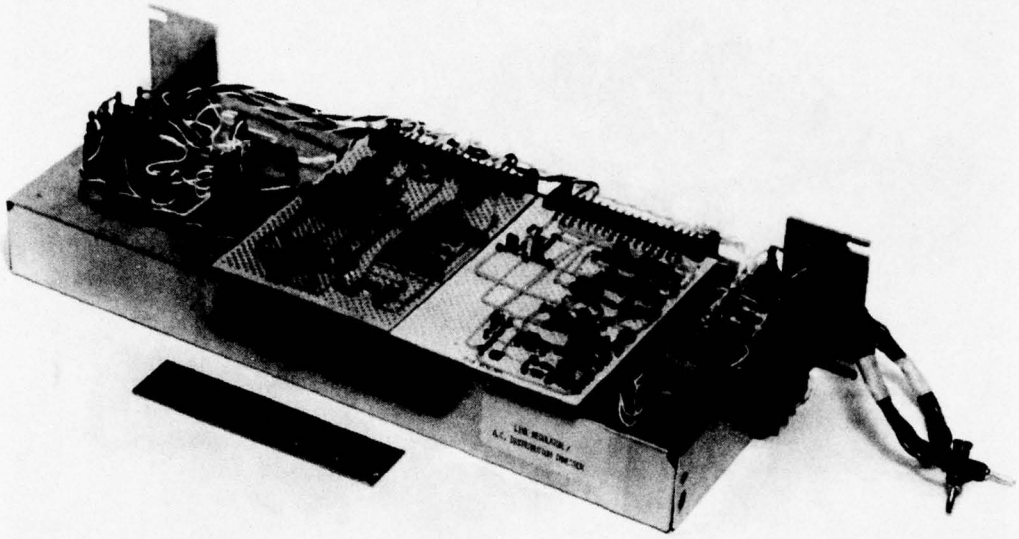

Figure 84. Breadboard PPA Chassis No. 1.

M11365

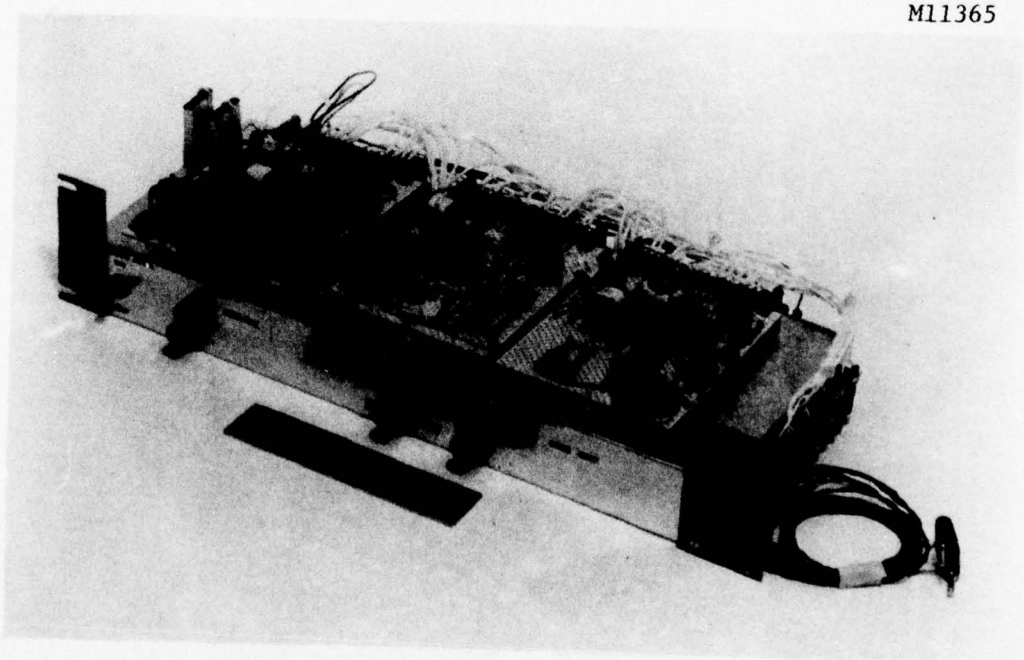

Figure 85. Breadboard PPA Chassis No. 2.

M11364

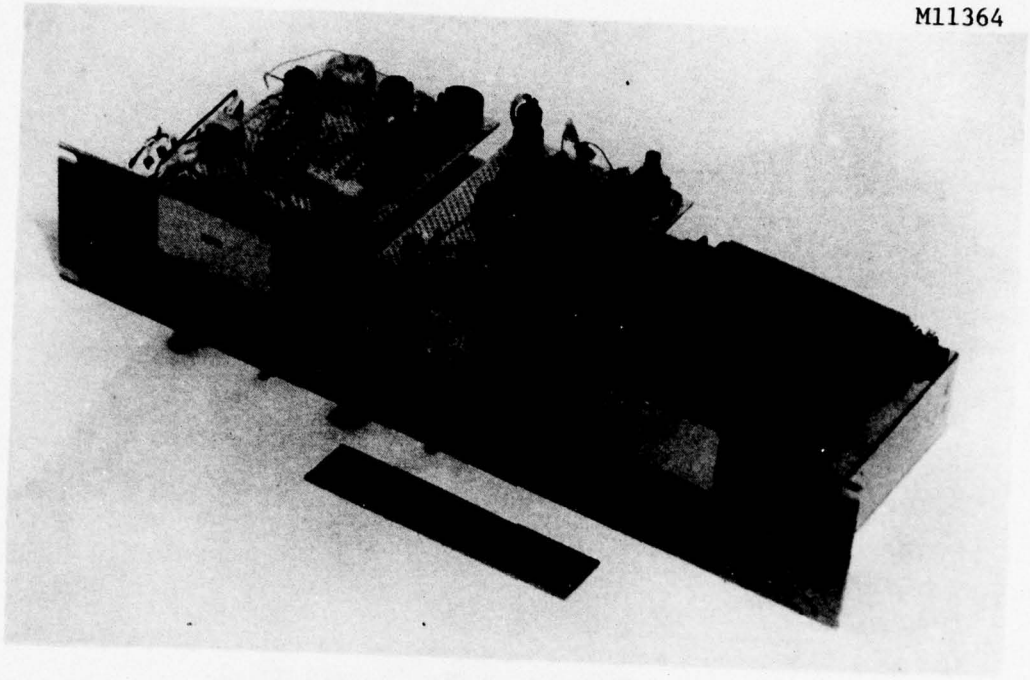

Figure 86. Breadboard PPA Chassis No. 3

M11367

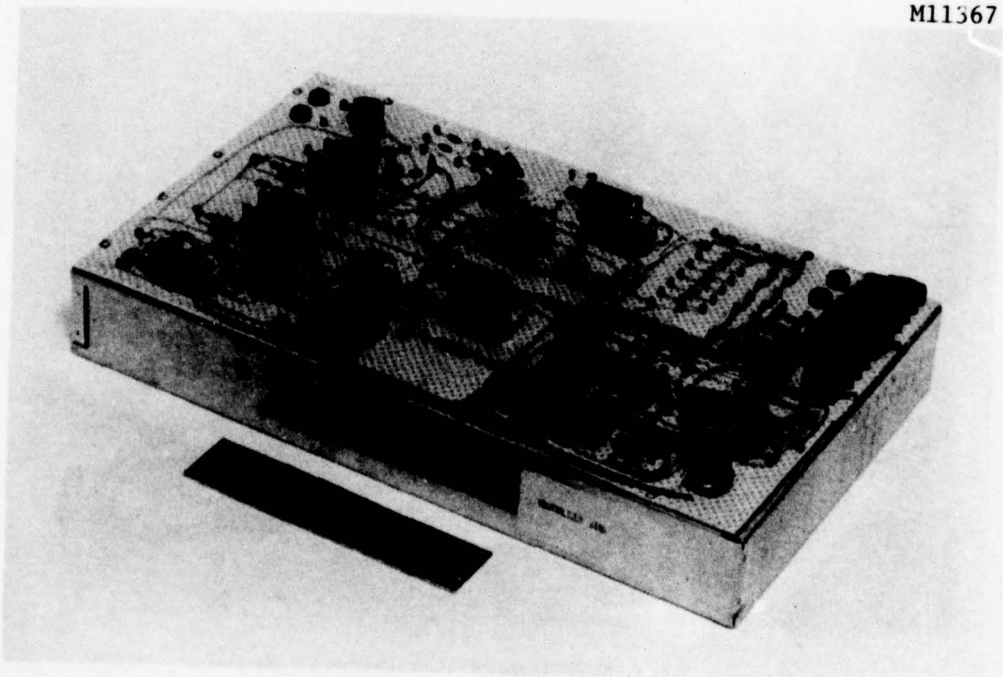

Figure 87. Breadboard PPA Chassis No. 4.

Table 9. Summary of Third Quarter Ion Source Testing

Test	Purpose	Remarks	Test Setup Changes Prior to Run
A-1A	First checkout of breadboard source	Successful run; accel to decel short (screw).	First test
A-1B	Operation with PPA; keeper requirements tests	Successful operation with PPA; keeper supply requirements clarified. Also noted multimode source operation.	Added PPA to test setup
A-2	Evaluate operation with smaller keeper orifice (0.038 in. diameter); evaluate neutral filament position	Multimode characteristics corrected. Continued keeper supply evaluation. Neutral filaments badly sputtered.	Changed keeper orifice; moved filament.
A-3	Evaluate neutral filament position; take beam probe measurements	Accel-decel short (flake). Obtained preliminary probe data. Poor neutral coupling to beam.	Moved filament; added beam probe.
A-4	Evaluate neutral filament position; beam measurements.	Coupling satisfactory at both positions tested; no apparent wear. Accel-decel short (nothing visible).	Cleaned optics; worked on probe.
A-5	Recheck accel-decel short.	Short re-occurred (optics had not been cleaned).	Checked optics.
A-6	Recheck optics after respacing; continue neutral evaluation.	Keeper to cathode heater short.	Respaced optics.
A-7	Performance evaluation; evaluate PPA keeper supply beam probe data.	Recommend inductive output on keeper supply. Obtained probe data. Accel-decel short (flake).	Repair cathode-keeper short at heater.
A-8A	Evaluate larger accel holes; evaluate 0.030 keeper orifice; probe data.	Accel currents essentially unchanged. Observed electron "backstreaming"; higher discharge voltage. Accel-decel short (flake).	Increased accel hole diameters and reduced keeper orifice diameter.
A-8B	Evaluate operation with higher accel voltage; evaluate modified beam probe.	Backstreaming eliminated; probe data improved.	Modified beam probe.
A-8C	Evaluate performance in large tank.	No observable difference in performance in large tank; accel-decel short.	
A-9	Evaluate operation on 99.9% purity xenon; continued evaluation of accel-decel short.	Performance not apparently affected by lower purity; accel-decel short after about 37 hours.	Gas purity; source unchanged from run A-8 (accel apertures of 0.15 cm dia.)
A-10	Continued evaluation of accel-decel short.	Source failed to start-appeared to be blockage in cathode.	Single 0.76 cm dia. decel aperture.
A-11	Extended test of cathode insert; continued evaluation of shorting. Startup tests; PPA integration.	Accumulated 220 hours of discharge operating time; about 40 restarts. Stopped to evaluate insert. Developed startup power profile and checked electrometer; accel-decel short after 190 hours.	New Ta foil cathode insert; kpr.orifice diameter increased from 0.076 to 0.090 cm.
A-12	Extended test of cathode insert; test of graphite grids.	Accumulated 160 hours of discharge and beam time; about 25 restarts; would not restart after weekend; no grid shorts.	New Ta foil cathode insert; graphite accel (0.102 cm) and screen (0.152 cm).
A-13	Evaluate porous tungsten insert; continue evaluation of graphite grids.	"Unstable" discharge operation; low beam current; short run.	"Deposit" on accel grid lapped off; install porous tungsten insert (#1); increase kpr. orifice dia. to 0.102 cm.
A-14A	Continue evaluation as in A-13; evaluate keeper baffle.	Beam current about half normal value: Short run.	Added 0.165 dia. baffle over kpr. orifice.
A-14B	Same as A-14A.	Baffle did not improve discharge characteristics; found a magnet reversed.	Checked grids for orientation.

Table 9. Summary of Third Quarter Ion Source Testing (Continued)

Test	Purpose	Remarks	Test Setup Changes Prior to Run
A-15	Extended test of porous tungsten insert and graphite grids.	Reversed magnet caused low beam current; accumulated beam and discharge times of 314 and 371 hrs. respectively; both neutral filaments failed at about 300 hrs.; about 25 restarts.	Corrected magnet polarity.
A-16	Evaluation of graphite-moly laminated accel grid; continued evaluation of porous tungsten insert.	Accel current increased to about 12% of beam from normal of 5-6%; about 20 restarts; would not restart after weekend.	Added a moly accel to setup of A-15. Insert unchanged. Replaced neutral filaments.
A-17	Evaluate new insert; evaluate gas line pumpout procedure.	Startup seems improved; mapped neutralizers; take perveance data on laminated grids.	New porous insert (#2); grids unchanged from A-16.
A-18	Evaluate accel coated with Aquadag graphite.	Aquadag coating in apertures sputtered away quickly; metal flake buildup on both faces of accel grid in less than 16 hrs.	Change to Aquadag coated (downstream) grids.
A-19	Neut. coupling mapping with biasing; PPA integration; startup.	Neut. coupling indicates filaments are too far from beam. Startups very easy.	Replaced Aquadag coated accel grid with solid graphite; molybdenum screen grid. Changed gas line pumpout procedure.
A-20	Neut. coupling; residual gas measurements; ion beam AC content.	Easy startups; decel-accel-screen leakage currents.	Filaments accurately spaced at 0.64 and 0.76 cm from centerline; added RGA head; reinstalled large collector.
A-21	Startup cycle tests; PPA integration; neut. coupling; backstreaming evaluation.	Accumulated over 750 cycles with typical startup procedure (cathode heating time of 2 min.).	Cleaned optics insulators; replaced broken decel insulator.
A-22	Evaluate operation with vacuum enclosure (blowoff cover open).	Source would not start.	Added vacuum enclosure assembly, cover open.
A-23	Same as A-22.	Operation normal. Short run.	Insert "flagpole" found separated from insert; install new insert (#3).
A-24	Neut. coupling; evaluate source modifications; PPA integration.	Telemetry calibrations and performance data; decel leakage.	Respaced new neut. filaments; cleaned optics; realigned cathode and keeper.
A-25	Evaluate operation with blowoff cover closed.	Completely successful operation with cover closed; beam currents up to 0.4 mA.	Closed cover; collector covered with graphite.
A-26	Evaluate operation using high pressure into latching valve and regulator.	Source started on lab (1 ℓ) gas system; feedthrough high voltage breakdown.	Setup gas system with latching valve and regulator. Shortened neut. filaments. Replaced accel grid (original broken by handling); opened cover.
A-27	Same as A-26.	Successful operation from high pressure system. Decel leakage again.	Switched feedthrough connections.
A-28	Prepare for design review demonstration.	Performance low for normal conditions; oscillatory operation under certain conditions.	Enlarged accel grid holes; clean decel "whiskers"; fix keeper orifice plate.
A-29	Same as A-28.	Performance improved; still oscillatory.	Added two magnets.
A-30	Investigate oscillatory behavior.	Oscillations are not apparent.	Moved insert away from cathode face; respaced neut. filaments to 0.58 and 0.64 cm off centerline.
A-31	Investigate optics leakage; continue insert evaluations; operate from high pressure gas system; operate for SAMSO visitors.	Operation reasonably normal; operation from high pressure for about 50 hours; total run time of about 100 hours; decel-accel leakage again.	Optics cleaned and respaced.
A-32	Investigate optics leakage; continue insert evaluations.	Operation rather erratic; discharge oscillatory again. Decel-accel leakage again.	Replace accel and screen grids. Install new insert (#4) with sheet metal-pin flatpole design; remove vacuum enclosure and add ground screen.

Table 9. Summary of Third Quarter Ion Source Testing (Continued)

Test	Purpose	Remarks	Test Setup Change Prior to Run
A-33	Evaluate insert design and positioning.	Discharge hard to start; operates only with cathode heater on at 3.5 A or more.	Move insert away from cathode face.
A-34	Evaluate insert design.	Acceptable performance for cathode. Starting made difficult by low flowrate; higher gas pressure required.	Installed new insert (#5) using wire loop attachment method.
A-35	Evaluate insert design; Extended optics test. Tried to clean porous plug.	Acceptable performance, except for high gas pressure. Observed flake buildup on decel after 210 hours.	No change in ion source. Worked on PPA.
A-36	Evaluate insert design; Extended optics test. Evaluate new porous plug.	Good performance without flake build-up. 615 hours operating time and 375 cycles. Neutralizer filaments failed after about 100 hours.	Increased decel aperture to 1.27 cm; increased accel apertures to 0.12 cm; installed insert (#6) having brazed wires for attachment.
A-37	Evaluate neutralizer heater control loop response.	Response tests show strong dependence on filament location; with good coupling, response time is less than one second.	Replace filament. (One filament was still intact).
A-38	Evaluate rebuilt cathode, keeper, and neutralizer filaments (new location).	Operated for about 330 hours with no apparent difficulty. Filament life projected to about 500 hours.	Replace cathode subassembly; replaced keeper subassembly; replaced and repositioned filaments.

M11361

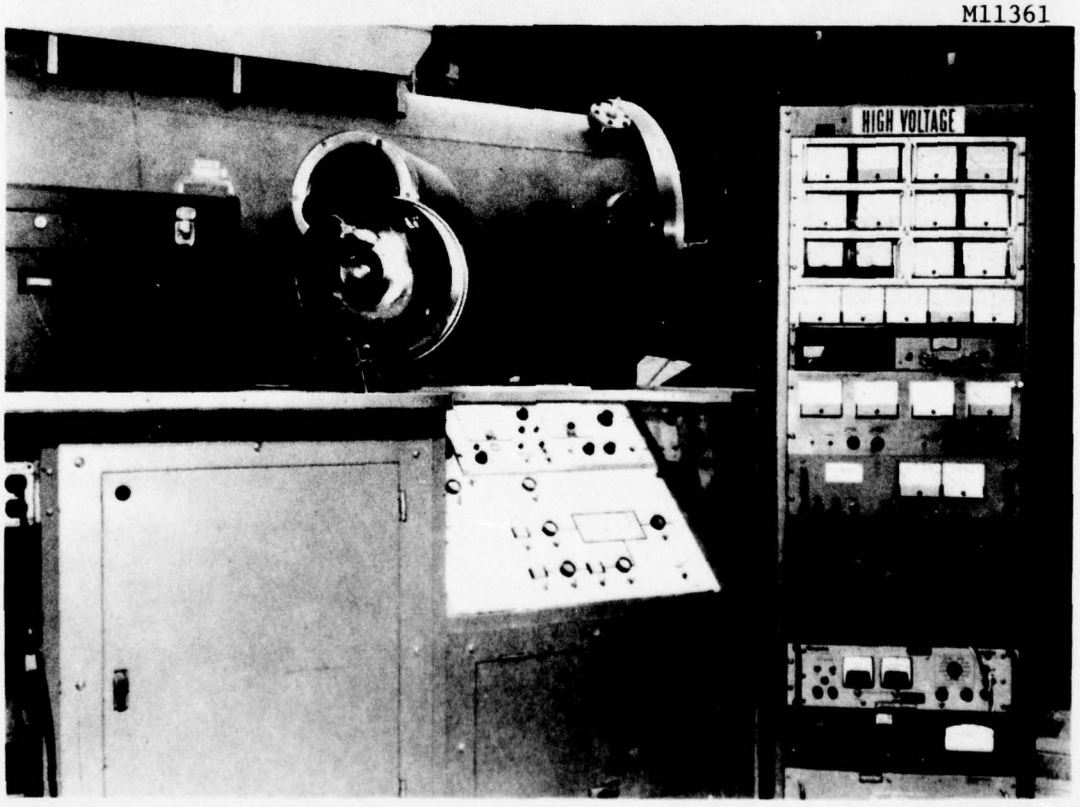

Figure 88. Breadboard ion source test configuration.

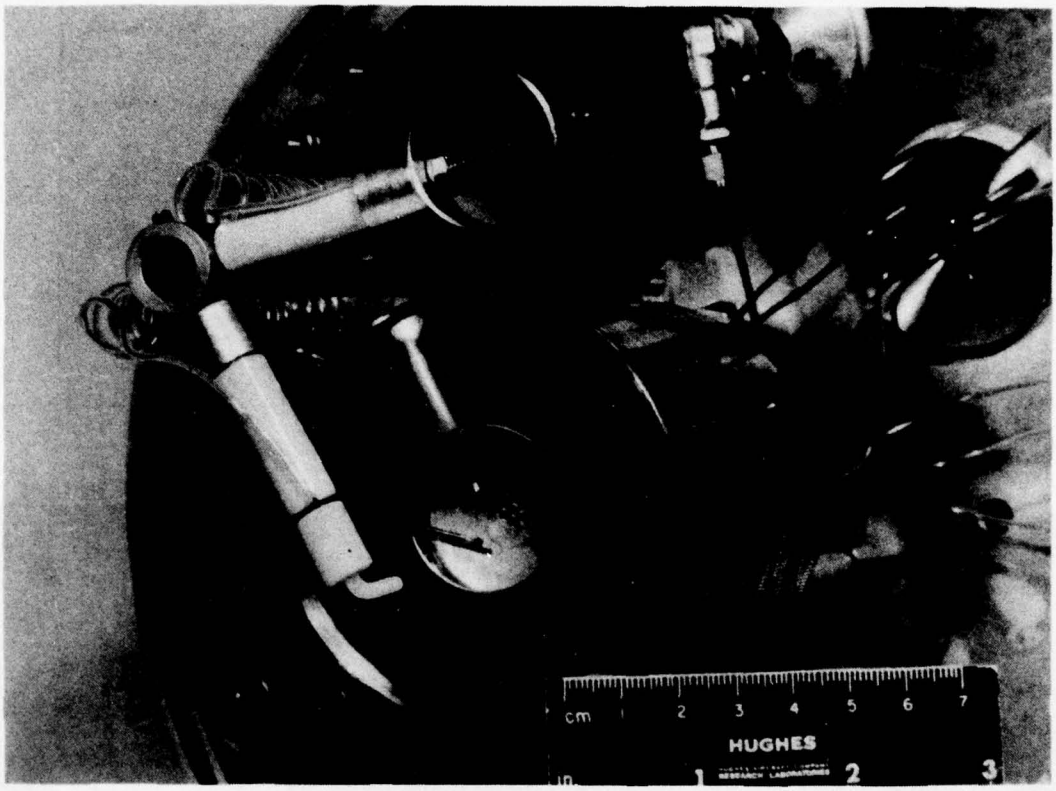

Figure 89. Ion source.

1. Ion Optics

The most troublesome area in the ion source development process was the ion optics. As indicated in Table 9, much of the breadboard ion source effort was expended in finding a satisfactory design. Indirectly, the cause of the ion optics difficulties was the low expellant utilization efficiency (i.e., the low fraction of the expellant exhausted as ions). The low utilization and associated high fraction of neutral atoms passing through the apertures leads to a relatively high production of charge exchange ions near the grids. Charge exchange ions formed near the grids sputter material from the accel grid. This sputtered material can deposit between the grids and build up to a significant thickness. Layers of deposited material eventually flake off and bridge the gaps between grids, as shown in Figure 90. Shorts between the accel and the decel were most frequent, although screen-to-accel shorts also occurred. Typically, the original breadboard optics configuration would operate for about 10 hr before shorting occurred.

Many tests were conducted in trying to eliminate the grid shorting problem. Two general approaches were considered: (1) reducing the charge exchange ion production and sputtering rates and (2) avoiding collecting the sputtered material. A combination of these approaches produced an acceptable design. Reducing the large neutral flux by source modification did not seem to be a simple matter within the time, cost, and weight constraints. Thus, the only logical alternative was to reduce the severity of the material buildup.

Two factors affecting the buildup of sputtered material were identified: sputtering rate and deposition site availability. The sputtering rate was reduced by a factor of from 5 to 10 by changing the screen and accel grid material from molybdenum to graphite. An alternate approach coating the molybdenum grids with Aquadag did not prove successful. Sputtered material was further reduced by increasing the accel aperture diameter from 1.0 mm to 1.2 mm. During long tests, the apertures are enlarged by ion machining; starting with a larger diameter simply removed this portion of the deposition material from the outset.

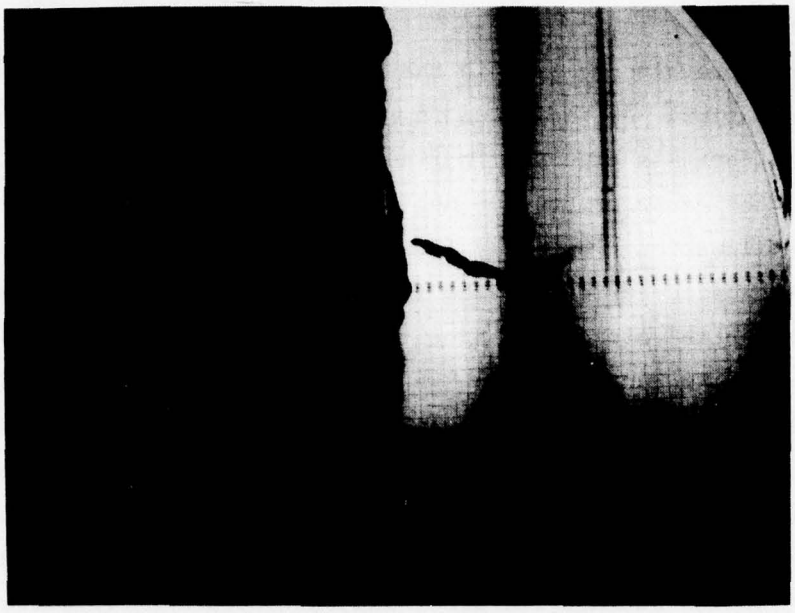

(a) Run A-7

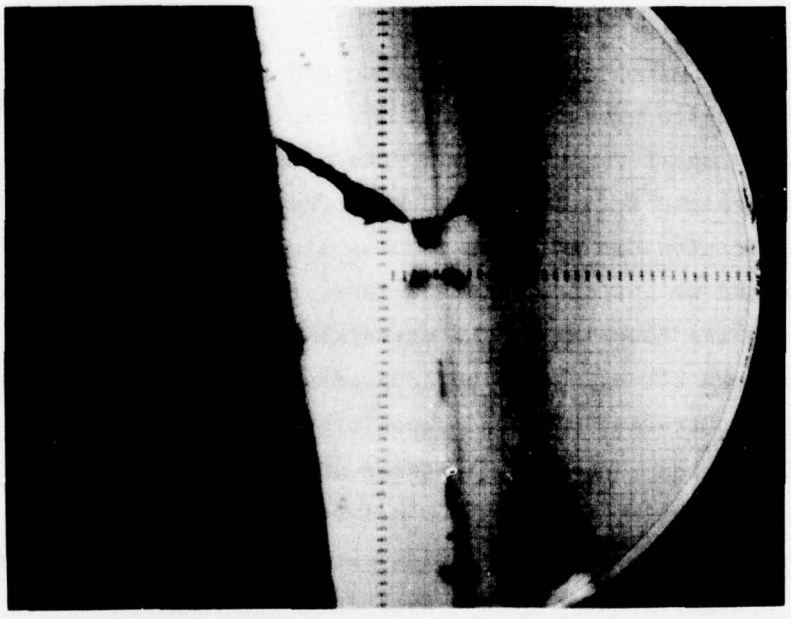

(b) Run A-8

Figure 90. Accel to decel flakes.

These reductions in sputtered material were significant but did not completely eliminate the flaking/shorting problem for runs of 40 to 50 hr. The next major improvement was obtained by replacing the seven decel apertures with a single large aperture. As noted in Table 9, runs up to about 200 hr were obtained with a 0.7-cm-diameter decel aperture. Late in the breadboard phase, the decel aperture was increased to .27 cm (see run A-36), and a test of 615 hr was performed without shorting. The larger decel apertures probably had two effects: (1) to reduce the neutral density in the accel region, resulting in less charge exchange, and (2) to increase the escape path for sputtered material. Since the source lifetime requirement was 300 hr, the ion optics design used in run A-36 was established as the baseline for SPIBS.

2. Cathode

The same basic cathode configuration was used throughout the SPIBS program. However, several small variations were made to improve reliability and resistance to air exposure. Virtually, all the modifications were associated with the cathode insert (see Figure 78).

All forms of foil inserts have similar problems: (1) the oxide coating is difficult to apply in a repeatable manner, (2) the coating is brittle and tends to flake off the metal foil, and (3) the large areas of the coating are exposed each time the cathode is exposed to air.

Tests with the prototype and with the breadboard source showed that the tantalum foil type insert deteriorated after a few hundred hours. Generally, these tests included periodic exposure to air, which allowed the active surface elements (barium and stontium) to be destroyed. However, run A-11 was a continuous test of a new insert that had not been exposed to air. After 220 hours of continuous test it had deteriorated significantly. This test provided positive proof that an insert improvement was required. For this reason, a porous insert was investigated and subsequently included in the final design.

The porous tungsten insert configuration used is shown in Figures 20 and 21. Before using the brazing method for attaching the support wires, several other welded designs were attempted. The welded

configurations used the same porous tungsten cylinder and performed well. However, the tantalum-to-tungsten E-beam weld was brittle and usually failed after a few test cycles.

The brazed configuration has two advantages: (1) the rhenium wires can be inserted into the tungsten and brazed to produce a flexible joint, and (2) the oxide mixture can be placed in the tungsten after brazing, assuring minimum contamination. With the oxide stored in the tungsten matrix, degradation from air exposure is probably limited to a few monolayers at each opening in the matrix. Thus, even repeated exposures should not significantly reduce the available active elements.

3. Keeper

The keeper electrode (see Figure 18) provides a means for starting and maintaining the discharge. In the SPIBS design all the xenon flows through the cathode and keeper. Although the keeper mounting insulators do not provide a gas-tight seal, the keeper orifice is a major gas flow path and is the principal charged particle path.

Results of tests to determine the effect of keeper orifice diameter on discharge voltage are shown in Figure 91. Data were conveniently obtained as a function of volume flowrate (psi/hr) using the blowdown expellant system. Based on these results, an orifice diameter of about 1.0 mm was selected. Significantly smaller diameters produced voltages that would tend to cause discharge chamber sputtering. Larger diameters results in low discharge voltages and low ionization efficiency. The 1.0 mm diameter produced a reasonable voltage for ionization over a broad range of flowrates and yet avoided possible sputtering problems.

4. Neutralizer Filaments

Neutralizer tests were performed (1) to prove functional capability, (2) to determine filament location (3) to establish power requirements, and (4) to establish filament life. Early in the program, basic neutralizer feasibility was demonstrated using a large beam probe to

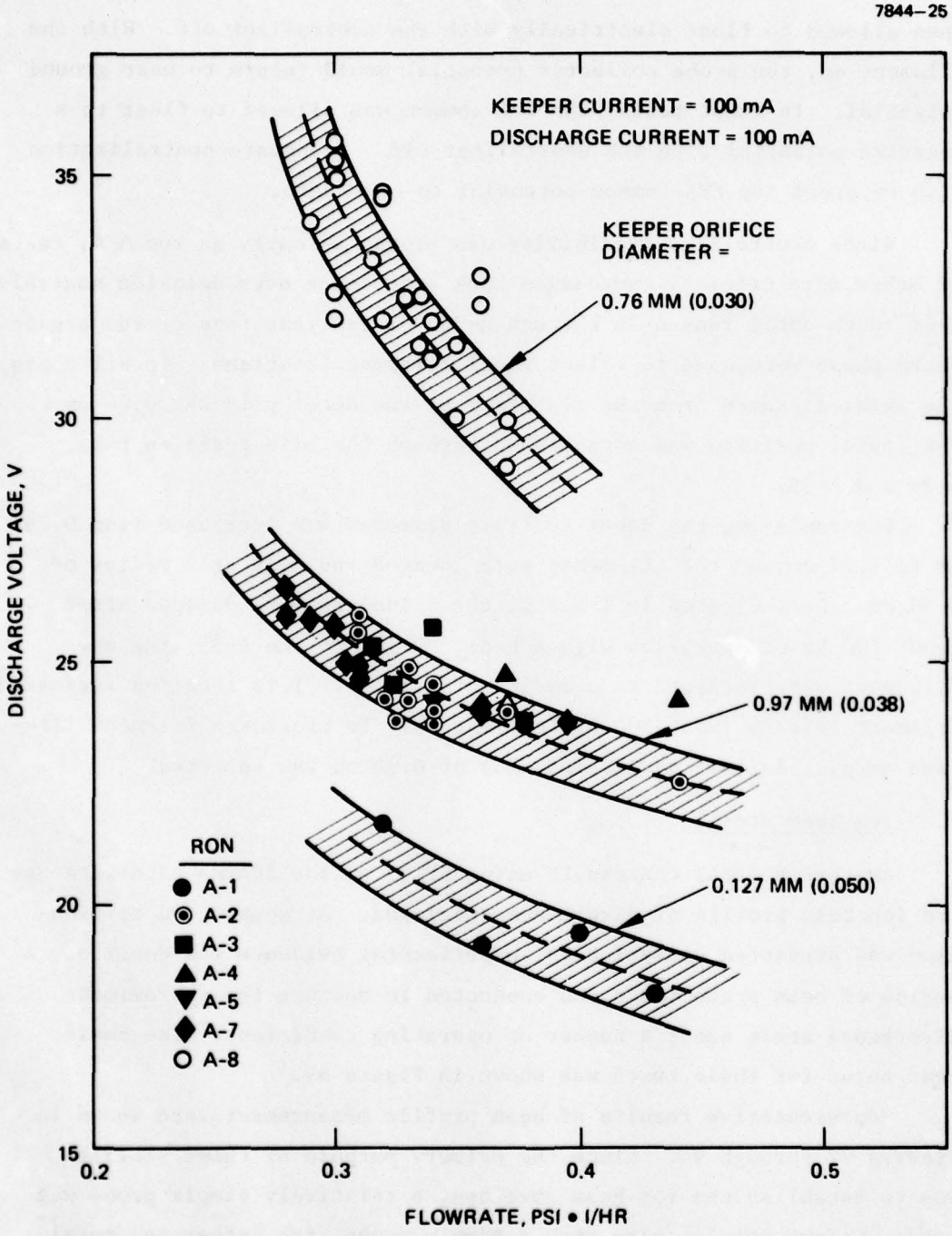

Figure 91. Effect of keeper orifice diameter on discharge voltage.

collect the total ion beam. The probe would attain a positive potential when allowed to float electrically with the neutralizer off. With the filament on, the probe collector potential would return to near ground potential. In these tests, the PPA common was allowed to float to a negative potential with the neutralizer off. Adequate neutralization also returned the PPA common potential to near zero.

Since neutralizer feasibility was proven as early as run A-4, tests of other more critical components took precedence over detailed neutralizer tests until runs A-36 through A-38. These last runs of the breadboard phase were used to select final filament locations. In all tests, the axial distance from the flat face of the decel grid was 0.44 cm. The radial position was established through the life tests in runs A-36 and A-38.

For run A-36, the decel aperture diameter was increased from 0.76 cm to 1.27 cm and the filaments were located radially at a radius of 0.50 cm. As indicated in Table 9, the filaments were damaged after about 100 hr of operation with a beam. Prior to run A-38, the new filaments were respaced to a radius of 0.53 cm. This location increased filament life to about 500 hr (estimated). To provide a filament lifetime margin, a final radial location of 0.56 cm was selected.

5. Ion Beam Profile

Another general concern in using SPIBS on the SCATHA satellite was the ion beam profile or divergence enveloped. Although good collimation was predicted analytically, experimental evidence was desired. A series of beam probe tests was conducted to measure the approximate divergence angle under a number of operating conditions. The basic test setup for these tests was shown in Figure 89.

Representative results of beam profile measurements are shown in Figures 92 through 94. Since the primary purpose of these profiles was to establish the ion beam envelope, a relatively simple probe was used. Unfortunately, with such a simple probe, the integrated total current was not equal to the metered beam current. Several factors could explain this difficulty, including secondary emission from the

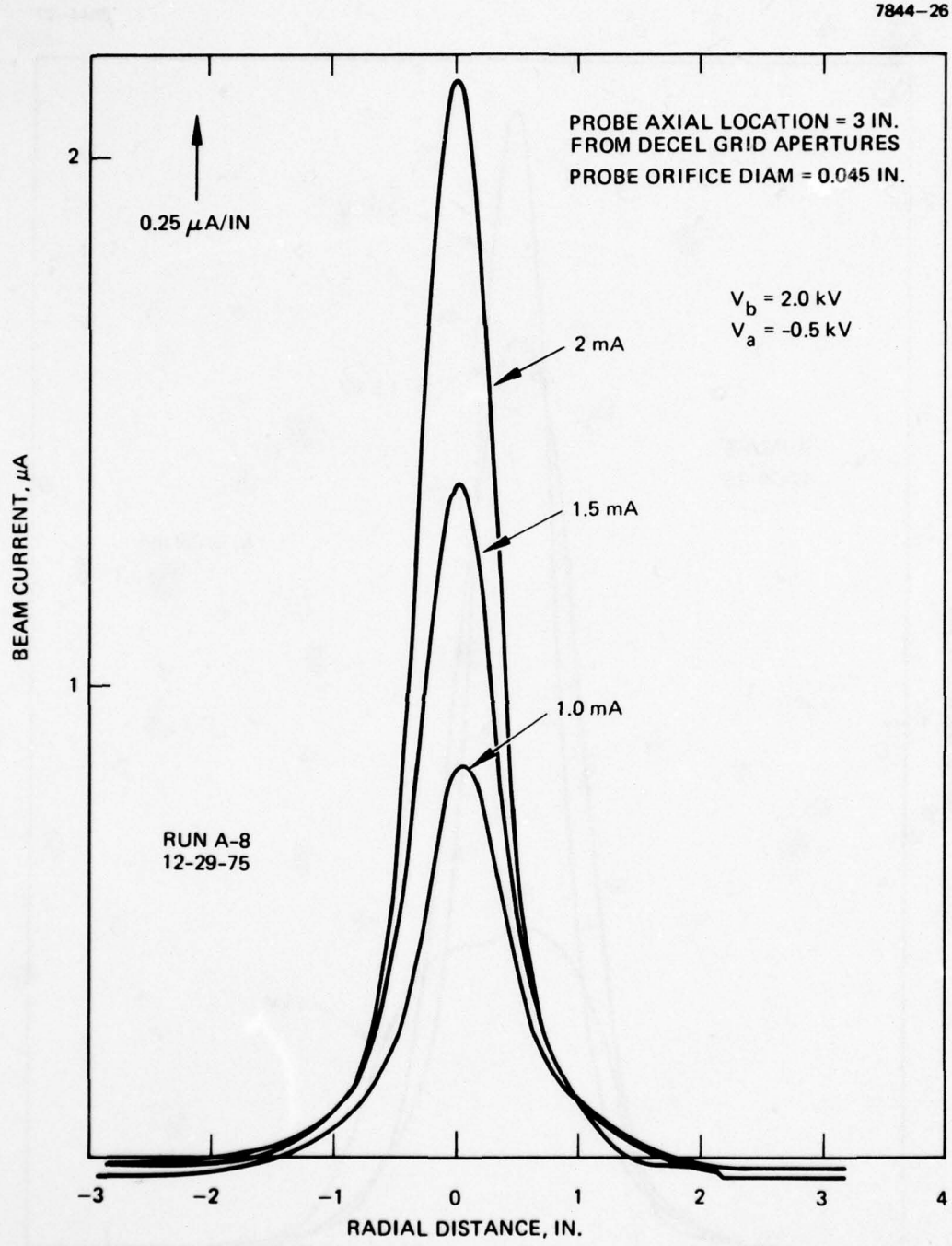

Figure 92. Ion beam profiles; beam voltage = 2 kV; variable beam current.

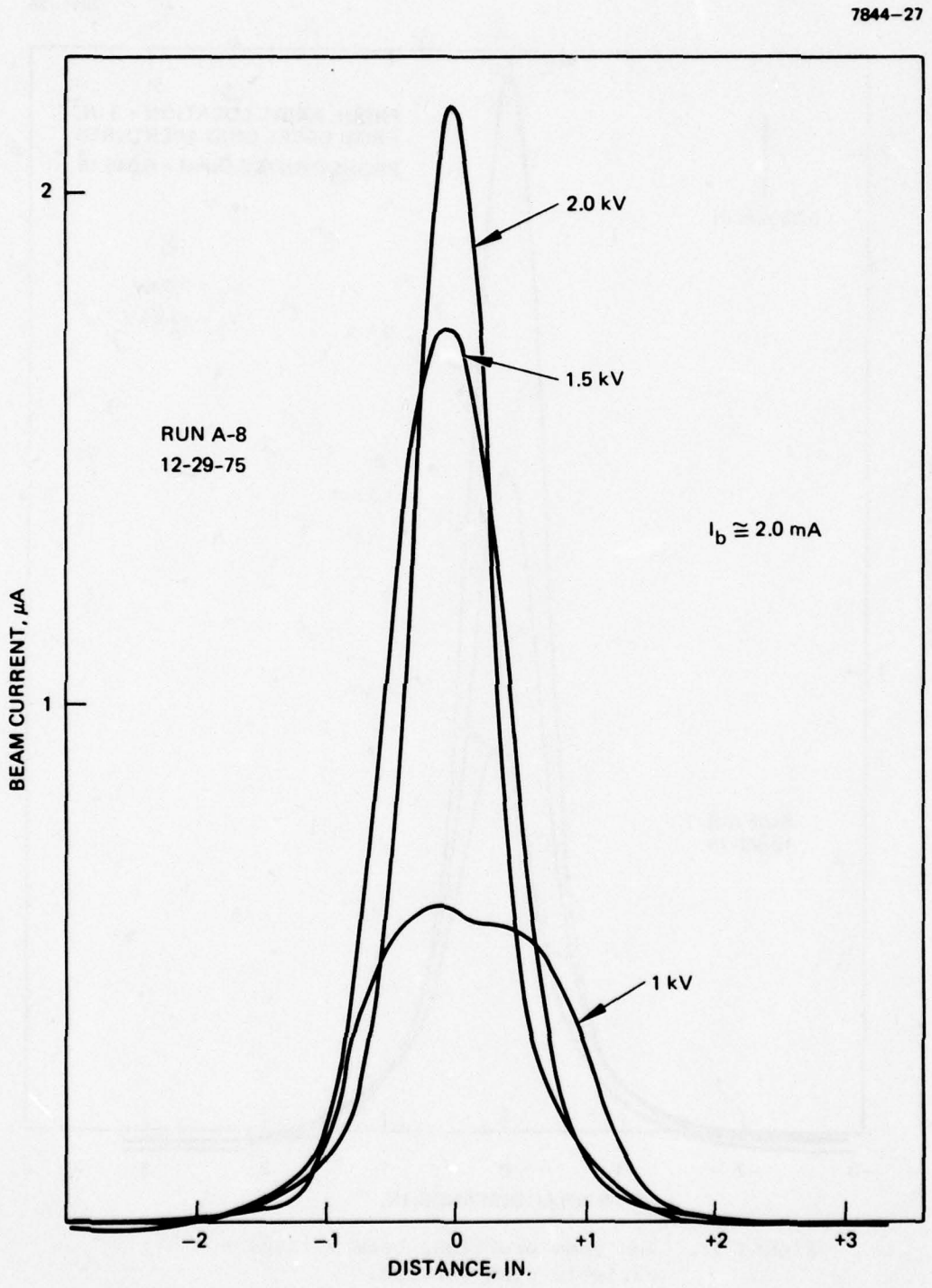

Figure 93. Ion beam profiles; beam voltage variable; beam current = 2 mA.

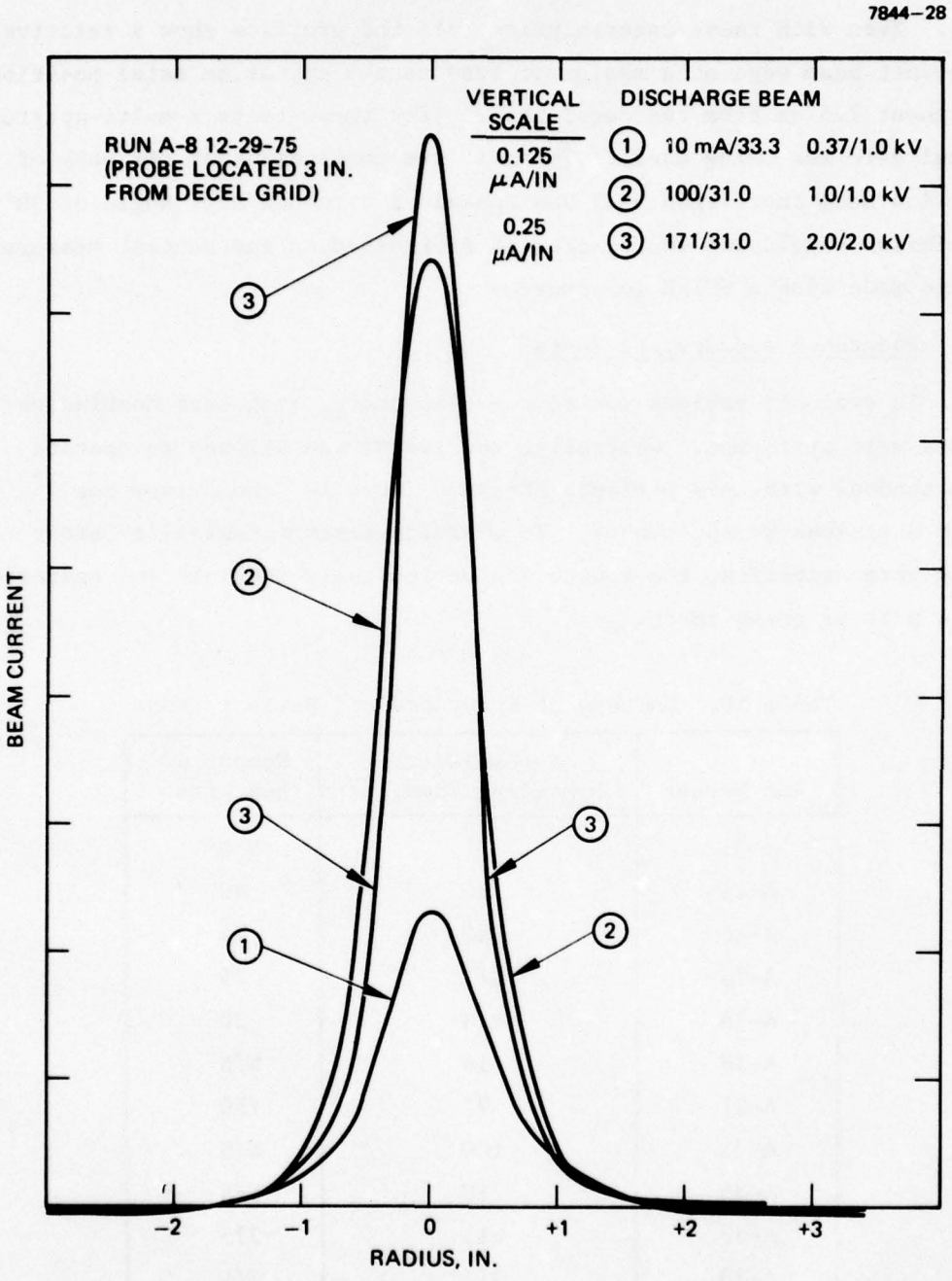

Figure 94. Ion beam profiles; beam voltage variable; beam current variable.

probe, surface charging on the dielectric around the probe wire, and EMI. Even with these uncertainties, all the profiles show a relatively distinct beam edge at a radius of less than 5 cm, at an axial position of about 7.5 cm from the decel grid. (For these tests a multi-aperture decel grid was being used). Thus, it was concluded that the bulk of the ion beam (more than 95%) was contained within a half angle of 30°. A similar conclusion was reached at AFGL based on independent measurements made with a SPIBS ion source.

6. Endurance and Restart Tests

To evaluate various ion source components, long term continuous tests were performed. Generally, the system was allowed to operate unattended, with only periodic checks. Table 10 summarizes the test durations by run number. To evaluate restart capability after long-term operation, the source was periodically shut off and restarted as a part of these tests.

Table 10. Summary of Endurance and Restart Tests

Run Number	Accumulated Operating Time, hr	Number of Restarts
A-9	37	N/N*
A-11	220	40
A-12	160	25
A-15	371	25
A-16	N/N	20
A-18	16	N/N
A-21	75	750
A-31	100	N/N
A-35	210	N/N
A-36	615	375
A-38	330	N/N

*Not noted, but usually more than 5 in typical test sequences.

As part of the reliability evaluation of the porous tungsten insert, cyclic ignition tests were performed on the breadboard ion source. An automatic cyclic controller was integrated into the SPIBS test rack to provide the sequence described below:

t = 0	Cathode heater and discharge voltage on
t = 2 min	Keeper voltage on - ignition. (If ignition does not occur within 10 sec, turn off keeper voltage and reapply 50 sec later.
t = 6 min	All power off
t = 10 min	Reset timer to zero and start next cycle.

More than 750 ignitions were accumulated during 7 days. The cyclic tests were run with a porous tungsten insert that had been operated approximately 120 hr before the start of the cyclic tests and had several exposures to air. There was no detectable different in its operating characteristics between the start and end of the cyclic tests. As a result of the endurance and restart tests, a high level of confidence was established in the ion source and system designs.

7. External Magnetic Field

One of the SPIBS program technical goals was to achieve a low external magnetic field. Quantitatively, the goal was to produce a dc field of less than 1 G at a distance of 10 cm from the system. The origin of the dc magnetic field is the ion source which uses permanent magnets.

Data taken with the ion source mounted in the EM configuration (i.e., on the vacuum enclosure baseplate and inside the vacuum enclosure) are presented in Figures 95 and 96. Data points were taken along the source centerline and along an axial line located 10 cm radially from the centerline. A correction of about 0.4 G was made for the ambient field in the measuring area. Data were taken with an "axial"-type probe.

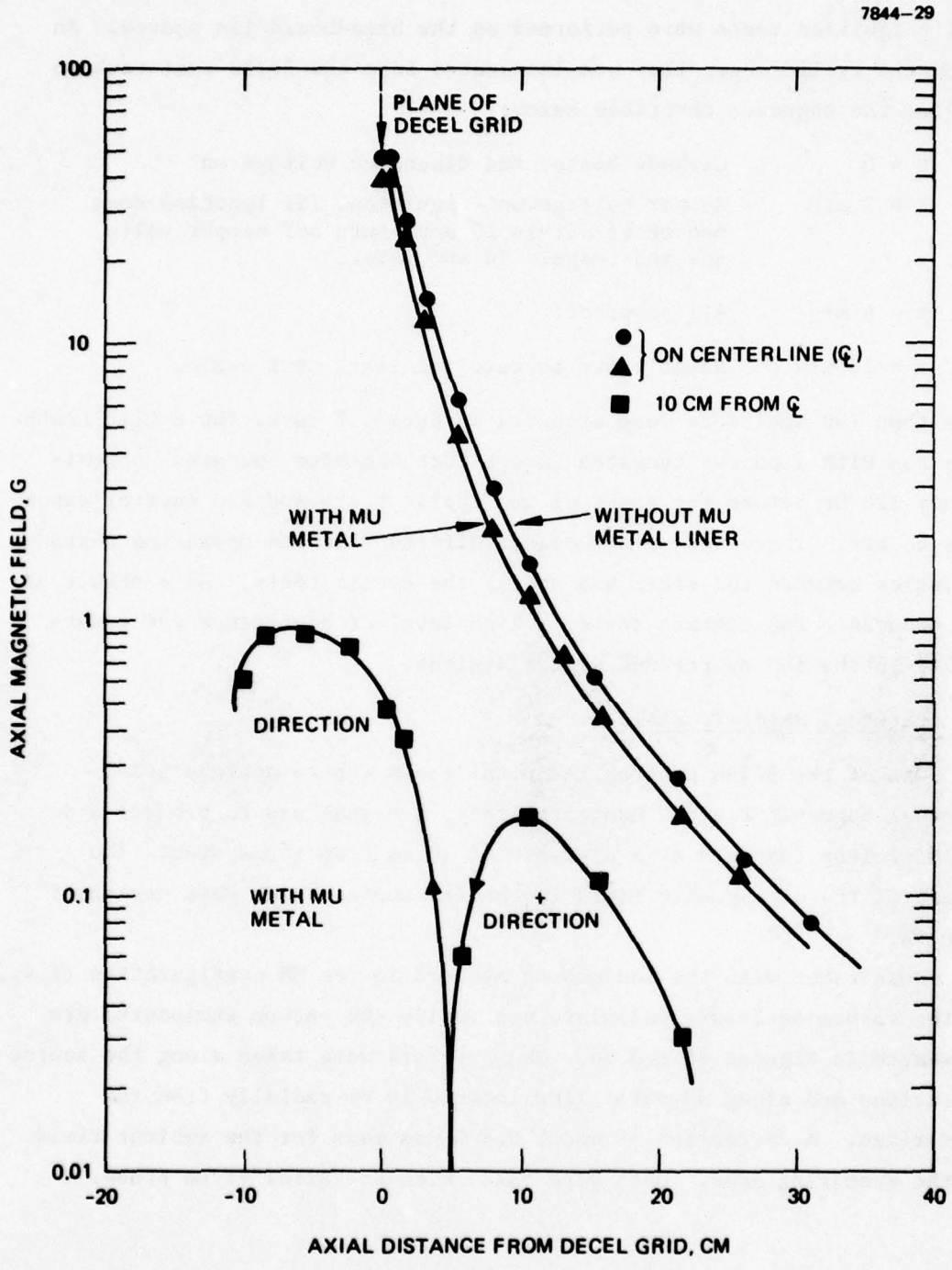

Figure 95. Magnetic field strength as a function of axial and radial position.

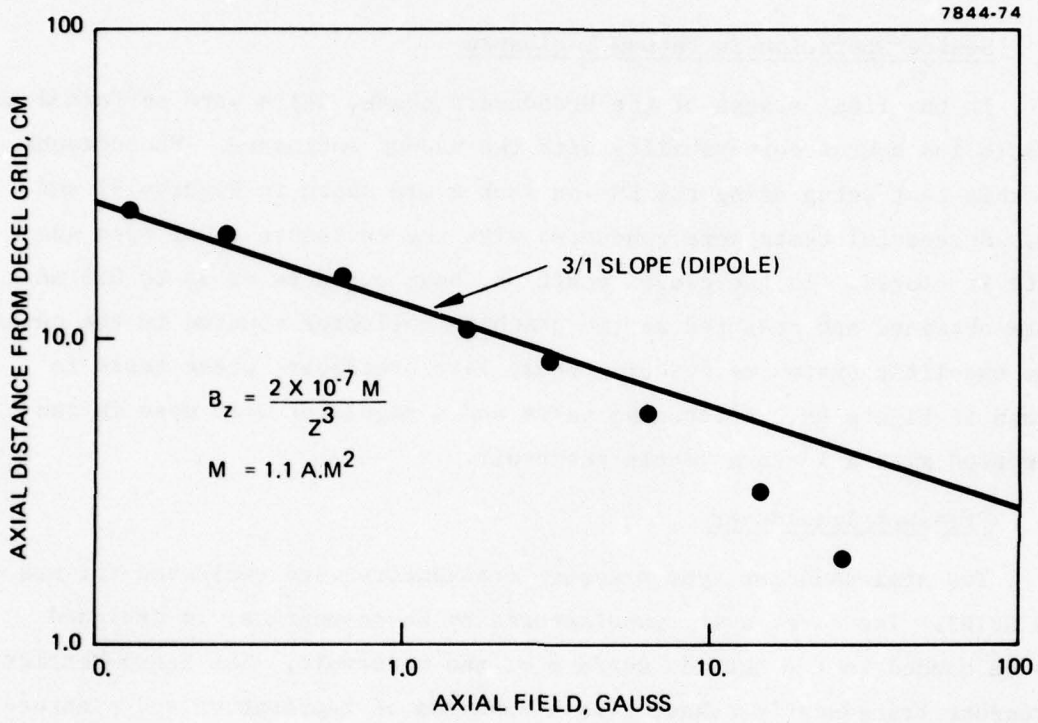

Figure 96. Magnetic field data from tests on May 4, 1976.

On axis, the field decreases continuously away from the source. At the 10 cm radial location, the expected field reversal occurs slightly ahead of the plane of the decel grid. Although further measurements in a "screened room" would improve the accuracy of these data, the external magnetic field appears to meet the 1 G level at 12 to 13 cm. As indicated in Figure 96, the field approximates that of a dipole having a strength of 1.1 $A\text{-}M^2$.

8. Source Operation in Vacuum Enclosure

In the final stages of the breadboard phase, tests were performed to assure ion source compatibility with the vacuum enclosure. Photographs of this test setup using the EM ion source are shown in Figures 97 and 98. Successful tests were conducted with the enclosure cover open and with it closed. In the closed position, beam currents of up to 0.5 mA were obtained and measured at the graphite collector mounted in the cover. The expellant system used during these late breadboard phase tests is shown in Figure 99. A latching valve and a regulator were used in conjunction with a lecture bottle reservoir.

9. Pressure Transducer

Two semiconductor type pressure transducers were evaluated for use on SPIBS. The first unit, manufactured by Sevso-metrics, is designed to be bonded to the outside surface of the reservoir. The Senso-Metrics pressure transducer's behavior as a function of temperature and pressure is shown in Figure 100. A more satisfactory behavior might have been obtained by masking a "flat" into the tank. However, such a change to the task would have jeopardized the tank's DOT rating. The Entran unit is mounted in a 10-32 screw and can be sealced into the pessure vessel with an O-ring as shown in Figure 29. Calibration data for the Entran unit is shown in Figure 101. The Entran unit was chosen for SPIBS.

M11565

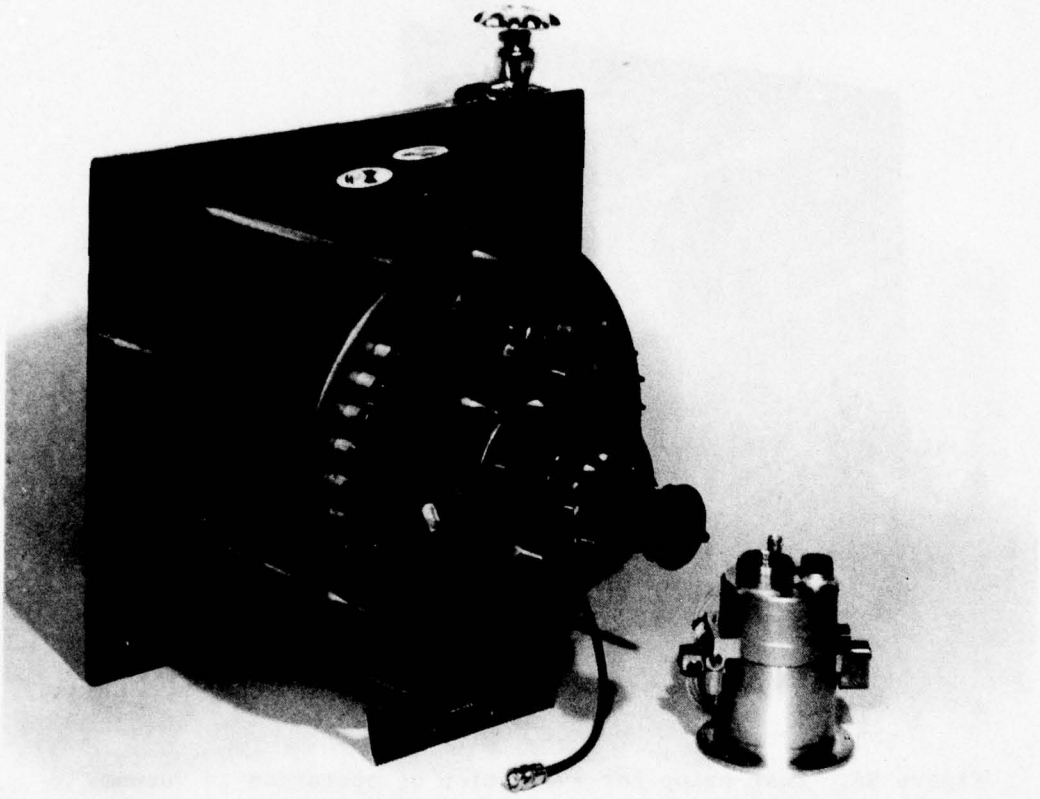

Figure 97. Test setup for evaluation of operation in vacuum enclosure: enclosure and ground screen removed.

M11568

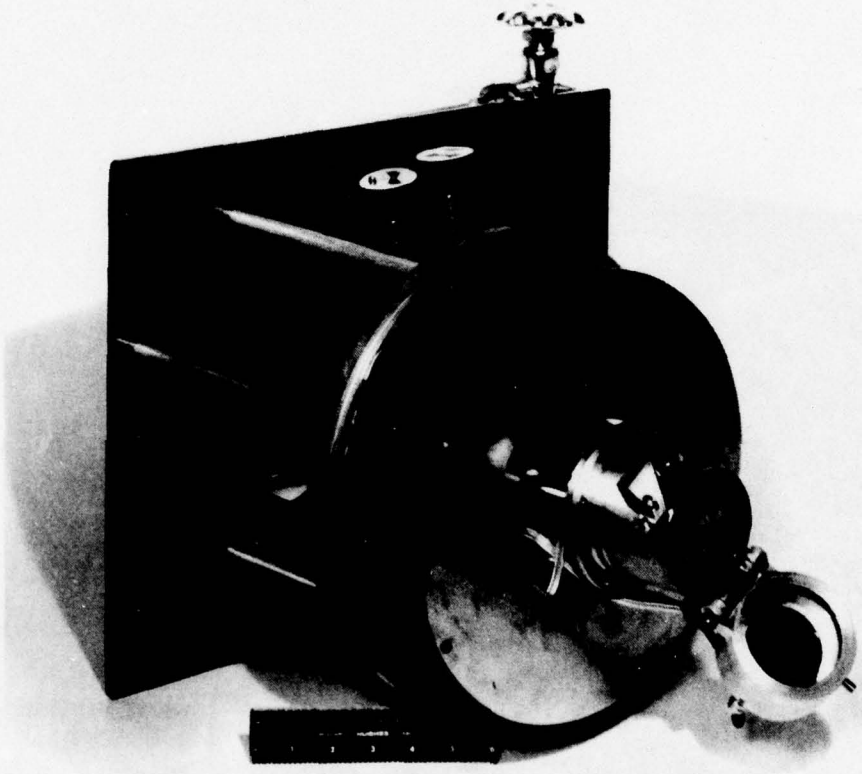

Figure 98. Test setup for evaluation of operation in vacuum enclosure: enclosure and ground screen installed; cover open.

M11570

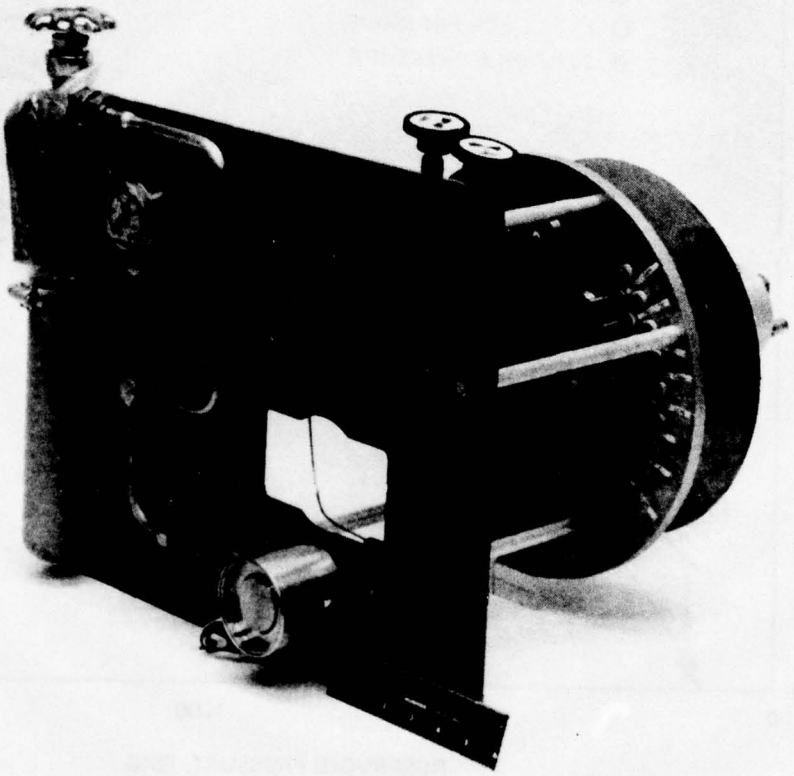

Figure 99. Test setup photograph showing latching valve and regulator.

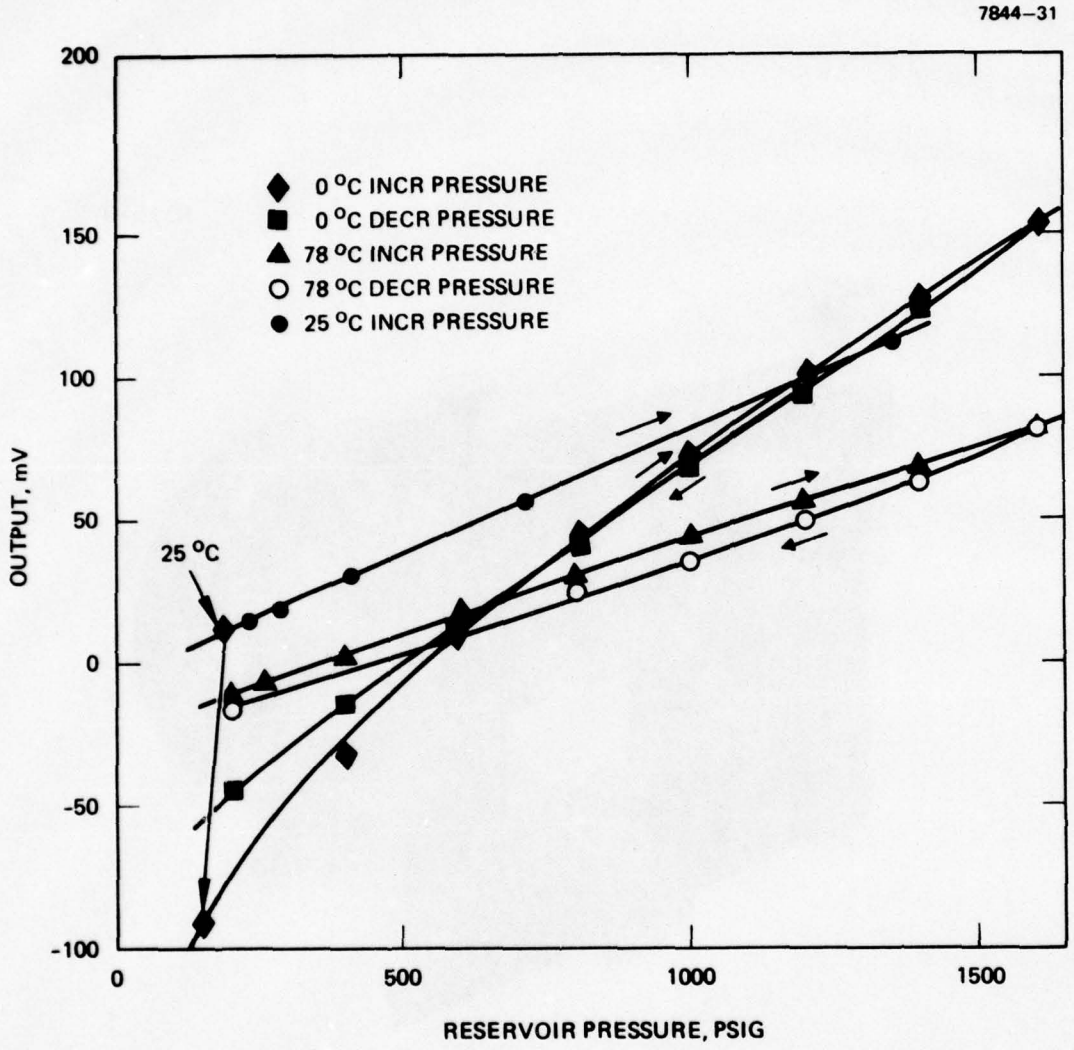

Figure 100. Calibration data for sensometrics pressure transducer.

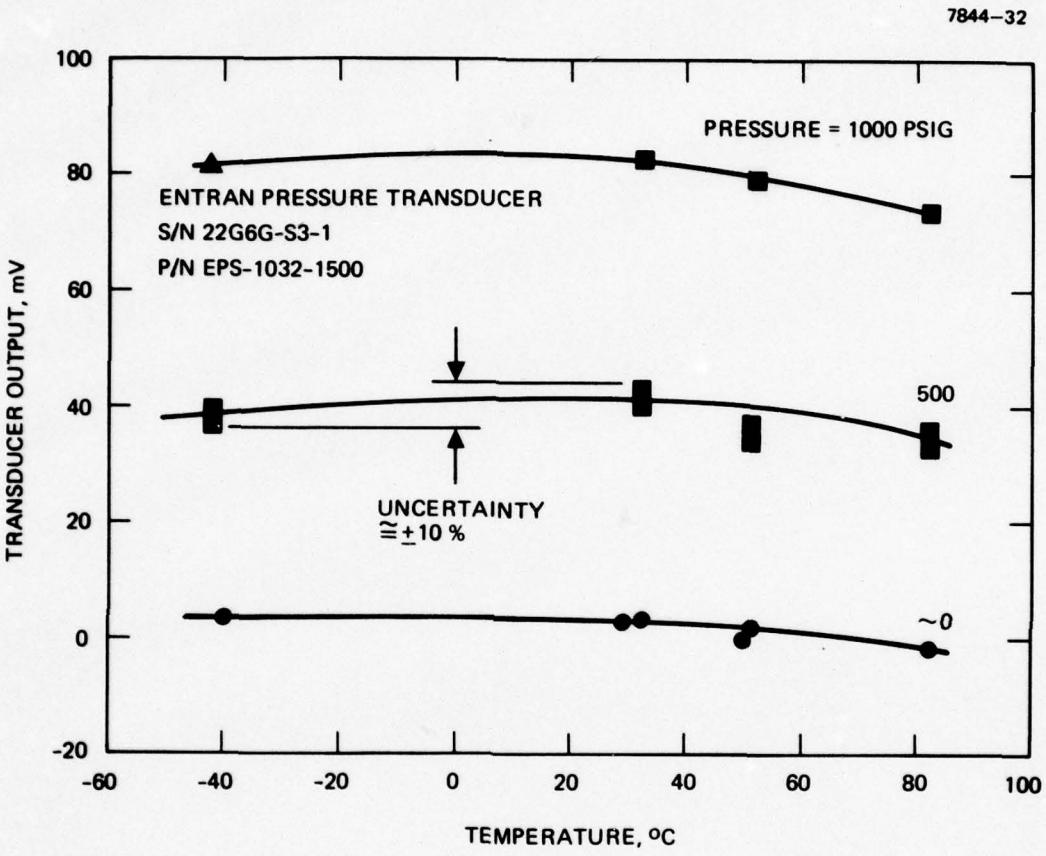

Figure 101. Calibration data for Entran pressure transducer.

SECTION 6

ENGINEERING MODEL SYSTEM

Near the end of the breadboard phase, a design review was held to present results of breadboard testing and to obtain approval for construction of the EM system. At that time (25 May 1976), the major open issues included: (1) ion source life and the continuing grid shorting problem, (2) system packaging, and (3) system mass. Although these items and several additional questions were of concern, it was agreed that fabrication of EM hardware should proceed.

Following the design review, ion source modifications were made and the shorting problems were eliminated for operating times of up to at least 600 hr. These tests were performed on the breadboard ion source and specific results were described in Section 5. These breadboard ion source modifications were incorporated into the final EM and flight source design, and no further significant source changes were made during the program. However, as discussed below, the EM and flight source porous plugs used for xenon flow control had less impedance than expected, and a minor modification of thepressure regulator was required. Except for this recalibration, most EM tests were associated with system integration and power processor set-point adjustment.

A. SYSTEM DESIGN AND ASSEMBLY

The initial system design concept is shown in Figure 102 (as presented in the first quarterly report). During the second quarter, PPA circuit card layouts were started and the need for more volume was identified. The width and height of the PPA enclosure were increased by about 2.5 cm, and the length of the cards was increased as shown in Figure 103. By the end of the third quarter, the PPA circuit card layouts were nearly complete after several iterations. To remain within the PPA volume constraint (agreed on after the previous volume increase), it was necessary to interdigitate portions of the three cards as indicated

Figure 102. Unavailable.
(Figure 2 of Quarterly 1)

Figure 103. Unavailable.
(Figure 2 of Quarterly 2)

by the dashed lines in Figure 104. Thus, "tall" components (e.g., magnetics) on one care were located next to "short" components (e.g., resistors mounted flat) on an adjacent card. The cards were extended to the maximum length and a "dog leg" was added to the middle card. Components were located on both sides of each magnesium channel section card at this point in the design evolution.

During the second quarter additional information on the pressure regulator had been obtained, and the regulator mount was updated. New details of the ion beam collector and blow-off cover were also incorporated. By the end of the third quarter the pressure transducer had been moved from the surface of the reservoir to the fill fitting, as shown in Figure 104.

The final SPIBS design is shown in Figures 105 through 107. Details to be noted in the layout drawing, Figure 105, include: (1) pressure regulator mounting; (2) the addition of connectors for the transducer, value, and cover; (3) right-angle not plates for securing the enclosure cover, and (4) the protrusion of the reservoir clamp beyond the edge of the base. The clamp was subsequently modified to move the clamp "loop" out of the way to minimize the width to about 23 cm. The photos in Figures 106 and 107 show many of the details of the EM system during and after final assembly. The wires protruding from the PPA enclosure in Figure 106 attach to terminals on the source.

Fabrication and assembly procedures for the EM system were somewhat different from those for the breadboard system, and documentation was increased. All mechanical or machined parts were trated as "controlled hardware." This process does not involve inspection of vendor facilities, but does provide 100% inspection of all fabricated parts. Electronics parts, except for magnetics, were purchased and controlled by HRL personnel. Magnetics parts were designed electrically at HRL and were built by the Hughes Components and Material Laboratory in Culver City.

During the fabrication of the EM (and rocket model) ion source, a written assembly procedure was developed. All process steps were clarified and documented for use on the flight source. The assembled ion

Figure 104. Unavailable.
(Figure 2 of Quarterly 3)

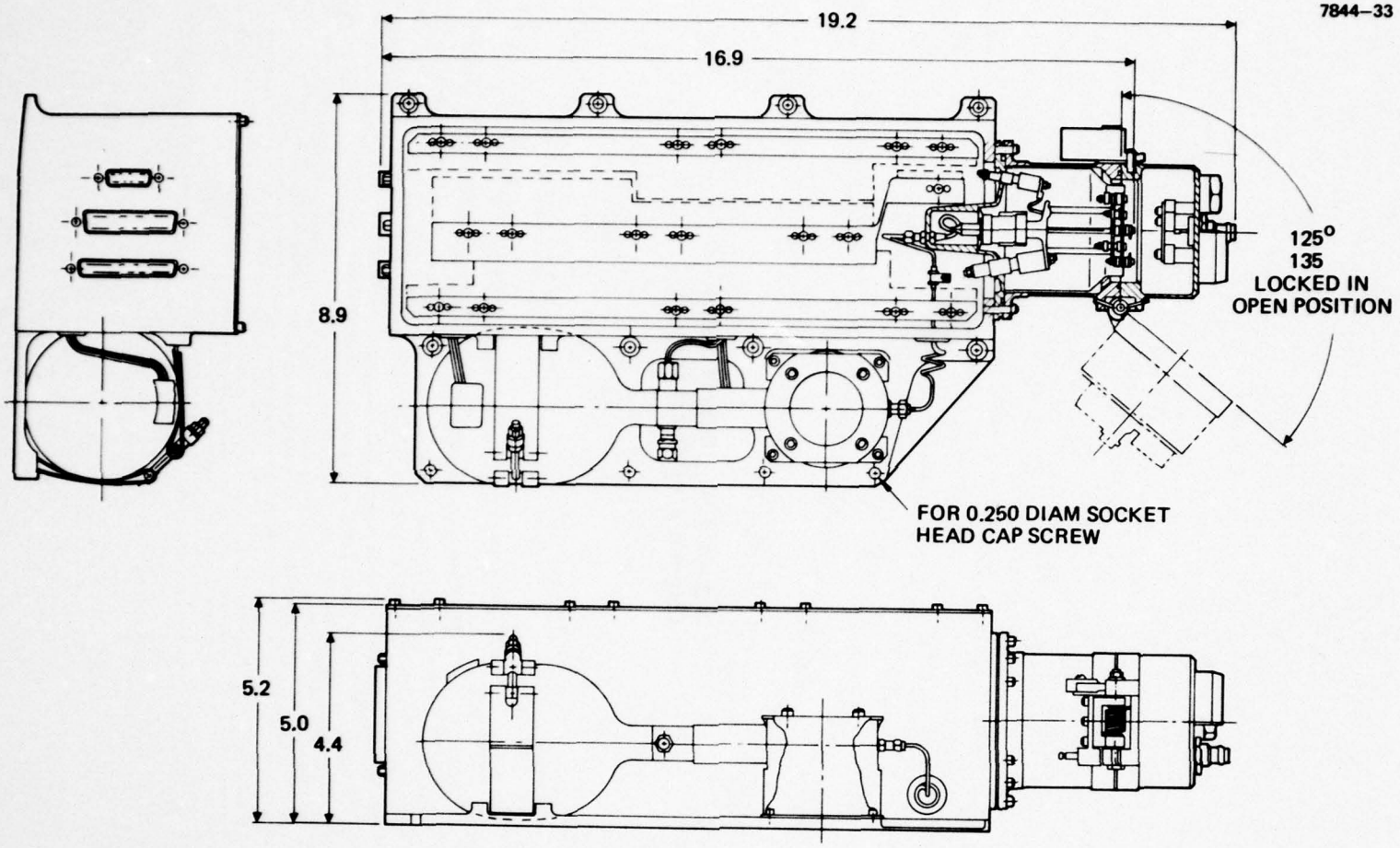

Figure 105. Final system layout drawing.

M12247

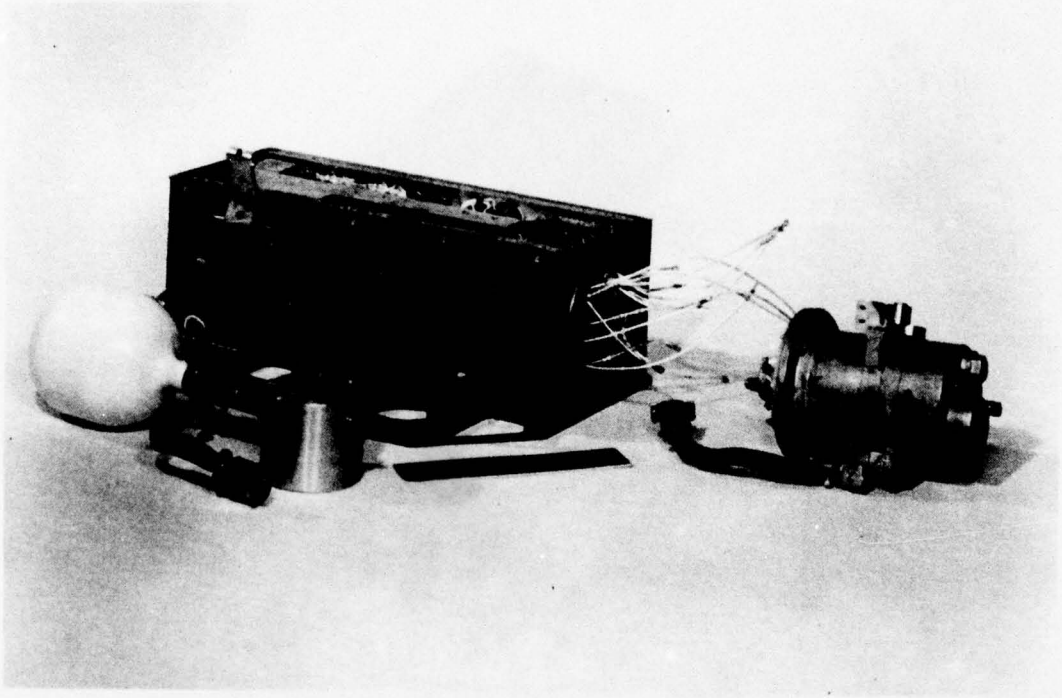

Figure 106. Exploded view of EM system during assembly.

M12244

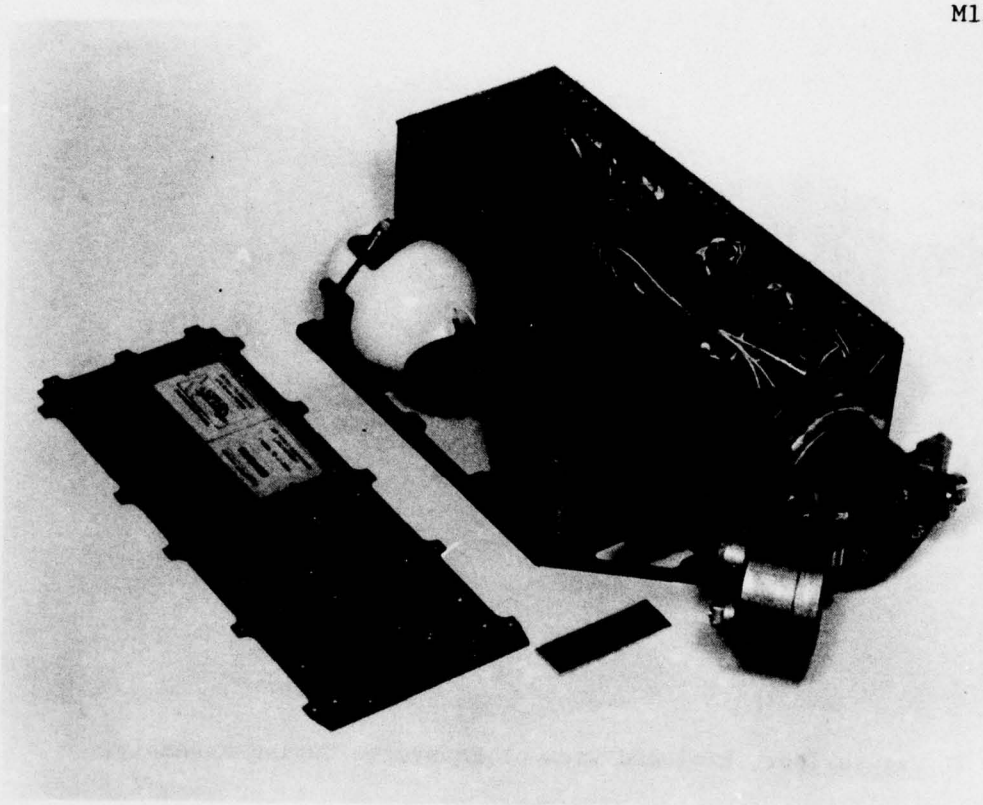

Figure 107. SPIBS hardware ready for delivery.

source was inspected by the assembly supervisor. Although the quality assurance program for the ion source was simple, few errors resulted. All sources operated properly from the first startup and had remarkably similar characteristics.

Assembly of the EM PPA was performed at the Hughes Culver City site. Harness design, point-to-point wiring lists, assembly, and inspection were handled at this facility. Parts kits were supplied by HRL. After the three circuit cards were assembled, electrical tests were made to verify proper assembly. The intra-card harness was then installed, and tests were performed on dummy loads and with an ion source. Select-by-test components were installed; all corrections were finalized; and a pre-conformal-coat test was made with the system. After system performance verification, the PPA was plotted (all high voltage areas) and conformally coated for environmental protection.

The ion source, PPA, and expellant assembly were then integrated. The various tests performed during the assembly phase are discussed in the following section.

In addition to meeting size and performance requirements, system weight was a major concern. The initial weight goal of 6.3 kg (14 lb) was based on estimates made during the proposal phase. However, after assessing the PPA design and packaging complexity, the estimate was raised to 7.36 kg (16.2 lb). This increase was mainly associated with PPA components; improved estimates of harness, potting, and conformal weights; and the larger enclosure. At the second design review, the weight estimate was increased to 7.5 kg based on the measured weight of portions of the EM system; fortunately, the actual final weight was less than 7.4 kg, as shown in Table 11.

To minimize SPIBS weight, magnesium was used extensively. Except for minor parts of the ion source vacuum enclosure, all machined parts were magnesium, including the PPA circuit card structure. The PPA enclosure and SPIBS structure were machined extensively to remove all excess material, as shown in Figure 108.

Table 11. Engineering Model Weight Breakdown

Element	Weight, g
	Revised Estimate
Ion Source Assembly (ISA)	
Ion Source Enclosure endplate Insulators, wiring, and fasteners	490[a]
Expellant Assembly (EA)	
Tank (empty) Valve, fill fitting, and transducer Regulator	1253[a]
Xenon	270
Lines and fittings	20
Connectors and Miscellaneous	50
Power Processor Assembly (PPA)	
Circuit card 1	961[a]
Circuit card 2	1026[a]
Circuit card 3	810[a]
Conformal coating and potting	300
Connectors and wiring	550[a]
Structure and Mechanisms	
Blowoff cover assembly	540
PPA enclosure	850[a]
Clamps and fasteners	230
Contingency	150
TOTAL	7,500 g

[a]Measured engineering model weights.

6326

M11949

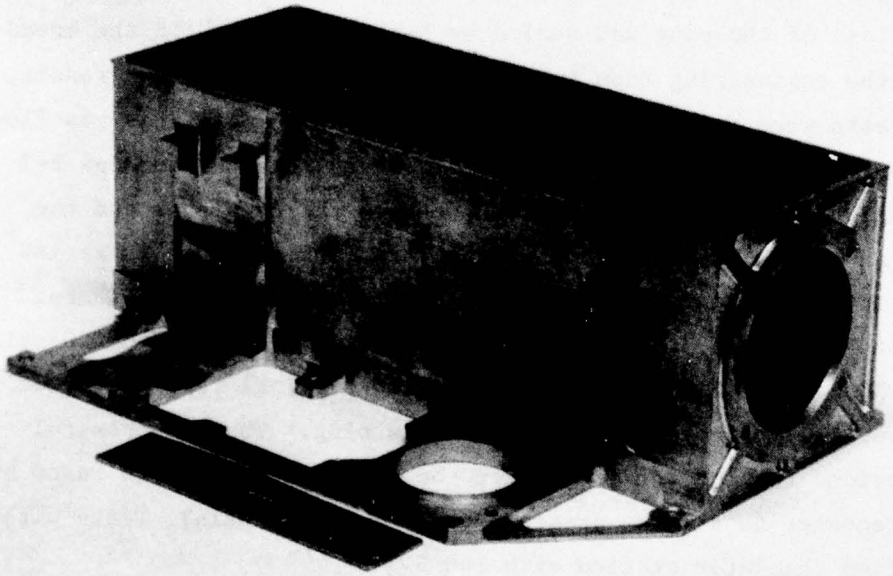

Figure 108. EM system setup for thermal testing.

B. SYSTEM TESTING

A broad range of tests with the EM system verified proper operation and satisfactory performance. The 22 test runs made are summarized in Table 12. The majority of these tests fall into a "verification" category. A few tests were of a development nature and resulted in modifications or system changes. Although several difficulties were encountered during this period, no significant redesign or rework was required.

Initially, the EM phase tests centered on the EM ion source, operated from the breadboard PPA. Due to differences in the ion source fabrication process, introduced to assure reproducibility for the flight source, the EM source porous plug had lower flow impedance than anticipated. (Less of the plug was sealed by E-beam "washing" in the breadboard in the engineering than in the breadboard model.) As a result, several tests were required to seek a method for reducing the gas flow to the source. As indicated in Table 12, tests runs B-2 through B-7 used additional plugs in the gas line between the regulator and the source. An equivalent impedance of about two normal plugs in series with the original plug was required to obtain the desired flowrate. In runs B-8 through B-13, the regulated pressure was reduced from 20 psia to about 7 to 8 psia (the lower limit of the original regulator), using the EM source with only the built-in porous plug. These successful tests provided the impetus for having the pressure regulators reset by the manufacturer to a lower pressure range (4 to 10 psia). Tests with the modified regulator started with run B-14.

In parallel with the porous plus impedance investigation, other system tests were continued. Starting with run B-9, the EM PPA was integrated into the system. A series of tests were then conducted to select various resistors for set-point adjustments. Demonstrations were conducted for AFGL personnel during runs B-10 and B-11.

During the installation of the PPA into the enclosure prior to run B-10, a cracked weld was found on card A-2 (at "dog leg"). It was mutually agreed that the A-2 card would be repaired, but that it would

Table 12. Summary of Engineering Model Tests During Sixth Quarter

Test	Purpose	Test Setup Change Prior to Run	Remarks
B-1	Initial operation of EM-ISA with BB-PPA and BB gas system.		Operated for 21 hr. Indication of high gas flow Level 3 - 0.89 mA. Regulator set at 20 psia.
B-2	Operate ISA with lower gas flow.	Two porous plugs with 0.125-in.-diameter open area placed in gas flowline. Laboratory supplies used.	Gas flow too high. Level 3 = 1.44 mA. Regulator set at 20 and 16 psia.
B-3	Operate ISA with lower gas flow.	Porous plug with 0.050-in.-diameter open area placed in gas flowline.	Gas flow too high. Level 3 = 1.62 mA. Regulator set at 16 psia.
B-4	Operate ISA with lower gas flow.	Porous plug with 0.039-in.-diameter open area placed in gas flowline.	Gas flow near desired value. Level 3 = 1.71 mA. Regulator set at 16 psia.
B-5	Operate ISA with lower gas flow.	Porous plugs with 0.038-in.- and 0.050 in. diameter open areas placed in gas line.	Consumed xenon gas before obtaining data.
B-6	Repeat B-5	New gas bottle. Source enclosure added.	Performance good. Level 3 - 1.98 mA. Regulator set at 17 psia. Startup time ≈30 min.
B-7	Checkout relay rack mounted BB-PPA.	BB-PPA	Performance good. Level 3 = 1.90 mA. Startup time ≈30 min. BB-PPA operational.
B-8	Throttle gas flow by varying regulator setting.	Only ISA porous plug in feedline.	With regulator at 7 psia. Level 3 = 1.9 mA, Level 2 = 0.9 mA, and Level 1 is unstable.
B-9	Operate ISA with EM-PPA	EM-PPA in air, out of box. Obtain input power values and select-by-test components.	With regulator at 8.1 psia. Level 3 = 0.51 mA and stable with I_D = 60 mA, Level 2 = 0.88 mA, and Level 1 = 1.7 mA.
B-10	Operate ISA with EM-PPA in Mg housing demonstrate operation at Design Review .	EM-PPA in Mg housing.	Discharge unstable for low discharge current values.
B-11	Continue demonstration for Design Review and operate with increase keeper and discharge current.	EM-PPA out of Mg housing for access to components.	Discharge current = 250 mA; keeper current >200 mA; regulator set at 8 psia. Level 1 = 0.3 mA; Level 2 = 0.9 mA; Level 3 = 1.9 mA
B-12	Evaluate PPA after conformal coating and potting.	Conformal coating and potting of PPA.	Successful test.
B-13	Evaluate eratic operation	None	Grounding problem resolved.
B-14	Checkout modified pressure regulator.	Installed modified regulator.	Regulator OK; burned out filament.
B-15	First full system test in vacuum.	Completed system assembly; new filament.	Successful test; keeper transformer failed.
B-16	Checkout keeper transformer.	Installed new transformer.	Successful test.
B-17	System test with known gas reservoir.	Installed lecture bottle reservoir.	Test results inconclusive.
B-18	Full system test with reservoir.	Installed new reservoir.	Successful test; electrometer failed.
B-19	Checkout electrometer repair.	Repaired electrometer.	Successful test.
B-20	Full system test with full reservoir.	Installed full reservoir.	Successful test.
B-21	Ground test simulation	Connected system only at pump-out port.	Successful test.
B-22	Final test after painting.	Disassembled system for painting; reassembled for delivery.	Successful test; system prepared for shipping.

6326

be switched with the same card in the rocket model system. This card substitution was made and the EM system was subsequently potted and conformally coated. Figure 109 shows the PPA and harness before potting. Checkout tests with the fully system in air were conducted in runs B-12 through B-14.

The EM PPA and system were instrumented with thermocouples for thermal vacuum testing as shown in Figure 110. These temperature measurements were designed to be used in conjunction with analytical thermal model results. Run B-15 was the first full system test in vacuum, and the only test run with thermocouples. The thermal model, presented in Appendix A, provides a reasonable representation of the hardware except on the blowoff cover and decel grid. For these areas, the model predicts much higher temperatures than those experienced. However, for the more critical areas, such as the PPA cards, the measured temperatures are close to those predicted. In specific terms, the temperature drop across the card (from center to base) was predicted to be about 9°C; measurements indicated a drop of about 6°C. Thus, if the SPIBS environment on the satellite is maintained within reasonable bounds, the electronics will remain within acceptable temperature limits. Other SPIBS components are expected to tolerate broader temperature ranges than the electronics.

During run B-15, the keeper power supply high voltage transformer failed. The cause was believed to be a marginal design and the use of relatively rigid potting material. This material apparently causes the ferrite cores to crack, resulting in low inductance. This is discussed in more detail in Appendix B.

The testing pause resulting from the transformer replacement allowed time to refill the xenon reservoir. Runs B-16 and B-17 were subsequently used to checkout the electronics and the system on a known gas system (lecture bottle). In run B-18, a resistor failed in the decel circuitry; a carbon composition type resistor was substituted for the original metal film type. Run B-19 was devoted to system checkout following the repiar of the decel circuit. At this point, a leak in one of the latching valves (rocket model) occurred. To deliver the rocket model, the

M12056

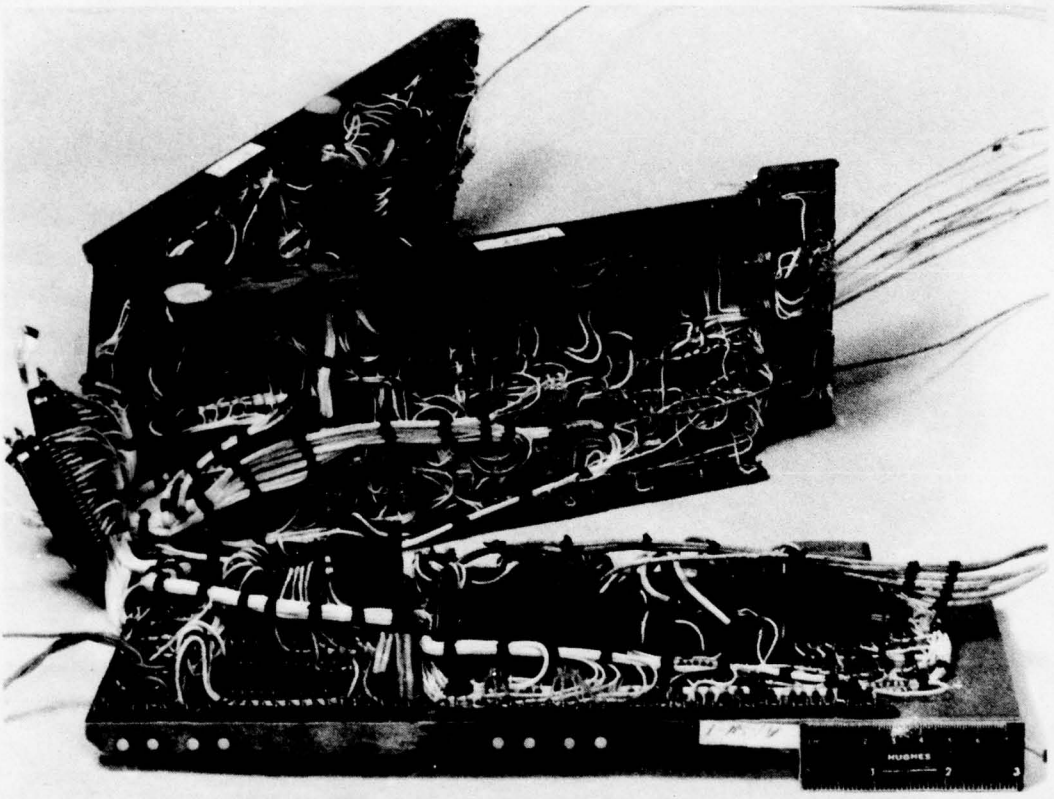

Figure 109. Photograph of PPA circuit cards harnessed, potted, and conformally coated.

AD-A063 964 HUGHES RESEARCH LABS MALIBU CALIF F/G 20/7
SATELLITE POSITIVE ION BEAM SYSTEM.(U)
OCT 78 T MASEK F19628-76-C-0066
UNCLASSIFIED AFGL-TR-78-0141 NL

3 OF 3
ADA
063964

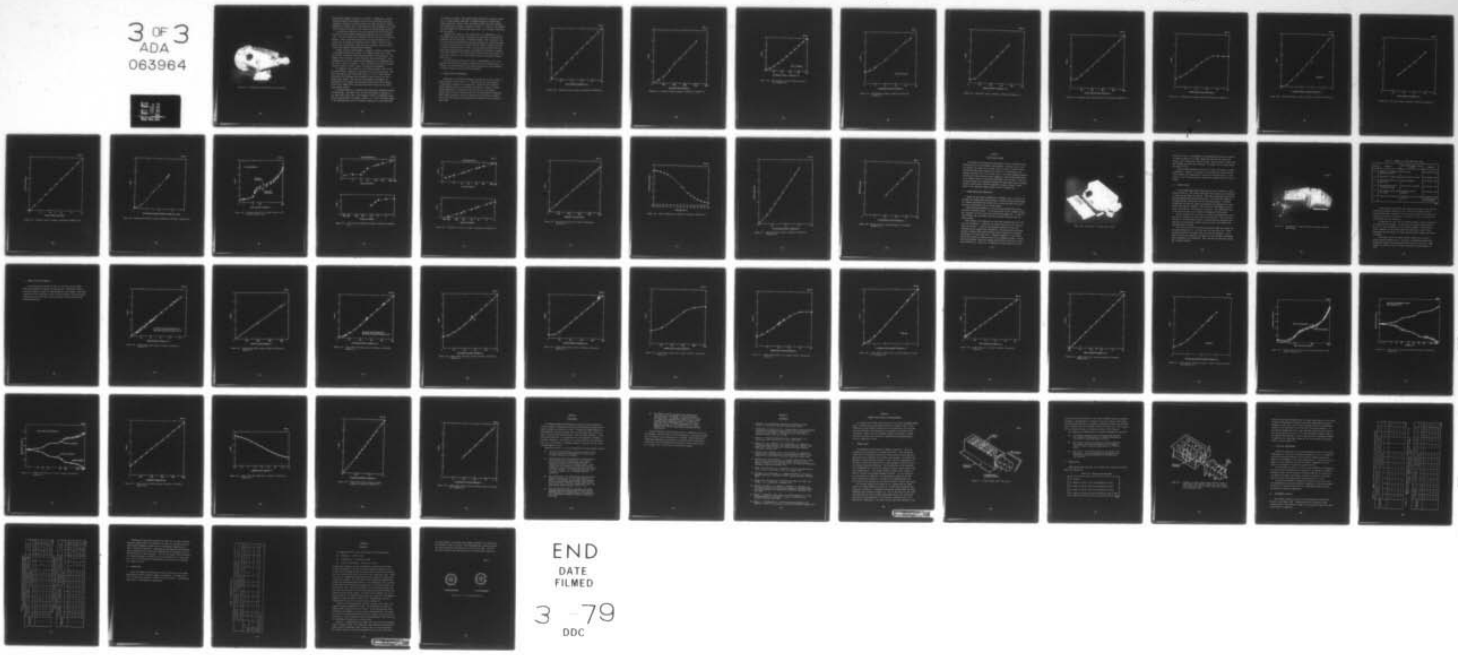

END
DATE
FILMED
3 -79
DDC

M12147

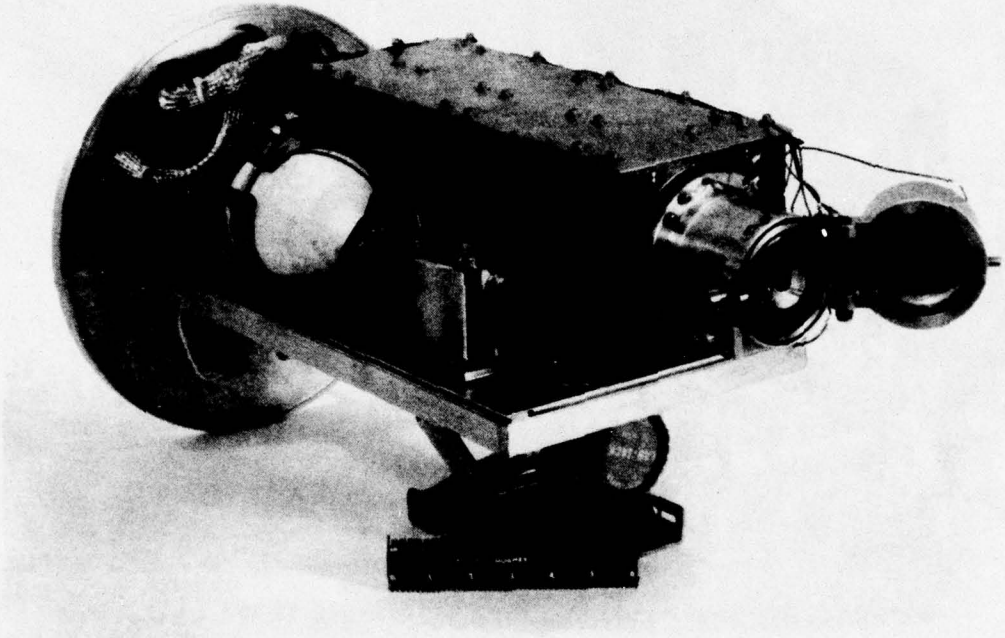

Figure 110. Photograph of PPA enclosure and structure.

EM expellant assembly was used on the rocket. Subsequently, another expellant assembly was prepared and filled (all latching valves were eventually returned to Carlton Controls for nickel plating of internal components to prevent rust.) The system was then integrated with a full xenon reservoir and given a final checkout in vacuum during run B-20.

A ground-test simulation test was conducted in Run B-21 with the system in air and evacuated through the pump-out port in the blowoff cover. No difficulties were encountered at the 1 mA and 1 kV beam conditions. Since the primary objective of the ground checkout is to assure that the system is functional before launch, a check of other levels is not appropriate. Long term source operation with the cover closed risks sputter coating various surfaces.

Toward the end of the EM phase, a change in exterior surface finish on the SPIBS was directed by AFGL. The original finish was a clear, electrically conductive oxide obtained through a dipping process. For thermal control reasons, a black conductive paint was desired. Thus, following run B-21, the system was disassembled and all magnesium parts were sent to AFGL for painting. After reassembly, the full system was tested in vacuum to verify correct operation and performance.

In comparison with results of the breadboard phase, tests of the EM system showed a significant improvement in ion source startup. The source discharge would consistently ignite in 2 min. After initial activation, the discharge would frequently ignite without the use of keeper high voltage. This excellent performance can probably be attributed to the compact and clean gas system and the short cathode heater wires (which allow relatively more heater power for the same power supply output).

An operating mode not originally anticipated was experienced during the EM testing. This mode is one in which the keeper is ignited at a low value (less than 30 mA), the discharge current is essentially zero, and the cathode heater is limited to about 1 A. Such a condition arises if the discharge goes out but the keeper remains at a level sufficient

to sustain the plasma. The cathode heater supply and the keeper supply share a high-voltage transformer to minimize parasitic power during normal operation. However, when the keeper drains even small currents, the cathode heater current is limited to about 1 A. Since it was expected that the keeper and cathode heater would never be on together, this mode was not planned.

However, as a result of the rocket test of the RM-SPIBS, it was determined that beam current levels below 0.3 mA might be desirable and necessary for full evaluation of SPIBS on SCATHA. The "low keeper current only" mode can probably be achieved repeatedly by turning the SPIBS on in the low discharge current mode (25 mA) without initially starting at higher discharge current. Such a startup process probably does not allow the cathode emission process to stabilize sufficiently to operate as an "auto cathode." The beam current obtained in this low keeper current mode is about 0.1 mA, giving SPIBS a beam current dynamic range of about 20 to 1.

The EM system was delivered to AFGL in mid-September, 1977. Subsequent tests performed at AFGL confirmed the results reported here. In addition, successful vibration and thermal-vacuum tests were performed to satisfy satellite qualification requirements.

C. ANALOG OUTPUTS (TELEMETRY)

Operation of the SPIBS instruments is monitored by means of the 18 analog outputs listed in Table 4. Calibrations for these channels are presented in Figures 111 through 128. These data were obtained using resisting loads on the supplies individually. However, during system integration, the PPA was connected through a meter panel (Figure 88) to verify calibrations and to set select-by-test components. Most of the calibration curves are believed to be accurate to within ±5% of the true value; the electrometers are believed to be accurate to about ±10%.

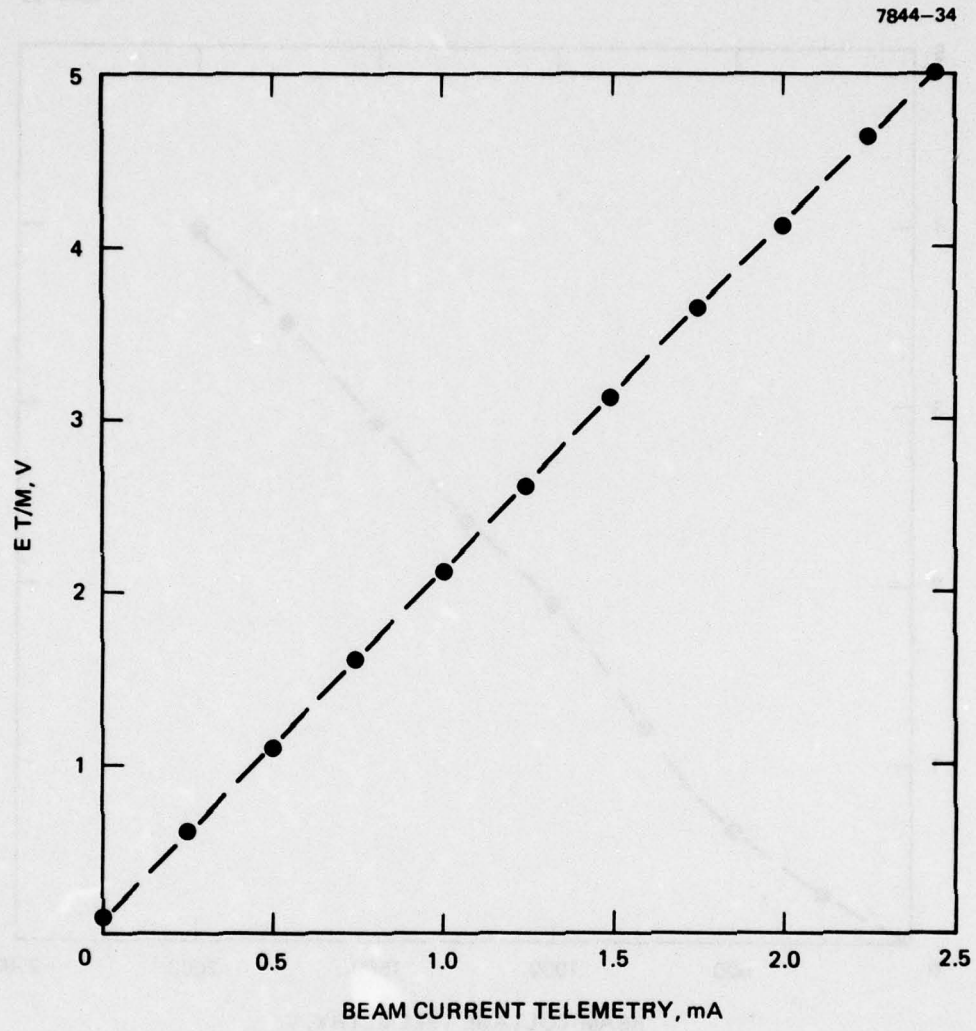

Figure 111. EM beam current telemetry calibration (Channel 1).

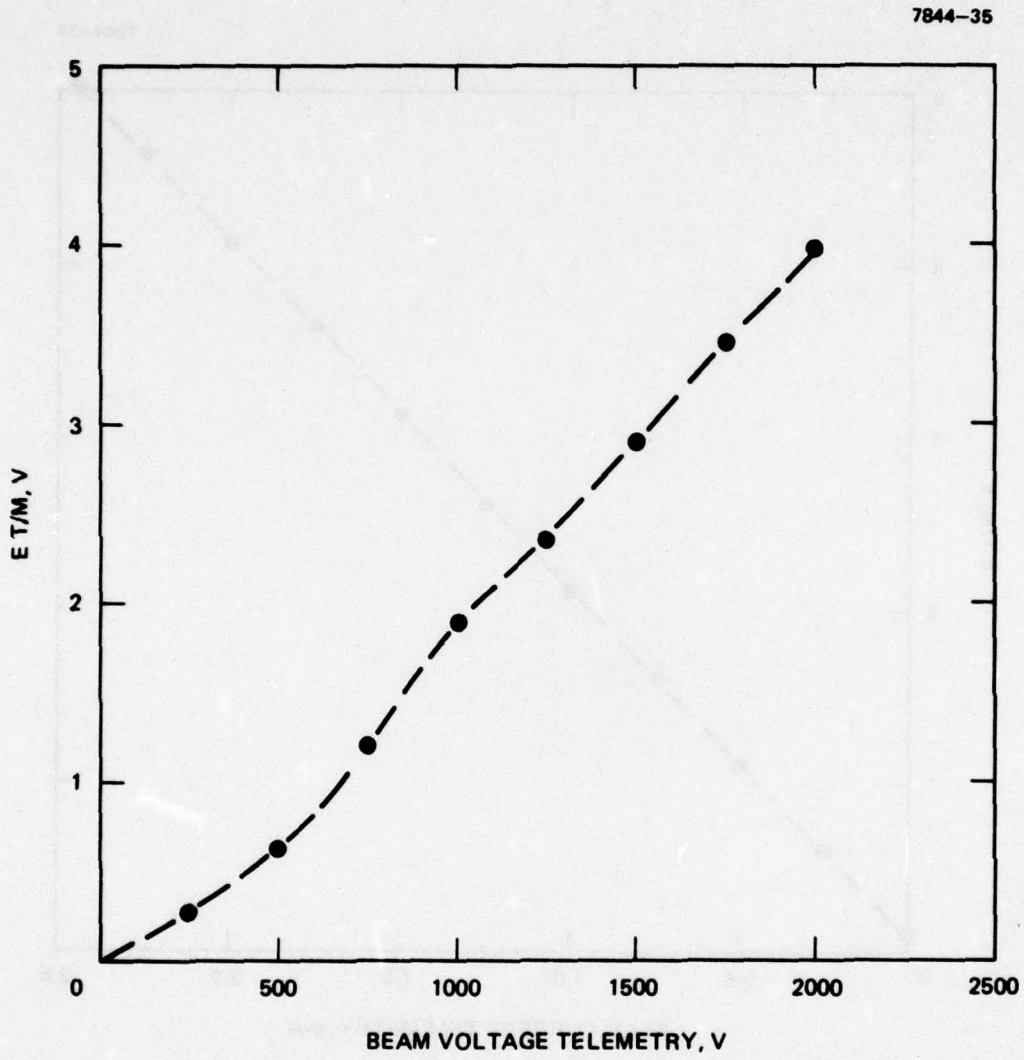

Figure 112. EM beam voltage telemetry calibration (Channel 2).

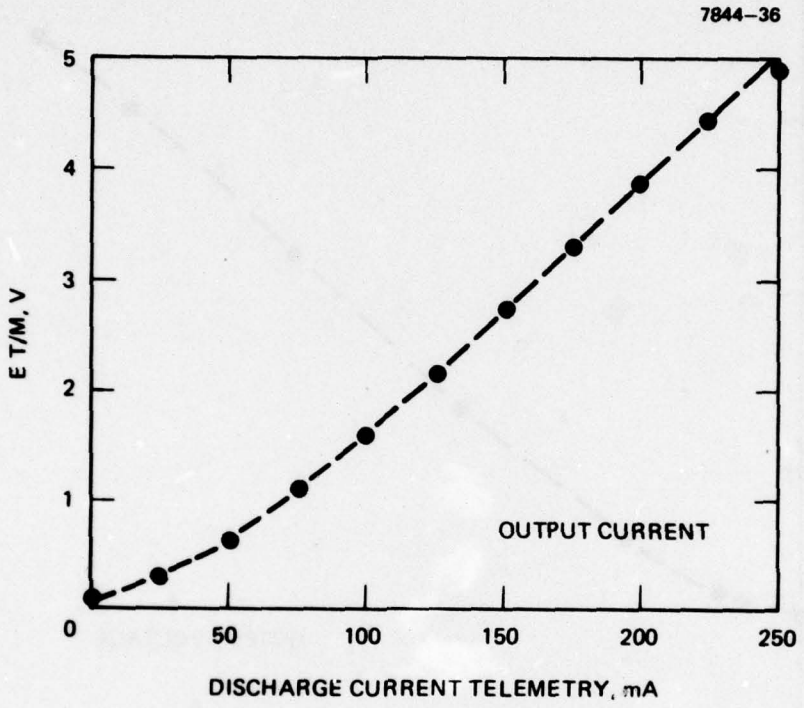

Figure 113. EM discharge current telemetry calibration (Channel 3).

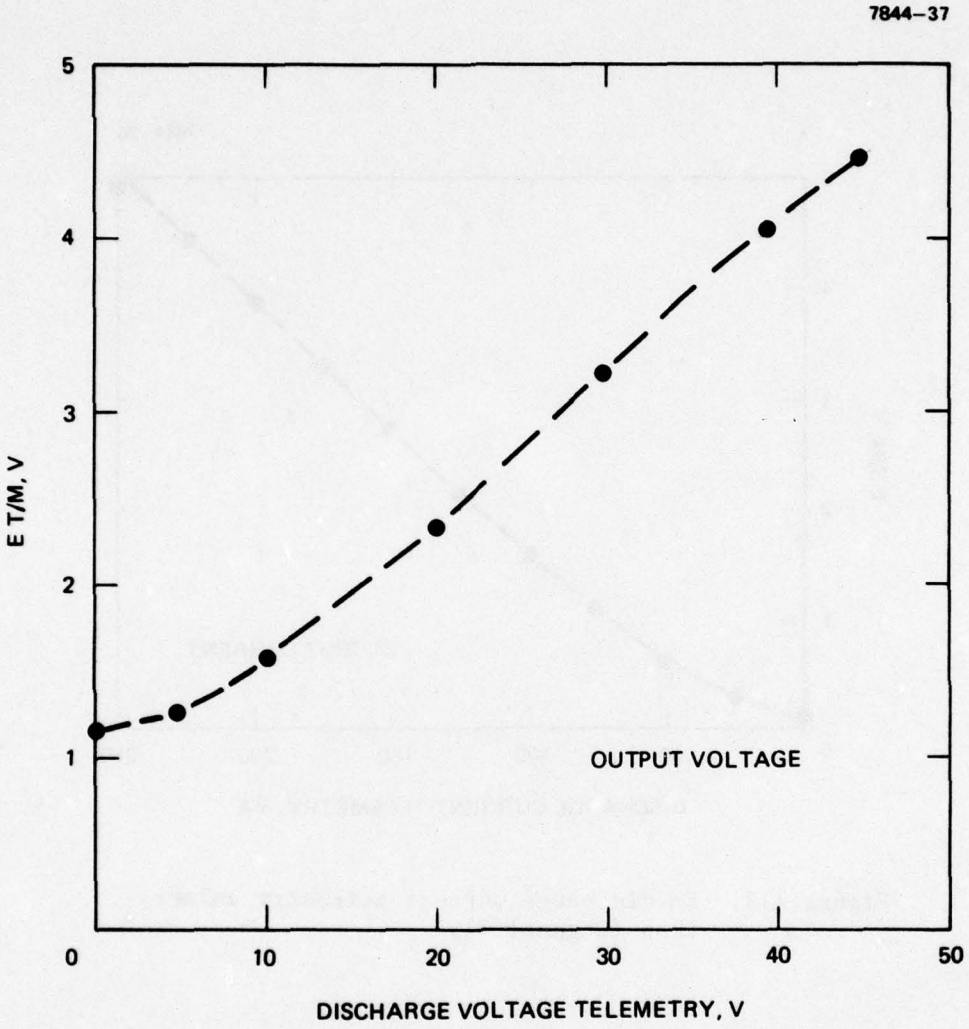

Figure 114. EM discharge voltage telemetry calibration (Channel 4).

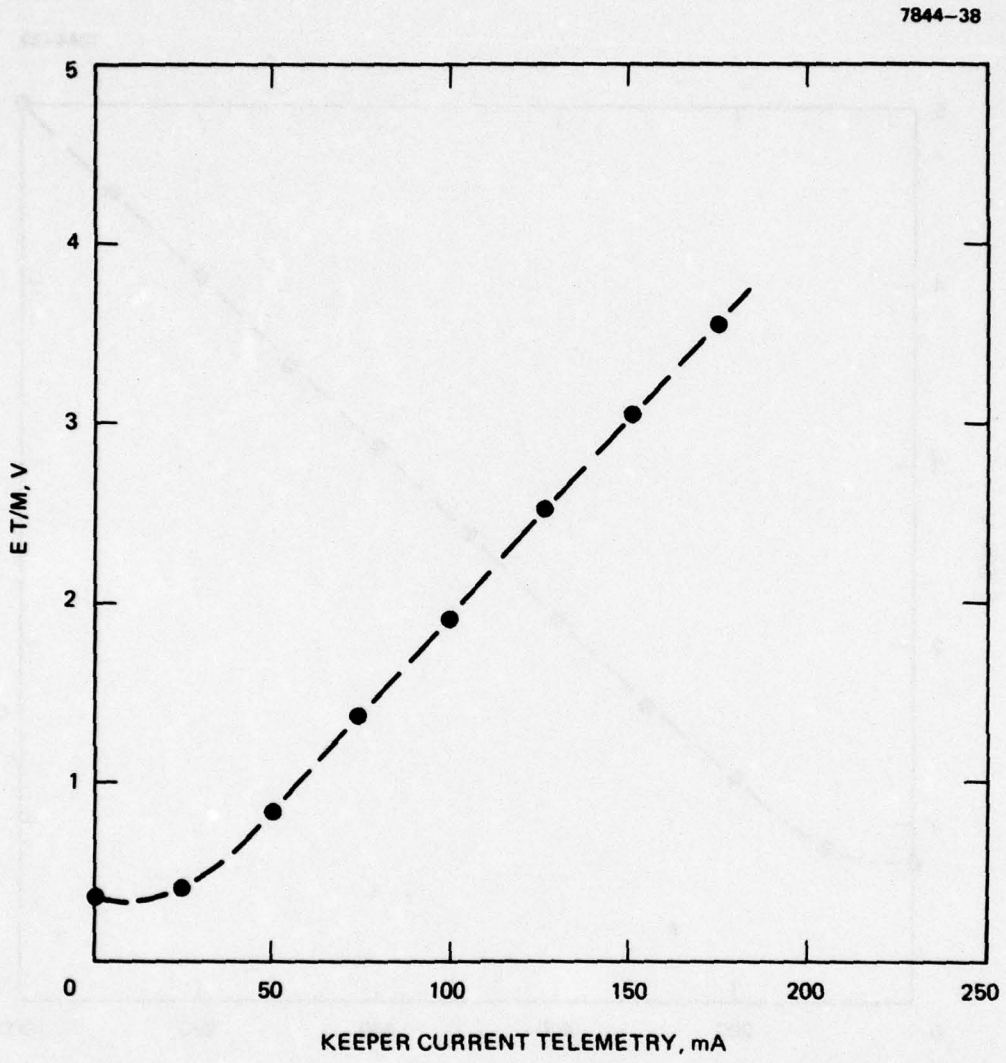

Figure 115. EM keeper current telemetry calibration (Channel 5).

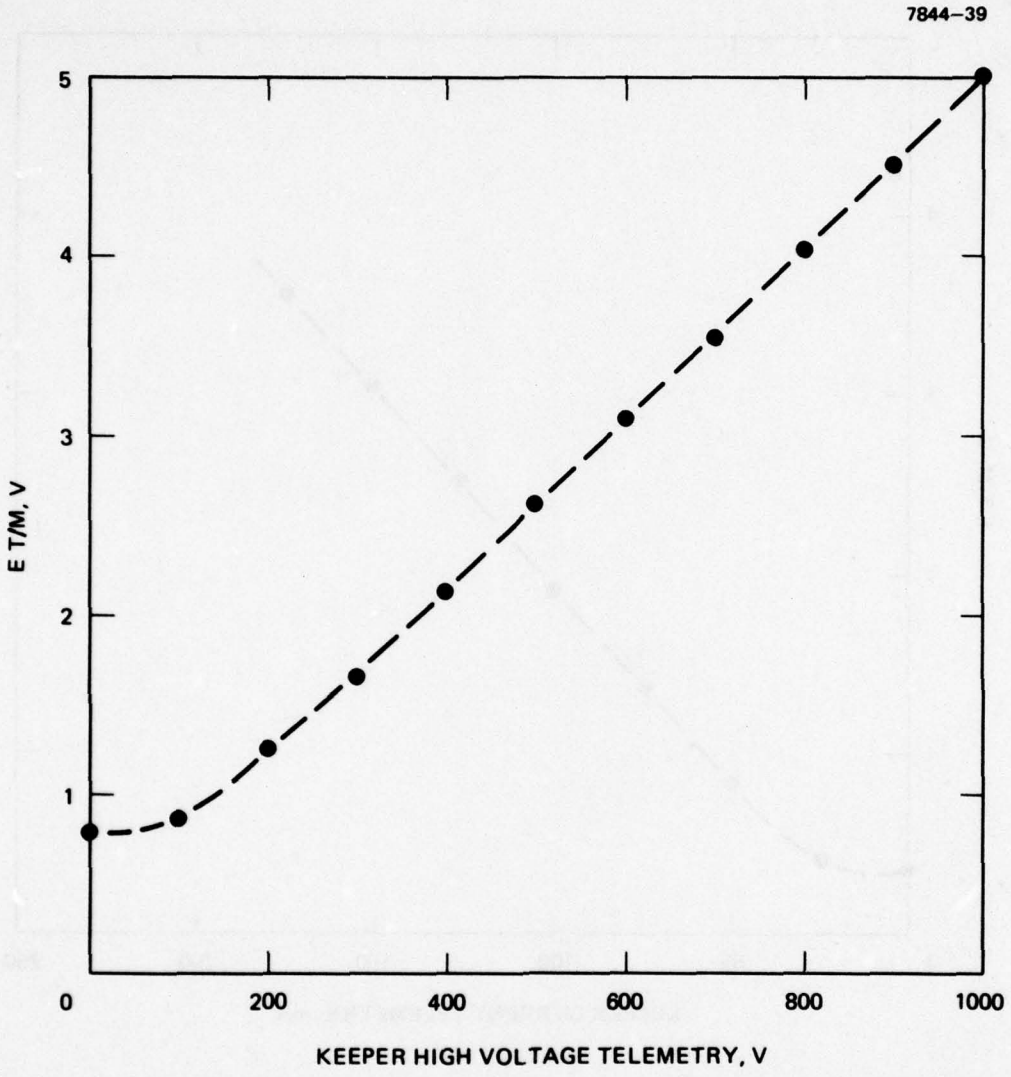

Figure 116. EM keeper high voltage telemetry calibration (Channel 6).

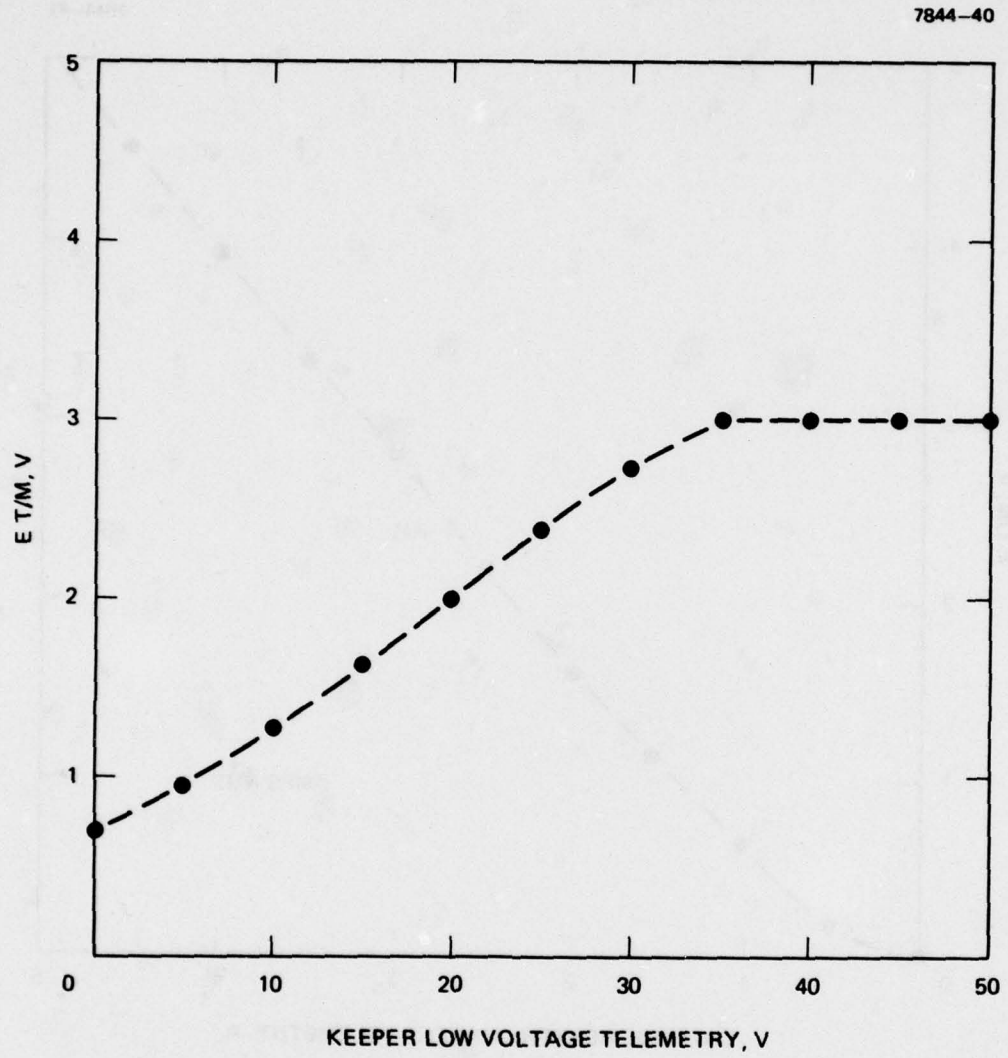

Figure 117. EM keeper low voltage telemetry calibration (Channel 7).

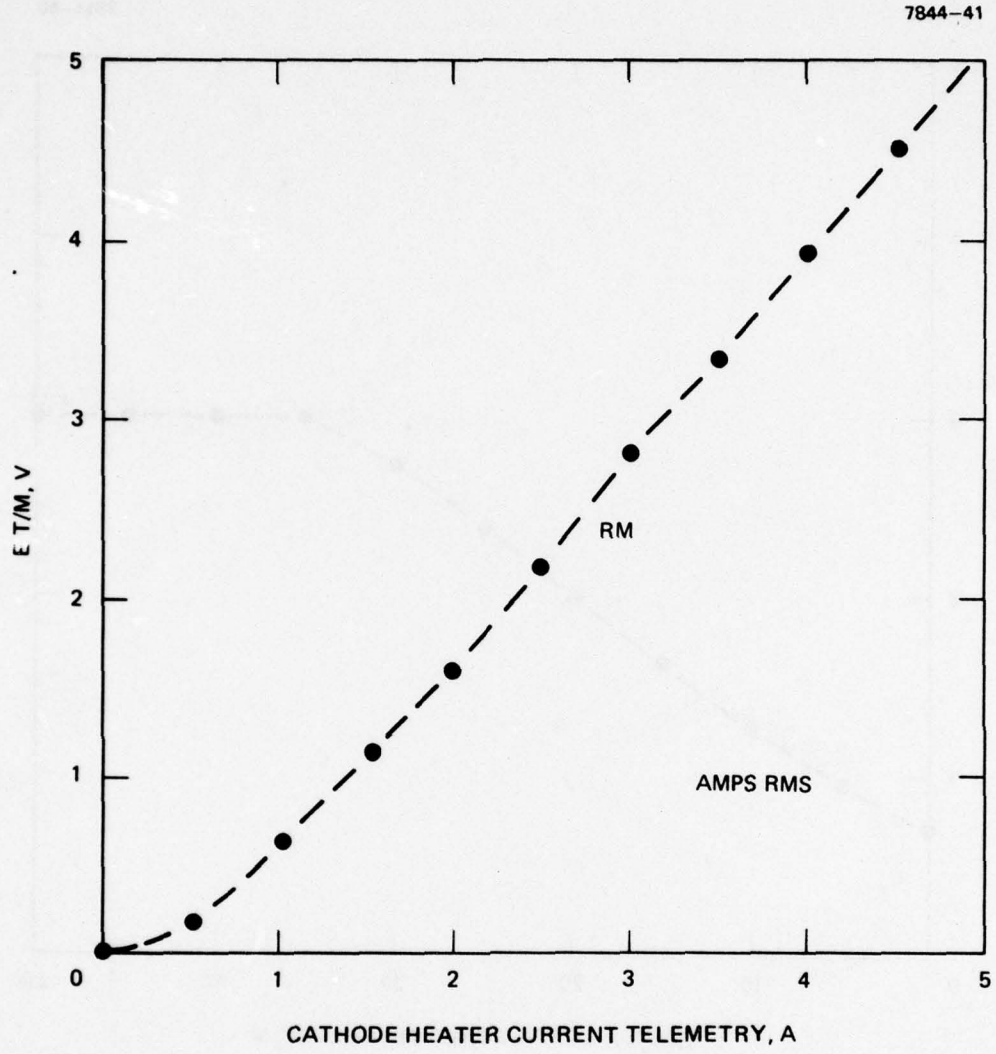

Figure 118. EM cathode heater current telemetry calibration (Channel 8).

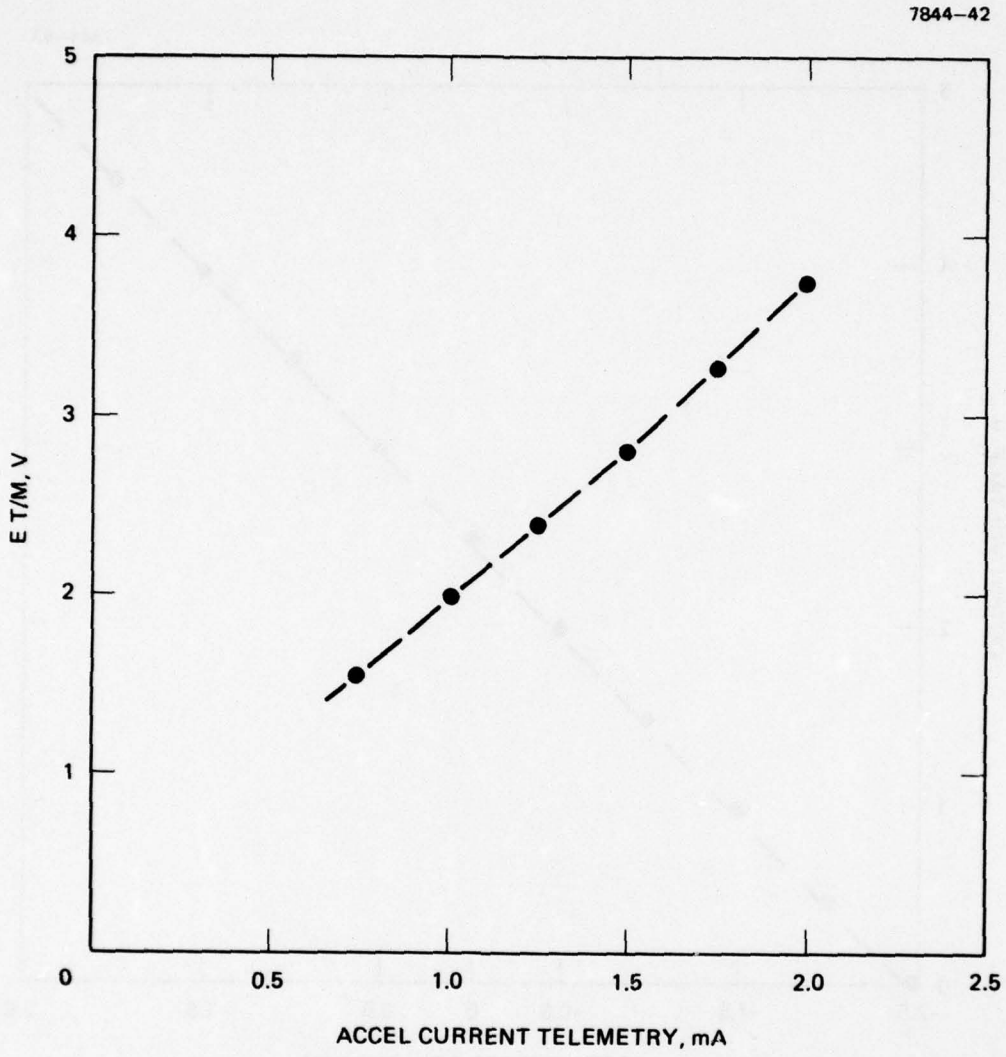

Figure 119. EM accel current telemetry calibration (Channel 9).

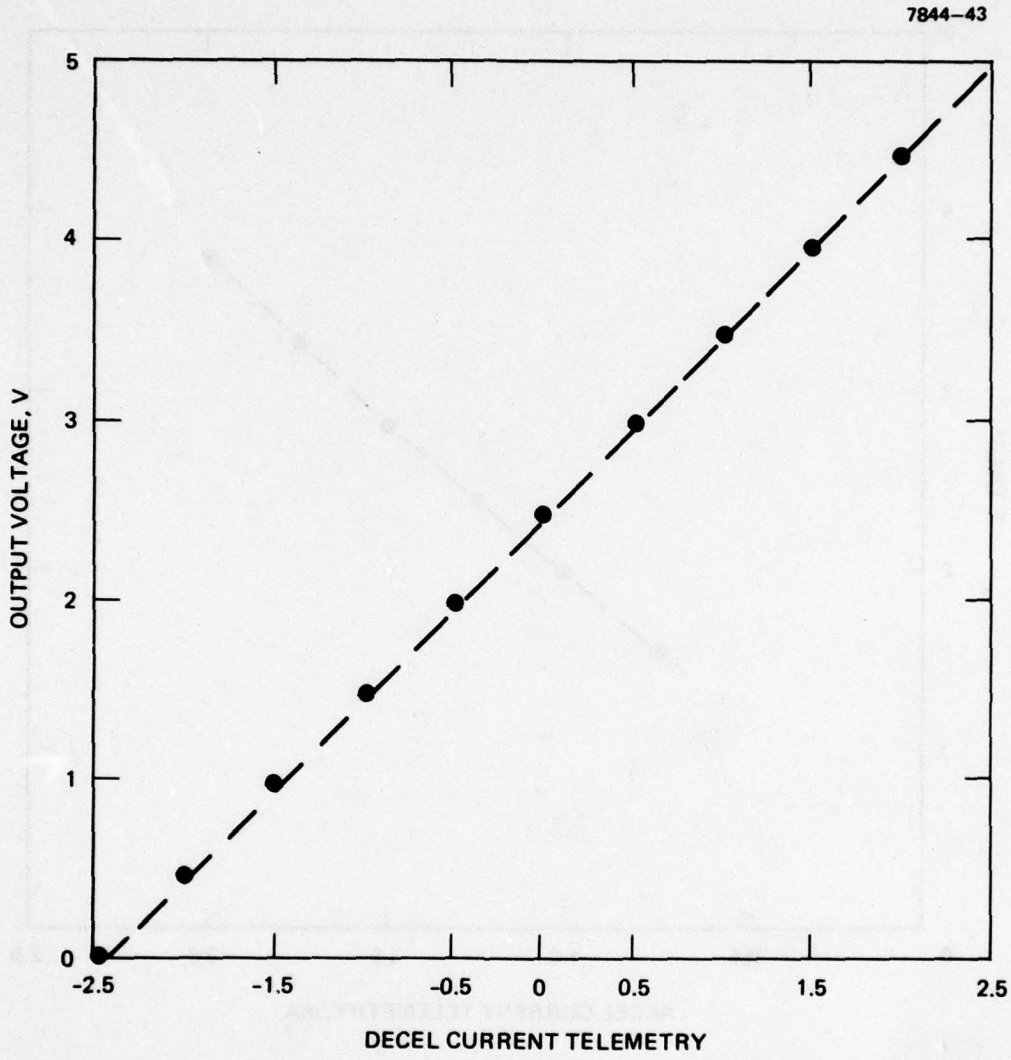

Figure 120. EM decel current telemetry calibration (Channel 10).

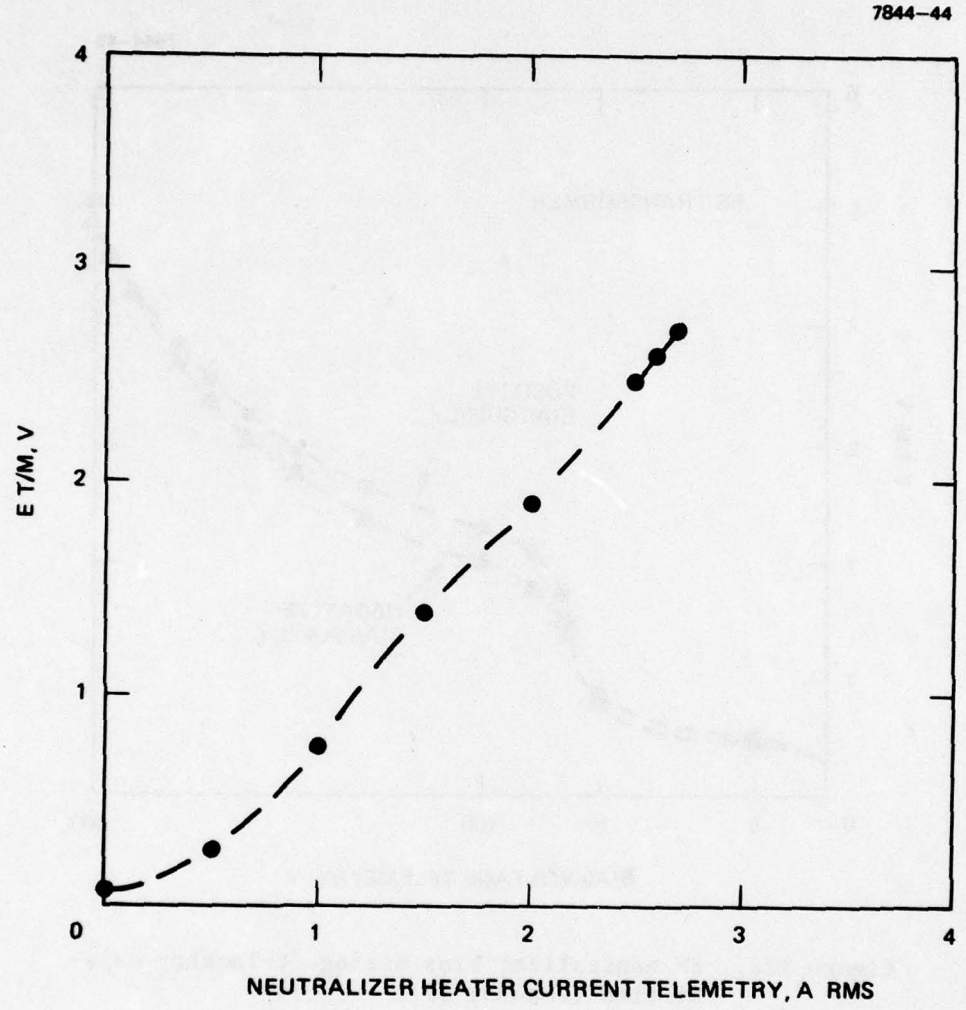

igure 121. EM neutralizer heater current telemetry calibration (Channel 11).

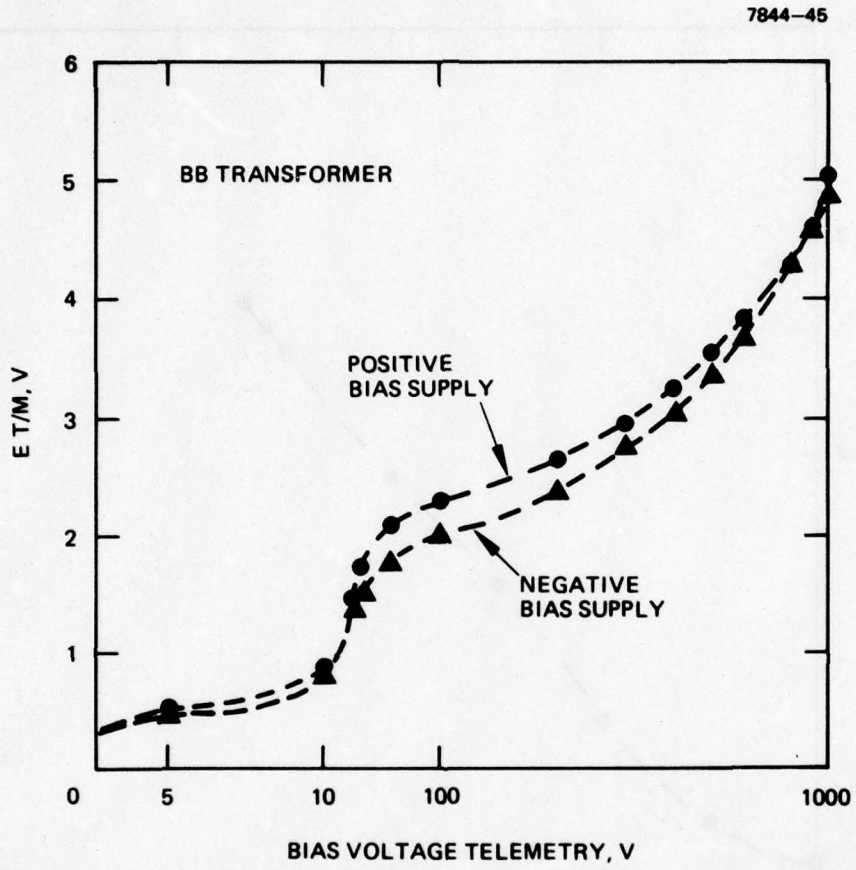

Figure 122. EM neutralizer bias voltage telemetry calibration (Channel 12).

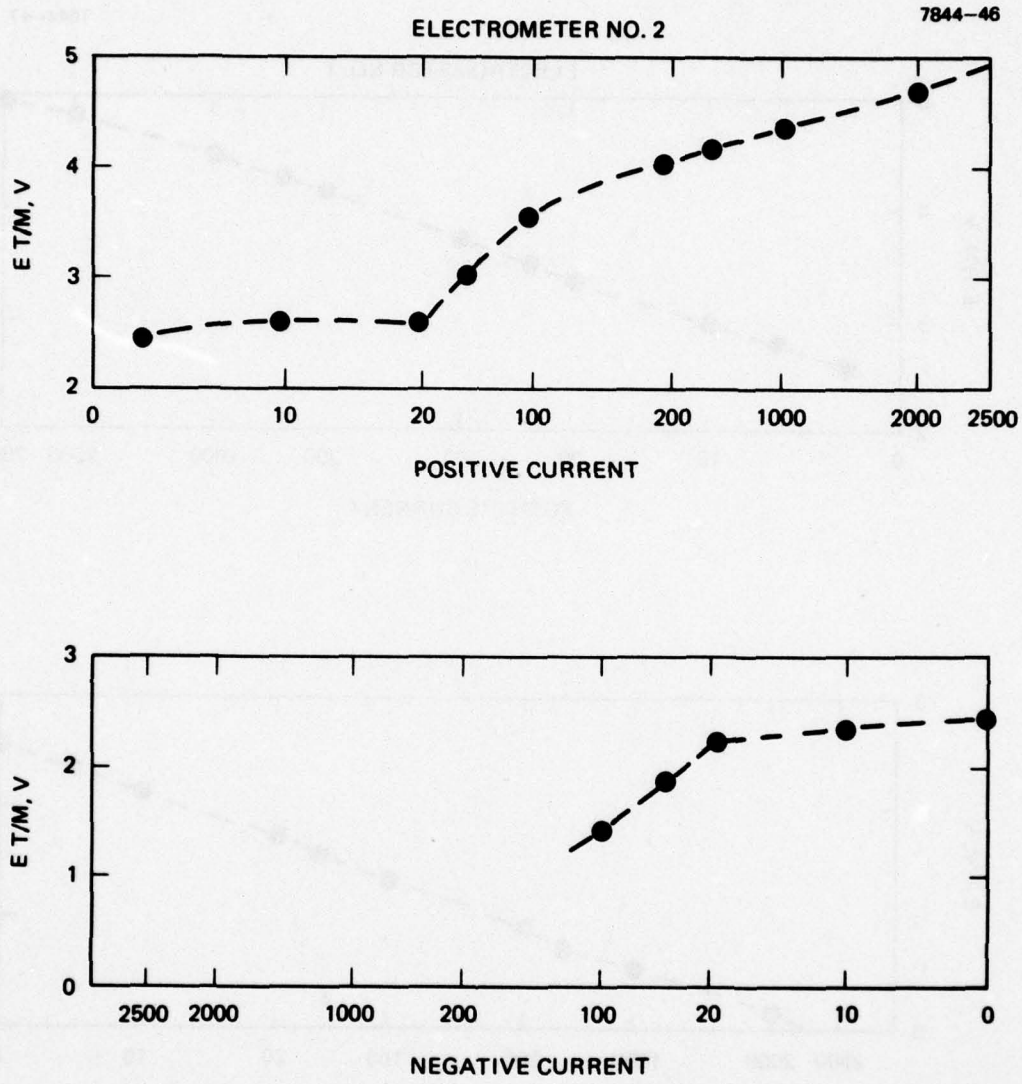

Figure 123. EM neutralizer emission telemetry calibration (Channel 13).

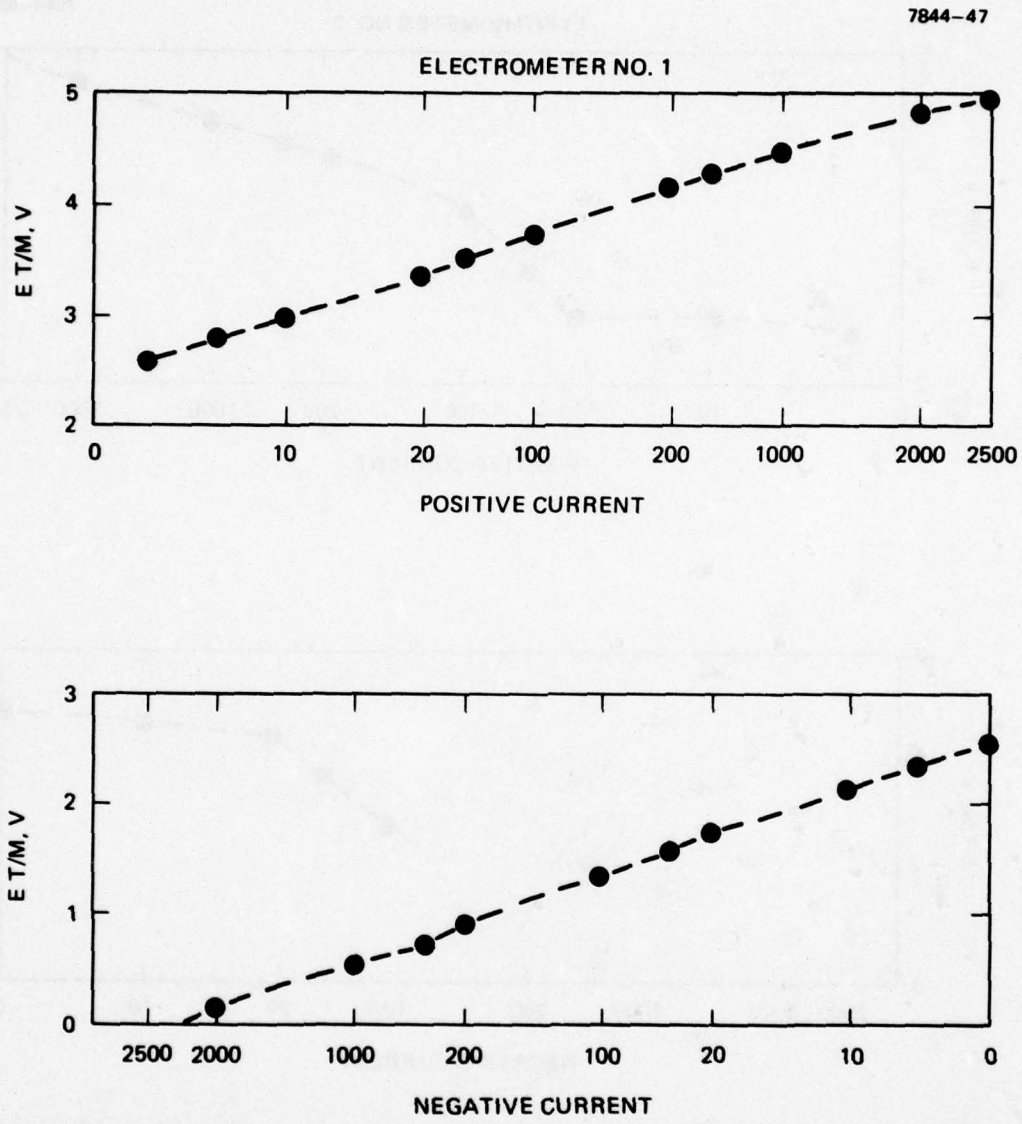

Figure 124. EM SPIBS net current telemetry calibration (Channel 14).

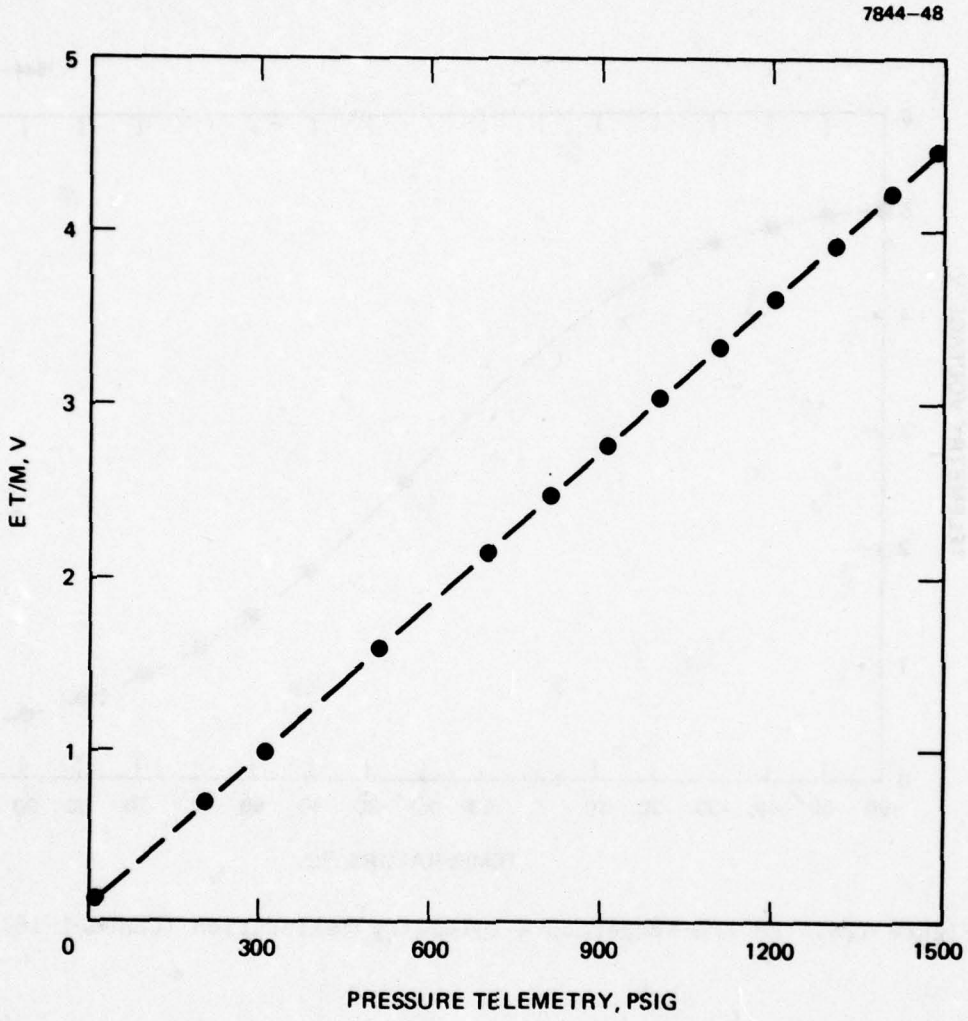

Figure 125. EM reservoir pressure telemetry calibration (Channel 15).

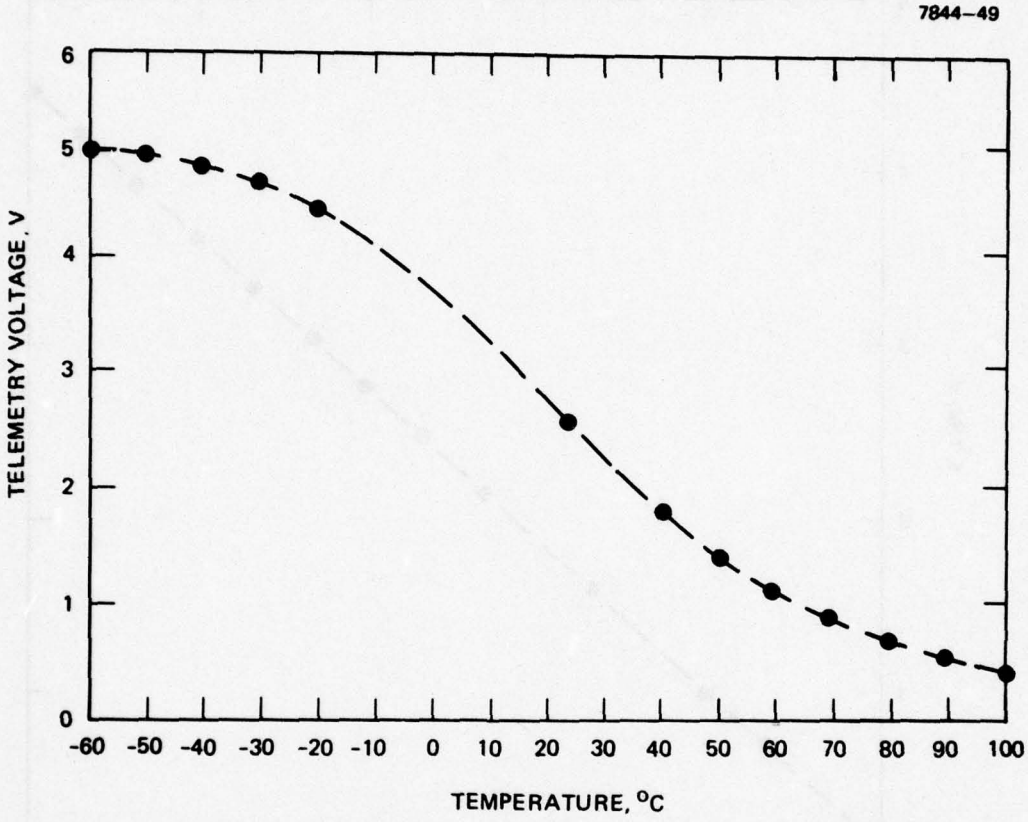

Figure 126. EM PPA temperature telemetry calibration (Channel 16).

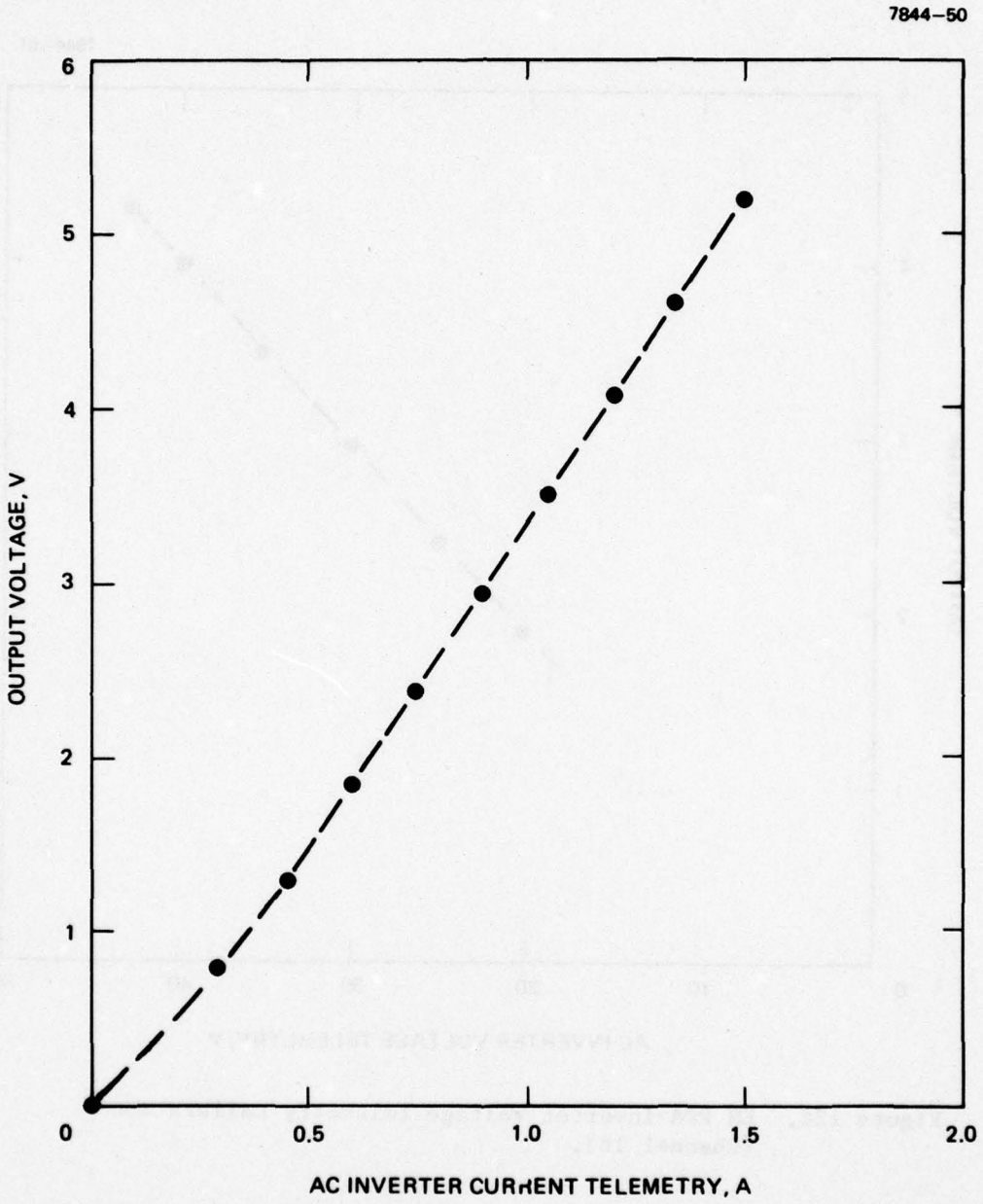

Figure 127. EM PPA inverter current telemetry calibration (Channel 17).

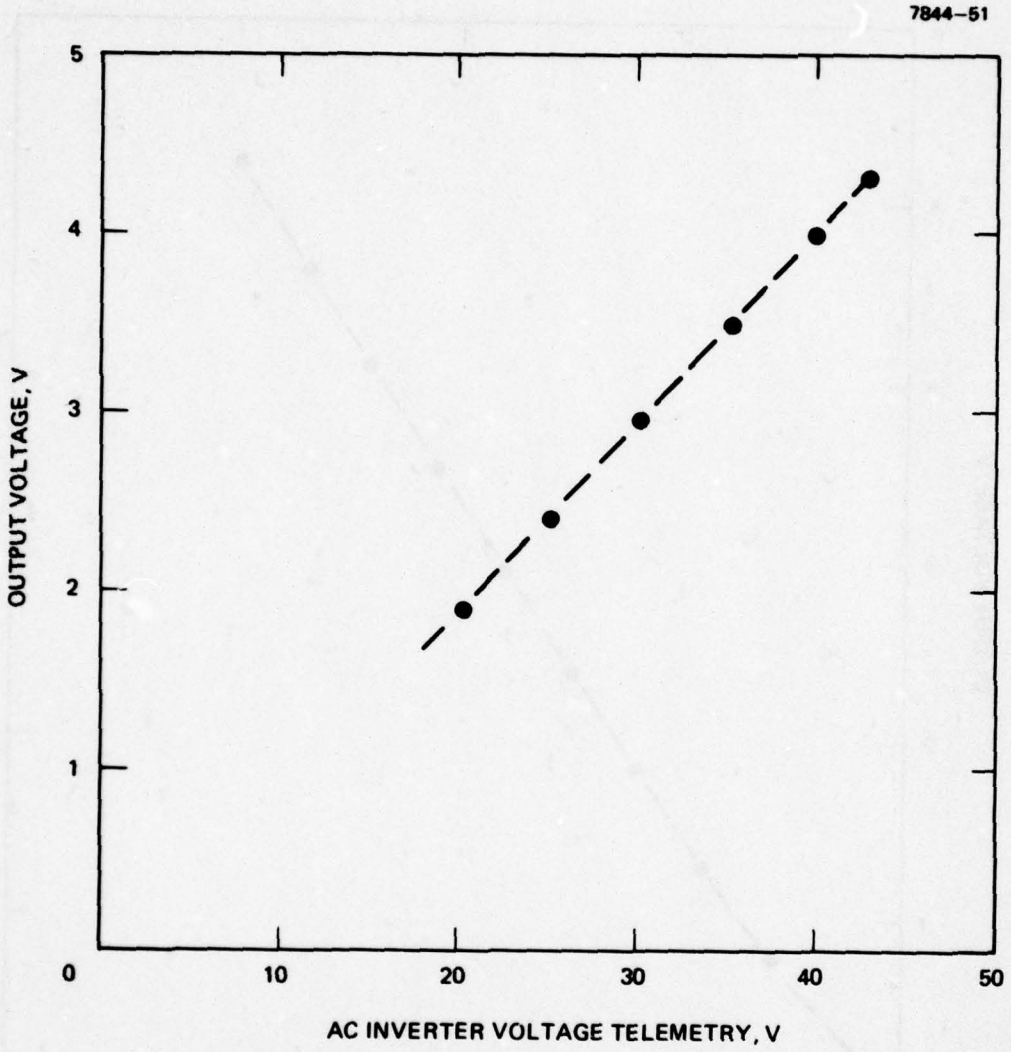

Figure 128. EM PPA inverter voltage telemetry calibration (Channel 18).

SECTION 7

FLIGHT MODEL SYSTEM

The flight system benefited significantly from our experiences and difficulties with the breadboard and EM phases. However, since a few new factors were added in the flight phase in terms of quality control and documentation, more emphasis was placed on the fabrication and assembly processes than for previous units. The flight hardware assembly records and various procedures were supplied to AFGL during fabrication or on hardware delivery and are not discussed in detail here. Very few serious problems were encountered during the flight model phase, although several untimely minor failures resulted in overall delays. A photograph of the completed flight system is shown in Figure 129.

A. SYSTEM DESIGN AND FABRICATION

Except for very minor differences in assembly (e.g., wire size and routing) the flight model system design is identical with the EM system. All changes introduced into the EM, such as exterior paint, were automatically incorporated into the flight model.

Fabrication and assembly of the ion source followed the written procedure developed earlier. At critical points in the assembly process, the completion of that portion was verified and signed off. A copy of this assembly log, including inspection tags was delivered with the flight system.

PPA assembly was documented and controlled significantly more than for previous models. A complete new point-to-point wire list was prepared and checked. A quality plan defining insepction levels and requirements was prepared and implemented. All electronics parts were ordered to Hughes "908" specifications, batch inspected in receiving, and locked in a controlled store. Complete inspection of all solder joints was provided at various points in the assembly process. As with the EM, individual cards were checked electrically at HRL prior to harness installation. Except for coordination, the PPA was built at the

M12380

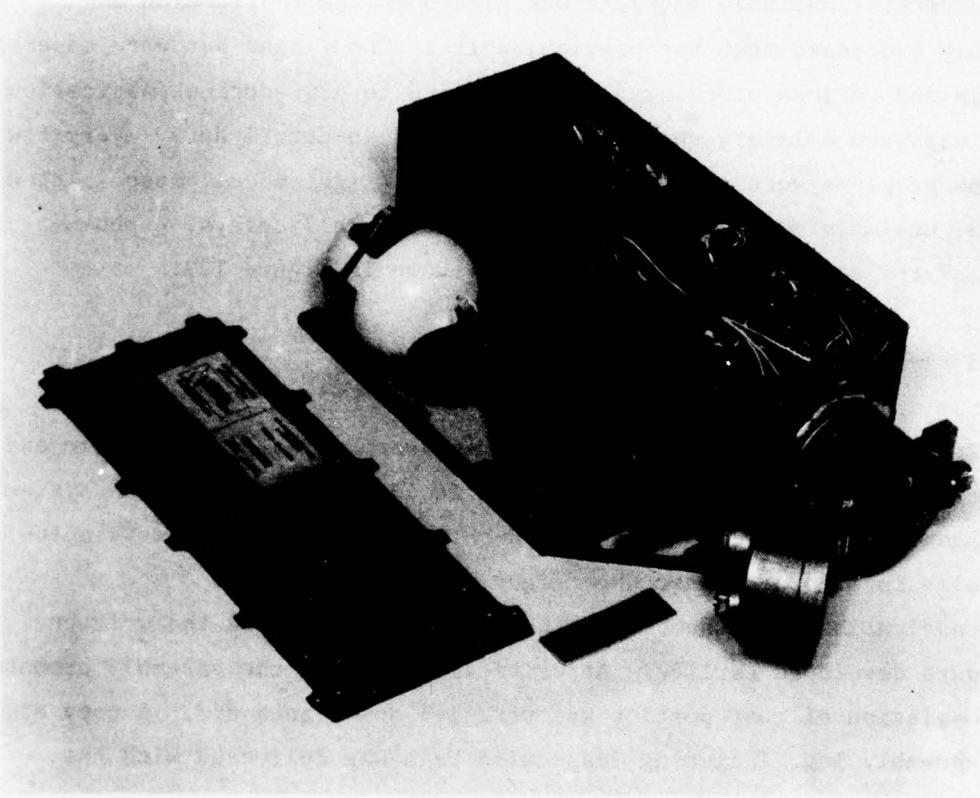

Figure 129. Photograph of flight model system.

Culver City site. A photograph of the harnessed PPA setup for checkout is shown in Figure 130. A small gauge wire was used for intra-card wiring in the flight model than in the EM. This resulted in a more compact package and eased wire bundling. The weight of the flight system was about 7.35 kg.

Flight system integration basically followed the process outlined in Section 6. However, the length of time needed for integration and final checkout was significantly reduced over the EM system. As discussed in the following section, testing was completed with only a few delays.

B. SYSTEM TESTING

In the flight model phase, six test runs were conducted, as indicated in Table 13. The first flight phase test, run C-1, was conducted to check out the flight ion source. This was accomplished using the EM PPA (between EM phase runs B-20 and B-21). The ion source operated properly and was checked over the full operating range. A problem encountered with the net current electrometer was diagnosed as a cold solder joint and was repaired. The neutralizer bias supply was also found to be missing a select-by-test capacitor. This additional test of the EM PPA proved to be valuable in debugging the EM system.

Having verified that the flight ion source was operational, run C-2 was used to integrate the source with the flight PPA. Select-by-test resistors in the neutralizer heater circuitry were set and minor problems with the bias supply telemtry and net current electrometer were identified and corrected.

The first test of the full system using the flight gas system was performed during run C-3. For this test, the PPA was in air. After correcting another cold solder joint in the accel telemetry, a full range of tests was conducted. All aspects of the system's performance were considered to be acceptable. Thus, the PPA was ready for potting and conformal coating.

77-60699

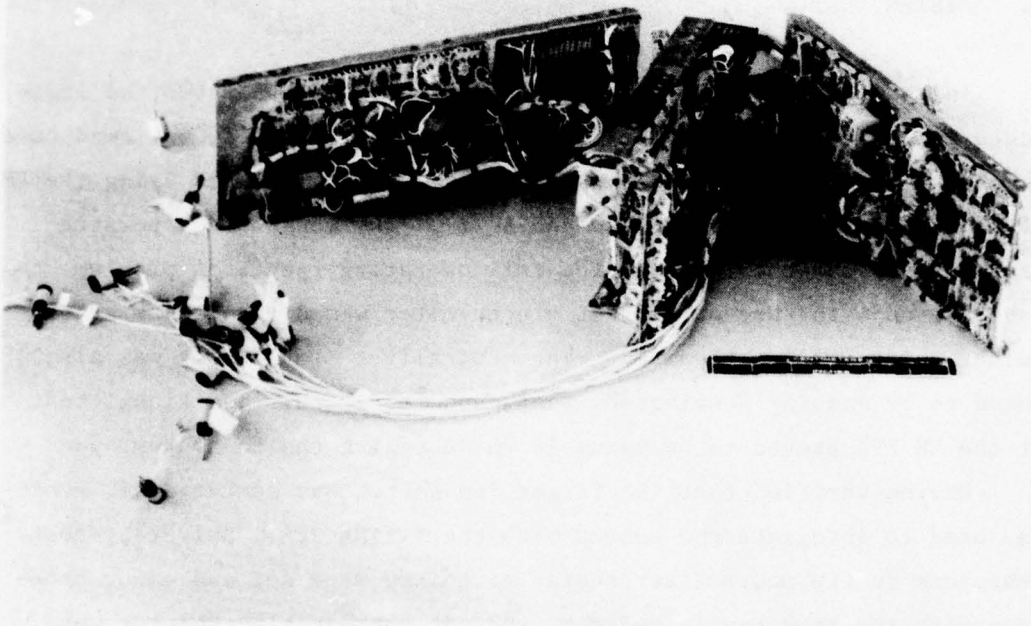

Figure 130. Photograph of flight PPA before conformal coating and potting.

Table 13. Summary of Flight Model Test Runs

Test	Purpose	Test Setup Change Prior to Test	Remarks
C-1	Checkout of flight ion source on EM PPA.	First test.	Successful test.
C-2	Checkout of flight PPA.	First PPA/source test	Successful test.
C-3	Full system test with reservoir.	System assembly.	Successful test.
C-4	PPA evaluation after conformal coating	Potting and conformal	Successful test.
C-5	Full flight system test in vacuum.	Completed system assembly.	Successful test.
C-6	Ground test simulation.	Installed system at pump out port	Successful test; system prepared for shipping.

6326

After potting and coating, the system was retested in run C-4 with the PPA and expellant assembly in air. Neutralizer emission levels required additional adjustment, and a cold solder joint in the decel circuitry was corrected. With these corrections, the PPA was prepared for installation into the enclosure.

During run C-5, with the full flight system in vacuum, essentially all operations were normal. At the time, this problem was believed to be due to a loose connection in the external harness. Subsequently, a failed component in the keeper supply was identified. After a full performance map was taken, the flight system vacuum checkout tests were concluded.

The final test of the flight system at HRL, run C-6, was a ground checkout simulation run. As before, the system was evacuated through the pumpout port and operated into the cover collector. Beam currents of about 0.2 and 0.9 mA were obtained at a beam voltage of 1 kV.

C. ANALOG OUTPUTS (TELEMETRY)

Analog outputs are listed in Table 4, and data for the flight model are presented in Figures 131 through 148. Calibration results are quite similar to those for engineering and rocket models. Data were obtained with the individual circuit cards operating on resistive loads. Additional data points were obtained through the meter panel during system integration.

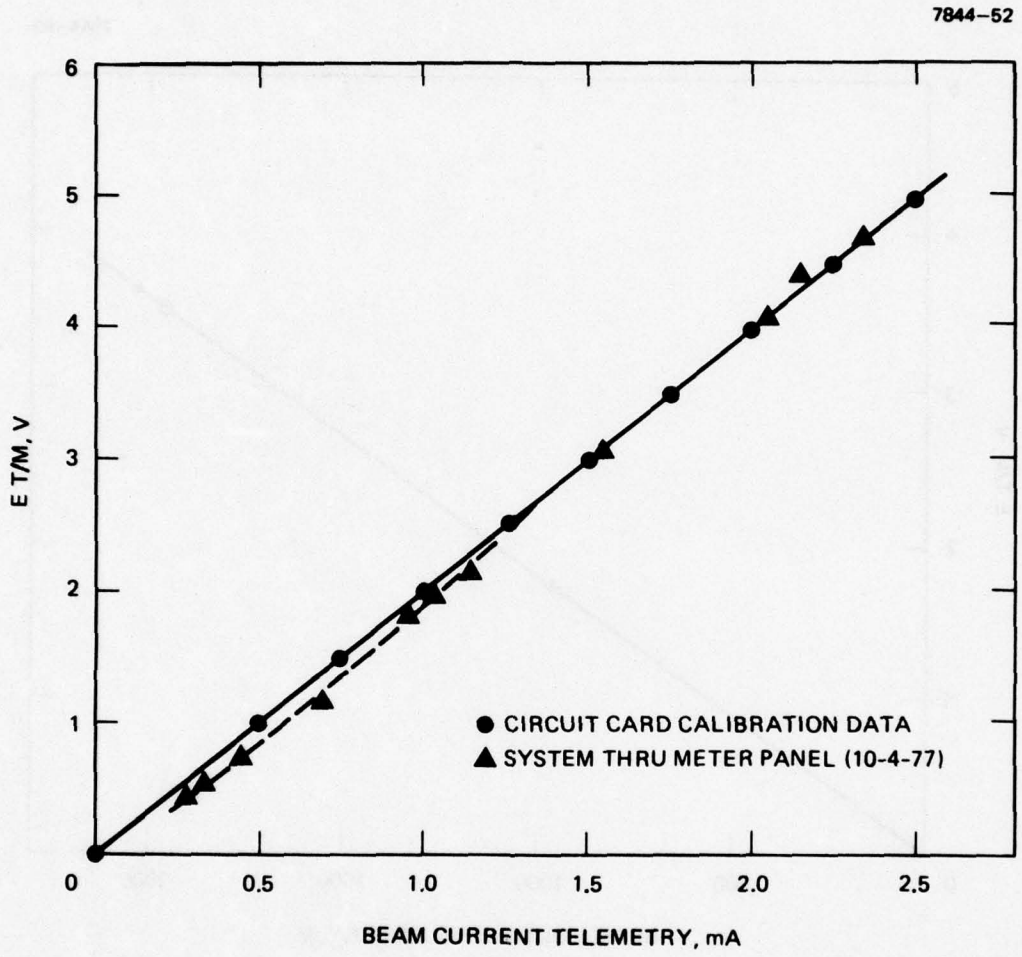

Figure 131. Flight model beam current telemetry calibration (Channel 1).

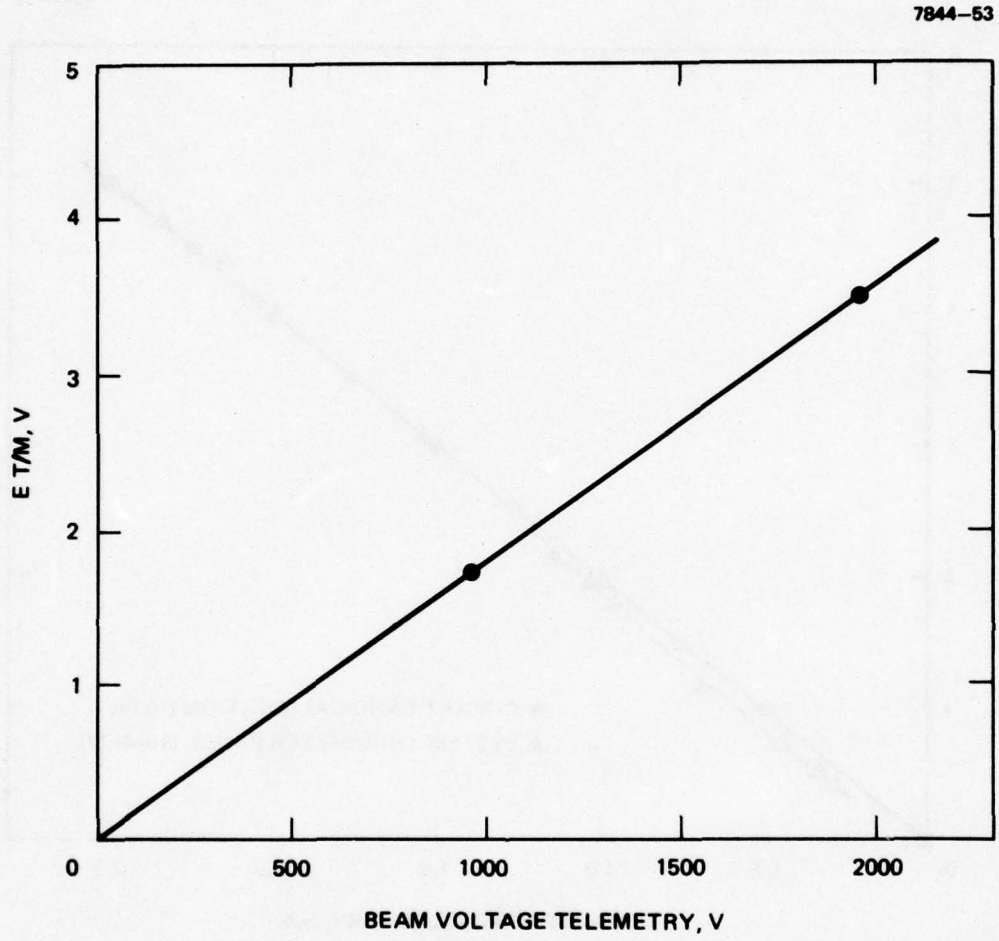

Figure 132. Flight model beam voltage telemetry calibration (Channel 2).

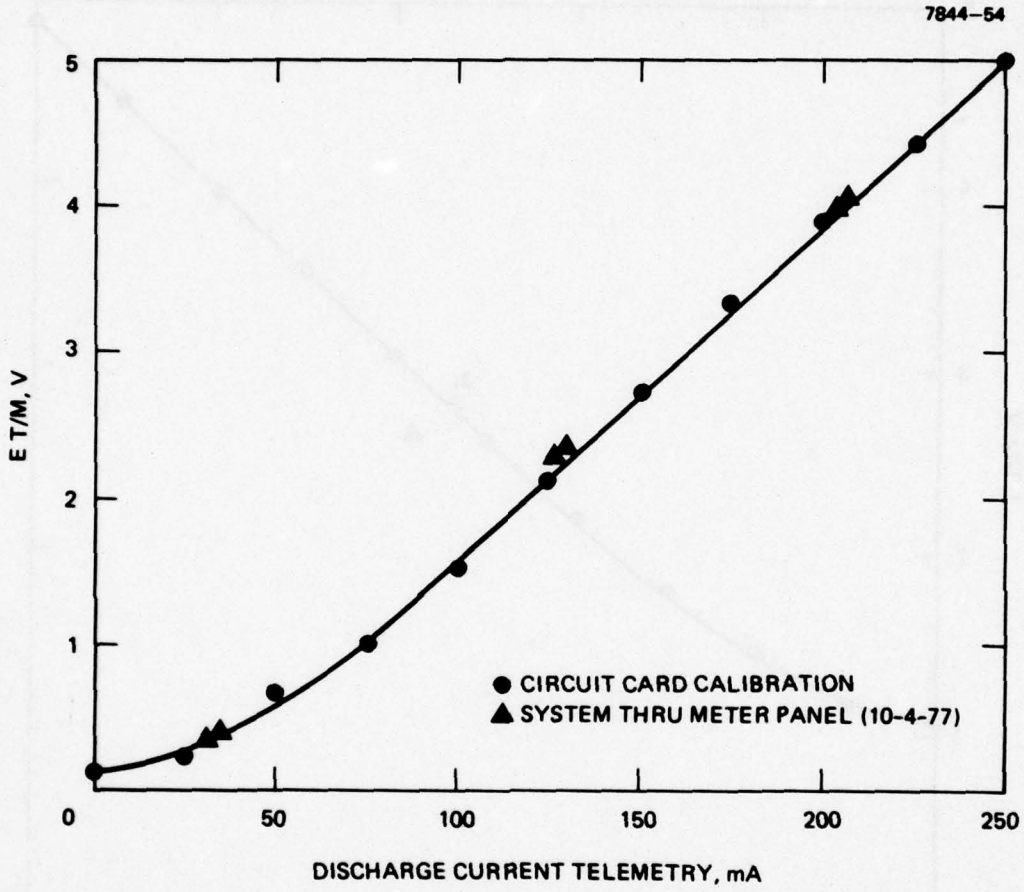

Figure 133. Flight model discharge current telemetry calibration (Channel 3).

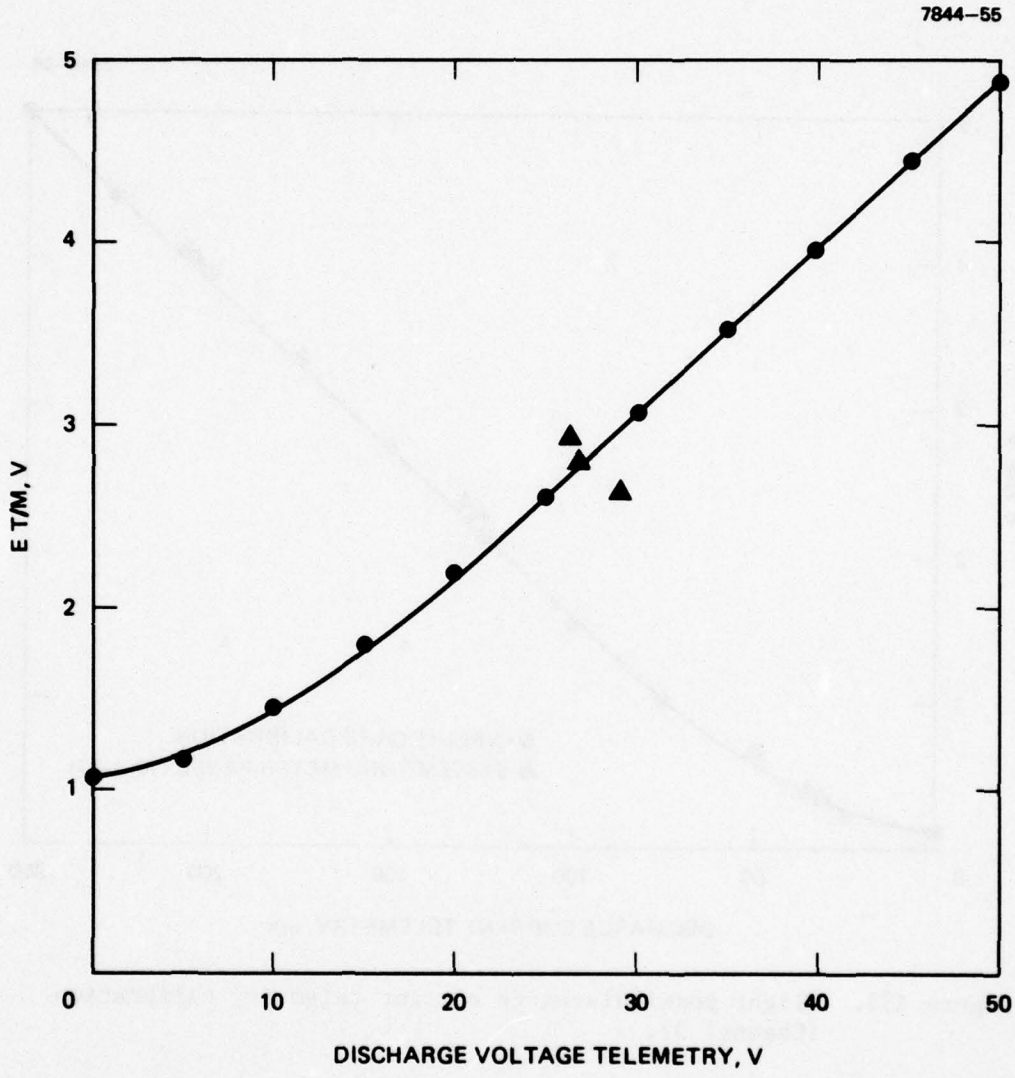

Figure 134. Flight model discharge voltage telemetry calibration (Channel 4).

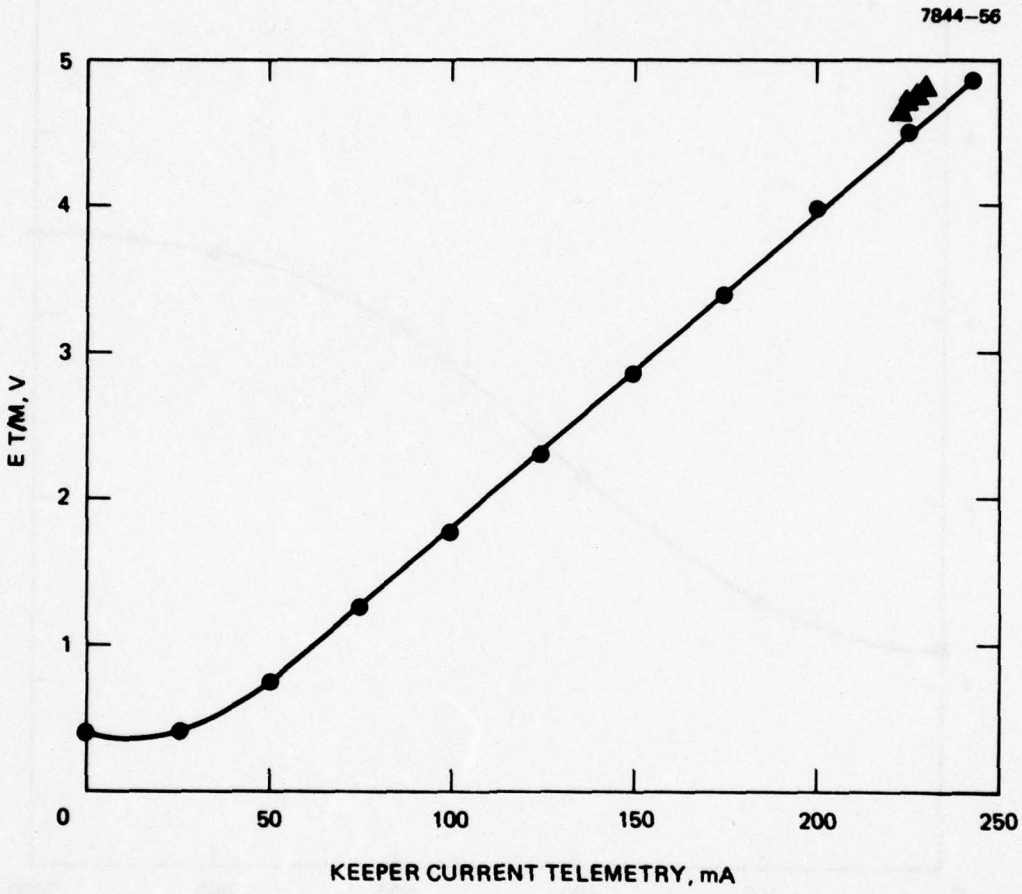

Figure 135. Flight model keeper current telemetry calibration (Channel 5).

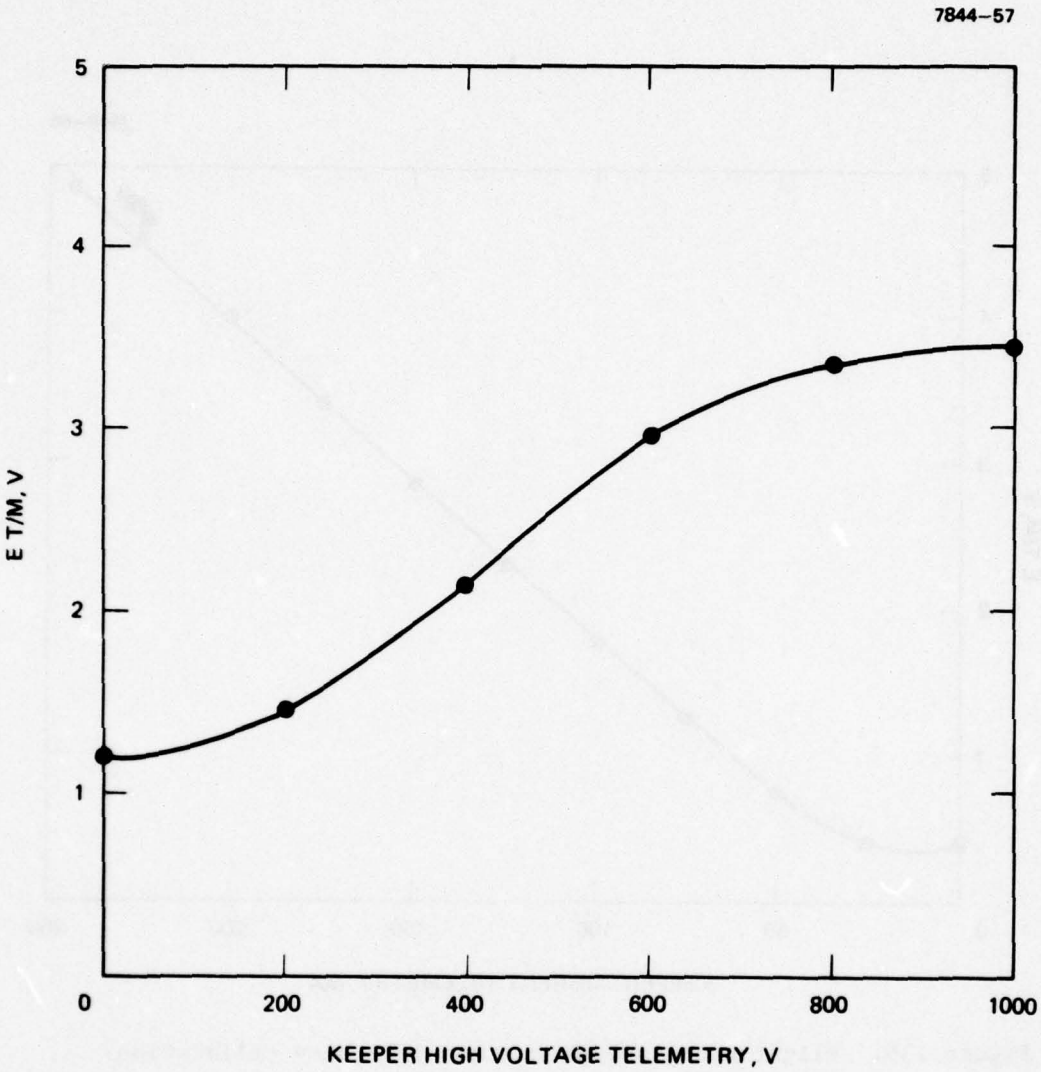

Figure 136. Flight model keeper high voltage telemetry calibration (Channel 6).

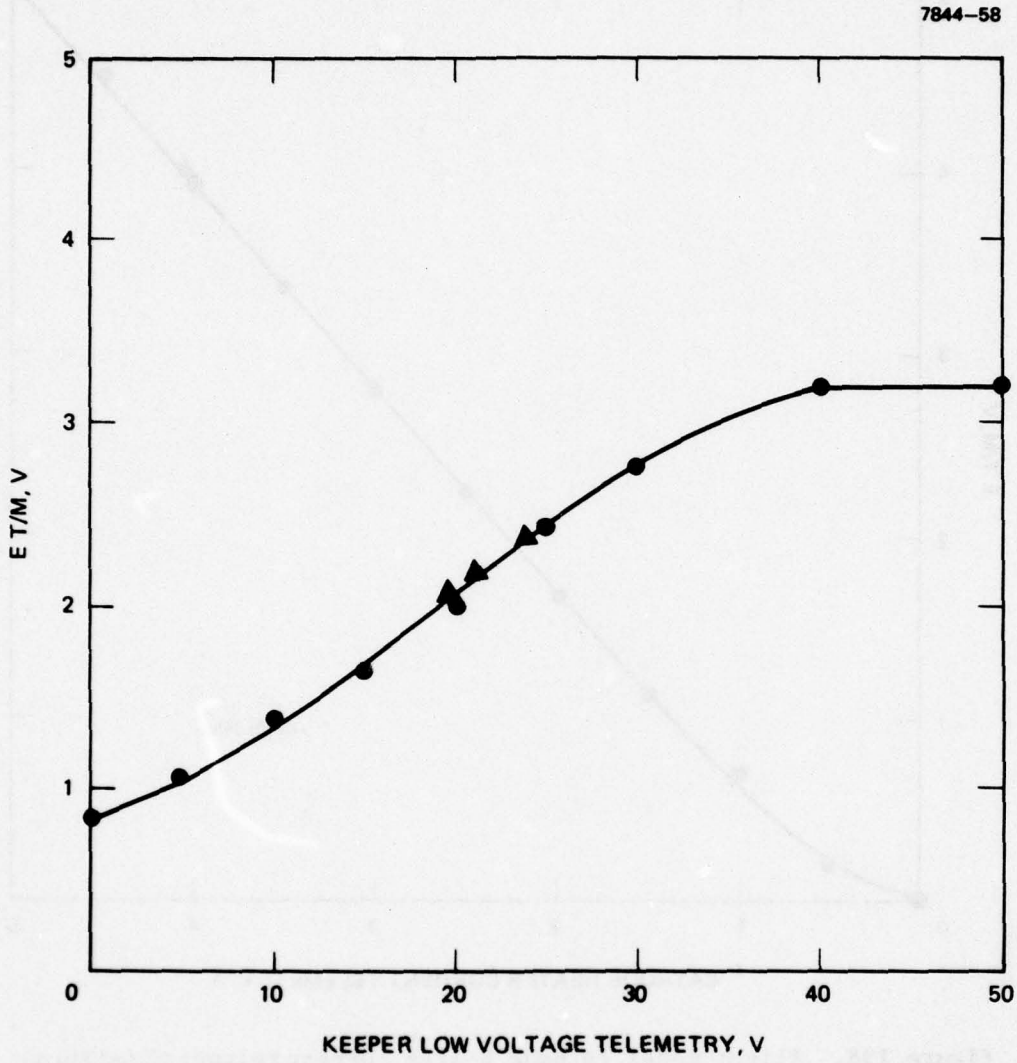

Figure 137. Flight model keeper low voltage telemetry calibration (Channel 7).

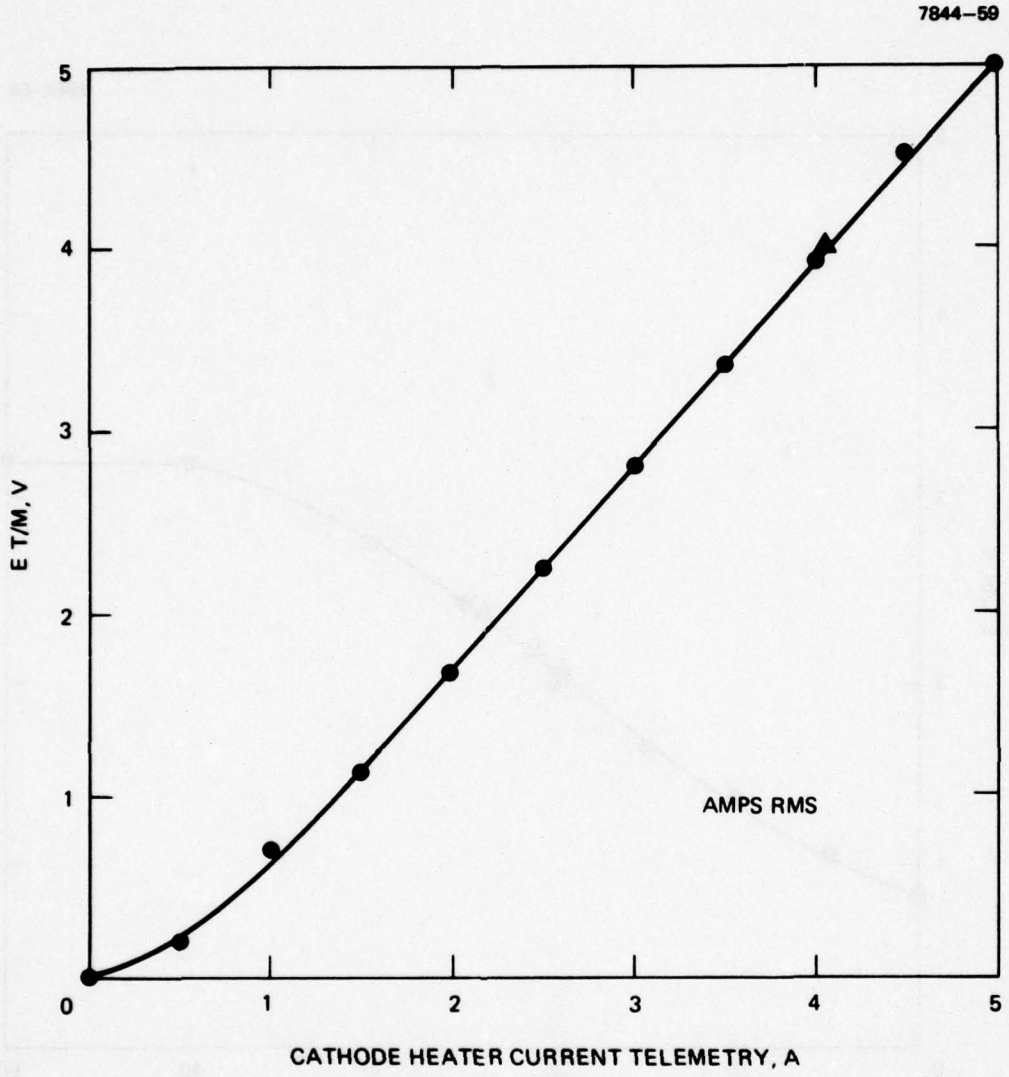

Figure 138. Flight model cathode heater current telemetry calibration (Channel 8).

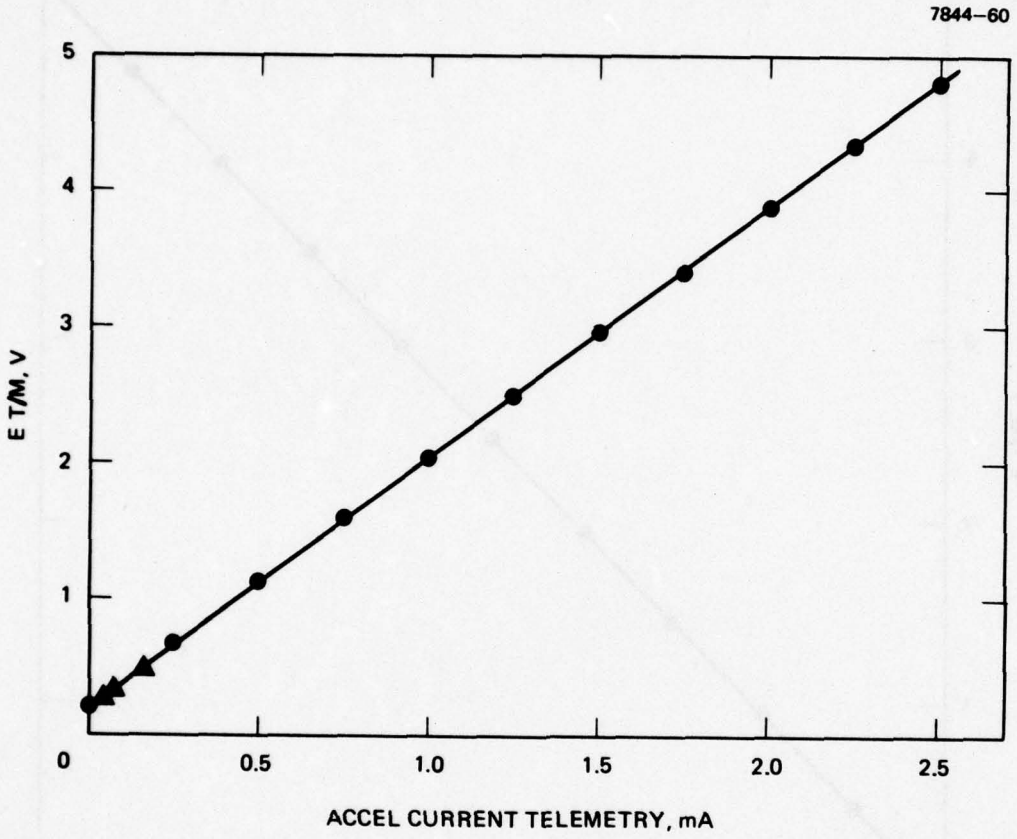

Figure 139. Flight model accel current telemetry calibration (Channel 9).

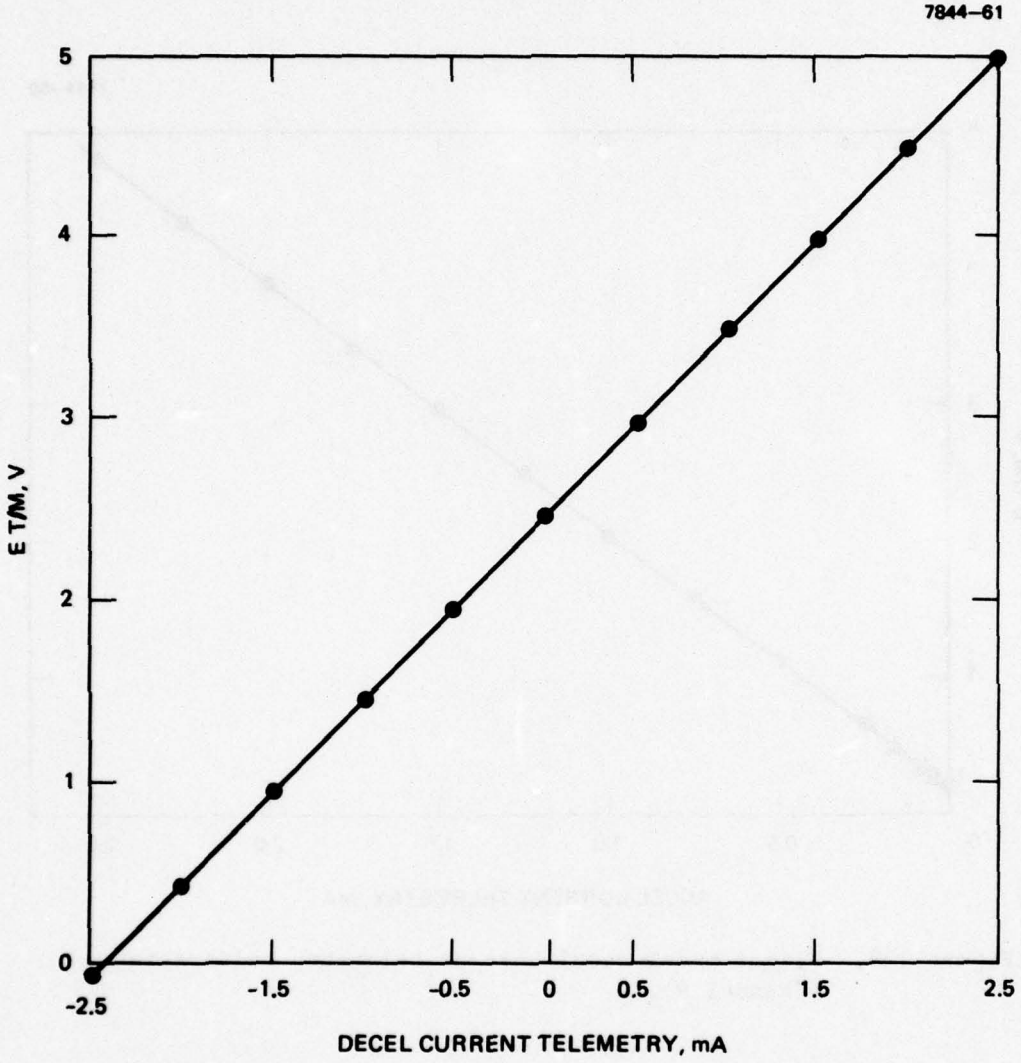

Figure 140. Flight model decel current telemetry calibration (Channel 10).

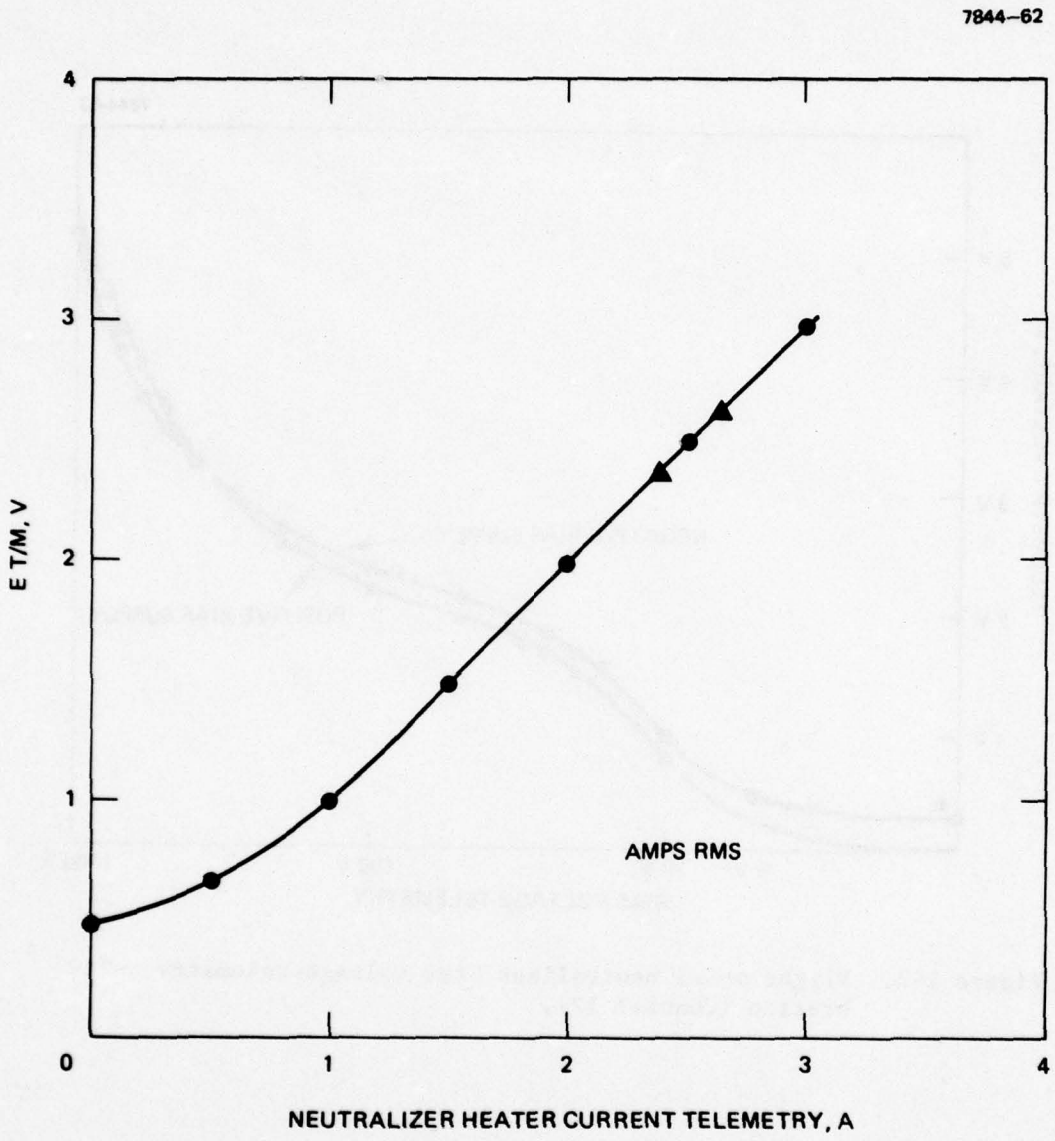

Figure 141. Flight model neutralizer heater current telemetry calibration (Channel 11).

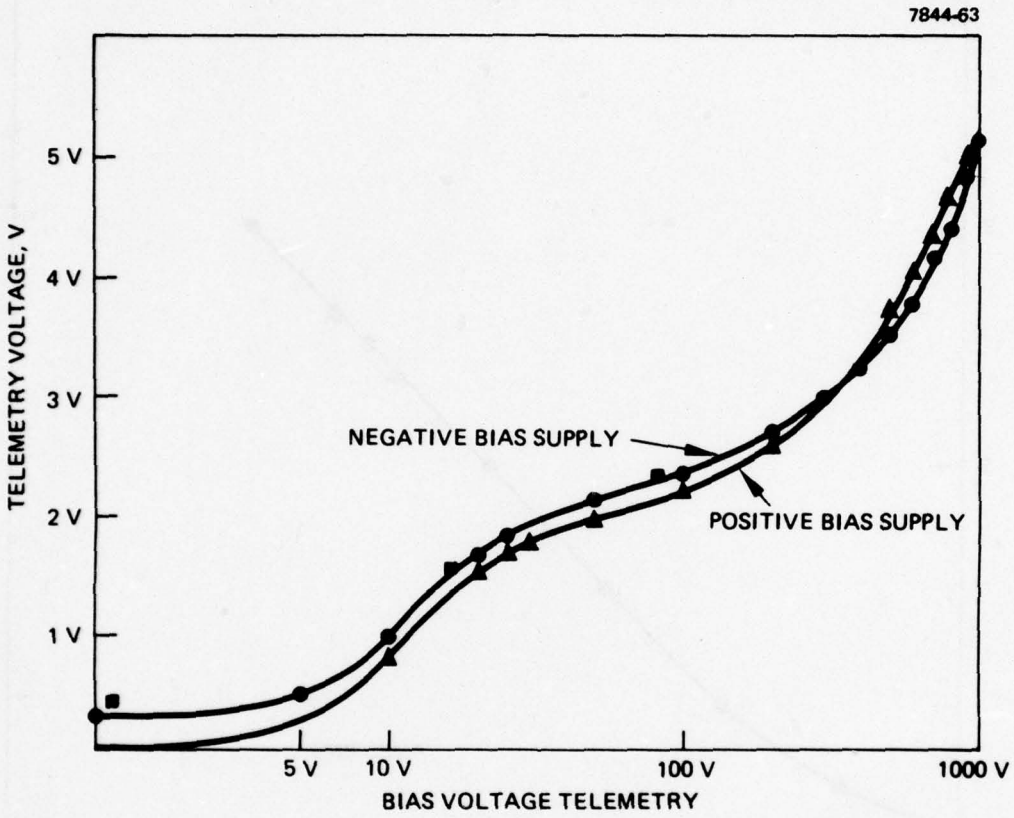

Figure 142. Flight model neutralizer bias voltage telemetry calibration (Channel 12).

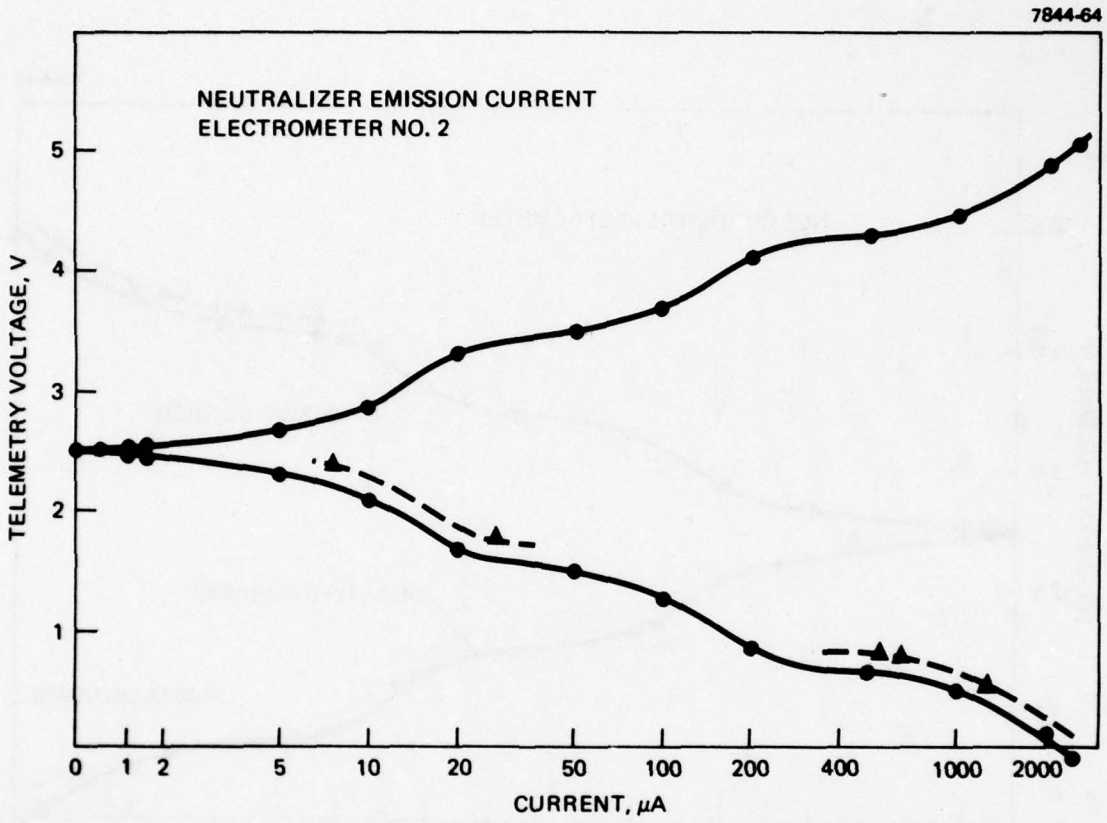

Figure 143. Flight model neutralizer emission telemetry calibration (Channel 13).

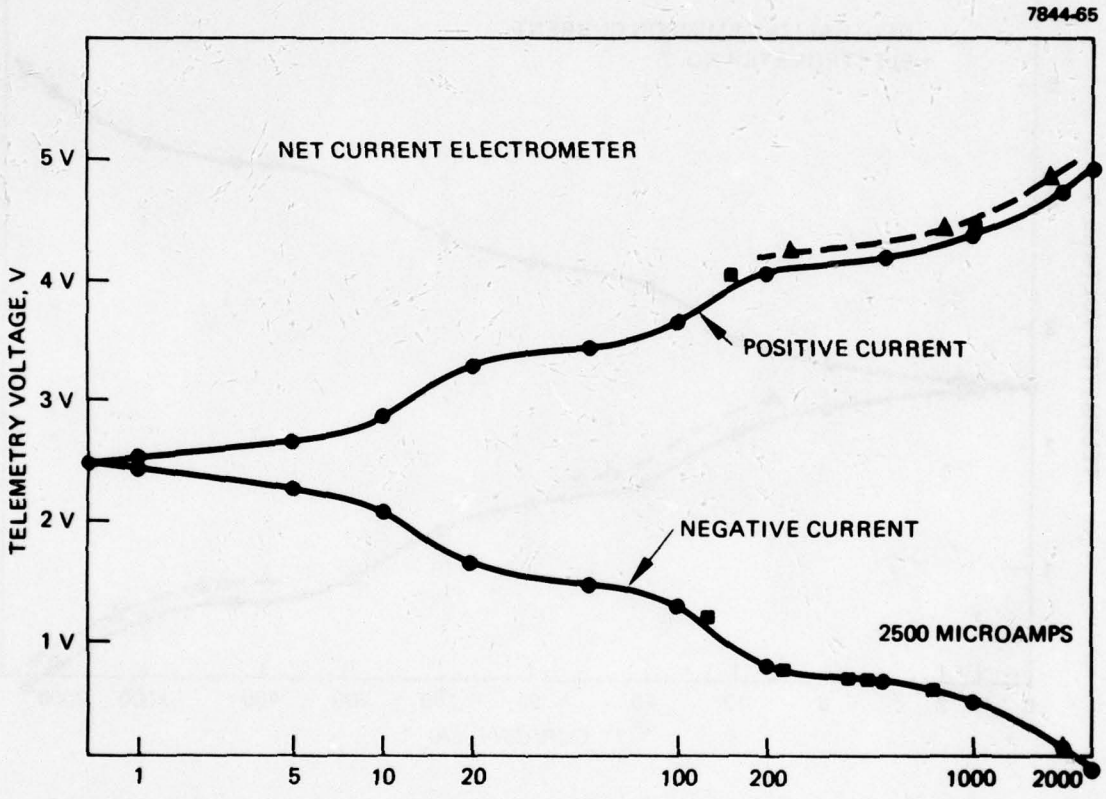

Figure 144. Flight model SPIBS net current telemetry calibration (Channel 14).

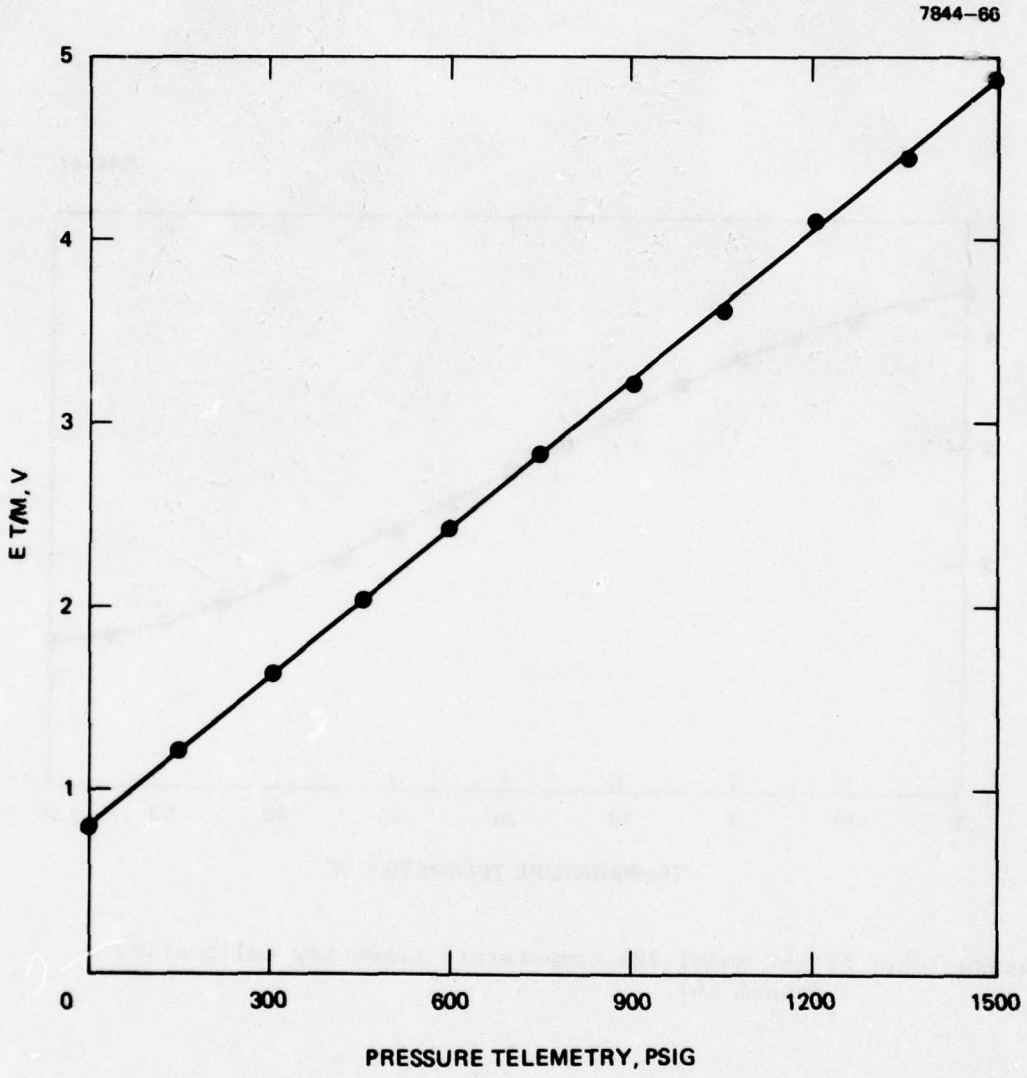

Figure 145. Flight model reservoir pressure telemetry calibration (Channel 15).

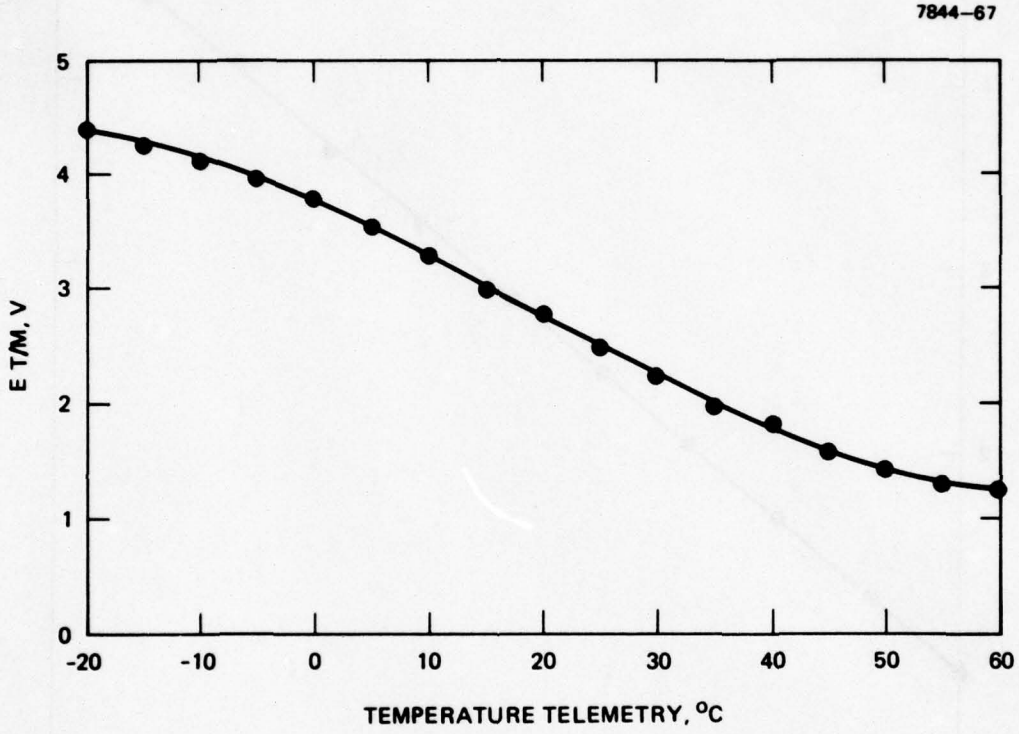

Figure 146. Flight model PPA temperature telemetry calibration (Channel 16).

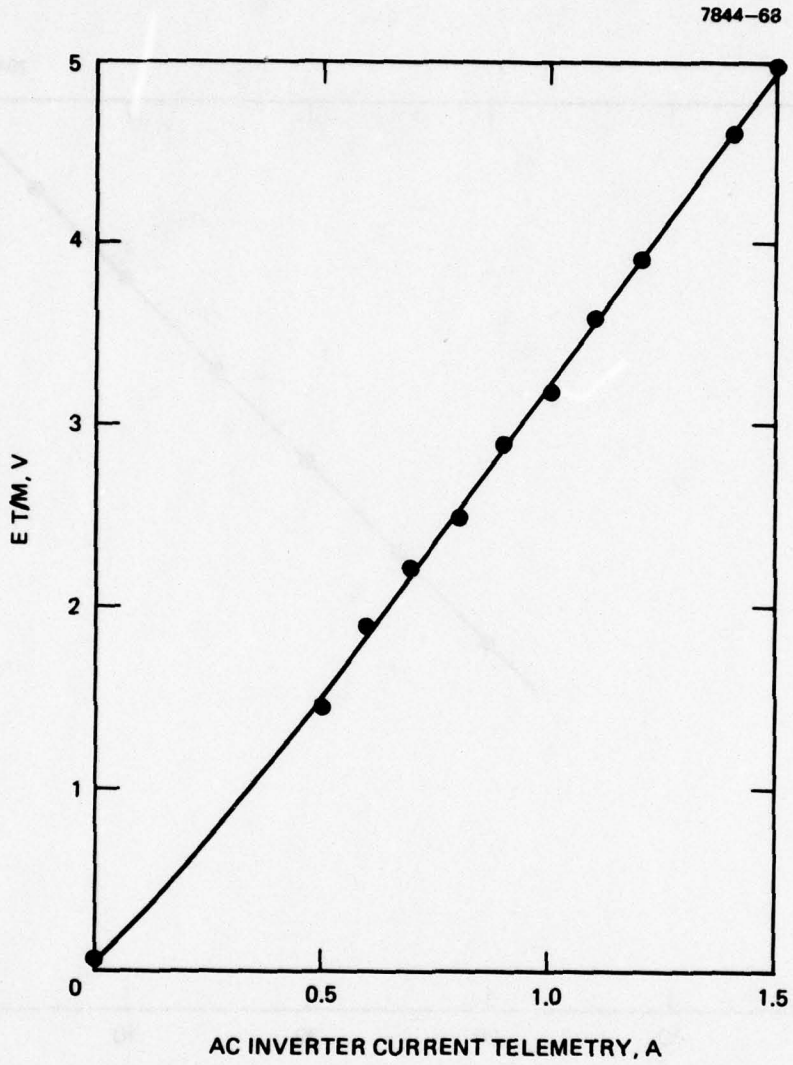

Figure 147. Flight model PPA AC inverter current telemetry calibration (Channel 17).

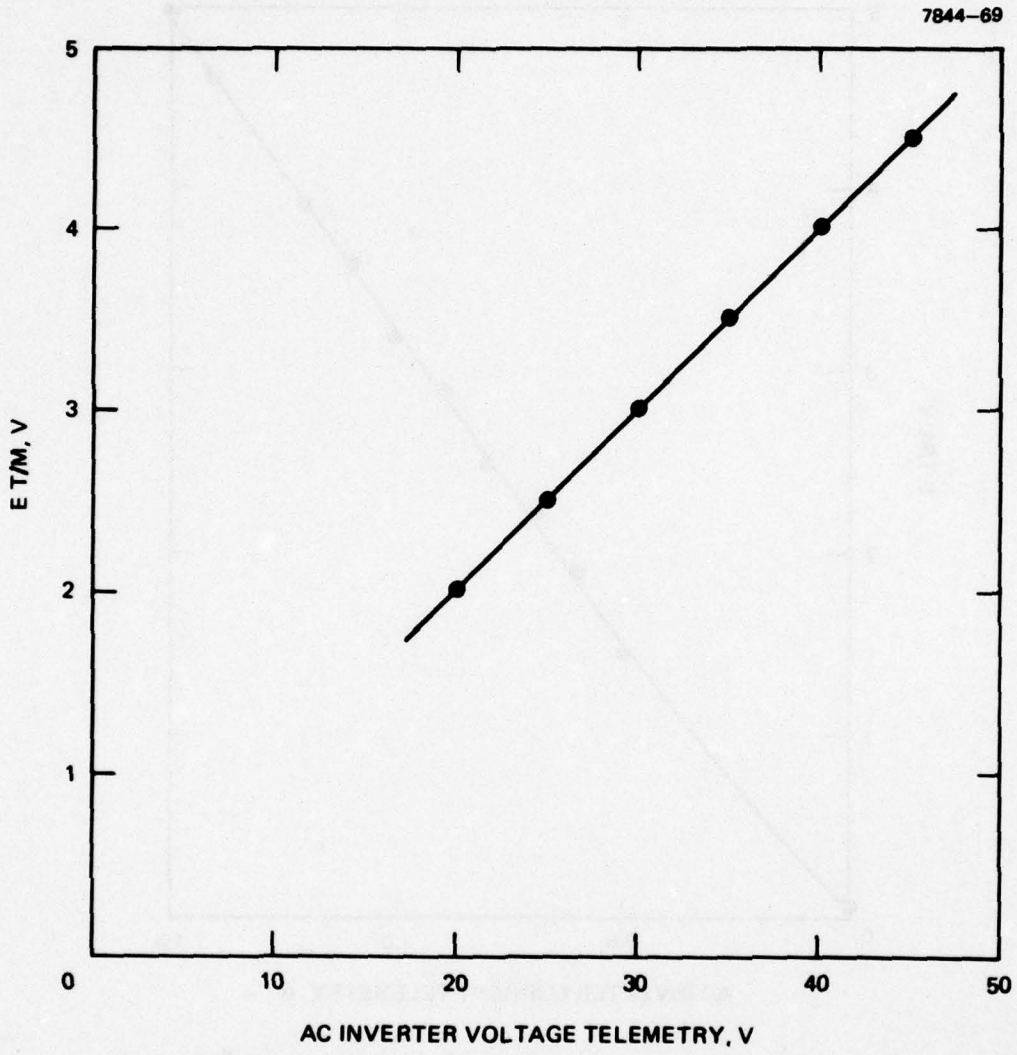

Figure 148. Flight model PPA AC inverter voltage telemetry calibration (Channel 18).

SECTION 8

CONCLUSIONS

The SPIBS program was successfully carried out with a minimum of serious setbacks. Essentially all objectives were met and three operational systems were delivered to AFGL. Although the SPIBS hardware as delivered had a vew shortcomings that were discovered late in the program, corrections were made relatively easily by AFGL personnel. These corrections included: (1) modification of the regulator to include a pressure transducer, (2) addition of a noise filter on the analog outputs, and (3) addition of permanent magnets to buck-out the ion source external magnetic field.

Significant points to be noted regarding the final hardware include:

- All units perform similarly; have reproducible characteristics; and satisfy requirements on input power, envelope dimensions, and weight.

- Qualification tests were completed by AFGL personnel and demonstrated that SPIBS meets rigid requirements on vibration, thermal-vacuum, and EMI. A transformer failure in the discharge supply of the flight model and transducer failures were the only problems encountered in AFGL qualification and acceptance level testing. The flight instrument has been delivered to Martin Co., the SCATHA satellite integrator.

- The flexibility of the SPIBS design was demonstrated during the flight test of the rocket model. As a result of this flight, an additional operating mode will be included on SCATHA to obtain beam currents as low as 0.1 mA. With this "keeper only" mode, the beam current dynamic range is about 20 to 1.

- Over 300 operating modes are available, including operation with an un-neutralized ion beam, partial neutralization, full neutralization, or neutralizer only. Neutralizer biasing of ±1000 V is possible in all modes.

- The SPIBS ion source has many novel features and characteristics, including: (1) xenon expellant, (2) decel grid, (3) graphite screen and accel grids, (4) compact and rugged hollow cathode using a porous tungsten oxide impregnated insert, (5) startup in less than 3 min, (6) stable operation over a wide beam current range, (7) operating life in excess of 1000 hr, and (8) low input power considering overall capabilities.

Several important related subjects were not addressed as part of this program. Neutral efflux, ion beam divergence, and charge exchange are of concern to other experimenters on SCATHA. AFGL personnel are conducting experiments and analyses to accurately define and assess these areas. Not withstanding these questions, SPIBS should prove to be a valuable tool in the study of spacecraft charging.

SECTION 9

REFERENCES

1. DeForest, S.E., "Spacecraft Charging at Synchronous Orbit," *Journal of Geophysical Research,* 77:4:651-659 (1972).

2. Fredericks, R.W. and Scarf, F.L. "Observations of Spacecraft Charging Effects in Energetic Plasma Regions," *Photon and Particle Interactions with Surface in Space,* D. Reidel Publishing Co., Doroecht-Holland, 1973, pp. 277:308.

3. Rosen, A., "Large Discharges and Arcs on Spacecraft," *AIAA Astronautics and Aeronautices,* p. 36-44, June 1975.

4. McPherson, D.A., Cauffman, D.P., and Schober, W., "Spacecraft Charging at High Altitudes: The SCATHA Satellite Program," AIAA Paper 75-92, AIAA 13th Aerospace Sciences Meeting, Pasadena, California, January 1975.

5. Bartlett, R.O., DeForest, S.E., and Goldstein, R., "Spacecraft Charging Control Demonstration at Geosynchronous Altitude," AIAA Paper 75-357, 11th Electric Propulsion Conference, March 1975.

6. DeForest, S.E. and Goldstein, R., "A Study of Electrostatic Charging of ATS-5 Satellite During Ion Thruster Operation," Final Technical Report, Contract NAS JPL 953675, Jet Propulsion Laboratory, Pasadena, California, December 1973.

7. Masek, T.D. and Cohen, H.A., "Satellite Positive Ion Beam System," *Jour. of Space and Rockets,* 15:1:27-33, January 1978.

8. Gallagher, H.E. and Knauer, W., "Advanced Thermionic Cathodes for Kaufman Thrusters," AIAA Paper 67-678, Colorado Springs, September 1967.

9. Kramer, N.B. and King, H.J., "Extraction of Dense Ion Beams from Plasma," *J.A.P.* 38:10:4021, September 1967.

10. Worlock, R., Davis, J.J., James, E., Ramirez, P., and Wood, O., "An Advanced Contact Ion Microthruster System," AIAA Paper 68-552, AIAA 4th Propulsion Joint Specialist Conference, Cleveland, Ohio June 1968.

11. Hyman, J., Dulgeroff, C.R., Kami, S., and Williamson, W.S., "One-Millipound Mercury Ion Thruster," *Journal of Spacecraft and Rockets* 13:366-372, June 1976.

12. Hyman, J., "Development of a 5-CM Flight-Qualified Mercury Ion Thruster," *Journal of Spacecraft and Rockets* 10:503-509, August 1973.

APPENDIX A

THERMAL MODEL RESULTS AND MEASUREMENTS

To evaluate the thermal characteristics of the SPIBS packaging design prior to fabrication, an analytical model was prepared. Since all the SCATHA spacecraft boundary conditions were not defined at the time this work was performed, the modeling was not intended to simulate flight conditions. However, given reasonable boundary conditions, the model provided confidence that electronics components would operate below critical temperature levels.

A. THERMAL MODEL

The temperature distribution of SPIBS is expected to vary as a consequence of variations in operating conditions. These variations result from the different power levels applied during startup and during operation at different beam currents and voltages. To evaluate the design, a thermal analysis was made to ensure that the temperatures of the three circuit cards did not vary beyond allowable limits for any of the various operating conditions. This steady-state thermal analysis was accomplished with the aid of a Hughes Aircraft Company digital computer program TAP-3. This thermal analyzer computes heat transfer in physical systems using lumped parameter networks. Any two nodes may be connected by two resistors, one representing conduction and the other representing radiation. In addition to exchanging heat with other nodes, each node may receive radiation and/or a direct heat input.

The thermal analysis was carried out by representing the SPIBS system as a lumped parameter network of 15 nodes and 36 radiation and conductor resistances. A schematic showing the thermal model and modal numbering used is shown in Figure A-1. Each of the three circuit cards was represented by three constant temperature nodes, each of which is connected to adjacent nodes, to the satellite interface, and to the PPA case by conductances. The three circuit card nodes adjacent to the

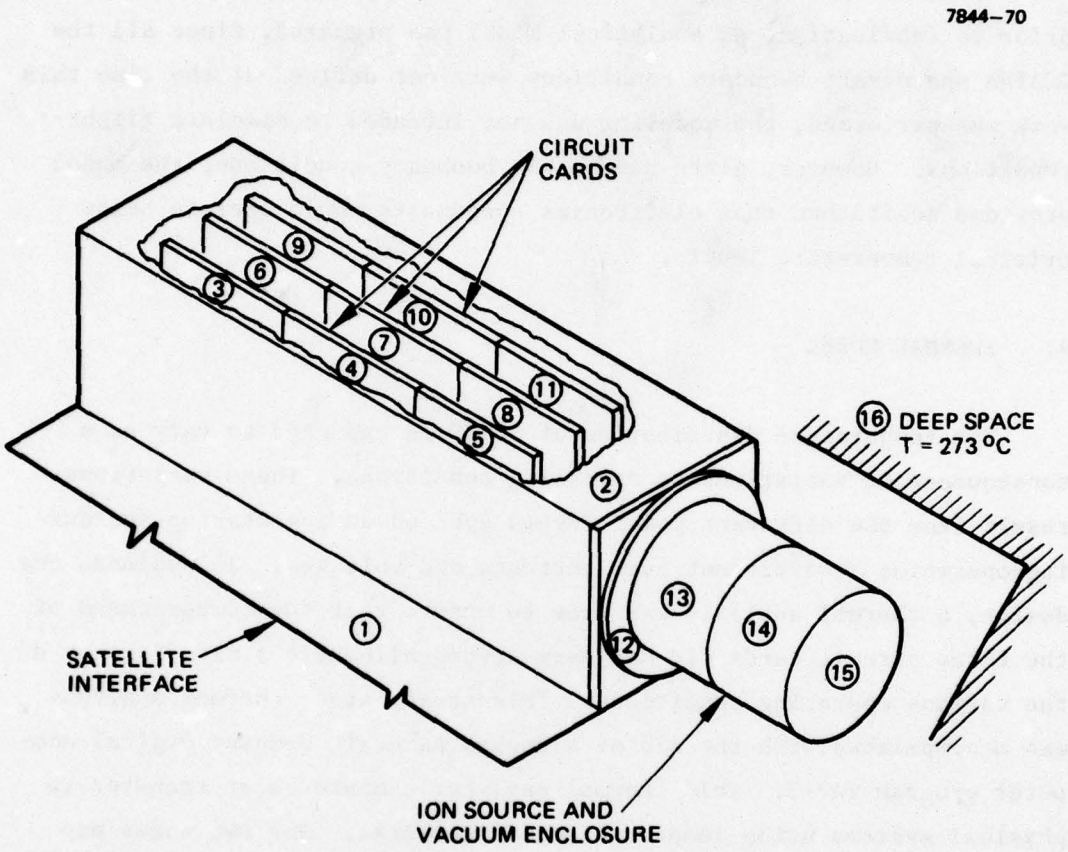

Figure A-1. SPIBS thermal model node layout.

ion source are also connected to the source backplate node via radiation resistors. The backplate is connected to the ion source by both radiation and conduction paths. A schematic showing the conductances and radiation resistors used in this model is shown in Figure A-2. (For clarity, only one typical circuit card network is shown in the figure.)

In preparing the SPIBS model, the following assumptions were made:

- The thermal properties were calculated using the handbook values for magnesium with a thermal conductance of 1.57 $W/cm^2/°C$ and an emissivity of 0.13.
- The thermal conductance between the circuit cards and PPA case was calculated assuming a 20 psi clamping force to produce a surface conductance of k = 0.05 $W/cm^2/°C$.
- Only the ion source body (nodes 13, 14, and 15) view deep space. All other nodes view the satellite, and radiation was neglected between the PPA nodes and the satellite.

B. POWER INPUTS

SPIBS system heat loads for the following five different operating modes are shown below

Table A-1. Thermal Operating Modes

(1) Startup
(2) Beam of 1 mA at 1 kV; no neutralizer; no bias
(3) Beam of 2 mA at 2 kV; no neutralizer; no bias
(4) Beam of 2 mA at 2 kV with neutralizer; no bias
(5) Beam of 2 mA at 2 kV with neutralizer; 1000 V bias

6326

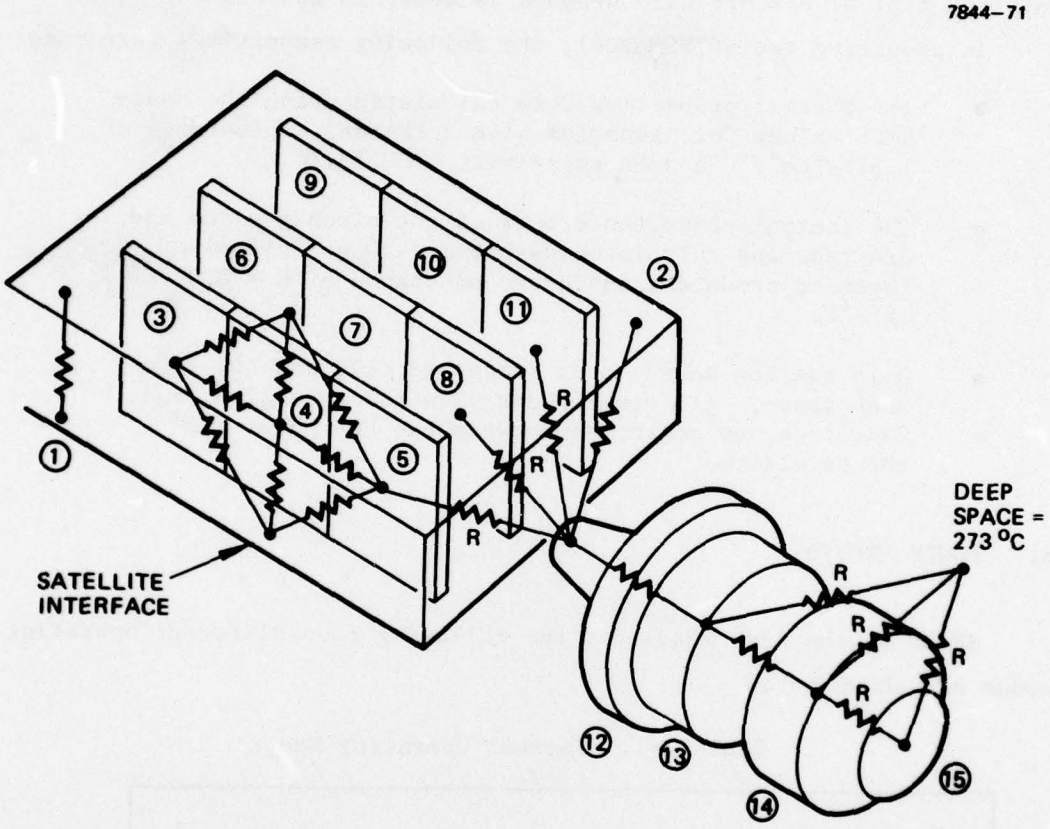

Figure A-2. Schematic of SPIBS thermal model showing network of conductances and radiation resistors. For clarity only, one circuit card is shown. Subscript R designates radiation paths.

Using the total powers shown above, the nodal power inputs to the circuit cards were distributed according to the power dissipated in the area assigned to each node. The ion source assembly power was distributed equally to the side nodes (13 and 14) and to the front node(15). It was further assumed that 25% of the transverse power goes into node 13 and that 75% goes into node 14. For the neutralizer filament power, it was assumed that 50% goes to node 15 and that 50% is radiated to space. A summary of the nodal power inputs for the five different operating modes is shown in Table A-1.

C. CALCULATED TEMPERATURES

Table A-2 summarizes the calculated temperatures for the five operating modes for a satellite interface temperature of 25°C. As might be expected, operating condition 5, which has the highest input power, results in the highest circuit card temperatures. Of the three circuit cards, the line regulator card has the highest temperature (∿54°C), while the screen/accel card has the lowest (∿41°C).

To investigate the effect of circuit card thickness on temperature, the circuit card conductances were adjusted to correspond to a 0.063 cm thickness rather than the baseline thickness 0.089 cm. The results of the reduced thickness calculations, presented in Table A-3, indicate that the circuit card temperatures are increased by 4° to 8°C.

A third run was made to determine the sensitivity of the circuit card temperature to satellite interface temperature. The results, shown in Table A-4, indicate a nearly linear relationship between the PPA and satellite interface temperature.

D. EXPERIMENTAL RESULTS

The thermal vacuum test setup for the EM system is described in Section 6 (see Figure 108). Thermocouples were installed at node locations used in the analytical model. All steady state data were taken in the "mode 2" condition.

Table A-1. Summary of Nodal Power Inputs (Watts) for Typicaly Operating Modes

Operating Condition	Circuit Card No. 1 Screen/Accel			Circuit Card No. 2 Cathod Keeper			Circuit Card No. 3 Line Regulator			Source End Plate	PPA Cover	Ion Source		
	Thermal Model Node													
	3	4	5	6	7	8	9	10	11	12	2	13	14	15
1	0.67	2.02	4.31	0.67	0.67	0.67	4.81	4.17	2.03	0	0	3.1	9.4	12.5
2	1.13	1.08	0.79	1.45	0.88	0.67	4.22	3.76	2.03	0	0	0.88	2.62	3.5
3	1.59	1.77	1.63	0.45	0.88	0.67	4.22	3.76	2.03	0	0	1.25	3.75	5.0
4	2.29	2.08	1.63	3.02	1.31	0.67	6.0	5.11	2.89	0	0	1.25	3.75	8.5
5	2.29	2.08	1.63	3.63	4.91	4.86	6.59	5.52	2.89	0	0	1.25	3.75	8.5

6326

Table A-2. Summary of Calculated Temperatures (°C) for SPIBS Thermal Model for Different Operating Conditions. Baseline Conditions: Satellite Interface of 25°C; 0.089 cm Thick Circuit Cards

Operating Condition	Circuit Card No. 1 Screen/Accel			Circuit Card No. 2 Cathode Keeper			Circuit Card No. 3 Line Regulator			Source End Plate	PPA Cover	Ion Source		
	Thermal Model Node													
	3	4	5	6	7	8	9	10	11	12	2	13	14	15
1	42.7	47.7	55.5	41.9	42.0	42.7	57.6	55.0	49.5	106	53.5	131	140	624
2	36.1	35.9	35.2	37.1	35.4	34.7	47.9	45.9	40.8	51.6	38.5	57.5	60.0	381
3	39.7	40.2	40.1	38.8	37.1	36.5	49.6	47.6	42.6	51.8	41.9	61.0	74.6	441
4	45.1	44.3	43.2	47.1	41.9	39.7	59.1	55.7	49.1	72.0	47.5	83.4	88.0	541
5	47.6	46.9	45.8	53.5	56.2	57.8	63.9	59.8	52.0	76.8	52.7	88.0	92.5	541

6326

Table A-3. Calculated Temperatures (°C) for SPIBS Thermal Model, Satellite Interface of 25°C. 0.063 cm Thick Circuit Cards

Operating Condition	Circuit Card No. 1 Screen/Accel			Circuit Card No. 2 Cathode Keeper			Circuit Card No. 3 Line Regulator			Source End Plate	PPA Cover	Ion Source		
	Thermal Model Node													
	3	4	5	6	7	8	9	10	11	12	2	13	14	15
1	38.7	42.2	47.8	38.1	38.1	38.7	49.3	47.5	43.5	101	47.5	125	135	624
2	33.4	33.3	32.7	34.1	32.9	32.4	41.8	40.4	36.7	48.9	35.6	54.9	57.4	381
3	36.1	36.5	36.4	35.5	34.2	33.8	43.1	41.7	38.2	58.5	38.3	67.9	71.4	441
4	40.1	39.6	38.8	41.6	37.9	36.3	50.1	47.7	43.0	67.7	42.7	79.3	83.9	541
5	42.2	41.6	40.8	46.3	48.3	49.4	53.7	50.8	45.3	71.4	46.8	82.9	87.5	541

6326

Table A-4. Calculated Temperatures (°C) for SPIBS Thermal Model; Satellite Interface at 50°C; 0.089 cm Thick Circuit Cards

Operating Condition	Circuit Card No. 1 Screen/Accel			Circuit Card No. 2 Cathode Keeper			Circuit Card No. 3 Line Regulator			Source End Plate	PPA Cover	Ion Source		
	Thermal Model Node													
	3	4	5	6	7	8	9	10	11	12	2	13	14	15
1	63.4	66.9	72.5	62.7	62.8	63.4	73.9	72.1	68.2	122	71.8	145	155	625
2	58.2	58.0	57.5	58.9	57.7	57.2	66.5	65.2	61.5	71.6	60.2	76.9	79.1	382
3	60.9	61.2	61.2	60.2	59.0	58.6	67.9	66.5	62.9	80.9	62.8	89.4	92.8	442
4	64.9	64.3	63.5	66.3	62.6	61.0	74.8	72.4	67.8	89.8	67.2	100	105	542
5	66.9	66.4	65.6	71.1	73.0	74.2	78.4	75.5	70.0	93.5	71.3	104	108	542

6326

Experimental results are presented in Table A-5 for three different baseplate temperatures. The information in Table A-5 includes a key for thermocouple designation number and the experimental temperature of node 1 (satellite interface). Comparing the experimental and analytical results indicates that the measured temperatures and gradients are less than predicted for the electronics. For the ion source, which should not be critical thermally, the model is also conservative but is less accurate. This is not surprising considering the uncertainties in modeling the source and cover.

E. CONCLUSIONS

These experimental and analytical results indicate that the SPIBS design should satisfy expected thermal requiremenqs. In terms of circuit card structure thickness, 0.089 cm is a good choice. A thinner web would result in unacceptable temperatures.

Table 5. Experimental Results

	Circuit Card No. 1 Screen/Accel			Circuit Card No. 2 Cathode Keeper			Circuit Card No. 3 Line Regulator			Source End Plate	PPA Cover	Ion Source		
	Thermal Model Node													
	3	4	5	6	7	8	9	10	11	12	2	13	14	15
TC No.[a]	1	2	3	4&7	5&8	6&9	10	11	12	22/24	15/16	21/28/27	21/23/27	28
Mode 2 (Node 1 = 29)	30	33	32	32/33	32/34	31/33	39	44	30	34/34	29/31	16/33/32	16/33/32	88
Mode 2 (Node 1 = 37)	40	44	44	43/43	44/45	43/44	48	53	42	52/53	40/41	10/50/49	10/50/49	90
Mode 2 (Node 1 = 45)	50	53	55	50/50	50/52	50/52	57	66	49	60/61	48/49	10/59/58	10/59/58	103

[a]Thermocouple designation.

6326

APPENDIX B

MAGNETICS

The magnetics used on this program were the following types:

- Inductors — cut "C" cores
- Transductors — tape wound toroids
- Current transformers — ferrite pot cores.

Of particular interest are the transformers, specifically the high-voltage transformers. The power processor operating frequency (20 to 25 kHz) and the program weight and volume goals indicated that ferrite pot cores would be well suited for use as the transformer cores. Fabrication of the transformers proceeded smoothly except for certain high voltage part numbers. For these parts, the problem was manifested as excessively high magnetizing current, or low inductance, after potting. Failure analysis of these parts showed that the cores had cracked during potting. There were two contributors to this problem. First, the pot cores that are used in high voltage applications are modified after being received from the vendor. The slot in the standard core is not large enough for the required high voltage wire. The slot is enlarged by grinding it open as shown in Figure B-1. This grinding, naturally, removes material from the core and thereby, weakens it.

Second, the potting material that was used was a hard epoxy that required elevated temperature curing. The combination of these two things is what caused the cores to crack. It was then decided, after evaluating test samples, to use a softer potting material. The material that was selected was HP 16-92, Type II, Class 1, which is a polyetylene wax. Since switching to this potting material, there have been no transformer failures due to cracked cores.

However, a transformer in the flight unit did fail during thermal-vacuum testing at AFGL. The transformer that failed was the discharge supply output transformer, which floats on top of the screen supply. The failure was not of the type mentioned above, but was a sort that

developed between the primary and secondary windings. The flight unit was returned to HAC for rework. The transformer was replaced, and the unit was electrically tested prior to its return to AFGL. The unit was again tested at AFGL and delivered to the spacecraft contractor.

7844-72

a. BEFORE GRINDING

b. AFTER GRINDING

Figure B-1. Pot core modification.